

AD-A162 631

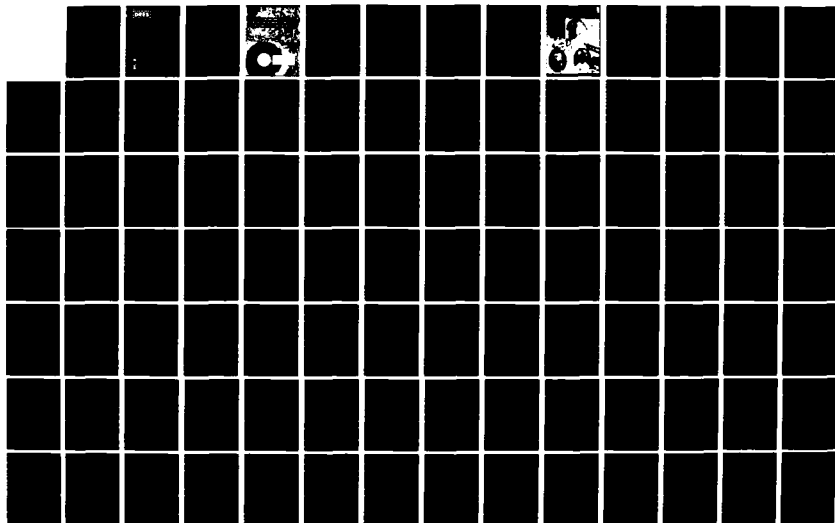
THE INFLUENCE OF INITIAL AND BOUNDARY CONDITIONS ON  
GASEOUS DETONATION WAVES (U) DEFENCE RESEARCH  
ESTABLISHMENT SUFFIELD RALSTON (ALBERTA) S B MURRAY  
SEP 85 DRES-SR-411

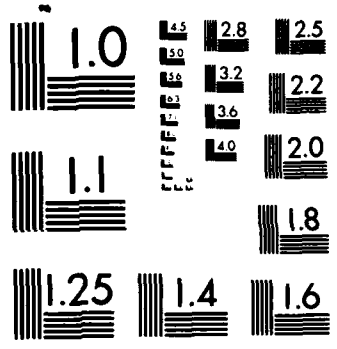
1/4

UNCLASSIFIED

F/G 19/4

NL





MICROCOPY RESOLUTION TEST CHART  
NATIONAL BUREAU OF STANDARDS-1963-A

# DRES

## SUFFIELD REPORT

NO. 411

2

AD-A162 631

### THE INFLUENCE OF INITIAL AND BOUNDARY CONDITIONS ON GASEOUS DETONATION WAVES\* (U)

by

Stephen Burke Murray

PCN No. 27C10

\* A thesis submitted to the Faculty of Graduate Studies and Research  
at McGill University, Montreal Canada in December of 1984

September 1985

DTIC  
ELECTE

DEC 26 1985

E

DTIC FILE COPY



DEFENCE RESEARCH ESTABLISHMENT SUFFIELD, RALSTON, ALBERTA

Canada

**WARNING**  
The use of this information is permitted subject to  
recognition of proprietary and patent rights.

This document is for public distribution in unclassified form.

85 12 20 015

UNCLASSIFIED

DEFENCE RESEARCH ESTABLISHMENT SUFFIELD  
RALSTON ALBERTA

SUFFIELD REPORT NO. 411

THE INFLUENCE OF INITIAL AND BOUNDARY CONDITIONS  
ON GASEOUS DETONATION WAVES\* (U)

by

Stephen Burke Murray

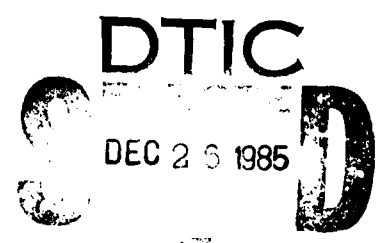
PCN 27C10

Accession For	
NTIS GRA&I	<input checked="" type="checkbox"/>
DTIC TAB	<input type="checkbox"/>
Unannounced	<input type="checkbox"/>
Justification	
By _____	
Distribution/	
Availability Codes	
Dist	Avail and/or Special
A-1	



\* A thesis submitted to the Faculty of Graduate Studies and Research at McGill University, Montreal Canada in December of 1984.

**WARNING**  
The use of this information is permitted subject to recognition of proprietary and patent rights.



UNCLASSIFIED

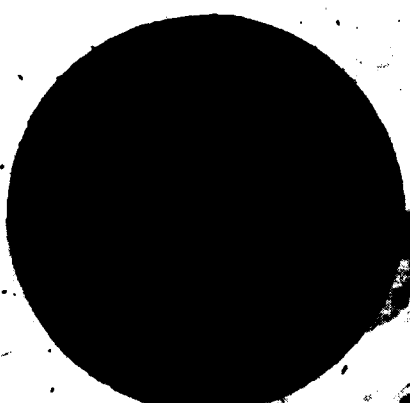
This document has been approved for public release and its distribution is unlimited.



# **THE INFLUENCE OF INITIAL AND BOUNDARY CONDITIONS ON GASEOUS DETONATION WAVES**

by  
**Stephen Burke Murray**

**Department of Mechanical Engineering  
McGill University, Montreal**



A thesis submitted to  
the Faculty of Graduate Studies and  
Research in partial fulfillment of  
the requirements for the degree of  
Doctor of Philosophy

© Crown Copyright  
December, 1984

ABSTRACT

The results of five experimental investigations on the initiation, propagation and transmission of detonation have shown that the wave behavior depends on the relative rates of gasdynamic expansion and chemical energy release occurring within the cellular detonation front. The former rate is controlled by the "boundary conditions" defined by the physical system, while the latter rate depends on the chemical and physical properties of the combustible mixture. The fractional increase  $\xi$  in the area of the post-shock "stream tube", evaluated over a chemical kinetic distance equal to the cell length, has been identified as a parameter which satisfactorily characterizes the competition between these two rate processes. For  $\xi$  less than about 20%, the chemical processes survive the gasdynamic expansion and self-sustained propagation is possible. However, under these "supercritical" conditions, the wave propagates with a velocity deficit which appears to be a universal and theoretically predictable function of  $\xi$ .

For  $\xi$  greater than 20%, the shock/reaction zone coupling breaks down, resulting in failure of the wave. The "critical" conditions for the propagation of detonation waves subjected to a wide range of expansion inducing mechanisms, including viscous boundary layers, compressible boundary gases and yielding walls, are all found to be consistent with the 20% criterion. However, the criterion becomes inapplicable as the cell size approaches the characteristic transverse dimension of the geometry.

In the case of direct initiation or transmission of detonation from one geometry to another, the critical conditions are shown to be linked to the requirement for the diverging wave to exceed some minimum radius of curvature. Such radius is geometry dependent and satisfies the stream tube criterion. The role of the "initial conditions" in this type of problem is to guarantee survival of the wave until it achieves the minimum radius for which shock/reaction zone coupling, and hence self-sustenance, are possible.

RESUME

Cette thèse présente cinq études expérimentales portant sur l'initiation, la propagation et la transmission des ondes de détonation. Il est démontré que ces trois phénomènes dépendent, d'une part, du taux d'expansion et, d'autre part, de la vitesse de réaction à l'intérieur du front cellulaire de la détonation. Ce premier est contrôlé par les conditions frontières du système physique tandis que le dernier dépend des propriétés physiques et chimiques du mélange combustible. L'effet compétitif de ces deux processus est très bien caractérisé par un paramètre  $\xi$ , soit la fraction d'expansion du "tube d'écoulement" sur une longueur d'une cellule. Les études effectuées démontrent que la propagation d'une onde de détonation stable n'est possible que si  $\xi$  est moins qu'environ 20%. Il existe, de plus, une relation théorique et universelle reliant le déficit de célérité de propagation et le paramètre  $\xi$ .

En raison du découplage éventuel entre le choc et la zone de réaction, la propagation d'une onde de détonation stable devient impossible si  $\xi$  est plus de 20%. Ce critère est valable pour une vaste gamme de mécanismes d'expansion due soit à une couche limite, une enveloppe de gaz compressible ou une paroi souple. Le critère n'est cependant pas valable lorsque la dimension transversale de la cellule approche celle du système physique.

Les conditions limites pour l'initiation d'une détonation et la transmission de celle-ci d'une géométrie à l'autre sont liées au rayon de courbure de l'onde divergente. De plus, le rayon de courbure minimum est en bon accord avec le critère du "tube d'écoulement".

Le role de "conditions initiales" dans se genre de problème est de garantir que la détonation survive jusqu'a ce quelle arrive au rayon minimum pour que l'accouplement du zone de choc/réaction, et en soi, la propagation stable est possible.



ACKNOWLEDGEMENTS

The author wishes to express his sincere gratitude to Professor J. Lee, not only for the academic guidance which he provided during the course of this work, but also for his constant encouragement, patience and friendship. In addition, the moral support, friendship and stimulating scientific exchanges with Dr. I. Moen, Dr. P. Thibault and Professor R. Knystautas are acknowledged with thanks. The author is indebted to the Department of National Defence for being given the privilege to undertake the studies described herein. Particular thanks is due to Dr. F. Christie, Dr. R. Heggie and Dr. J. Gottlieb, whose efforts were instrumental in making possible the opportunity for educational leave.

An endeavor of this magnitude would not have been successful without the assistance of many qualified and spirited individuals. The technical support provided by Mr. J. Funk, Mr. S. Ward and Mr. C. Coffey was of extremely high calibre. Their dedication and ingenuity were invaluable during the design and construction of the field apparatus and in assisting with the experiments therein. The Photography Group, the Electronic Design and Instrumentation Group, the Munitions Group, the Computer Group, the Field Operations Section, the Meteorological Section, the Chemistry Section, and the machine shops at both McGill and DRES provided high quality services in the true spirit of cooperation. The author also wishes to express his gratitude to Mrs. N. Smart and Ms. H. Collier for their patience and hard work in preparing the typewritten manuscript. The exceptional quality of the graphics is due to the talents of Mrs. S. Kelly and Mrs. L. Wall. In conjunction with the experience of Mr. N. Bonin, the final volume is truly a handsome and polished looking piece of work.

Without question, the moral support and encouragement provided by my parents, my two sisters and their respective families, my many relatives and friends, and in particular the Bannister and Moen families, were responsible for keeping my progress sustained through some very difficult times. Finally, I would like to thank Wendy, who supported me like a soldier throughout most of my post-graduate studies.

To Stephanie and Kirt  
with love. They have  
brought much joy and  
happiness into my life.  
They made this  
endeavour all  
worthwhile...

vi)



TABLE OF CONTENTS

	Page No.
ABSTRACT .....	ii
RESUME .....	iii
ACKNOWLEDGEMENTS .....	v
DEDICATION .....	vi
TABLE OF CONTENTS .....	vii
LIST OF TABLES .....	xii
LIST OF FIGURES .....	xiii
NOMENCLATURE .....	xxi
PREFACE .....	xxvi
1.0 INTRODUCTION .....	1
1.1 Motivation .....	1
1.2 Historical Background .....	2
1.2.1 The Discovery and Chapman-Jouguet Theory .....	2
1.2.2 The Structure of a Detonation Wave .....	3
• Early Notions .....	3
• An Important Discovery Long Overdue .....	5
• The Effort to Understand the Intricacies of the Cellular Front .....	7
• The "Hydrodynamic Thickness" of the Detonation Front .....	8
1.2.3 The Formation of Detonation .....	9
• Two Modes of Initiation .....	9
• Early Studies - Initiation of Detonation in Fuel-Oxygen Mixtures .....	12
• More Recent Work - Initiation of Detonation in Fuel-Air Mixtures .....	13
• Theoretical Efforts to Predict the Initiation Energy .....	15
1.2.4 The Transmission of Detonation .....	17
• The Critical Tube Diameter for Transmission to an Unconfined Region .....	17
• The Critical Channel Width for Transmission to an Unconfined Region .....	20
• Transmission Phenomena in Other Geometries .....	20
1.2.5 The Detonability Limits and Velocity Deficits .....	21
• Limits and Near Limit Phenomena .....	21
• Velocity Deficits .....	23

TABLE OF CONTENTS (cont'd)

	• Influence of Confinement - Early Studies Related to High Explosives .....	25
	• Influence of Confinement - The Extension to Gaseous Explosives .....	27
1.3	Objectives and Format of the Thesis .....	30
1.3.1	A Brief Recap - Where We Are Today .....	30
1.3.2	An Outline of the Present Undertaking .....	32
2.0	THE CRITICAL CONDITIONS FOR THE TRANSMISSION OF PLANAR DETONATION TO SPHERICAL OR CYLINDRICAL DETONATION .....	34
2.1	Introduction .....	34
2.2	Experimental Details .....	35
2.3	Experimental Results and Discussion .....	37
2.3.1	Cell Width Measurements .....	37
2.3.2	The Two Modes of Reinitiation .....	38
	• Smoke Records Corresponding to Spontaneous Reinitiation .....	39
	• Smoke Records Corresponding to Reinitiation by Reflection .....	41
2.3.3	The Annular Ring - What Does It Tell Us? .....	42
	• Reinitiation by Reflection - the Formation of Cylindrical Detonation .....	45
	• Spontaneous Reinitiation - the Formation of Spherical Detonation .....	48
2.3.4	Wave Front Curvature as a Means of Quantifying the Gasdynamic Expansion .....	53
2.4	Summary .....	54
3.0	LARGE-SCALE EXPERIMENTS ON THE TRANSMISSION OF PLANAR DETONATION TO SPHERICAL DETONATION IN ETHYLENE-AIR MIXTURES .....	57
3.1	Introduction .....	57
3.2	Experimental Details .....	58
3.3	Experimental Results and Discussion .....	61

TABLE OF CONTENTS (cont'd)

3.3.1	High-Speed Cinematography of the Diffraction Phenomenon .....	61
3.3.2	Critical Tube Diameter Measurements .....	63
3.3.3	Cell Width Measurements .....	64
3.3.4	The $13\lambda$ Correlation - Difficulty Interpreting the Smoke Records .....	65
3.4	Summary .....	68
4.0	THE INFLUENCE OF YIELDING CONFINEMENT ON LARGE-SCALE ETHYLENE-AIR DETONATIONS .....	70
4.1	Introduction .....	70
4.2	Experimental Details .....	72
4.3	Experimental Results and Discussion .....	73
4.3.1	Cell Width Measurements .....	73
4.3.2	High-Speed Cinematography of the Transmission and Propagation Phenomena .....	74
	• The Transient Reinitiation Phase .....	74
	• The Steady Propagation Phase .....	79
4.3.3	Estimating the Magnitude of the Controlling Chemical Length .....	82
	• A Criterion for Criticality .....	82
	• The Particle Thermodynamic History .....	83
	• Results of the Calculations .....	85
4.3.4	The "Stream Tube" Area Increase as a Means of Quantifying the Chemical-Gasdynamic Competition .....	86
	• A Check on the Stream Tube Criterion Using Tapered Yielding Tubes .....	88
	• Other Support for the Stream Tube Criterion .....	89
4.4	Summary .....	91
5.0	THE INFLUENCE OF YIELDING CONFINEMENT ON THE VELOCITY OF PROPAGATION OF GASEOUS DETONATION WAVES .....	94
5.1	Introduction .....	94
5.2	Experimental Details .....	96

TABLE OF CONTENTS (cont'd)

5.3	Experimental Results and Discussion .....	98
5.3.1	Cell Width Measurements .....	98
5.3.2	The Transmission Phenomenon .....	99
5.3.3	Critical Conditions for Propagation .....	100
5.3.4	The Behavior of the Wave Under Supercritical Conditions .....	103
	• Velocity Deficits and the Steam Tube Area Increase .....	103
	• Velocity Deficits Reported by Other Investigators .....	104
5.3.5	Limitations of the Stream Tube Approach .....	107
5.4	Summary .....	108
6.0	DIRECT INITIATION OF DETONATION IN ETHYLENE-AIR MIXTURES .....	111
6.1	Introduction .....	111
6.2	Experimental Details .....	112
6.3	Experimental Results and Discussion .....	114
6.3.1	High-Speed Cinematography of the Initiation Phenomenon .....	114
6.3.2	Velocity Deficits and Oscillations .....	114
6.3.3	The Critical Energy for Direct Initiation .....	117
	• Wave Front Curvature and the Stream Tube Area Increase .....	117
	• The "Kernel" Theory in Light of the Stream Tube Criterion .....	119
	• Other Models for the Critical Energy .....	123
6.4	Summary .....	124
7.0	CONCLUSIONS AND RECOMMENDATIONS FOR FUTURE RESEARCH .....	126
7.1	Highlights of the Individual Experimental Studies .....	126
7.2	A Unified Description of Detonation Based on the Present Results .....	132

TABLE OF CONTENTS (cont'd)

7.3 Recommendations for Future Research ..... 138

8.0 ORIGINALITY AND CONTRIBUTION TO KNOWLEDGE ..... 141

LIST OF REFERENCES

TABLES

FIGURES

APPENDICES

LIST OF TABLES

- Table I Critical conditions for transmission from a rigid tube of 0.89 m diameter to various yielding tubes and to an unconfined region.
- Table II Initial post-shock conditions and results from calculations to determine the relevant chemical length scale associated with detonative propagation.
- Table III Calculated stream tube area increases for the constant diameter yielding tube configurations.
- Table IV Calculated stream tube area increases for the tapered yielding tube configurations.
- Table V Summary of critical conditions for propagation of  $C_2H_2-O_2-N_2$  detonations in square channels with various rigid/yielding wall combinations.



LIST OF FIGURES

- Figure 1 Smoke records produced by a detonation wave in low-pressure equimolar oxyacetylene showing the cellular structure recorded on walls parallel to and normal to the direction of propagation.
- Figure 2 Stroboscopic laser-shadow photographs of a detonation wave propagating in a hydrogen-oxygen mixture.
- Figure 3 Schlieren interferogram and interpretive sketch showing details of the double Mach reflection associated with the cellular structure of a detonation wave.
- Figure 4 Sketch illustrating the cyclic nature of detonative propagation.
- Figure 5 Spark Schlieren photographs of a spherical detonation illustrating the subcritical, supercritical and critical regimes of direct initiation.
- Figure 6 Photographs of the apparatus used to investigate the transformation of planar detonation to cylindrical or spherical detonation.
- Figure 7 Schematic diagram of the apparatus and diagnostic techniques used to study the transformation of planar detonation to cylindrical or spherical detonation.
- Figure 8 Transverse wave spacing or cell width versus initial mixture pressure for equimolar oxyacetylene mixtures.
- Figure 9 Schematic diagrams of the spontaneous reinitiation mechanism and the process of reinitiation by reflection from a wall.
- Figure 10 Smoke record from the back wall of the cylindrical chamber showing features of the annular ring formed during spontaneous reinitiation.

- Figure 11 Collection of smoke records from the back and front walls of the cylindrical chamber showing supercritical transmission, critical transmission and failure to transmit.
- Figure 12 Normalized ring radius ( $R_s/R_0$ ) versus relative mixture sensitivity ( $\lambda_s/\lambda$ ).
- Figure 13 Normalized ring radius  $(R_s - R_0)/\lambda$  versus relative mixture sensitivity ( $\lambda_c/\lambda$ ).
- Figure 14 Normalized critical ring radius versus ratio of tube diameter to plate separation.
- Figure 15 Schematic diagrams of the spontaneous reinitiation process showing the spherical detonation bubble model and the transversely propagating detonation model used to calculate the axial location of reignition downstream of the tube exit.
- Figure 16 Normalized axial location of reignition versus relative mixture sensitivity for spontaneous reinitiation.
- Figure 17 Collection of smoke records from the outer surface of the thin-walled hollow cylinder showing failure to transmit, critical transmission and supercritical transmission.
- Figure 18 Photograph showing the large-scale experimental configuration for a critical tube diameter test and a schematic diagram of the gas mixing system.
- Figure 19 Fuel concentration versus time for a typical critical tube diameter experiment.
- Figure 20 Selected photographs of the large-scale experimental test facility.

- Figure 21 Selected frames from a high-speed cinematographic record showing near critical transmission of detonation from a rigid tube of 0.89 m diameter to a large gas bag simulating an unconfined environment.
- Figure 22 Selected frames from a high-speed cinematographic record showing supercritical transmission of detonation from a rigid tube of 0.89 m diameter to a large gas bag simulating an unconfined environment.
- Figure 23 Critical tube diameter versus fuel concentration for the ethylene-air system at atmospheric pressure.
- Figure 24 Detonation cell width versus fuel concentration for the ethylene-air system at atmospheric pressure.
- Figure 25 Comparison between the cellular structure recorded on a smoked plate and the plastic strips produced by an ethylene-air detonation propagating in a plastic bag.
- Figure 26 Photograph of a smoked plate produced by an ethylene-air detonation along with the author's interpretation of the cellular structure.
- Figure 27 Photographs of smoke records showing the difference between the cellular structure of a fuel-air detonation at atmospheric pressure and a fuel-oxygen detonation at low pressure.
- Figure 28 Large-scale field facility showing the rigid/yielding tube combination prior to testing.
- Figure 29 Photographs showing both the initiation scheme employing an oxyacetylene slug, and the protective housing containing the camera and microwave unit.

- Figure 30 Measured cell aspect ratios for the  $C_2H_4$ -air system at atmospheric pressure.
- Figure 31 Cinematographic sequence showing supercritical transmission to a yielding tube of nominal 10 mil wall thickness and 0.89 m diameter.
- Figure 32 Cinematographic sequence showing slightly supercritical transmission to a yielding tube of nominal 5 mil wall thickness and 0.89 m diameter.
- Figure 33 Schematic diagrams showing details of the reinitiation process typical of transmission to a tube with yielding walls.
- Figure 34 Cinematographic sequence (looking into the tube exit) showing critical transmission to a yielding tube of nominal 1 mil wall thickness and 0.89 m diameter.
- Figure 35 Cinematographic sequence (looking along the axis of propagation) showing transmission of detonation to a yielding tube of nominal 6 mil wall thickness and 1.83 m diameter.
- Figure 36 Cinematographic sequence (looking normal to the direction of propagation) showing critical transmission to a yielding tube of nominal 1 mil wall thickness and 0.89 m diameter.
- Figure 37 Reaction front axial velocity and normalized radius of curvature as a function of axial distance from the rigid tube exit.
- Figure 38 Cinematographic sequence showing subcritical transmission to a yielding tube of nominal 5 mil wall thickness and 0.89 m diameter.
- Figure 39 Summary of test results for transmission of detonation from a rigid tube of 0.89 m diameter to yielding polyethylene tubes having various wall thicknesses.

- Figure 40 Cinematographic sequence showing recovery of a detonation wave perturbed at the boundary.
- Figure 41 Photograph of the yielding tube configuration prior to testing showing a high-explosive initiation charge in place of the linear detonation tube.
- Figure 42 Cinematographic sequence showing gradual failure of detonation induced by a series of perturbing obstacles around the periphery of a tube of nominal 10 mil wall thickness.
- Figure 43 Comparison between measured wall trajectories and those calculated using a cylindrical piston analogy.
- Figure 44 Comparison between calculated contact surface trajectories from a bursting cylinder.
- Figure 45 A plot of the chemical histories for various assumed controlling chemical times, given the expansion corresponding to the 10 mil thick yielding polyethylene wall.
- Figure 46 Apparatus used to investigate the phenomenon of velocity deficits in the presence of yielding confinement.
- Figure 47 Photographs showing the test section used to investigate the phenomenon of velocity deficits; prior to being prepared for testing, after preparation for an experiment, and after completion of a test.
- Figure 48 Cell width versus mixture composition for stoichiometric oxyacetylene mixtures with nitrogen dilution at atmospheric pressure.

- Figure 49 Comparison between the reinitiation phenomenon proposed from cinematographic records of large-scale transmission and that evident from smoke records in laboratory experiments.
- Figure 50 A series of smoke records from the side wall of a square channel having three rigid walls and a yielding acetate top.
- Figure 51 Experimentally measured velocity deficits versus the calculated increases in stream tube area for the data from tests in square channels with yielding walls.
- Figure 52 Experimentally measured velocity deficits versus the calculated increases in stream tube area for the data of other investigators.
- Figure 53 General layout of the field facility used to determine the critical energy for direct initiation of ethylene-air mixtures.
- Figure 54 Schematic diagrams of the test section used to determine the critical energy for direct initiation of detonation in  $C_2H_4$ -air mixtures, showing the location of pressure transducers and ionization-gap probes.
- Figure 55 Photographs showing the configuration of the gas bag test section used to determine the critical energy for direct initiation of  $C_2H_4$ -air mixtures.
- Figure 56 Selected frames from a cinematographic record showing unsuccessful initiation of detonation in a gas mixture of 6.40%  $C_2H_4$  in  $C_2H_6$ -air using an initiator charge of 9 grams Detasheet.
- Figure 57 Selected frames from a cinematographic record showing successful initiation of detonation in a gas mixture of 6.40%  $C_2H_4$  in  $C_2H_6$ -air using an initiator charge of 18 grams Detasheet.

- Figure 58 Detonation velocity observed at various positions along the test section showing steady propagation for 6.40%  $C_2H_4$  in  $C_2H_4$ -air and unsteady propagation for 3.90%  $C_2H_4$  in  $C_2H_4$ -air.
- Figure 59 Spherical initiation energy versus concentration of  $C_2H_4$  in  $C_2H_4$ -air mixtures at atmospheric pressure.
- Figure 60 Spherical initiation energy versus stoichiometry for various fuel-air mixtures at atmospheric pressure.
- Figure 61 A summary of experimental studies on the influence of initial and boundary conditions on the behavior of detonations away from the spin limit.
- Figure 62 Proposed experimental configuration to investigate the nature of the chemical-gasdynamic competition and the magnitude of the relevant chemical kinetic thickness of the detonation front.
- Figure A-1 Plan view of the DRES FAE facility.
- Figure A-2 Mounting channels in the concrete test pad.
- Figure A-3 Concrete test pad.
- Figure A-4 Gas delivery system.
- Figure A-5 Centrifugal blower used for mixing combustible gases.
- Figure A-6 Gas mixing system.
- Figure A-7 Gas analysing system schematic.
- Figure A-8 Fuel concentration versus time for a typical experiment.

Figure A-9 Diagnostic systems.

Figure A-10 Instrumentation and gas flow control bunkers.

Figure B-1 The  $x - t$  diagram for a simple launcher.

Figure B-2 Wave diagram for the motion following the one-dimensional impact of a shock wave on a movable wall.

Figure C-1 One-dimensional detonation wave.

Figure C-2 Hugoniot-Rayleigh representation of shock and detonation waves.

Figure C-3 Quasi one-dimensional representation of a detonation wave with area increase.

Figure C-4 Changes in C-J conditions due to area increase.



NOMENCLATURE

<u>Symbol</u>	<u>Description</u>
a	exponent in induction-time or other chemical kinetic time formula.
A	area of shock or detonation front, cross-sectional area of stream tube, or surface area of yielding wall material.
(A)	denotes dark annular band corresponding to region of quenched detonation wave.
b	exponent in induction-time or other chemical kinetic time formula.
c, C	sonic velocity in a gas.
(C)	denotes circular core of a detonation wave, or cylindrical detonation wave.
$d_0$	diameter of a thin-walled hollow cylinder.
D	tube diameter.
(D)	denotes diffracted shock wave or detonation wave.
$D_c$	critical diameter for transmission of detonation from a circular tube to an unconfined region.
e	internal energy of a gas.
E	initiation energy, or effective activation energy.
(E)	denotes explosion or reignition nuclei.
$E_c$	critical energy for direct initiation of detonation.
$E_s(t)$	energy of initiation source.
f	dimensionless pressure $P/\rho_0 R_s^2$ .
(F)	denotes trailing reaction zone or flame.
h	axial distance from tube exit at which reignition occurs.
(H)	denotes head of rarefaction wave.
I	dimensionless energy integral.

<u>Symbol</u>	<u>Description</u>
j	specifies geometry; equal to 0, 1 or 2 for planar, cylindrical or spherical geometry, respectively.
k	pre-exponential factor in induction-time or other chemical kinetic time formula, or constant of proportionality between predicted and experimentally observed quantities.
$k_j$	numerical constant; equal to 1, $2\pi$ or $4\pi$ for planar, cylindrical or spherical geometry, respectively.
K	curvature of the shock front $A^{-1}dA/dR$ ; equal to $1/R$ and $2/R$ for cylindrical and spherical fronts, respectively.
l, L	length of a rigid tube or a plastic bag.
(L)	denotes luminous patches indicative of a renewed detonation front.
$L_c$	detonation cell length.
m	mass of a yielding wall or a piston.
m/A	area density of yielding wall material.
M, $M_s$	Mach number of a shock wave or a detonation wave.
$M_s^*$	critical shock Mach number for direct initiation of detonation.
( $M_1$ )	denotes cylindrical Mach stem caused by reflection of a detonation wave from a wall.
( $M_2$ )	denotes detonative Mach stem responsible for "petal"-like structures on the back wall smoke records.
$\Delta M$	change in Mach number of a shock wave or a detonation wave.
$\Delta M/M_{C-J}$	Mach number deficit resulting from an increase in the stream tube area.
p, P	pressure of a gas.
(P)	denotes planar detonation wave.
$P_2$	Riemann invariant; equal to $2c_2/(\gamma_2 - 1)$
q	exponent in the power law density profile expression.
Q	heat release per unit mass liberated through combustion.

<u>Symbol</u>	<u>Description</u>
$Q_1$	Riemann invariant; equal to $2c_1/(\gamma_1 - 1)$
$r, r(t)$	radial position of a particle or a yielding wall.
$r_s(t)$	radial position of the diffracted wall shock.
$R$	gas constant.
$(R)$	denotes reignition centres.
$R_0$	tube radius.
$R_s, R_s(t)$	shock radius, or radius of the annular ring observed on the back wall smoke record.
$R_s^*$	critical shock radius for direct initiation of detonation.
$\dot{R}_s$	velocity of a shock wave or a detonation wave.
$(R_1), (R_2)$	denote reflected shock wave or detonation wave.
$(S)$	denotes spherical detonation wave.
$t$	time, or thickness of the yielding wall material.
$\Delta t$	elapsed time between two events, or the period of oscillations from pressure-time signatures.
$T$	temperature of a gas.
$(T)$	denotes transversely propagating detonation wave.
$u_r, u_r(t)$	radial velocity of a particle or a yielding wall.
$u_s$	post-shock relative particle velocity.
$u, U$	absolute particle velocity.
$V$	velocity of a shock wave, a reaction front or a detonation wave.
$\Delta V/V_{C-J}$	velocity deficit resulting from an increase in the stream tube area.

<u>Symbol</u>	<u>Description</u>
w	separation between the front and back plates in planar-to-cylindrical transmission experiments.
W	mass of the initiator charge in experiments to determine the critical energy for direct initiation of detonation, or channel width.
$W_c$	critical width for transmission of detonation from a channel to an unconfined region.
x	relative distance behind a shock wave, or distance from the rigid tube exit.
$\beta$	nitrogen-to-oxygen dilution ratio.
$\gamma$	ratio of specific heats for a gas.
$\delta^*$	boundary layer displacement thickness.
$\Delta$	induction-zone or other chemical kinetic length.
$\zeta$	dimensionless position $r/R_s(t)$ .
$\lambda$	detonation cell width or transverse wave spacing.
$\lambda_c$	cell width required for critical transmission of detonation from a circular tube to a cylindrical volume.
$\lambda_s$	cell width required for critical transmission of detonation from a circular tube to an unconfined region.
$\mu_e$	dynamic viscosity of a gas at the edge of a boundary layer.
$\nu$	term in Dabora's velocity deficit expression; equal to $\xi/(1 + \gamma_2)/(1 + \xi)$ .
$\xi$	relative increase in the cross-sectional area of a stream tube of particles entering the shock front.
$\xi_{in}$	stream tube area increase due to the motion of yielding walls.
$\xi_t$	stream tube area decrease due to the taper of a yielding tube.
$\pi$	numerical constant; approximately equal to 3.1415926.
$\rho$	density of a gas.

<u>Symbol</u>	<u>Description</u>
$\tau$	induction or other chemical kinetic time.
$\tau_0$	induction or other chemical kinetic time based on initial post-shock conditions.
$\Delta\tau$	increase in induction or other chemical kinetic time.
$\phi$	angle of cone traced out by a rarefaction wave penetrating a detonation wave, or equivalence ratio for a gas mixture, or dimensionless velocity $U/R_s$ .
$\psi$	dimensionless density $\rho/\rho_0$ .

Subscripts

a	value immediately ahead of the piston.
b	value immediately behind the piston.
c	critical condition, or value associated with cylindrical geometry.
C-J	Chapman-Jouguet condition.
e	condition at the edge of a boundary layer.
s	shocked condition, or value associated with the shock front, or value associated with spherical geometry.
w	condition at the wall.
0	initial condition.
1	initial condition in low-pressure reservoir ahead of the piston, or condition ahead of the detonation wave.
2	initial condition in high-pressure reservoir behind the piston.

Superscript

*	denotes value for critical initiation.
---	--

Other

[ ]	denotes concentration of a gas specie.
$\infty$	denotes infinite value.

## 1.0 INTRODUCTION

### 1.1 Motivation

Throughout the evolution of man, his standard of living has been closely tied to the discovery and subsequent exploitation of new forms of energy and new types of material. This has been particularly true over the past century, during which the growth of the chemical and petrochemical industries has proceeded at an astounding pace. However, the benefits derived from these advances have not been without cost. In recent years, vapour cloud explosions have become the cause of the largest losses in these industries. This has been the result of a trend toward higher plant capacities, higher pressure and temperature processes and prolonged inventory holdup. In a survey of accidental explosions prior to 1976 (Davenport, 1977), over 30% of all incidents were attributed to vessel failures, while more than 60% of accidents resulted from piping, valve or fitting failures. Following the escape of a combustible vapour, it diffuses and mixes with the surrounding air. If a suitable ignition source is present, the ensuing rapid rate of energy release, either in the form of a deflagration wave or a detonation wave, can be catastrophic. The incident in Flixborough, England in 1974, which claimed the lives of 28 chemical plant workers, is a vivid example. In the more recent incident (1979) at the Three Mile Island Nuclear Plant in Harrisburg, Pennsylvania, a potentially devastating explosion of the hydrogen-air bubble inside a reactor pressure vessel did not occur. Here in Canada, the ethylene plant explosion in Edmonton in 1982 is a recent reminder.

Although it is thought highly improbable that detonation has been the mechanism involved in any accidental vapour cloud explosion to date (the incident at Port Hudson, U.S.A. in 1970 may be an exception), the damage potential of detonation is so great that some organizations concerned with risk analysis still consider it a possibility, albeit remote. The recent observations (Pfortner, 1983; Moen et al., 1984) of transition to detonation in large-scale experiments have generated renewed concern about the possibility of detonation in an accidental scenario.

Apart from accidental explosions, detonable clouds have been used to advantage by military engineers in applications such as minefield breaching, defoliation, demolition and penetration of fortified structures. The rotating detonation wave rocket engine is another example of the controlled use of detonation (Nicholls et al., 1962a, 1962b, 1963). In all situations, whether they be accidental or applications oriented, the detonability of the combustible mixture is of key importance. Detonability is usually quantified by parameters such as the critical energy required for direct initiation of detonation, or the range of mixture composition over which detonation is possible. Most often, these quantities are measured either in unconfined clouds or in rigid tubes. However, in any practical situation, they depend strongly on both the initial and boundary conditions. The present study is motivated by the need to know to what extent the initial and boundary conditions influence the detonability of a combustible mixture.

## 1.2 Historical Background

### 1.2.1 The Discovery and Chapman-Jouguet Theory

It has been more than one hundred years since studies on combustion were first carried out by Mallard and Le Chatelier (1881, 1883) at the School of Mines in Paris where the first streak photographs of transition to detonation were obtained using a rotating drum camera. At the same time, Berthelot (1881) with Vieille (1882) at the School of Pharmacy measured detonation velocities in long tubes on the premise that detonation was a wave phenomenon characterized by a specific velocity of propagation. In fact, they formulated a theory to rationalize their measurements based on the hypothesis that the entire heat of combustion was converted into kinetic energy of the gas. It was not until several years later that the thermodynamic character of a planar steady detonation wave was revealed in the classical works of Chapman (1899), Jouguet (1905, 1906, 1917, 1927) and Crussard (1907a, 1907b). These authors pointed out the significance of a reactive wave front in relation to the shock front studied earlier by Hugoniot (1887-1889). They were also the first to postulate that a

detonation wave consisted of a shock wave followed by a deflagration. The Chapman and Jouguet (C-J) theory was able to successfully predict the detonation velocity and detonation gas states for the steady one-dimensional wave using equilibrium thermodynamics. A cornerstone premise in the theory, which has become known as the C-J condition, is that the detonation products travel at sonic velocity relative to the shock front. The calculation of C-J properties has been thoroughly refined (Eisen et al., 1960; Glassman, 1977). Computer software packages incorporating extensive libraries of thermodynamic data are readily available for this purpose (e.g., Gordon and McBride, 1976). The C-J theory is based on the assumptions of steady velocity and equilibrium thermodynamics. It provides no information about the behavior of the wave under transient conditions. In such cases, the rate of reaction or the structure of the wave must be taken into account.

### 1.2.2 The Structure of a Detonation Wave

#### Early Notions

Owing to the success of the C-J theory, several decades were devoted to improving the thermodynamic and hydrodynamic interpretation of the theory. Jouguet (1917) and Crussard (1907a), in particular, advanced the understanding by formulating the fundamental properties of the steady one-dimensional wave. Lewis and Friaf (1930) were noteworthy in addressing the chemical aspects of detonation using chain reaction theory with dissociation effects, while Becker (1936) was concerned with the dynamics of shock waves and was credited for having contributed a detailed description of shock wave formation in nonsteady flows. The understanding of planar detonation was further enhanced during the Second World War by the analyses of Zeldovich (1940-1944), von Neumann (1942), and Döring and Burckhardt (1944). These authors described the detonation as a shock wave followed by a steady-flow, inviscid reaction zone which is terminated by a plane at sonic conditions. This model of the wave, which has become known as the ZND model, triggered a number of studies. On the one hand, many investigations were concerned with the influence of transport properties and attempted to discredit the inviscid assumption (Hirschfelder et al., 1958a, 1958b, 1959; Oppenheim and



Rosciszewski, 1963). On the other hand, several studies addressing the interaction between the steady reaction zone and a nonsteady rarefaction to the rear of it questioned the validity of the Chapman-Jouguet hypothesis (Brinkley and Kirkwood, 1949; Kirkwood and Wood, 1954). By the end of the fifties, the understanding of the planar steady wave had peaked. Excellent reviews of the work carried out during this era are provided by Gross and Oppenheim (1959), Oppenheim (1961), Strehlow (1968, 1969), Edwards (1969), Lee et al. (1969), Oppenheim (1970), Oppenheim and Soloukhin (1973) and Fickett and Davis (1979).

One of the anomalies in the generally accepted view was the observation of the transverse wave phenomenon in detonation. It was originally thought to be a transient mechanism seen only near the detonability limits, as first reported by Campbell and Woodhead in 1927. These authors observed single-head spinning detonations in round tubes containing carbon monoxide-oxygen mixtures. Subsequently, Campbell and Finch (1928) established from phasing photographs and deposits on the tube wall that this structure describes a helical trajectory as the wave propagates axially. Shortly afterward, Bone with Frazer (1930) and with Townsend (1927a, 1927b) carried out a systematic study on the properties of detonation. The former pair of investigators noted that multiple heads could appear in large diameter tubes. A theory dealing with the origin of spin was later advanced by Bone, Fraser and Wheeler (1935) based on Schlieren records obtained using a rotating mirror camera. However, it was Manson (1946) and later Fay (1952) who were the first to propose independent mechanical acoustic theories for the prediction of the spinning frequency of the transverse vibrations in and behind the reaction zone. The frequency of the single-head spinning detonation was found to correspond approximately to the fundamental acoustic mode of the tube. The multiple heads observed by Bone and Frazer simply corresponded to other higher acoustic modes. An excellent description of the fine mechanical details of low-mode spinning detonations is given by Voitsekhovskii et al. (1963) and by Schott (1965).

An Important Discovery Long Overdue

It was not until the end of the fifties that a revolution of sorts began which made it apparent that the "anomaly" of spinning detonation was, in fact, a limiting case of the more universal cellular structure of detonation. This revolution, which was led in the Soviet Union by Denisov and Troshin (1959) and in the United States by White (1961), virtually shattered the concept of the steady one-dimensional wave. White obtained photographic records by means of spark-lit interferometry which demonstrated that the structure was highly three-dimensional, nonsteady and "turbulent" in nature, showing signs of transverse wave phenomena. Denisov and Troshin arrived at the same conclusion using the smoke-record technique discovered nearly a century earlier by Mach and Sommer (1877). After eighty years of detonation research, the true universal cellular character of the wave was finally revealed.

The smoke records shown in Figure 1 illustrate the cellular mechanism. Such records can be obtained by applying a thin layer of carbon soot, either from a richly burning kerosene lamp or a piece of smoldering wood, to a sheet of mylar, steel or glass. The record on the top (Figure 1a) was "written" by a wave propagating parallel to the sheet, while that on the bottom (Figure 1b) is due to normal reflection of a wave from the end wall of a tube. Figure 2 shows a sequence of laser Schlieren photographs of a detonation propagating in a rectangular tube. One of the windows of the test section was coated with soot prior to the experiment in order to illustrate the nature of the writing process. The boundary of each cell is a history of the trajectories of triple points associated with the detonation front.

The details of the triple-shock configuration are apparent from the interferogram in Figure 3. An explanatory diagram appears at the top left of the figure. With the triple point denoted by A, line segments AI and AM represent the incident shock and Mach stem, respectively, while AB is the reflected shock. A second triple point, labelled B, is the centre of yet another three-shock configuration. Collectively, the pair of triple points

and associated shock waves is referred to as a double Mach reflection. In the case of marginal detonations, the second triple point may be absent. The reflected shock complex ABCDE is generally called a "transverse wave" due to its direction of propagation being more or less normal to that of the overall front. It propagates with a velocity very near the sonic velocity in the burned gases. The zone of heat release, denoted by hatched lines in the schematic diagram, trails the strong Mach stem quite closely but lags behind the weaker incident shock due to the lower post-shock temperature and thus longer induction period. The fact that the reflected shock complex ABC propagates through unburned gas which has already been compressed by the incident shock is responsible for the zone of heat release following the transverse shock quite closely. The dotted lines represent slip planes or shear discontinuities associated with the three-shock configuration. It is thought that the high shear across these discontinuities is responsible for eroding the soot from the smoked plates (Crooker, 1969), although the exact mechanism of "soot writing" is not well understood.

Figure 4 emphasizes the cyclic nature of the phenomenon. Starting at the apex of a cell, denoted by A, the shock wavelet is highly overdriven, propagating at about 1.6 times the one-dimensional equilibrium velocity  $V_{C-J}$ . Throughout the first half of the cell (i.e., from A to BC), the wavelet serves as a Mach stem to a pair of incident shocks in the neighbouring cells. However, it becomes the incident shock throughout the second half of the cell (i.e., from BC to D) for the more recently generated Mach stems in the adjacent cells. Toward the end of the cell, the wavelet velocity decays to about seventy percent of the C-J value just before approaching transverse waves collide. It is thought that this collision, perhaps in combination with an explosive recoupling of the reaction zone and shock wavelet near the end of the cell, gives rise to a rejuvenated overdriven Mach stem which begins another cycle. Hence, propagation of detonation is characterized by a cyclic, self-sustained cellular structure, with the heat release from chemical reaction furnishing the driving energy. Dimensions of the cell to which reference will be made throughout this thesis include the cell length  $L_c$  and the cell width  $\lambda$ , denoted by AD and BC in the figure, respectively. Note that  $\lambda$  is the maximum spacing achieved by

pairs of transverse shocks and is therefore often referred to as the (maximum) "transverse wave spacing".

#### The Effort to Understand the Intricacies of the Cellular Front

A great deal of work has been done to elucidate the details of the cell dynamics. For example, the flow field associated with the triple-point configuration has been analyzed in shock matching calculations (Oppenheim et al., 1970). Other computations to determine the flow conditions before and after a transverse wave collision have been carried out assuming a knowledge of the entrance and exit angles at the end and beginning of adjacent cells (Strehlow and Biller, 1969; Oppenheim et al., 1970; Strehlow et al., 1972). The variation of wavelet velocity throughout the cell has also been a subject of intense investigation (Steel and Oppenheim, 1966; Lundstrom and Oppenheim, 1969; Takai et al., 1974; Libouton et al., 1981), while efforts to model the observed results using conventional blast-wave theory have been ongoing (Lundstrom and Oppenheim, 1969; Edwards et al., 1970; Urtiew, 1976). Experimentally, Thomas and Edwards (1983) have attempted to simulate the cell kinematics by using cylindrical reactive blast waves in a diverging two-dimensional sector.

In addition to the cell dynamics, the measurement and correlation of cell sizes has commanded the attention of several investigators. Strehlow and Engel (1969) were the first to report numerous cell size data for low-pressure mixtures of  $H_2$ ,  $C_2H_2$ ,  $C_2H_4$  and  $CH_4$  with oxygen, and to correlate the cell dimensions with the calculated one-dimensional induction and recombination times. A similar study was carried out by Libouton and Van Tiggelen (1976) on the  $CO-H_2-O_2-Ar$  system using the chain-branching inhibitor  $CF_3Br$  and variable initial pressure to alter the mixture induction time. More recently, Lee et al. (1981), Westbrook (1982) and Westbrook with Urtiew (1982) attempted similar correlations between the cell size and the induction time. However, rather than employing an overall reaction rate as had been done by Strehlow and Engel, Westbrook utilizes a complex multistep reaction scheme to calculate induction times. Edwards et al. (1979, 1981b) and Knystautas et al. (1982) have recently measured cell sizes for a variety

of fuel-oxygen mixtures at subatmospheric initial pressures. Bull et al. (1982), Guirao et al. (1982), Knystautas et al. (1983) and Moen et al. (1983) have reported cell sizes for the less sensitive fuel-air mixtures at atmospheric initial pressure. The regularity of the cellular structure has been studied by Strehlow (1968, 1969), who classified it in one of four categories ranging from excellent to irregular, and by Libouton and van Tiggelen (1976). Takai et al. (1974) have suggested that chemical species which interfere with the chain reaction processes may be responsible for irregular structure. Along theoretical lines, attempts have also been made to predict the transverse wave spacing (Strehlow, 1970; Barthel, 1972, 1974; Erpenbeck, 1969; Vasiliev and Nikolaev, 1978; Ul'yanitskii, 1980), while the nature of transverse waves has been studied in detailed numerical simulations (e.g., Taki and Fujiwara, 1981; Oran et al., 1981).

The birth and reproduction of cells is a subject which has been studied to a lesser extent. Strehlow with Cohen (1962) and with Liaugminas, Watson and Eymen (1967) have investigated the evolution of structure following reflection of a shock wave from the closed end of a tube containing combustible mixture. Lee, Soloukhin and Oppenheim (1969) have shown that new transverse waves are generated at a rate required to maintain a constant spacing in successfully propagating cylindrical detonations, whereas no new waves are produced in the case of failing detonations. Gordeev (1976) has studied the influence of strong perturbations on cell reproduction and has proposed that disturbances such as sudden transitions from one gas to another, or rarefaction waves originating at openings in the tube wall, can act to upset the three-shock balance, causing it to split into two or more new three-shock complexes.

#### The "Hydrodynamic Thickness" of the Detonation Front

From the foregoing brief review, it is apparent that a real detonation has a three-dimensional and nonsteady structure very unlike that proposed by Zeldovich, von Neumann and Döring. This structure is characterized by a cell length over which successive chemical-gasdynamic cycles occur. Therefore, it would seem reasonable that the controlling length might be on the

order of the cell length. However, it has been noted recently that the sonic plane, which prevents the rarefaction to the rear of the wave from overtaking it, trails the shock front by much more than a cell length, giving rise to speculation that another phenomenon may control the effective thickness of the wave. Edwards and associates (1976b) have suggested that the gasdynamic flow structure aft of the frontal shock requires a finite time to equilibrate. These authors have found, by examining pressure-time signatures from oxyacetylene and oxyhydrogen detonations, that the transverse shocks dissipate their oscillation energy some 2 to 4 cell lengths behind the leading shock. They concluded that this might be one mechanism accounting for the downstream displacement of the sonic surface and, consequently, a "hydrodynamic thickness" larger than the cell length. Related experiments have been performed by Vasiliev et al. (1972), who photographed detonations in cellophane tubes and estimated the sonic surface to be located a minimum of 3.6 cell lengths behind the shock front. They subsequently confirmed this result in a more direct manner by photographing the bow shock caused by the passage of a detonation wave over a thin plate mounted perpendicularly to the oncoming flow. In the case of steady flow, such a bow shock is detached if the oncoming flow is supersonic. It was postulated that the sonic plane could therefore be identified by determining the location at which the bow shock detached itself from the plate. Over a range of initial pressures for a variety of gases, it was found that the sonic plane could be located as far back as 3 cell lengths when the tube diameter was large in comparison with the cell size (i.e., when wall effects did not play a role). The relative importance of the cell length and the hydrodynamic thickness in the behavior of detonation has yet to be resolved.

### 1.2.3 The Formation of Detonation

#### Two Modes of Initiation

There exist two basic means of establishing or "initiating" a detonation wave. The first of these is a slow mode where detonation evolves from an accelerating flame. Interactions between pressure waves and the

flame, as well as turbulence, are the principle acceleration mechanisms which lead to the onset of detonation. This mode is usually referred to as transition from deflagration to detonation or "self initiation" since the ignition source does not play a role in the transition process. Mallard and Le Chatelier (1883) were the first to obtain streak photographs of transition to detonation, while extensive studies involving the measurement of the predetonation distance were carried out by Le Chatelier (1900), Dixon et al. (1903) and Lafitte (1923, 1924). Shchelkin (1940) was the first to demonstrate that this distance could be substantially reduced through the generation of turbulence. In fact, the predetonation distance depends on a vast array of parameters, including the tube dimensions, the geometry and wall roughness, the nature, strength and location of the igniter, the boundary conditions at the ends of the tube, the flame speed, the heat of combustion and the sound speed of the mixture. More recently, the transition of a hot turbulent gas jet to spherical detonation has been studied by Knystautas et al. (1978). The present thesis will not be concerned with these aspects of detonation. The interested reader is directed to the reviews by Lee (1977) and Lee with Moen (1980).

The other mode of initiation is a fast mode where the detonation forms nearly instantaneously in the vicinity of either a powerful igniter or a violent chemical reaction. The source must be capable of generating a strong shock which is sustained for a long enough period so that chemical energy release can become coupled with the shock. Since the blast wave is responsible for bringing the mixture to a state which promotes the onset of detonation, this mode is often referred to as "blast" or "direct" initiation. The spark Schlieren photographs shown in Figure 5 [from Bach et al. (1969)] illustrate the phenomenon. Three regimes of propagation are generally observed. Below a certain threshold value of igniter energy, it is found that the blast wave produced by the igniter progressively separates from the reaction zone. This regime is termed the "subcritical" energy regime (Figure 5a). The blast wave eventually decays to an acoustic wave, while the subsequent propagation of the reaction front is identical to that of a flame. In the "supercritical" energy regime (Figure 5b), the igniter energy exceeds some threshold value. The blast and reaction zone are

coupled in the form of an overdriven multiheaded detonation which expands outward from the source and asymptotically decays to the C-J state. The "critical" energy regime (Figure 5c) is characterized by a blast wave and reaction zone which are initially coupled but which separate with increasing distance from the igniter. The decoupling process terminates as the chemical energy released through combustion begins to play a significant role in the blast motion. At this point, the shock wave and reaction zone propagate as a coupled complex at a constant velocity near  $0.6V_{C-J}$  during a so-called "quasi steady period". This period ends abruptly with the formation of localized explosion "bubbles" which lead to a rapid increase in the front velocity toward the C-J value.

The dip in velocity to a value well below  $V_{C-J}$  has been observed by several experimenters (e.g., Brossard et al., 1972; Atkinson et al., 1980). The quasi steady period has been studied by Edwards et al. (1978). Ul'yanitskii (1980) has used the term "flashing" to describe the explosive reignition and catch-up phenomenon. In a study by Edwards et al. (1981c) involving the initiation of detonation by planar shock waves, it was demonstrated that the onset of detonation may be related to the time coherent release of energy by particles entering the shock at different times, causing the wave to accelerate. The role of colliding transverse waves in the reinitiation process has been queried by Bull et al. (1979b) in their study of sympathetic initiation. In those tests, a shock from a "donor" detonation was transmitted across an air gap to an "acceptor" volume of detonable mixture. Elsworth et al. (1983) have proposed that a narrow range of fuel concentration exists (for a given spherical initiation energy) over which reestablishment of the front is characterized by a cyclic "galloping" phenomenon rather than by a monotonic acceleration of the front toward the C-J velocity. A similar observation, noted earlier by Bull et al. (1978), was explained in terms of the reaction zone repeatedly attempting to couple with the shock front. The recent experiments in tubes by Donato (1982) show that galloping can be sustained over very long distances.



Early Studies - Initiation of Detonation in Fuel-Oxygen Mixtures

Many of the early studies on direct initiation focused on the measurement of the critical energy for various fuel-oxygen mixtures (Lafitte, 1923; Manson and Ferrié, 1953; Zeldovich et al., 1956; Carlson, 1973). Litchfield et al. (1962), for example, reported minimum energies for mixtures of hydrogen, ethylene or propane with oxygen at various initial pressures, employing both spark and exploding wire ignition. Apart from finding that a well defined stored capacitor energy existed for initiation of detonation in a given fuel-oxygen mixture, it was observed that less stored energy was required in the case of exploding wire ignition, suggesting that the igniter characteristics play an important role in the process. One such characteristic, the igniter geometry, has been investigated in some detail by Matsui and Lee (1976) in their study of initiation in low-pressure oxy-acetylene mixtures. It was found that the critical energy for spark ignition depends on both the electrode spacing and the physical configuration of the igniter. For large electrode spacings, it was observed that the energy per unit length of spark gap approached a constant value indicating that, although the detonation eventually becomes spherical, it is first formed as a cylindrical wave. There also existed a range of electrode spacings over which the critical energy per unit length of spark gap increased linearly with decreasing spark length, thus giving a constant total spark energy. It was concluded that this regime corresponds to spherical initiation of detonation since, in spherical geometry, the critical energy should be independent of the spark length. Ramamurthi (1976) has proposed that the geometry of initiation can be established by comparing the spherical explosion length associated with the source energy (i.e., a length scale which characterizes the blast decay) to the characteristic dimension of the igniter. For an explosion length much larger than the characteristic length of the igniter, initiation is spherical since the onset of detonation occurs far from the igniter (i.e., the igniter is effectively a point source). However, for an explosion length smaller than the characteristic igniter dimension, the igniter configuration will dictate whether initiation corresponds to planar or cylindrical geometry.

The critical initiation energy has also been found to depend on the energy-time characteristics of the source for a specified igniter geometry. Bach et al. (1971) have carried out an investigation on direct initiation of low-pressure oxyacetylene mixtures and found that the critical initiation energy for a given mixture can vary by as much as three orders of magnitude, depending on the time history of the energy deposition. Lee et al. (1974) and Knystautas with Lee (1976) have conducted studies to clarify the dependence of the critical initiation energy on the energy-time characteristics of the source. These studies, which employed spark ignition, varied the R-L-C parameters of the discharge circuit to alter the energy-time profile. The spark energy was deduced from the simultaneous measurement of the discharge current and the voltage drop across the spark. The results indicated that only the energy released before the igniter achieves maximum power is important in the initiation process. The discharge frequency was also varied in order to determine the dependence of the useful spark energy (i.e., the energy released up to the peak power condition) on the time taken to reach peak power. These experiments showed that the critical energy decreases with the duration of energy release until a certain duration is reached, below which more rapid deposition of the energy does not alter the minimum required. Therefore, a limiting value of critical energy is obtained as the source power tends to infinity. Abouseif and Toong (1982), as well as Kailasanath and Oran (1983), have investigated the correlation between the igniter's energy and power using a simple theoretical model based on a constant-velocity piston. U'yanitskii (1979) has developed a closed model for direct initiation and has studied the dependence of the critical energy on the space-time characteristics of the source.

#### More Recent Work - Initiation of Detonation in Fuel-Air Mixtures

For practical reasons, the critical energy for direct initiation of detonation in fuel-air mixtures, rather than fuel-oxygen mixtures, has commanded much attention over the last couple of decades since fuel-air mixtures arise in accidental situations. Owing to the lower detonation sensitivity of fuel-air mixtures, spark or exploding wire ignition cannot

generally be used to determine the critical energy for initiation. Manson and Ferrié (1953), for example, were successful in initiating acetylene-oxygen detonation using a spark, but could not initiate any acetylene-air detonation with the same system. In general, more powerful igniters are required to initiate detonations in fuel-air mixtures. In experiments to measure the critical initiation energy, high explosives are often used for this purpose. Such tests are usually conducted in the field because of the large volumes of explosive mixture involved (a few liters up to tens of cubic meters) and the significant amounts of solid explosive employed (a few grams up to tens of kilograms). Large volumes of mixture are required in order to ensure that the detonation wave is self-supported far from the source. Data on the hydrogen-air system has been obtained by Cassut (1961) and by Atkinson et al. (1980), and on the acetylene-air system by Freiwald and Koch (1963) and by Kogarko et al. (1965). Initiation energies for ethylene-air mixtures have also been reported by several investigators (Hikita et al., 1975; Pfortner, 1977; Bull et al., 1978). Some very large experiments involving methane-air mixtures contained in rectilinear plastic bags of 2.4 m square cross section were carried out by Benedick (1979). Critical energies for liquid fuel spray-air mixtures have been determined at Eglin Air Force Base (Vanta et al., 1973; Parsons et al., 1973). An excellent review of available high-explosive initiation energy data has been compiled by Bull (1979).

The question of igniter geometry appears to be equally valid for high-explosive initiation as evidenced by the results of Benedick (1979). This author was apparently successful in initiating a stoichiometric methane-air detonation with only 4 kg of explosive, whereas estimates of the critical energy for spherical initiation are much larger [e.g., Bull et al. (1976) predict 22 kg]. It is possible that the sheets of explosive mounted on a plywood backing produced a blast wave which corresponded more to planar rather than to spherical initiation. The container walls (thin plastic material) may also have influenced the initiation process.

Theoretical Efforts to Predict the Initiation Energy

Along theoretical lines, a criterion linking the critical energy to the chemical properties of the mixture was proposed as early as 1956 by Zeldovich et al. Their hypothesis was based on the fact that the blast wave generated by the source decays rapidly. Thus, in order for the chemical energy released in the wake of the blast to sustain the shock, a sufficient time must be available for the fluid particles to release their chemical energy after being processed by the shock. Choosing the induction period as the representative chemical kinetic time, Zeldovich postulated that, for successful initiation, the time required for the blast wave to decay to the C-J Mach number must be equal to the mixture induction time. Based on this criterion, it was demonstrated that the critical energy was proportional to the cube of the induction time for spherical initiation. Lee et al. (1966) attempted to use the Zeldovich criterion for the quantitative prediction of critical energies by using the strong blast theory of Taylor (1950) to determine the blast-wave trajectory. However, when the induction times based on properties behind a C-J shock were substituted into the criterion, the calculated energies were seen to be smaller than the experimentally measured ones by about three orders of magnitude. Agreement improved to within one order of magnitude when the experimentally determined wave thicknesses (deduced from radiation measurements) were used in place of the calculated induction-zone lengths. Both Edwards et al. (1976a) and Sichel (1977) have also proposed relations for obtaining the critical energies. In the expression given by the former authors, experimental values for the wave thickness are again required. In the proposal of Sichel, an experimental value for the critical energy is required at a reference mixture composition before the critical energies can be evaluated at other compositions.

The theories described above are based on a nonreacting blast-wave model. An attempt to include the influence of chemical energy release on the blast-wave motion was made by Bach et al. (1971) and later reviewed by Lee (1972) and by Fry and Nicholls (1974). The model was quite successful in describing the three energy regimes (Figure 5) identified in an earlier study (Bach et al., 1969). In the critical energy regime, the calculations

gave velocities below the C-J value prior to the wave accelerating toward the theoretical velocity. Such behavior has been observed by many experimenters (e.g., Brossard et al., 1972). Furthermore, instabilities were predicted to occur during the approach to steady velocity. Such instabilities have also been seen in the numerical calculations of others (Kyong, 1972; Levin and Markov, 1976) and are consistent with the observations from recent initiation experiments (Bull et al., 1978; Elsworth et al., 1983). For parameters typical of acetylene-oxygen mixtures, the calculations of Bach et al. showed that acceleration of the sub C-J wave begins when the shock front achieves a radius of 8.2 induction-zone distances, suggesting the existence of some minimum volume prerequisite for the onset of self-sustained detonation.

A more recent theory for direct initiation (Lee and Ramamurthi, 1976), which is based on the concept of such a minimum volume requirement, is formulated around an analogy between the critical volume for detonation and the minimum size of a flame kernel. In flame ignition, the source generates a volume of hot gas. Successful ignition requires the flame kernel to be of a minimum size so that the rate at which heat is generated through chemical reaction exceeds the rate of heat loss from the volume. In the case of detonation initiation, the source must be capable of producing a strong enough blast wave so that the blast radius exceeds some minimum size by the time the wave decays to some critical Mach number. It is postulated that the blast motion will be dominated by chemical energy release, rather than by the source, if the detonation "kernel" is larger than the critical size. If instead the kernel is too small, the energy released through combustion plays a minimal role in the blast motion and the wave will continue to decay, resulting in a deflagration. The critical radius selected is that for which the heat energy liberated through combustion equals the source energy. The critical Mach number chosen is that which gives a post-shock temperature corresponding to the auto-ignition temperature of the mixture. This theory has been moderately successful in the prediction of the critical energies. Its weakness stems mainly from the difficulty in the choice of the critical Mach number.

#### 1.2.4 The Transmission of Detonation

##### The Critical Tube Diameter for Transmission to an Unconfined Region

One of the problems associated with initiation energy measurements is that the results depend strongly on the source geometry and energy-time profile. This has led to difficulties in the comparison of data and in the correlation of data with prediction. One means of initiation which does not suffer these disadvantages involves the use of a linear detonation tube. Experimentally, it is observed that a planar detonation wave in a tube of circular cross section is capable of initiating a spherical wave upon emerging from the tube into an unconfined space containing the same mixture, provided the tube exceeds some minimum diameter. Although transmission of this type in fuel-oxygen and fuel-air mixtures was studied earlier by Zeldovich et al. (1956), it was Freiwald and Koch (1963) who first suggested the linear tube as an ignition source. As long as the tube is long enough so that an equilibrium wave exists prior to exiting into an unconfined region, it should be possible for any two experimenters to arrive at the same "critical tube diameter" for a given mixture or, equivalently, to determine the same critical mixture composition for a given diameter of tube.

This suggestion paved the way for a new wave of investigations into the critical conditions required to initiate a spherical detonation. Matsui and Lee (1979) proposed that the critical tube diameter be used as an alternative to the critical initiation energy for assessing the relative sensitivity of explosive mixtures to detonation. These authors carried out a systematic study involving the measurement of critical diameters for the common fuels (i.e.,  $\text{CH}_4$ ,  $\text{C}_2\text{H}_2$ ,  $\text{C}_2\text{H}_4$ ,  $\text{C}_2\text{H}_6$ ,  $\text{C}_3\text{H}_6$ ,  $\text{C}_3\text{H}_8$  and  $\text{H}_2$ ) with oxygen over a limited range of fuel concentration and with varying degrees of nitrogen dilution. Since the available tubes covered a narrow range of diameters ( $6.5 \text{ mm} < D < 53 \text{ mm}$ ), experiments had to be performed at above and below atmospheric pressure (in order to accommodate the available tubes). An extrapolation was then made to estimate the critical diameters at atmos-

pheric pressure. To estimate the critical diameters for fuel-air compositions, experiments were conducted with fuel-oxygen mixtures at low degrees of nitrogen dilution. Curve fits to these results were then extrapolated to the dilution corresponding to fuel-air. For the less sensitive fuels, such as  $\text{CH}_4$ ,  $\text{C}_2\text{H}_6$  and  $\text{C}_3\text{H}_8$ , extrapolation over two orders of magnitude was necessary. Knystautas et al. (1982) have minimized the degree of extrapolation by undertaking a similar study employing tubes up to 200 mm in diameter. Their investigation involved  $\text{C}_4\text{H}_{10}$  and MAPP (a common multicomponent welding gas) in addition to the fuels used by Matsui and Lee. Although higher degrees of nitrogen dilution were possible, the extrapolation to fuel-air composition was still significant for the less sensitive fuels.

Since fuel-air mixtures are of most interest insofar as accidental explosions are concerned, a clear need existed to carry out such tests on a larger scale. This need has been the motivating force behind the recent large-scale tests carried out at Raufoss, Norway (Knystautas et al., 1981; Rinnan et al., 1982; Jenssen, 1983) employing acetylene-air and ethylene-air mixtures in tubes up to 1.36 m in diameter. A similar effort by Moen et al. (1983) involving  $\text{C}_2\text{H}_2$ -,  $\text{C}_2\text{H}_4$ -,  $\text{C}_2\text{H}_6$ - and  $\text{C}_3\text{H}_8$ -air mixtures in tubes up to 1.83 m in diameter has been undertaken at DRES. As well, Guirao et al. (1982) at Sandia have obtained critical tube diameter data on the hydrogen-air system for diameters up to 1.21 m. The tests at Raufoss, and more recently at McGill (Liu et al., 1984), also demonstrated the equivalence between the critical tube diameter and the critical diameter for transmission through a circular orifice hole. Since the rarefaction to the rear of a shock wave diffracting from a tube is very different from that of a shock transmitting through an orifice hole, reinitiation must depend on conditions in the neighbourhood of the shock front. This implies the existence of a wave thickness which is rather small in comparison with the shock radius.

A theoretical model linking the critical tube diameter and the critical initiation energy was proposed by Lee and Matsui (1977). The model assumes that the planar detonation wave emerging from the tube delivers energy to

the gas in the outside volume via compression work done by the interface separating the combustion products and the gas originally in the larger volume. Under critical conditions, it has been observed experimentally that spherical detonation is formed near the tube axis at about one diameter from the tube exit. This observation suggests that only the work done by the wave up to this point in time is important in the initiation process. Assuming the only meaningful work (i.e., work which contributes to the initiation process) is done by that portion of the wave unaffected by the expansion moving radially inward, a simple integration shows that the critical energy is proportional to the cube of the tube diameter. Urtiew and Tarver (1981) have modified the analysis, arguing that initiation must occur before the rarefaction wave converges on the tube axis. Their argument is based on the idea that a finite unattenuated detonation core must exist for initiation to be possible.

Mitrofanov and Soloukhin (1965) studied the transmission of detonation from a circular tube to an unconfined region in oxyacetylene mixtures and suggest that a link exists between the cellular structure and the critical tube diameter. Specifically, they propose that the critical diameter  $D_c$  is related to the cell width  $\lambda$  characteristic of the mixture by the relation  $D_c \cong 13\lambda$ . The recent study of Knystautas et al. (1982), involving a wide variety of fuel-oxygen and fuel-nitrogen-oxygen mixtures covering a range of initial pressures, suggests that the  $13\lambda$  correlation may be a universal feature of planar-to-spherical transmission in gaseous media. Ungut et al. (1983) have found this to be the case for the  $C_2H_6-O_2-N_2$  and  $C_3H_8-O_2-N_2$  systems as well. The large-scale test results of Guirao et al. (1982) indicate that the correlation is likely valid for hydrogen-air mixtures. The data of Moen et al. (1983), also obtained in large-scale tests, indicate that the correlation may be valid for other fuel-air mixtures. However, some doubt exists due to the difficulty in the interpretation of the cellular structure appropriate to fuel-air detonations. Liu et al. (1984) have studied transmission through orifices of square, triangular, elliptical and rectangular shape and found the  $13\lambda$  correlation to hold if an effective diameter (equal to the mean of the longest and shortest dimensions of the orifice) is employed.



### The Critical Channel width for Transmission to an Unconfined Region

Mitrofanov and Soloukhin (1965) further propose that, for transmission from a narrow two-dimensional channel to an unconfined region,  $w_c \cong 10\lambda$  where  $w$  is the channel width. This geometry corresponds to the initiation of a cylindrical rather than a spherical detonation. Reestablishment of the wave in planar-to-cylindrical transmission has also been studied by Soloukhin and Kagland (1969), by Edwards et al. (1979, 1981b) and by Subbotin and Mitrofanov (1980). Edwards and colleagues have provided evidence that the  $10\lambda$  correlation is true for low-pressure oxyhydrogen mixtures as well. However, preliminary results using oxygen with ethane, propane, methane or acetone place  $w_c$  between  $14\lambda$  and  $18\lambda$ , depending on the system. The regularity of the cellular structure is suggested as a factor which may account for the difference. Results from the recent laboratory experiments of Liu et al. (1984) and the field tests of Benedick et al. (1983) support the  $10\lambda$  correlation for channels having an aspect ratio  $L/W$  near unity, but show that  $w_c$  tends to about  $3\lambda$  as  $L/W$  becomes large.

Theoretical models linking the dynamics of the diffracting shock to the chemical kinetics of the mixture have been advanced by Dremin and Trofinov (1965), with improvements by Enig and Petrone (1970), and by Edwards et al. (1979). These models recognize that reestablishment of detonation is via an explosive reinitiation in the vicinity of the head of the expansion following failure of the transverse waves. However, the theory of the latter authors appears to be more realistic in that it incorporates the chemical kinetic behavior in nonsteady flow by drawing from observations about the decaying wavelet in an individual detonation cell.

### Transmission Phenomena in Other Geometries

Apart from transmission from a tube or a channel to an unconfined region, more complex geometries have been studied. Bjerketvedt et al. (1981) investigated transmission through multiple orifice holes and perforated plates. Klug and Simpson (1982) studied transmission from a two-dimensional channel of constant width to one having a pair of diverging

walls. Detonations negotiating bends (Edwards et al., 1981a) and sharp corners (Lee and Lee, 1965) have also been studied. Martin and Lee (1982) looked at the problem of detonations transmitting through screens. Correlations linking the gasdynamic and the chemical aspects of transmission in these geometries have either not been attempted or have been unsuccessful. One class of transmission problem for which some degree of success has been experienced with correlations is that involving transmission to an unconfined region from either a channel or a tube in which a central blockage has been placed in the exit plane (Bjerketvedt et al., 1984; Sulmistras et al., 1984). The blockage area ratio appears to be the relevant parameter in this type of problem.

### 1.2.5 The Detonability Limits and Velocity Deficits

#### Limits and Near Limit Phenomena

A very important issue with respect to accidental explosions is whether a combustible mixture will detonate and, if so, over what range of mixture composition is detonation possible. These questions are of particular importance because the concentration gradients are very small at the edge of a fuel-air cloud arising from the accidental release of combustible material. Thus, a slight change in the lean detonability limit can result in a significant increase in the size of the detonable volume. To date, no quantitative theory exists which is capable of successfully predicting the detonability limits. However, several attempts have been made to formulate a general theory. Belles (1959), for example, used the criterion of a precursor shock just strong enough to ignite the mixture. He then determined whether the heat released through combustion was sufficient to support a shock of that strength. The prediction for oxyhydrogen mixtures was seen to differ from the experimental results of Lafitte (1938) by about 15% in concentration of the minor reactant but became worse when the mixture was diluted with nitrogen, argon or helium. Patch (1961) found that correlations were more successful when a constant temperature criterion was used. By choosing a vibrationally unrelaxed post-shock temperature of 1314 K, the average error in the predicted limiting concentration was about 13%. Nolan

(1973) used the criterion that the energy required to establish a C-J shock must equal the chemical energy release of the mixture at the limit. Fair agreement between predicted and observed limiting concentrations was obtained for a variety of lean mixtures. Agreement was not as good for fuel-rich mixtures.

The traditional method for determining the detonability limits has been to carry out experiments with mixtures contained in tubes. Such studies have been undertaken by Zeldovich and Kompaneets (1960), Lewis and von Elbe (1961), Shchelkin and Troshin (1965), Borisov and Loban (1977), Wolanski et al. (1981) and Donato (1982). However, the results obtained can vary markedly, depending on the tube diameter and length, and on the nature and magnitude of the initiation source. Kogarko and Zeldovich (1948), for example, showed that the lower limit for hydrogen-air mixtures dropped from 19.6% to 15%, while the upper limit increased from 58.8% to 63.5% when the tube diameter was increased from the 10 - 20 mm range to 305 mm. Similarly, Rivan and Sokolik (1936) found that the limiting diameter increased as the mixture initial pressure (and hence, mixture sensitivity) decreased. Wagner (1963) also showed the existence of narrowing limits with decreasing tube diameter. It was Manson and Guénoche (1957) who first formally pointed out that the specification of limits must be accompanied by an associated tube diameter. In their words, "to determine the lower and upper limits of detonation,  $C_i$  and  $C_s$ , means that we are really determining the limiting diameters for mixtures of concentration  $C_i$  and  $C_s$ ".

As the limits for a given tube are approached, several interesting phenomena are possible. The most common of these is the single-head spinning detonation which occurs when the cell size characteristic of the mixture is approximately equal to the tube diameter (Campbell and Woodhead, 1927; Bone et al., 1930, 1935). Experimentally, owing to a strong coupling between the walls of the tube and the chemical energy release, single-head spin can persist as the mixture is made less and less sensitive. However, it has been found that such detonations are delicate and become unstable and fail if subjected to boundary induced perturbations (Donato, 1982). Another type of instability which has been observed near the detonability limits

is longitudinal in nature and is characterized by large oscillations in velocity of the front. These were first reported by Mooradian and Gordon (1951) and studied afterward by others (Saint-Cloud et al., 1972; Edwards and Morgan, 1977). They were given the name "galloping" detonations by Duff (1963). Edwards et al. (1974) have obtained detailed velocity data for such waves using microwave interferometric techniques, while Brochet (1966) has studied the mechanism using streak photography. Moen et al. (1981) observed from pressure records that the phenomenon begins with an initial decoupling between the reaction zone and the shock wave, followed by an amplification of pressure oscillations in the reaction zone. These intensify and lead to an explosive recoupling of the reaction zone with the shock. The result is an overdriven wave which subsequently decays to begin another cycle.

Several attempts have been made to define the detonability limits in terms of near limit phenomena. Manson et al. (1963) devised a criterion based on the velocity fluctuations of the wave in different diameter tubes. They linked the amplitude of the velocity fluctuations to the detonation Mach number but were forced to select some arbitrary amplitude of fluctuation in order to define the "stable" regime. Dove and Wagner (1962) proposed that the appearance of spin be used as a criterion for the limit. However, it was Moen et al. (1981) and Donato (1982) who established that the onset of spin in a given tube corresponds to a unique mixture composition.

#### Velocity Deficits

Hand in hand with a narrowing of the detonability limits has been the observation of detonation velocity deficits. By "deficit" we mean the difference between the theoretical and observed velocities. These have been measured in smooth round tubes covering a large range of diameters and mixture compositions (Mooradian and Gordon, 1951; Kistiakowsky et al., 1952a, 1952b; Manson and Guénoche, 1957; Edwards et al., 1963; Brochet, 1966; Pujol, 1968; Renault, 1972). Similar investigations have been carried out using smooth tubes of rectangular cross section (Edwards et al., 1963;

Boisleve, 1970; Renault, 1972). Shchelkin (1947) and Kistiakowsky et al. (1952b) have also measured velocity deficits in tubes whose walls have been roughened by the installation of helical spirals into the tube. It has been customary for experimenters to plot the velocity against the reciprocal of the characteristic transverse dimension of the tube and to extrapolate to infinite tube size in order to estimate the velocity in an unconfined space. However, the French in particular suggest that the velocity obtained by this method is overpredicted [see Desbordes and Manson (1981), for example].

Several theoretical efforts have been undertaken to quantify the dependence of the deficit on both the properties of the mixture and the characteristics of the tube. Zeldovich (1940) proposed that the drag exerted by the wall on the fluid between the shock and the C-J plane is responsible for the deficit, but this model underpredicted the deficit considerably. Fay (1959) argued that distributing the losses uniformly throughout planes normal to the axis was not physically correct and thus accounted for the lack of success of the Zeldovich model. Instead, Fay proposed that the wall effects were confined to a thin (boundary) layer and could only influence the bulk of the flow through pressure changes propagated throughout the subsonic reaction zone; that is, via a "stream line divergence" or displacement effect between the shock and the C-J plane. A quasi one-dimensional "nozzle" type analysis revealed that the velocity deficit was proportional to the displacement thickness of the boundary layer and inversely proportional to the tube diameter. Tsugé (1971) and Dove et al. (1974), who also modelled the influence of the tube on the propagation by quasi one-dimensional schemes, arrived at similar conclusions. They were also successful in predicting the existence of a tube diameter below which propagation is not possible; i.e., a "limiting" or "quenching" diameter. Rybanin (1969) has modelled the same phenomenon for tubes having rough walls. Williams (1976) estimated the quenching diameter by postulating that the post-shock flow could only accelerate to sonic conditions if the Mach number decrease due to area expansion is outweighed by the Mach number increase due to heat release.

Influence of Confinement - Early Studies Related to High Explosives

The limiting cylindrical diameter is a parameter of key importance in the design of high-explosive cylindrical charges. The first comprehensive theoretical effort was carried out by Jones (1947). Like much of the early work in this area, his investigation centred around the fact that, while gaseous detonation in a rigid tube was thought to involve essentially one-dimensional flow, there exists no practical means of preventing a certain degree of radial expansion in the case of solid explosives. Since it was known from experience that the detonation velocity increased with the initial density of the explosive, Jones reasoned that the lower density following radial expansion in the reaction zone of a detonating explosive should give rise to a measurable velocity deficit. Jones' intention was to calculate this deficit with a view to estimating the reaction-zone thickness from the experimentally measured deficits. His analysis employed both the Rankine-Hugoniot jump conditions across the shock and the conservation equations across a quasi one-dimensional stream tube reaction zone. The severity of the expansion was estimated by drawing an analogy between the post-shock reacting explosive and the expansion of a high-pressure, high-temperature free jet issuing into a vacuum. The analysis revealed the deficit to be proportional to the reaction-zone length and inversely proportional to the charge diameter. Owing to the lack of reliable chemical kinetic data for high explosives, absolute quantitative results were not obtainable. However, Jones was successful in demonstrating that the post-shock expansion could be reduced by the application of a heavy casing over the charge.

It was also reasoned by Jones that the only way in which all of the boundary conditions could be satisfied is if the detonation front was curved. Later, Eyring et al. (1949) treated this aspect of the problem formally. These authors computed the wave front shape in a cylindrical charge of specified diameter by modelling the front as a series of spherical detonation segments. The radius of curvature for each segment was selected so that the post-detonation velocity equalled the normal component of velocity of the oncoming flow. The inclination angle at the edge of the charge

was established by matching the flow direction and the pressure behind the detonation to the corresponding quantities behind the oblique shock in the inert boundary material. Wood and Kirkwood (1954) carried out an analysis of the same problem using a vector form of the Rankine-Hugoniot jump conditions and the conservation equations in the reaction zone. Instead of concerning themselves with the connection between the boundary conditions and the curvature of the front, these authors addressed the relation between the curvature and the velocity deficit. They were able to demonstrate that the deficit was proportional to the reaction-zone thickness and inversely proportional to the radius of curvature of the front. This result is consistent with that of Jones (1947) if the charge diameter and the radius of curvature of the front are proportional. It is likely this is the case, since a decrease in diameter leads to a more severe expansion for a given reaction-zone length which, in turn, must cause the front to assume a greater curvature (i.e., a smaller radius of curvature) in order for the deflected particles to satisfy the boundary conditions at the edge of the charge.

Much later, Sichel (1965) clarified the connection between the curvature, the charge diameter, the boundary conditions and the velocity deficit in proposing a hydrodynamic theory which employed the conservation equations in orthogonal curvilinear coordinates coincident with the curved shock surface. His analysis showed that the transverse and axial equations of motion could be decoupled if the reaction zone was thin in comparison with the radius of curvature of the front. It was further demonstrated that, locally, the equations describing the reaction-zone flow behind a curved shock are the same as for a one-dimensional stream tube with area increase and heat addition. The rate of area increase was shown to depend on only the local curvature and the density profile across the reaction zone.

Experimentally, most of the features of detonation phenomena described by the above analyses have been borne out. Cook (1958), for instance, confirmed the notion of a curved wave front in a charge. Some of the most enlightening experiments were conducted by Campbell et al. (1955). In one test series, it was found that a detonation wave in liquid nitromethane was

sustained when the explosive was contained by either brass tubes of 3 mm inside diameter and 1.6 mm wall thickness, or by Dural tubes of the same wall thickness but 4.8 mm in diameter. However, the detonation wave was seen to fail when the explosive was contained by glass tubes of less than 17 mm inside diameter. It was also found that, by lining the inside of a glass tube with a 2 mil thick layer of aluminum foil, the wave could be sustained in tubes of much smaller diameter.

Another interesting experiment performed by the same authors involved lining a glass tube with platinum foil. One section of the tube was lined with 1 mil thick foil, while the second and third sections were lined with 0.5 mil thick and 0.2 mil thick foil, respectively. Under these conditions, a detonation wave was seen to propagate successfully through the first two sections, but fail in the least confined third section. In all cases, the failure process originated at the boundary and proceeded inward to the charge axis. A similar study involving ammonium nitrate charges cased in aluminum, copper or steel was carried out more recently by Tarasenko (1974a). However, this author was concerned with the trajectory of the casing material for the purpose of evaluating the severity of the expansion on the reaction zone. The same author investigated the influence of an annular layer of water placed between a cylindrical charge and a coaxial metal casing (Tarasenko, 1974b). Two important qualitative conclusions were drawn from the latter tests. First, for a given explosive and charge diameter, there existed a limiting thickness of water, beyond which the metal casing was of no consequence. Second, as the explosive was made less sensitive (i.e., as the reaction zone was made longer), the limiting water layer thickness was seen to increase. These two observations suggested to the author that the limiting water layer thickness could be used to infer the reaction-zone length, but the idea was not pursued.

#### Influence of Confinement - The Extension to Gaseous Explosives

Although a general understanding of the influence of confinement on condensed-phase explosives had been gained by the end of the fifties, the details of the interaction between the wave and the container housing the



charge were not understood. This was due mainly to experimental efforts being hampered by the destructive power of explosives, while theoretical studies were stalled by the lack of knowledge about the equation of state and the thermodynamic properties appropriate to high-explosive materials. Consequently, some attention was directed toward the possibility of investigating a suitable analogous phenomenon. The idea of a solid boundary becoming compressible under the influence of the high detonation pressures and temperatures suggested that some insight into the problem might be gained by studying the behavior of gaseous detonation waves bounded by inert gases of various density. The first study of this type was undertaken by Sommers (1961) and Sommers with Morrison (1962) using explosive mixtures of hydrogen, methane, propane or ethane with oxygen. In their initial experiments, a jet of oxyhydrogen mixture was allowed to issue from a circular tube into surrounding quiescent air. It was found that the confinement imposed on the cylindrical column of combustible mixture by the higher density air was not sufficient for a detonation wave emerging from the tube to continue propagating in the column.

Undaunted by this attempt, a second experimental configuration was investigated; a narrow channel consisting of a metal bottom wall and a pair of parallel glass side walls. A jet of explosive mixture exiting a slot was used to establish a flow over the bottom wall. This flow was bounded on the top by a second parallel jet flow of inert boundary gas (air or helium). The result was a rectangular column of combustible mixture bounded on three sides by rigid confinement and on the top by a compressible medium. Mixing and diffusion were minimized by maintaining approximately equal velocity laminar jets. Schlieren photographs showed that a detonation wave emerging from the slot into the channel always became curved, with the curvature process beginning at the compressible boundary and proceeding toward the bottom wall. Furthermore, after propagating some distance, the front always achieved an equilibrium shape.

In an attempt to evaluate the confining ability of the boundary gas, these authors carried out a simple analysis. Ignoring the reaction-zone thickness, it was argued that for the correct flow configuration the

pressure and the direction of the gas leaving the detonation wave at C-J conditions must equal the corresponding quantities behind the oblique shock wave in the inert boundary gas. Assuming the "best" container for a charge to be the one which gives the highest pressure ratio across the oblique shock in the boundary gas, it was shown that the largest ratio of acoustic impedance ( $\rho c$  where  $\rho$  is the density and  $c$  is the sonic velocity) between the boundary gas and the explosive gas provided the most effective confinement. This criterion proved to be valid in explaining the hierarchy of confining materials reported earlier by Campbell et al. (1955) for nitromethane detonations.

Although Sommers and Morrison (1962) ignored the finite reaction-zone length in their analysis, it was nonetheless recognized that successful propagation in their second test configuration was the result of a lesser degree of expansion in the reaction zone, resulting from both a larger gas column size and the two-dimensional nature of the latter apparatus. A more comprehensive study in the same geometry, which attempted to take into account the finite reaction zone, was later carried out by Dabora and colleagues (1963, 1965). The test section used by these investigators was essentially the same as that employed by Sommers and Morrison except that the slot height was adjustable, thus allowing the charge size to be varied. Hydrogen-oxygen and methane-oxygen mixtures bounded by nitrogen, butane, helium or hydrogen were employed. Schlieren photography and ionization-gap probes were used to determine the success or the failure of propagation and to deduce velocity deficits in cases of sustained propagation. The theoretical model formulated by these authors was centred around the ZND concept of a detonation wave. That is, the wave was assumed to consist of a shock wave followed by a zone of heat release terminating at the C-J plane. The "stream tube" area increase over the reaction zone was determined by first calculating the deflection angle of the inert/explosive interface. A pseudo one-dimensional shock tube analogy was used for this purpose. The reaction-zone length employed was deduced by Fay (1959) based on the calculations of others (Kistiakowsky and Kydd, 1954). The velocity deficit resulting from this area increase was then computed using a slightly modified version of the "nozzle" model employed

by Fay in his study of the post-shock divergence resulting from the growth of viscous boundary layers in the wake of the frontal shock. Good agreement was found to exist between the predicted area increase/velocity deficit variation and that observed in the experiments. It was also found that the maximum velocity deficit was on the order of 10% for propagation in a rectangular channel bounded rigidly on three sides and by an inert gas on the fourth side. Attempts to predict the limits of detonability based on criteria such as those advanced by Belles (1959), Patch (1961) and Shchelkin (1959) were, for the most part, unsuccessful. However, the analysis did show that the confining ability of the inert boundary gas depended on the ratio of  $(\rho\gamma)^{\frac{1}{2}}$  in the inert gas to that in the explosive mixture ( $\rho$  is the density and  $\gamma$  is the ratio of specific heats). This quantity is closely related to the acoustic impedance ratio suggested by Sommers (1961) and Sommers with Morrison (1962) to be the important parameter.

Very little attention was paid to the inert boundary gas problem until many years later when Adams (1972, 1978), motivated by the earlier observations of Sommers (1961), Dabora (1963) and Lu (1968), conducted a study on the effect of low-density boundary gases on the propagation of detonation. These earlier authors had observed that the oblique shock in the inert gas became detached from and ran ahead of the front if the inert gas was of low enough density, resulting in detonations which propagated at about half the C-J velocity. It was proposed that the detached shock wave running ahead of the detonation was making it "believe" that it was confined by a gas of higher density. The work of Adams, however, indicated that the wave was quenched and simply propagating at a velocity equal to the sonic velocity in the boundary gas.

### 1.3 Objectives and Format of the Thesis

#### 1.3.1 A Brief Recap - Where We are Today

It is evident from the historical review in Section 1.2 that the formation and sustenance of detonation waves depend on an intimate competition

between the rates of post-shock gasdynamic expansion and heat release due to chemical reaction.

The gasdynamic expansion is a function of both the initial conditions (energy, energy-time characteristics and geometry of the source, etc.) and the boundary conditions (geometry, compressibility or motion of walls, boundary layer growth, etc.). Past studies have been reasonably successful in addressing these aspects of the phenomenon. In general, there exist two types of problems. The first class includes those in which the flow entering the frontal shock wave is globally steady as viewed by an observer moving with the shock. Problems of this type include propagation in a column of explosive mixture bounded by either an inert gas (Jones, 1947; Sommers and Morrison, 1962; Dabora, 1963; Vasiliev, 1980) or a yielding casing material (Jones, 1947; Vasiliev et al., 1972; Tarasenko, 1974a, 1974b). Even if the casing does not yield in the wake of the passing wave (i.e., propagation inside a rigid tube), expansion of the flow can still be brought about by the growth of viscous boundary layers at the edge of the column (Fay, 1959). The gasdynamic expansion in the above described cases is usually treated from a "stream line divergence" point of view.

The second class of problems is that in which the flow entering the front is not globally steady to an observer riding on the shock. Initiation and transmission problems in which the fronts diverge are two common examples. Analysis of such phenomena generally focuses on the shock motion rather than on the motion of the post-shock fluid particles. In the case of initiation problems, for example, the gasdynamic expansion can be characterized by the distance over which the initiating shock wave decays to some specified strength (Zeldovich et al., 1956; Lee and Ramamurthi, 1976). Other parameters which have been used in the analysis of detonation transmission include the local rate of growth of the detonation frontal area (i.e.,  $A^{-1}dA/dR$ ) or the local velocity gradient ( $dM/dR$ ) of the diffracted shock front (Edwards et al., 1979). **It is certainly not clear how the many different means of characterizing the gasdynamic expansion are inter-related. This is, no doubt, one of the reasons why a unified description of detonation behavior has not yet been proposed.**

The rate at which energy is liberated within the detonation front is a function of the chemical properties of the mixture for a specified post-shock thermodynamic history (i.e., for a given gasdynamic expansion). To date, the one-dimensional induction-zone length based on properties behind a C-J shock has generally been selected as the representative chemical kinetic length. However, when used in theoretical models, agreement between the prediction and experiment has been poor. Perhaps the best example of this is the Zeldovich (et al., 1956) criterion relating the critical energy for direct initiation in spherical geometry to the cube of the induction time. Quantitatively, this theory underpredicts the critical energy by orders of magnitude. **Clearly, the biggest stumbling block in the road to unifying the detonation field has been our inability to identify the controlling chemical kinetic length scale.** The reason for this is that the universal nature of the nonsteady, three-dimensional cellular front managed to evade scores of researchers until only twenty-five years ago. Up to that point in time, the only hint that the controlling chemical kinetic length in detonative propagation might be much larger than the induction-zone length was the observation of single-head spinning waves near the detonability limits in rigid tubes (e.g., Manson and Guénoche, 1957). Shortly after the revelation of universal cellular structure, Mitrofanov and Soloukhin (1965) proposed the  $13\lambda$  correlation linking the critical tube diameter to the cell width in oxyacetylene mixtures. More recently, Edwards et al. (1979) observed that reignition following diffraction of a planar detonation wave from a tube occurs at a fixed number of cell widths from the tube exit. These observations give rise to speculation that the controlling chemical kinetic length is closely tied to the cell size.

### 1.3.2 An Outline of the Present Undertaking

The contributions of the present thesis are based on a series of detailed experimental investigations focusing on both the critical conditions and the behavior of detonation waves under supercritical conditions. The intimate competition between the gasdynamic expansion and the chemical heat release under a variety of initial and boundary conditions is analyzed with particular emphasis on the cellular structure of the wave. These investi-

gations are described in Chapters 2 through 6. Chapter 2 deals with the critical conditions required for a planar wave emerging from a tube to continue propagating as either a diverging spherical or cylindrical wave. Chapter 3 addresses the planar-to-spherical transmission problem as well, but for explosive mixtures with relatively longer characteristic chemical kinetic times (i.e., fuel-air mixtures) in a large-scale field apparatus. The objective is to examine the universality of conclusions drawn from the laboratory study described in Chapter 2. The tests outlined in Chapter 4 involve long cylindrical gaseous charges in which the gasdynamic expansion imposed on the detonation wave is controlled by varying the density of the confining walls which are shed in the wake of the wave. A corresponding laboratory study described in Chapter 5 is similar, except that the gasdynamic expansion is regulated by varying the fraction of the boundary which is allowed to yield, more so than by varying the density of the yielding wall material. Particular attention is paid to the phenomenon of velocity deficits. Selected experiments on the direct initiation of ethylene-air mixtures using high-explosive charges are described in Chapter 6. Drawing from the results of these five experimental investigations, a simple theory is proposed to describe macroscopic detonation behavior. The theory addresses the competition between the gasdynamic expansion and the global rate of chemical reaction by incorporating the features of the cellular structure into the conventional stream line divergence philosophy. When the findings of previous investigators are interpreted in the light of the proposed theory, it is found that many studies which were seemingly unrelated are, in fact, just variations of the same chemical-gasdynamic dependence. Conclusions and recommendations for future research are summarized in Chapter 7. A statement outlining the original contributions of the present work is given in Chapter 8.

## 2.0 THE CRITICAL CONDITIONS FOR THE TRANSMISSION OF PLANAR DETONATION TO SPHERICAL OR CYLINDRICAL DETONATION\*

### 2.1 Introduction

The critical tube diameter  $D_C$  for the transformation of a planar detonation in a circular tube to a spherically diverging detonation has been proposed as a measure of the detonability of combustible mixtures (Matsui and Lee, 1979). Mitrofanov and Soloukhin (1965) first proposed that the critical diameter is linked to the cell size  $\lambda$  of the nonsteady three-dimensional detonation front via the simple relation  $D_C \cong 13\lambda$ , based on experiments using low-pressure oxyacetylene mixtures. The same authors proposed a similar correlation for the case of transmission from an infinite slit of width  $W$  to an unconfined medium. The proposed relation,  $W_C \cong 10\lambda$ , is based on the assumption that the real phenomenon is satisfactorily simulated by sandwiching between two confining plates a thin sheet into which a channel and an abrupt area increase have been machined. Essentially, the idea is to examine a thin slice of an infinite geometry. Edwards et al. (1979, 1981b) have confirmed the  $10\lambda$  correlation for oxyacetylene mixtures in a similar test arrangement and further suggest the correlation should be approximately valid for all detonative systems. Liu et al. (1984) and Benedick et al. (1983) agree with this conclusion, in principle, but claim that  $W_C$  tends to about  $3\lambda$  as the aspect ratio of the slit increases, putting in question the "thin slice" philosophy of previous investigators. Nonetheless, an empirical relation linking a global detonation parameter ( $D_C$  or  $W_C$ ) to a smaller scale parameter ( $\lambda$ ) characteristic of the cellular structure appears to be generally valid for transmission-type phenomena.

Although most studies to date have focused on relatively simple geometries for which the critical condition depends on the mixture sensitivity

---

\*The bulk of the material in this chapter has been published in the paper "On the Transformation of Planar Detonation to Cylindrical Detonation". *Combustion and Flame* 52, 269 (1983). Authors: Murray, S.B. and Lee, J.H.

(i.e., on  $\lambda$ ) and on one geometric length, investigations of more complex geometries have also been conducted. These include studies of detonations negotiating bends and sharp corners (Lee and Lee, 1965; Edwards et al., 1981a) and detonations transmitting through multiple orifice holes, perforated plates (Bjerketvedt et al., 1981), annular passageways (Jenssen, 1983) and screens (Martin and Lee, 1982). Such investigations have been valuable in providing insight into the fundamental processes of failure and reinitiation involved in the transformation of detonation from one geometry to another, but they have not yet been successful in quantifying the critical conditions in terms of general correlations.

The mere identification of such correlations, even if only for simple geometries, strongly suggests the existence of a critical balance between the global rate of reaction, characterized by  $\lambda$ , and the rate of gasdynamic expansion, characterized by a length typical of the geometry ( $D$  or  $w$ , for example). The experimental study to be described in this chapter involves the transformation of a planar detonation in a circular tube to a cylindrical wave expanding radially outward from the tube axis between a pair of parallel plates separated by a distance  $w$ . This geometry is of interest in that a gradual change in the phenomena can be observed as the plate separation is varied between a large value (in comparison with the tube diameter  $D$ ) where only one nondimensional parameter,  $D/\lambda$ , is important, to smaller values where two parameters,  $D/\lambda$  and  $w/\lambda$ , are expected to play a role. The objective of the study is to elucidate the nature of the critical chemical-gasdynamic balance for these relatively straightforward cylindrical and spherical geometries, with a view to extending the criterion to the more general case.

## 2.2 Experimental Details

The test facility shown in the photograph of Figure 6 and the schematic diagram of Figure 7 was designed to enable investigation of both cylindrical and spherical initiation phenomena. The apparatus consisted of two components. The first of these was a round plexiglass detonation tube 1.83 m



long with an inside diameter of 63.2 mm, giving a length-to-diameter ratio L/D of about 30. The ignition end of the tube was capped by an igniter plug with two brass electrodes. Initiation of detonation in the tube was achieved by capacitor discharge (0.1  $\mu$ F charged to 20 kv) through a thin copper wire of 50 mm length. This system provided reliable initiation of the test mixture (equimolar oxyacetylene) at initial pressures as low as 4 Torr.

The second component of the apparatus was a cylindrical chamber consisting of two circular aluminum plates separated by an annular spacer. The chamber was oriented normally to the longitudinal axis of the tube so that a wave emerging from the tube would be diffracted around a sharp 90° corner. The plate separation  $w$  was varied by installing different combinations of steel and plexiglass annular spacers between the plates. Separations of 6.3, 12.1, 24.7, 48.5, and 70.8 mm were investigated, corresponding to  $w/D$  ratios of 0.099, 0.191, 0.391, 0.767, and 1.12, respectively. The chamber diameter was 560 mm. For the limiting case of "infinite" plate separation, a steel pipe of 362 mm length and 250 mm inside diameter, giving a value for  $w/D$  of 5.73, was used as a cylindrical chamber.

The oxyacetylene mixture was premixed using the method of partial pressures. The error in mixture composition was estimated to be less than 1 part in 2000. For each experiment, the test volume was first evacuated to 0.1 Torr absolute pressure and then filled to 75 Torr with the test mixture. It was subsequently evacuated to 1 Torr and filled a second time to 75 Torr before finally evacuating to the required initial pressure. The error in determining pressure using a mercury manometer was less than  $\pm 1$  Torr.

The diagnostic methods employed are illustrated in Figure 7. These included pressure transducers, smoked mylar films and open-shutter photographs. Three pressure transducers (PCB 113A24) were installed in the tube just upstream of the exit to the chamber. A fourth transducer at the edge of the cylindrical chamber (in the annular spacer between the plates) was used to determine whether transmission was successful. The structure of the

detonation wave was recorded using smoked mylar films, prepared by applying a thin layer of soot to 0.13 mm thick sheets of transparent mylar. These films were taped to the walls of the apparatus at strategic locations. One smoked film was placed in the tube just upstream of the exit. Another two films were attached to the walls of the cylindrical chamber; one on the back plate surrounding the tube exit and the other on the front plate opposite the exit. The purpose of these was to record the details of the interaction between the diffracted wave and the boundaries during the transformation from one geometry to another. For tests near criticality, an additional smoked film was attached to the inner surface of the annular spacer to aid in determining whether transmission had occurred. The third method of diagnosis was open-shutter photography, used when the plate separation was on the order of the cell size.

Photography was made possible by replacing the aluminum front wall of the chamber by one of plexiglass. A 35 mm camera with ultraviolet filter and ASA 400 film was then positioned on the tube axis looking normal to the direction of propagation in the chamber. With the shutter open throughout the course of an experiment, a time-integrated record of the triple-point trajectories was captured on film. The chemical luminescence of equimolar oxyacetylene was one of the criteria used in the selection of a suitable test gas.

In all, a total of 174 experiments were carried out.

## 2.3 Experimental Results and Discussion

### 2.3.1 Cell Width Measurements

All detonation pressures and velocities measured in the tube were within  $\pm 5\%$  of the corresponding C-J values, confirming that equilibrium propagation was established before the wave encountered the abrupt area change. This was further supported by transverse wave spacing or cell width measurements from smoked films and open-shutter photographs. A summary plot of cell width versus initial pressure is shown in Figure 8. It should be noted

that, from an experimental point of view, the cell width  $\lambda$  is better defined than the length  $L_C$  due to the difficulty in determining the end of the "cusp"-like tail on the cell. Consequently, the cell width has been measured and the length inferred from a typical cell aspect ratio ( $\lambda/L_C \cong 0.6$  for the present  $C_2H_2-O_2$  mixtures). This will be the approach throughout the remainder of the thesis, although the aspect ratio used will be seen to depend weakly on the detonative system. Data include measurements from both the tube and the cylindrical chamber. Cell widths were obtained from the records using two different sampling methods. In the first method, the average width of many individual cells was computed. The second method was to identify and measure the average width of dominant diagonal bands of cells. This latter procedure was used to discriminate between substructure and primary structure, since substructure seldom persists in bands for this system. Also shown in Figure 8 are transverse wave spacings computed from the period of oscillations  $\Delta t$  on the leading portion of the pressure-time signatures obtained from transducers in the tube. The cell aspect ratio noted above was used along with the one-dimensional Chapman-Jouquet velocity  $V_{C-J}$  to give  $\lambda = 0.6 V_{C-J} \Delta t$ . Finally, an indirect measure of the cell width was obtained from the  $13\lambda$  correlation. For the present tube, this gives  $\lambda = 63.2/13 = 4.9$  mm at the critical initial pressure of 16.5 Torr.

The present data are in good agreement with the recent cell width data of Knystautas et al. (1982) which are also included in Figure 8. The dashed line through the data has been derived from the critical tube results of Matsui and Lee (1979), again using the  $13\lambda$  correlation. In fact, this line describes the trend of the present data quite well and will be used as a reference in calculations involving the cell width later in this chapter. Substantial scatter in the data, particularly at lower initial pressures, may be due to confinement effects in cases where the cell width was on the order of the transverse dimension of the test volume.

### 2.3.2 The Two Modes of Reinitiation

The contributions of this study are centred around observations on the two distinct modes of reinitiation sketched in Figure 9. In both cases, the

planar multilineated detonation wave (P) which emerges from the tube is initially threatened by the inward propagating rarefaction wave originating at the area change. When the cylindrical gap is large (Figure 9a) in comparison with the cell size characteristic of the mixture, reinitiation commences by the formation of one or more reignition or explosion nuclei (E) before the diffracted wave interacts with the wall opposite the tube exit. Subsequently, detonation bubbles evolving from these nuclei propagate both ahead into the unburned gas and transversely (T) through the compression heated gas bounded by the diffracted shock (D) and the trailing reaction zone (F). Individual bubbles collide to form a complex system of interacting Mach stems which eventually coalesce into a symmetric, reestablished spherical wave (S). Since reinitiation occurs prior to the interaction of the wave with the opposing wall, it will be referred to as "spontaneous reinitiation". It is the same mechanism by which a detonation wave in a tube transforms into an unconfined spherical detonation.

In the second mode of reinitiation (Figure 9b), reignition nuclei are not born spontaneously but form due to the reflection of the incident wave from the opposing wall. Upon reflection, a cylindrical Mach stem ( $M_1$ ) is driven radially outward along the front wall and a reflected shock ( $R_1$ ) travels back toward the tube exit. Owing to the strength of the reflected shock and the fact that a portion of it propagates through unburned but compressed mixture, a sizable volume of high-temperature unreacted gas is realized almost immediately and detonation results. The subsequent process, whereby the transversely propagating detonation engulfs the diffracted shock to form an equilibrium cylindrically diverging detonation, is similar to that which occurs in the spontaneous case. Since this mode of reinitiation is boundary induced, it will be referred to as "reinitiation by reflection".

#### Smoke Records Corresponding to Spontaneous Reinitiation

Figure 10 shows a smoke record from an experiment in which spontaneous reinitiation was the mechanism by which the wave reestablished itself in the cylindrical volume. This particular record is from the back wall (the black circle shows the tube cross section) for the largest plate separation (i.e.,

w/D = 5.73). The most dominant feature is the narrow asymmetric annular ring. The inner and outer boundaries of this ring mark the positions of the diffracted wall shock (D) and the trailing reaction zone (F) at the moment the transversely propagating detonation wave (T) arrives at the back wall. Since the collision is from a direction more or less normal to the wall, the resulting cellular writing is of the end wall variety (i.e., like Figure 1b). Furthermore, it is of small scale, emphasizing the increased detonation sensitivity of the preshocked mixture. Asymmetry of the ring is due to the fact that reignition does not occur along a circular locus of points, as depicted in the idealized sketch of Figure 9a, but rather at several discrete "hot spots" around the periphery of the attenuated detonation core. Consequently, different times are required for points on the surfaces of expanding detonation bubbles to arrive at the back wall. The "fan"-like structures, which originate at discontinuities in the curvature of the annular ring and grow circumferentially with increasing radius, are written by detonative Mach stems caused by the collision between two such detonation bubbles. The scale of the structure within the fan is small near the annular ring, emphasizing the localized overdriven nature of the Mach stem, but grows with increasing radius until the equilibrium cell size is approached as the Mach stem decays to the steady state.

The annular ring and the tube bound an area characterized by a lack of cellular structure. This is the region over which the diffracted shock is not driven by a coupled reaction zone. Since the detonative mechanism had broken down, the wave did not write on this portion of the smoked film.

Outside the annular ring, the usual side wall writing (i.e., like Figure 1a) is seen, confirming that propagation near the back wall is in the radial direction. The small "petal"-like structures around the periphery of the annulus are written by numerous detonative Mach stems ( $M_2$ ) created by the reflection of the transversely propagating detonation wave from the back wall. Each Mach stem is bounded on the sides by a pair of transverse waves which move toward one another as the Mach stem propagates radially outward along the wall. The "point" of each petal marks the location where a pair of circumferentially moving (i.e., in a direction normal to the plane of the sketch in Figure 9a) transverse waves meet.

Smoke Records Corresponding to Reinitiation by Reflection

The collection of four pairs of smoke records shown in Figure 11 is from experiments in which the opposing wall ( $w/D = 0.391$ ) plays a role in the transformation process (i.e., reinitiation by reflection). Prints on the left (a) are from the back wall, while those on the right (b) are from the front wall. Sets of prints are presented in order of decreasing mixture sensitivity. The annular rings in Figures 11.1a and 11.2a, corresponding to experiments for which  $D/\lambda$  was approximately 34 and 15, respectively, exhibit rotational symmetry and are of nearly identical radius, despite the appreciable difference in mixture sensitivity as evidenced by the scale of both end wall and side wall cellular structure. The symmetry is due to reignition being induced by reflection of the diffracted wave from the front plate, as illustrated in Figure 9b. Since reignition of this type is geometrically controlled, taking place along a circular locus of reignition nuclei in the preheated gas near the front wall, formations on the smoked films are rotationally symmetric. The fact that the rings are of nearly identical size over a considerable range of sensitivity is due to two factors. First, the shock trajectories are invariant over the narrow range of pressures used to adjust the mixture sensitivity, both in the early diffraction stages before reignition and at later times when the transversely propagating detonation sweeps rearward. Second, the reflected shock is of sufficient strength so that the delay to reignition is negligible in comparison with the time taken for the reinitiated wave to sweep to the back wall. This is confirmed in both Figures 11.1b and 11.2b in that the transition from end wall to side wall structure is sudden, occurring over a distance much smaller than the cell length itself.

As the sensitivity of the mixture is reduced, a limit is approached for which the reflected wave is barely capable of reignition. Smoke records from a test near criticality are shown in Figure 11.3. The annular ring is highly asymmetric, exhibiting a ragged outer boundary, a varying ring thickness (i.e., the distance between the inner and outer boundaries of the ring), and a mean radius which increases rapidly with decreasing mixture

sensitivity. Diminishing symmetry is evidence that reignition is marginal and therefore spotted, occurring at some locations near the front wall in the vicinity of the head of the expansion but not at others. The trend of increasing radius with decreasing sensitivity is probably the result of the reflected shock having to travel a substantial distance through the preheated gas behind the diffracted shock before the onset of renewed detonation (see Figure 11.3b). Therefore, as the limit is approached, reignition is no longer instantaneous in comparison with other time scales which influence the ring size.

As the mixture sensitivity is reduced even further, a point is reached where the reflected wave cannot reignite the gas and failure results. The smoke records in Figure 11.4 clearly demonstrate that transmission was unsuccessful. Only a vague outline of the ring is present on the record from the back plate. The corresponding smoke record from the front plate shows a core of end wall structure surrounded by a region of side wall writing which grows rapidly in scale with increasing radius and finally terminates. Despite the formation of numerous reignition centres around the periphery of the core, the decay of the cylindrical Mach stem is too rapid for chemical reactions to remain coupled with the shock. Transmission with this plate separation is not possible for less sensitive mixtures.

### 2.3.3 The Annular Ring - What Does It Tell Us?

The radius of the annular ring seen on most of the back wall smoke records is an informative parameter describing the transformation from one geometry to another. It is an indirect measure of the time required for the detonation emerging from the tube to reestablish itself in the cylindrical geometry. More specifically, the time taken by the wall shock to propagate from the edge of the tube to a radius of  $R_s$  (see Figure 9) is equal to the sum of the "reignition time" plus the "sweepback time" at the instant the ring is written on the smoked film. The reignition time is defined as the interval between the arrival of the planar wave at the tube exit and the occurrence of reignition downstream of the exit. The sweepback time is that

taken by the reinitiated expanding detonation bubbles to sweep back to the rear wall. A plot of the ring radius versus the relative mixture sensitivity is shown in Figure 12. Data include measured ring radii for all plate separations. The ring radius is normalized with respect to the tube radius  $R_0$ . The relative mixture sensitivity is quantified in terms of a normalized cell size,  $\lambda_s/\lambda$ . Here,  $\lambda$  is the cell width characteristic of a particular initial pressure (see Figure 8) and  $\lambda_s$  is a reference cell width; namely, that required for critical transmission of a planar wave from a tube of radius  $R_0$  to an unconfined medium. As such, mixtures more sensitive than that required for critical transmission to free space are characterized by values of  $\lambda_s/\lambda$  greater than unity, while those less sensitive are denoted by values of  $\lambda_s/\lambda$  less than unity. Open symbols in Figure 12 depict successful transmission, whereas shaded symbols denote failure to transmit. Half shaded symbols indicate marginal cases in which transmission appeared to be successful judging from some portions of the smoke record but not so from others. These marginal cases covered a very narrow range of initial pressures (~1-2 Torr) for a given plate separation. Hence, as is the case for critical transmission to an unconfined region, the mixture sensitivity for critical transformation to cylindrical detonation is well defined for a specified plate spacing.

For the largest plate separation (i.e.,  $w/D = 5.73$ ), where reignition can only occur spontaneously, the normalized ring radius  $R_s/R_0$  decreases with increasing mixture sensitivity, as illustrated by the broken line in Figure 12. This is a consequence of the fact that the point of reignition moves toward the tube exit as the mixture is made more sensitive. Therefore, the transversely propagating detonation sweeps to the back wall before the wall shock has travelled any appreciable distance. In the limit of high sensitivity, it is likely that  $R_s/R_0$  approaches unity. As the sensitivity is lowered, the point of reignition moves away from the tube exit so that the ring radius takes on a maximum value of about three tube radii in the critical limit.

The solid lines in Figure 12 show the ring size data for the five smaller plate separations (i.e.,  $0.099 < w/D < 1.12$ ). All curves are of



similar shape in that each consists of three distinct branches. Using the data for the plate separation of  $w/D = 0.391$  as an example, each curve has a central branch ( $1.2 < \lambda_s/\lambda < 2.6$ ) over which the ring radius is practically constant for a significant range of sensitivity, a lower branch ( $0.85 < \lambda_s/\lambda < 1.2$ ) over which the radius increases rapidly as the critical mixture sensitivity is approached, and an upper transitional branch ( $2.6 < \lambda_s/\lambda < 3.1$ ) which connects the central branch to the curve for spontaneous reinitiation (i.e., the dashed curve corresponding to  $w/D = 5.73$ ). The reasons for the variation in ring radius with mixture sensitivity over the central and lower branches of the curve have already been discussed with the aid of the smoke records shown in Figure 11. In fact, the ring radii obtained from the smoke records in Figures 11.1 - 11.4 are labelled 1-4 in Figure 12.

At high enough mixture sensitivity, the ring size must eventually be identical to that for spontaneous reinitiation, regardless of the plate separation, since it is always possible to choose a sensitivity for which reignition takes place spontaneously long before the emerging wave is aware of the front wall. The smoothness of the upper transitional branch suggests that the changeover from one mode of reinitiation to another is a gradual one in which the plate plays a role of diminishing importance as the sensitivity is increased. It is thought that a range of sensitivity exists over which reignition is of the spontaneous type, but for which the resulting ring radius is still governed by the wall due to a subsequent reflection later in time. This is probably why the curve for a given plate separation crosses over that for spontaneous reinitiation and then approaches it asymptotically from above. The ring size will be unaffected by the presence of the plate only if reignition occurs well before the wave encounters it.

The fact that the ring radius is independent of  $\lambda_s/\lambda$  over a large range suggests that the phenomena do not depend on the nondimensional parameter  $D/\lambda$  over that range since  $D \cong 13\lambda_s$ . This is not surprising since gasdynamic interactions in the cylindrical chamber control the phenomena. Furthermore, the critical condition for transmission does not appear to correlate with

$D/\lambda$  since the front plate makes critical transmission to cylindrical geometry more difficult (i.e.,  $\lambda_s/\lambda > 1$ ) than to an unconfined region for small plate separations, but less difficult (i.e.,  $\lambda_s/\lambda < 1$ ) for larger separations. Both of these observations suggest that  $\lambda_s$  may not be an appropriate reference mixture sensitivity for describing transmission to this geometry. Perhaps  $\lambda_c$ , the equilibrium cell width for critical transmission to a particular gap, is more suitable.

Figure 13 shows the ring size data replotted in the form  $(R_s - R_0)/\lambda$  versus  $\lambda_c/\lambda$ . The expression  $(R_s - R_0)/\lambda$  for the ring radius is simply the distance travelled by the wall shock, in terms of cell widths, up to the time when reestablishment has been completed. As might be expected, the data follow one of two trends corresponding to the two modes of reinitiation. It is convenient to discuss the implications of each trend separately.

#### Reinitiation by Reflection - the Formation of Cylindrical Detonation

The ring size data for the five plate separations fall onto a single curve. The fact that the ring radius is a unique function of  $\lambda_c/\lambda$  confirms that the process is controlled by the plate and emphasizes the similarity of the reignition and sweepback mechanisms in this type of transmission. Further support is provided by the observation that, within the bounds of experimental error, the plate spacing is a constant multiple of the cell size at critical conditions. Specifically, the computed values for  $w/\lambda_c$  are 5.2, 5.6, 5.4, 6.1, and 6.2 for each of the five plate separations, beginning with the smallest. That is,  $w = 5.7\lambda_c$  to within  $\pm 10\%$ . These conclusions provide a posteriori justification for the selection of  $\lambda_c$  as an appropriate reference sensitivity and confirm that the phenomena do indeed scale with  $w/\lambda$ . If the detonation tube is looked upon as an ignition source for the initiation of cylindrical detonation, the critical plate spacing of  $5.7\lambda$  is consistent with observations by Matsui and Lee (1976) that it is difficult to initiate cylindrical detonation in low-pressure oxyacetylene using flanged electrodes if the electrode spacing is reduced below about five cell widths. Combining the above  $5.7\lambda_c$  correlation with the  $13\lambda_s$  cor-

relation gives the connection between the cell width required for transmission to a cylindrical gap and that required for transmission to an unconfined region. Thus,  $\lambda_c/\lambda_s \cong (13/5.7)w/D = 2.3w/D$ , for the range of  $w/D$  ratios investigated.

One of the objectives of this study is to determine the minimum conditions required for the formation of cylindrical detonation. Consider the "work-done" model of Lee and Matsui (1977) which proposes, for the analogous case of spherical initiation, that the minimum conditions can be expressed in terms of the compression work done on the gas in the unconfined volume by the planar wave emerging from the tube. In essence, the model treats the tube as an initiation source of specified energy, with the amount of energy depending on the tube diameter ( $E \propto D^3$  according to the above model). Experimentally, the minimum conditions for transmission or, alternatively, for the formation of spherical detonation, can be identified by reducing the tube diameter and, hence, the initiation energy to the point where transmission is just possible. A similar philosophy should be valid for cylindrical geometry. However, it is the minimum energy per unit length of gap which is important for cylindrical initiation, not simply the energy itself. If it is assumed, as in the work-done model, that a fixed amount of energy is available from the wave emerging from the tube, we need only to increase the plate separation  $w/D$  and, thus, decrease the energy per unit gap width until the minimum conditions for cylindrical initiation are identified.

Having determined the critical set of boundary conditions, the minimum radius of a self-sustained cylindrical detonation front can be deduced from the smoke records. Following reflection of the diffracted wave from the front wall, a detonative Mach stem is driven out radially along the wall. As the Mach stem grows in height, the particles entering it undergo a three-dimensional expansion. For mixtures less sensitive than the critical one, the expansion is too severe for the reaction zone to remain coupled with the shock. The cellular structure seen on the front wall smoke record grows in scale with increasing radius and terminates abruptly, despite the successful formation of numerous reignition centres in the wake of the reflected shock (see Figure 11.4b, for example). As the mixture sensitivity is increased,

the detonative Mach stem propagates further before failing. If the mixture sensitivity is such that the diverging wave can survive the expansion until such time that it becomes strictly two-dimensional, then propagation appears to be guaranteed from that point onward. This occurs when the Mach stem has grown to occupy the entire gap width, an event which is synonymous with the forming of the ring on the back wall smoke record. In this context, we could interpret the role of the reflected shock as being similar to a high-explosive charge during critical initiation; specifically, to maintain the detonation until such time that the expansion becomes mild enough for the wave to sustain itself through chemical heat release alone.

With the present apparatus, it was not possible to use annular spacers larger than  $w = 1.12D$ . Consequently, the maximum plate separation  $w/D$  and corresponding ring radius  $R_s/\lambda$  could not be determined directly. Nonetheless, one can estimate the minimum ring radius from the available data by plotting  $R_s/\lambda$  against  $D/w$  and extrapolating to the case of  $D/w$  approaching zero (i.e., to the case of a line source). Such a graph, plotted in Figure 14, shows that as  $D/w \rightarrow 0$  the ring radius  $R_s \rightarrow 6\lambda \cong 3.6L_c$ . The same result could have been obtained more directly from Figure 13 where it is apparent that  $(R_s - R_0)/\lambda \cong 6$  at criticality for all plate separations. But as  $D/w \rightarrow 0$  so does  $R_0/\lambda$  so that  $(R_s - R_0)/\lambda + R_0/\lambda \cong 6$ . **Thus, it would appear that the minimum radius of a self-sustained cylindrical detonation wave is about  $6\lambda$ .**

The question must be answered as to why a critical condition exists for each plate separation smaller than the maximum one for which transmission can occur. This is somewhat puzzling since a smaller plate separation than the limiting one corresponds to a higher energy per unit gap width if our assumption regarding a fixed amount of available energy from the tube is correct. Two possible reasons for this observation come to mind. First, one might hypothesize that propagation is simply not possible unless the separation between plates exceeds  $5.7\lambda$ . Although this argument would help to explain the observation about initiation using flanged electrodes, as reported by Matsui and Lee (1976), it is inconsistent with the results reported by others. Vasiliev (1982), for example, has recently found that

stable detonation between parallel plates is possible as long as the spacing between plates exceeds the cell width. The second possibility may lay in the fact that both energy and power are of importance in initiation phenomena (Matsui and Lee, 1976; Lee, 1977). For initiation by electrical spark, it has been demonstrated that only the energy deposited up to the time when peak power is achieved is relevant in the formation of detonation (Lee et al., 1974; Knystautas and Lee, 1976). In the present transmission problem, reinitiation occurs near the edge of the attenuated detonation core in the wake of the reflected wave. Since the conditions behind a reflected shock are more elevated than behind the respective incident shock, we could make the claim that the peak power condition is associated with the reflection. Once the reflected shock decays (i.e., once the peak power condition subsides), the remaining available energy is of no consequence in the initiation of the cylindrical detonation.

#### Spontaneous Reinitiation - the Formation of Spherical Detonation

The ring size data for spontaneous reinitiation shown in Figure 13 indicate that the distance ( $R_s - R_0$ ) is a constant multiple of the cell width. Specifically,  $(R_s - R_0) \cong 11\lambda$ , which is in agreement with the value of  $10\lambda$  noted by Mitrofanov and Soloukhin (1965) from open-shutter photographs of transmission from a two-dimensional channel. This distance is independent of the relative mixture sensitivity  $\lambda_c/\lambda$  (or equivalently  $w/\lambda$ ) over the entire range since, by definition, the phenomena are not controlled by interactions between the diffracted wave and the front boundary of the chamber. The fact that the ring radius is a constant number of cell widths is the consequence of some intimate relation between the chemical kinetics of the mixture and the dynamics of the diffracting shock, no doubt a similar chemical-gasdynamic coupling to the one responsible for the structure of detonations in the first place.

It has been mentioned that the time required by the wall shock to propagate from the edge of the tube to a radius of  $R_s$  is equal to the sum of the reignition time plus the sweepback time at the moment the ring is written on the smoked film. If some assumptions are made about the dynamics of the

transformation process, it is a simple matter to formulate expressions for these three time intervals and to work backward, starting with the known ring radii, in order to evaluate the axial distances from the tube exit at which reignition occurs.

The wall shock will be dealt with first. For the present purpose, its distance-time trajectory  $r_s(t)$  is assumed to be that which results when a C-J detonation in a circular tube transmits to unreactive mixture in an unconfined region. This trajectory was calculated (Thibault, 1982) using the finite difference flux-corrected transport computer code developed by Boris et al. (1976). All properties at the exit plane of the tube were maintained at C-J condition throughout the computation.

In order to calculate the reignition time, an assumption must be made about the possible locus of reignition points. In all cases, reignition was considered to occur along the characteristic defining the head of the expansion; that is, on a conical surface defining the furthest point of advance of the rarefaction wave. The angle  $\phi$  describing the cone (see Figure 15) is  $\tan^{-1}[(U_{C-J} + C_{C-J})/C_{C-J}]$  where  $U_{C-J}$  and  $C_{C-J}$  are the particle velocity and the sonic velocity in the products of a C-J detonation. The time for reignition to occur at a point on this cone is  $h/V_{C-J}$  where  $V_{C-J}$  is the detonation velocity. These assumptions are supported by open-shutter photographs of detonation diffraction from a two-dimensional channel in low-pressure oxyacetylene mixtures which show that the core is well described by the value of  $\phi$  above and that reignition nuclei do indeed form in the proximity of the leading characteristic (Moen et al., 1982). Edwards et al. (1979, 1981b) have also reported reignition that occurs in the vicinity of the head of the expansion. In the critical case, if reignition must take place before the incoming rarefaction wave arrives at the axis of the tube to quench the reaction, the most downstream location of reignition would be at  $h = (D/2) \tan \phi$ , or about  $0.92D$  for most mixtures. This estimate is consistent with the observation by Lee and Matsui (1977) that a spherical detonation forms at about one tube diameter from the exit in the critical case.

The third and final time interval which must be evaluated is the sweep-back time. Two different approaches were taken. These are described individually below and illustrated in Figure 15. In the first model, a spherical C-J detonation bubble is assumed to expand about the reignition nucleus, consuming the diffracted wave as it does so. Eventually, it engulfs the entire wave and arrives at the back wall after the wall shock has propagated to a radius of  $R_s$ . The annular ring is formed where these independent trajectories intersect. In the second model, the path of the transversely propagating detonation wave in the precompressed mixture behind the diffracted shock is calculated. This detonation is assumed to be moving in a direction normal to that of the local diffracted front at any point in time. The two assumptions which are necessary before a solution is possible are those relating to (i) the shape of the diffracted shock, and (ii) the velocity of the transversely propagating detonation. With respect to the first assumption, the shock at any point in time was considered to be an elliptical segment with a major radius of  $V_{C-J}t$  and a minor radius of  $r_s(t) + C_{C-J}t$ , where  $r_s(t)$  is given by the finite difference calculations described earlier and  $C_{C-J}t$  defines the extent to which the expansion wave has advanced into the core. Time  $t$  is measured from the moment the wave arrives at the tube exit. Regarding the second assumption, the velocity of the transversely propagating wave was calculated to be that of a C-J detonation in a mixture already compressed by the diffracted shock. For this purpose, the local Mach number along the diffracted shock was assumed to vary linearly between  $M_w$  at the wall and  $M_{C-J}$  in the detonation core. The program of Gordon and McBride (1976) was used to compute the velocity in the precompressed mixtures.

A plot of the normalized location of reignition  $h/\lambda$  versus the relative mixture sensitivity  $\lambda_s/\lambda$  appears in Figure 16. Agreement between the results from the two models described above is good. The data reveal that the location of reignition is a fixed number of cell widths from the tube exit. Specifically,  $h \approx 11.5\lambda \pm 10\%$ . This value is in agreement with that of  $10\lambda$  reported by Edwards et al. (1979, 1981b) for transmission from a two-dimensional channel. Further evidence to support this conclusion can be

drawn from the transitional branch of each ring size curve in Figure 12. As noted earlier, this branch links the ring size data for purely spontaneous reinitiation to those for reinitiation by reflection. Its existence is a result of the fact that the ring can still be influenced by the plate even though spontaneous reignition may take place well before the plate. The above described calculations for the trajectory of the transversely propagating detonation show that it traces out an arclike path (Figure 15b) which initially heads away from the tube exit before reversing direction and veering toward the back wall. This trajectory is readily apparent in the open-shutter photographs of detonation reestablishment following diffraction from a two-dimensional channel. If it is assumed that the plate can no longer influence the ring once the transversely propagating wave has reversed direction, the location of reignition is calculated to be at  $h \cong 0.8w$ . These results are included in Figure 16 and are seen to agree well with those from the calculations involving the ring radius.

The results presented so far have been arrived at somewhat indirectly in that they depended on an associated calculation of one sort or another. A more direct means of identifying the location of reignition would be to observe it on a smoked film aligned with the direction of propagation. In order to achieve this end, tests were conducted in which a thin-walled hollow cylinder with sharpened leading edges was positioned concentric with the tube axis. The cylinder was situated in such a manner that its leading edge was flush with the exit plane of the tube. As such, when a planar wave arrived at the tube exit, part of it was allowed to transmit through an annular opening into the unconfined region, while a circular core of the wave was directed into the cylinder. On a trial and error basis, an initial pressure was identified for which reignition occurred marginally above the surface of the cylinder, yielding both the position and the details of reignition on a smoked film wrapped around the outside of the cylinder. This approach assumes that the gasdynamic field is not altered by the presence of the cylinder before reignition and that the cylinder provides a reflective surface which emulates an opposite family of transverse waves. Two diameters of cylinder  $d_0$  were used. These were 37.0 mm and 50.9 mm, giving



values for  $d_0/D$  of 0.585 and 0.804, respectively. As expected, for high enough mixture sensitivities, where reignition takes place well outside the cylinder, the observed ring radii were identical to those measured in the absence of such a cylinder.

A series of smoke records from tests involving the larger cylinder are shown in Figure 17. Prints appear in order of increasing sensitivity. Propagation in all cases is from bottom (starting at the exit plane of the tube) to top. The first record (a), which shows failure of transmission, exhibits equilibrium cellular structure up to the point where the rarefaction wave arrives at the surface of the cylinder (shown as a broken line calculated from  $\phi = 61.3^\circ$  for this mixture). These cell widths are included in Figure 8. Beyond this line, the structure increases rapidly in scale and terminates abruptly as the reaction is quenched. The second record (b), corresponding to critical transmission, is similar except that a few points of reignition are seen in the middle of the print. These points, labelled 1, 2, and 3, are at distances of  $12.2\lambda$ ,  $11.6\lambda$  and  $11.4\lambda$ , respectively, from the tube exit. Similar results were observed for the smaller cylinder. These data are included in Figure 16. Agreement with calculated values of  $h/\lambda$  is excellent. The third record (c), for supercritical reinitiation, shows only equilibrium detonation structure since reignition takes place well above the cylinder's surface. No evidence of this is apparent on the smoked film. All of the results shown in Figure 16 reinforce the conclusion that spontaneous reignition occurs at approximately a fixed number of cell widths from the tube exit.

A final point of interest is that the cell size approximately doubles just prior to the birth of new reignition centres in a region of critical expansion (see Figure 17b). Similarly, it can be seen in Figure 11.3b that, for near critical transmission to cylindrical geometry, the cell size approximately doubles prior to the wave recovering and establishing itself as a cylindrically diverging detonation. Both observations suggest that failure under critical conditions occurs over a distance of propagation of  $2L_c$ . During this interval, the particle migrates approximately  $2L_c \times C_{c-J}$  or about one cell length aft of the shock since  $C_{c-J}/V_{c-J}$  is about a half.

This suggests that the effective thickness of the three-dimensional cellular wave front is about one cell length. Another hint that this might be true can be drawn from the back wall smoke records for the experiments involving transmission to an unconfined region (see Figure 10, for example). In all cases of supercritical reinitiation, the separation between the diffracted wall shock and the trailing reaction zone increases with radius until it reaches approximately  $1.5\lambda$ , or about one cell length, at which time the transversely sweeping reinitiated wave arrives at the back wall. One possible interpretation of this observation is that reestablishment of the wave cannot take place if the reaction zone falls behind the shock by more than one characteristic chemical kinetic distance.

#### 2.3.4 Wave Front Curvature as a Means of Quantifying the Gasdynamic Expansion

The calculations described in the previous subsection model the diffracted wave as an elliptical segment having a major radius of  $V_{C-J}t$  and a minor radius of  $r_s(t) + C_{C-J}t$ . Since  $r_s(t)$  is slightly less than  $\frac{1}{2}V_{C-J}t$  and  $C_{C-J}t$  is slightly more than  $\frac{1}{2}V_{C-J}t$ , the diffracted shock is very nearly spherical by the time the rarefaction converges on the centre line. In this context, we could interpret a test to determine the critical conditions for transmission to an unconfined region as being equivalent to finding the minimum radius of curvature for which particles entering a spherical front can react in time for the coupling between the shock and the reaction zone to remain intact. **Thus, we could conclude that the minimum radius of curvature for a self-sustained spherical detonation wave is about  $11.5\lambda$ .** If it is assumed that reignition cannot occur much later than when the rarefaction arrives at the tube axis a distance of about  $0.92D_c$  from the exit, as discussed previously, then the critical tube diameter  $D_c$  and the critical radius of curvature  $R_s$  for a spherically diverging wave are related by  $R_s \cong 11.5\lambda = 0.92D_c$ ; that is,  $D_c = 12.5\lambda$ . This may be the very basis of the  $13\lambda$  correlation.

It is of interest to note that the critical radius of curvature for spherical expansion (i.e.,  $11.5\lambda$ ) is about twice that for cylindrical expan-

sion (i.e.,  $6\lambda$ ). This may be a consequence of the fact that the rate of gasdynamic expansion behind the shock is proportional to the rate of growth of the detonation surface area (i.e.,  $U_{C-J}/V_{C-J} \cong \text{constant}$ ). For a given radius, the relative rate of increase of surface area with radius can be expressed approximately by the curvature  $K = A^{-1}dA/dR$ . For cylindrical geometry  $K = 1/R$ , while for spherical geometry  $K = 2/R$ . In terms of the cell dimensions, the critical curvatures for the two geometries are  $(6\lambda)^{-1}$  and  $(5.75\lambda)^{-1}$ , respectively, according to the present experimental results. Thus, it would appear that a necessary requirement for successful initiation of a self-sustained detonation in a given geometry is that conditions be close to C-J when the wave curvature becomes less than about  $(6\lambda)^{-1}$ . Since smoked films were the major diagnostic tool, there is no way of determining the corresponding wave velocity at the point where the critical curvature is realized. Consequently, it is not possible to specify what "close to C-J" really means. This issue will be addressed in a later chapter.

The curvature criterion is closely related to the velocity gradient criterion employed by Edwards et al. (1979, 1981b). An underlying assumption of the Whitham (1957) shock diffraction theory used by these authors is that decreases in the Mach number of the front are the result of area increases alone (i.e.,  $dM/dR \propto dA/dR$ ). The velocity gradient and curvature concepts are therefore related ways of quantifying the rate of gasdynamic expansion. Both deal with the rate of growth of the detonation surface area. As far as the rate of reaction is concerned, both the present study and that of the above authors appeal to the cellular structure for the relevant chemical time scale.

## 2.4 Summary

The study described in this chapter is concerned with the critical conditions for the transformation of planar detonation in a circular tube to cylindrical detonation expanding radially outward between a pair of parallel

plates (Figure 6). Low-pressure equimolar oxyacetylene mixtures were used throughout. Numerous smoke records show that reinitiation of the diffracted wave is via one of two mechanisms. When the plate separation  $w$  is large in comparison with the cell size (i.e.,  $w > 11.5\lambda$  where  $\lambda$  is the cell width), "spontaneous reinitiation" occurs via the formation of reignition nuclei in the neighbourhood of the head of the expansion a distance of about 11.5 cell widths from the tube exit (Figure 9a). This is precisely the mechanism responsible for successful transmission from a tube to an unconfined region. Reignition at a fixed number of cell widths from the tube exit (Figure 16) confirms the similarity of the supercritical reinitiation process for all mixtures more sensitive than the critical one. In the case of critical transmission,  $11.5\lambda$  is also the radius of curvature  $R_s$  of the nearly spherical diffracted wave. If it is assumed that reignition cannot take place much after the incoming rarefaction has converged on the tube axis (a distance of  $0.92D$  from the tube exit based on equilibrium calculations), then the critical radius of curvature and the critical tube diameter  $D_c$  are related by  $R_s \cong 11.5\lambda = 0.92D_c$ ; that is,  $D_c \cong 12.5\lambda$ . Thus, it is proposed that the requirement for the radius of curvature to exceed some critical radius in order for the chemical processes to survive the gasdynamic expansion could be the basis of the  $13\lambda$  correlation.

For plate separations smaller than  $11.5\lambda$  but greater than  $6.7\lambda$ , "reinitiation by reflection" occurs when the diffracted wave collides with the front plate to induce a circular locus of reignition centres near the plate in the wake of the reflection (Figure 9b). Measurements from the smoke records show that both the reignition and subsequent processes which lead to the formation of cylindrically diverging detonation are similar for different plate spacings, scaling with  $w/\lambda$  (Figure 13). The minimum conditions for the formation of self-sustained cylindrical detonation are shown to be associated with the largest plate separation  $w/D$  for which successful transmission of this type can occur. The maximum plate separation corresponds to the minimum linear energy density across the gap if a fixed amount of energy is available from the wave emerging from the tube. Following reflection of the wave from the plate opposite the tube exit (Figure 9b), a detonative

cylindrical Mach stem is driven out radially along the plate, but is seen to decay as the flow expands in both the radial and axial directions. However, if the Mach stem can survive this three-dimensional expansion until it grows to occupy the entire gap width, at which time the expansion becomes purely cylindrical, then propagation is guaranteed from that point onward. Based on the smoke record observations, this minimum radius of curvature for self-sustained cylindrical detonation appears to be about  $6\lambda$ . For plate spacings smaller than  $5.7\lambda$ , transmission is not possible. Despite the formation of numerous reignition centres in the wake of the reflected shock (Figure 11.4b), the expansion is too severe behind the cylindrical Mach stem for the reaction zone to remain coupled with the shock.

The fact that the critical radius of curvature for a spherically diverging wave is about twice that for a cylindrically diverging wave may be the consequence of the gasdynamic expansion behind the shock being proportional to the rate of growth of the front,  $A^{-1}dA/dR$ . This term represents the "curvature" of the detonation surface. It evaluates to  $1/R$  and  $2/R$  for cylindrical and spherical geometries or, in terms of the cell width  $\lambda$  which characterizes the global rate of reaction, to  $(6\lambda)^{-1}$  and  $(5.75\lambda)^{-1}$ , respectively. Essentially identical curvatures suggest that the critical conditions for transmission in various geometries may be governed by the same chemical-gasdynamic competition occurring within the detonation front.

Finally, smoke records indicate that both failure of detonation prior to critical reignition (Figure 17b), and recovery of detonation from near critical disturbances (Figure 11.3b), are characterized by a sudden increase in the cell size by a factor of about two. This observation suggests that the critical processes are linked to the time it takes the front to propagate about  $2L_c$ . Since a particle migrates rearward of the shock through about half this distance during the same period, the effective thickness of the cellular wave front would appear to be about one cell length.

### 3.0 LARGE-SCALE EXPERIMENTS ON THE TRANSMISSION OF PLANAR DETONATION TO SPHERICAL DETONATION IN ETHYLENE-AIR MIXTURES\*

#### 3.1 Introduction

It was proposed in Chapter 2 that relations such as the  $13\lambda$  correlation, first proposed by Nitrofanov and Soloukhin (1965), are the result of a critical balance existing between the rate of gasdynamic expansion and the rate of chemical reaction. However, the experiments of Chapter 2, as well as those of most other investigations in which correlations have been attempted, employed rather sensitive fuel-oxygen mixtures. From the point of view of accidental scenarios or applications, it is the less sensitive fuel-air mixtures which are of interest. It is not clear whether correlations of the above mentioned type hold for these mixtures and, if so, whether the constants of proportionality are the same as for fuel-oxygen mixtures. The work of Strehlow and Engel (1969) shows that the cell size for highly diluted mixtures appears to be controlled by the induction time in the relatively low-temperature post-shock gas. For undiluted mixtures, the induction time is much shorter and the recombination time is thought to be controlling the cell dimensions. If the nature of the chemical processes which are a key ingredient in the makeup of the cellular structure changes with increasing dilution, it is quite conceivable that the  $13\lambda$  correlation may not hold or may involve a different numerical constant. There is also some evidence to suggest that the inclusion of nitrogen as a diluent may result in some degree of chain branching inhibition (Takai et al., 1974) which is thought to lead to more irregular cellular structure. Edwards et al. (1981b) have proposed that irregular structure may be the reason why between 14 and 18 cell widths appear to be necessary for transmission in some fuel-oxygen mixtures recently investigated. The objective of the

---

\*The bulk of the results presented in this chapter has been published in the paper "Diffraction of Detonation from Tubes into a Large Fuel-Air Explosive Cloud". Proceedings of the Nineteenth Symposium (International) on Combustion, p. 635. The Combustion Institute (1982). Authors: Moen, I.O., Murray, S.B., Bjerketvedt, D., Kinnan, A., Knystautas, R. and Lee, J.H.

experiments to be described in this chapter is to investigate the validity of the  $13\lambda$  correlation in ethylene-air mixtures and to gain further insight into the reinitiation process through photographic means not employed in the laboratory study of Chapter 2.

### 3.2 Experimental Details

Large-scale tests were carried out at the Defence Research Establishment Suffield (DRES) in Ralston, Alberta. The field facility was built in order to carry out both the present experiments and those planned as part of the DRES research program in this discipline in the foreseeable future. The design criteria and some of the technical details have been reported both internally at DRES (e.g., Funk and Murray, 1982) and in the open literature (e.g., Funk et al., 1982). One such report is included as Appendix A. The facility is centred around a concrete pad measuring 18.3 m in length by 7.6 m in width. The pad is equipped with a series of steel channels, running longitudinally from one end to the other, onto which a variety of apparatus can be fastened. A photograph of the test section used for the present diffraction experiments appears in Figure 18. The test section consists of a steel tube of circular cross section connected to a large "bag" constructed from 3.5 mil (i.e., 0.089 mm) thick polyethylene sheeting. Tube diameters of 0.31 m, 0.45 m and 0.89 m were employed in the study. The bag diameters were chosen so that the walls were deemed not to be interfering with the phenomenon under investigation (i.e., transmission to an "unconfined" volume). See the inset table of Figure 18 for the relevant tube lengths and bag diameters.

Ethylene (CP grade, 99.5% pure  $C_2H_4$ ) was chosen as a fuel because it is a gas at atmospheric conditions and is therefore easy to handle, and because other detonability data on this system are available. It is also of a sensitivity which does not require the apparatus to be immense in size. Fuel was delivered from a remote bunker to the test section via an underground line. Its flow rate was regulated by a "Matheson" mass flow controller.

Once introduced into the test volume, the fuel was mixed with initial ambient air using a multipath recirculation system driven by a high-capacity (20 m<sup>3</sup>/min) explosion-proof centrifugal blower. The mixture was supplied to one end of the test section from an underground manifold attached to the high-pressure side of the blower. It was subsequently returned to a manifold on the low-pressure side of the blower after travelling the length of the test volume. Flexible "dryer hose" was used to connect the test section to steel headers stemming from the manifolds. Mixing was enhanced by branching the flow at multiple points on the test section and on the manifolds. The bag was kept inflated by pressurizing it slightly with the aid of the blower. This recirculation system was designed to compensate for outward leaks by replacing any escaped mixture with an equal volume of air entrained into the loop at a point on the low-pressure manifold.

The composition and homogeneity of the mixture were monitored throughout each experiment using a precalibrated "Wilks Miran 80" infrared (IR) analyzer. Gas samples were drawn from four ports on the apparatus; two on the tube and two on the bag. These samples were relayed to the bunker through a series of underground lines using individual noncontaminating diaphragm pumps. Samples were isolated sequentially in the analyzer test cell, vented to atmospheric pressure (the pressure at which the IR calibration was done), tested for IR absorption, and finally routed via a return line back to the test volume. This entire operation was microprocessor controlled. The analyzer was calibrated under carefully controlled laboratory conditions using both industrially prepared gas samples and others prepared in-house by the method of partial volumes. Infrared absorption measured in the field was corrected to account for differences between ambient and calibration gas temperatures and pressures. The above described sampling and analyzing system was considered adequate to guarantee the composition and homogeneity of the mixture to within  $\pm 0.1\%$  C<sub>2</sub>H<sub>4</sub>. A composition-time history for a representative test is shown in Figure 19. Typically, a homogeneous mixture was obtained within 5 minutes from the time the fuel flow was terminated. An additional 30 to 60 minutes were required to converge on the desired fuel concentration. The falling concentration of ethylene seen in the figure is due to small amounts of mixture leaking out



of the system and being replaced by air. Just before the desired composition is reached, a pressure control valve is closed, preventing further entrainment of air into the loop. Thereafter, the composition levels out as the bag slowly softens.

An intended backup means of verifying the composition a posteriori involved bleeding samples off the supply line to the analyzer into flow-through type gas sampling tubes. The intention was to return these to the laboratory for either mass spectroscopic or gas chromatographic analysis. These efforts proved unsuccessful, however, when it was learned that the sampling tubes failed to retain a valid sample for more than a few hours.

Once the desired fuel concentration was achieved, the test volume was isolated by closing butterfly valves located at each manifold port. Afterward, both the manifold and the gas analyzing system were purged with air to afford them protection against potential blast damage. Initiation of gaseous detonation was achieved by a disc of high-explosive PETN which was initiated using a standard industrial electric detonator. The PETN disc was fastened to a plywood end cap covering the ignition end of the tube.

Four diagnostic techniques were employed. A series of eight piezoelectric pressure transducers (PCB 113A24) were positioned along the tube and in the vertical members of the bag support frame (see Figure 18). Pressure-time signatures from the transducers were retained using a high-speed (~80 kHz) analogue tape recorder (Honeywell 101), and were subsequently played back on an ultraviolet oscillograph (Honeywell 1858). Peak pressures, along with velocities deduced from the elapsed time between neighbouring transducers, were used to confirm that the wave in the tube was propagating at equilibrium conditions and, further, to determine success or failure of transmission from the tube to the bag. Velocities were verified independently using a 20-channel ionization-gap probe system and associated time interval counter manufactured at DRES.

Cinematographic records were obtained with a "Hycam" camera (15,000 - 18,000 half frames per second) looking normal to the direction of propaga-

tion and a "Fastax" camera (~5,000 full frames per second) looking into the tube exit from approximately 40° off the axis of propagation. Kodak video news film 7250 (ASA 400 high-speed tungsten 3200 K) was used exclusively. Both cameras were housed for protection against blast damage and against the elements. The startup times of the cameras and the tape recorder were synchronized with the firing of the detonator by a DRES-manufactured programmable countdown sequencer.

The final means of diagnosis, used to record the cellular structure of the wave, was smoked metal plates mounted in the tube near the exit to the bag. Each plate was coated with a thin layer of soot produced by a richly burning kerosene flame. The principle of this technique is identical to that involving smoked mylar sheets, as described in Chapter 2, except that metal plates had to be employed in tests at an initial pressure of one atmosphere for reasons of survivability. Plate sizes ranged from 260 mm by 360 mm to 350 mm by 500 mm.

The experimental procedure was simply to converge on the critical mixture composition for transmission from each size of tube by a series of "GO" - "NO-GO" tests. Once the critical conditions were identified, additional tests were carried out with diminishing amounts of PETN to ensure that the initiation charge was not influencing the transmission phenomenon. Photographs showing various experimental details appear in Figure 20.

A total of 21 experiments were conducted.

### 3.3 Experimental Results and Discussion

#### 3.3.1 High-Speed Cinematography of the Diffraction Phenomenon

Selected frames from a high-speed cinematographic record, showing successful but near critical transmission of detonation from the 0.89 m diameter tube to a large 1.75 m diameter bag simulating an unconfined region, are shown in Figure 21. The direction of propagation is from right

to left and approximately normal to the line of sight of the camera. In frame 1, the planar detonation wave can be seen just as it emerges from the tube. Frame 2 shows the shrinking detonation core and a distinct curvature of the front as the rarefaction originating at the tube exit converges on the axis, quenching the detonation in its wake. For the mixtures used in the present experiments, equilibrium calculations show that the rarefaction arrives at the axis after the front has moved a distance of  $0.90D$  downstream of the exit. Recall this distance compares quite closely to that of  $0.92D$  for the low-pressure oxyacetylene mixtures used in the laboratory study. Unless reignition occurs in the preheated gas behind the frontal shock somewhere in this vicinity, the wave fails and the remaining combustible mixture in the bag is consumed by a deflagration. In the sequence of Figure 21, reignition behind an almost spherical diffracted front is seen to occur at a nucleus near the axis (frame 3) at precisely this streamwise location. The subsequent formation of detonation bubbles which sweep transversely through the preconditioned mixture behind the diffracted shock can be seen in frames 4 through 6. The two curved luminous tails which appear to be extending to the rear of the front in frame 5 are, in fact, a pair of tangentially sweeping waves approaching one another. The collision between these waves is apparent in frame 6. The final two frames of the sequence show a fully reestablished detonation in the bag. Asymmetry of the reinitiation process is likely due to vertical temperature gradients in the tube and the bag which alter both the local sonic velocity and the mixture sensitivity.

Figure 22 shows a similar high-speed cinematographic sequence involving a mixture more sensitive than the critical one. In this supercritical case, reignition nuclei materialize much closer to the tube exit and at several random locations near the edge of the shrinking detonation core. The sequences shown in Figures 21 and 22 provide support for the description of the reestablishment process deduced from the smoke records obtained in the laboratory study (Chapter 2). They are also consistent with the Schlieren and smoke-record observations of diffraction in fuel-oxygen mixtures in a narrow chamber (Edwards et al., 1979, 1981b).

### 3.3.2 Critical Tube Diameter Measurements

In spite of the apparent randomness in the appearance of the reinitiation centres, the critical mixture composition for transmission from a given tube is well defined provided i) the wave emerging from the tube is no longer influenced by the energy from the initiating charge, and ii) the plastic bag is sufficiently large so as not to influence the transmission process. In the present tests, care was taken to ensure that an equilibrium planar wave had been established and that the PETN charge did not influence the critical fuel-air composition. This was accomplished by varying the charge mass once the critical fuel concentration had been identified and by carefully monitoring both the pressure and velocity of the wave in the tube. In order to ensure that wave interactions with the plastic bag were not responsible for successful reinitiation, tests were performed using different sizes of bags. See the inset table of Figure 18.

The results from the critical tube experiments are summarized in Figure 23 where the outcome of tests with different diameter tubes is shown as a function of ethylene concentration by volume. Open symbols signify "GO" or successful reinitiation, while shaded symbols denote "NO-GO" or failure to transmit. In only one instance was it suspected, through close examination of film records, that the plastic bag walls may have been instrumental in aiding the transmission. The apparent "GO" result from this test (0.45 m diameter tube and 0.89 m diameter bag at 6.3%  $C_2H_4$ ) has been discounted. Included in the figure are results from similar field tests carried out by Moen et al. (1983) at DRES and by Jenssen (1983) at Raufoss, Norway using tubes of 1.83 m diameter and 0.35 m diameter, respectively. Also included on the graph is a point at stoichiometric composition obtained by Knystautas et al. (1982) by extrapolating laboratory results for oxygen-enriched mixtures ( $0.375 < \beta < 3$  where  $\beta$  is nitrogen-to-oxygen volume ratio) to the dilution corresponding to air; that is, to  $\beta = 3.76$ . This result lays considerably below those from the three sets of field tests. However, the discrepancy can easily be accounted for by what appears to be a rather arbitrary extrapolation of the curve through the data at low values of  $\beta$ .

It is important to note that no detonation reestablishment was observed with a 0.31 m diameter tube up to an ethylene concentration of 10.5%. Since it is very unlikely that reinitiation would occur in richer, less sensitive mixtures, we can conclude that the critical tube diameter is larger than 0.31 m for all C<sub>2</sub>H<sub>4</sub>-air mixtures.

The solid line through the data is a correlation assuming the variation of critical tube diameter  $D_c$  over the range of composition to be described by a standard induction-zone length formula of the form:

$$D_c = k u_s [O_2]^a [C_2H_4]^b \exp(E/RT), \quad (3-1)$$

where  $D_c$  is in meters and  $u_s$ ,  $[O_2]$ ,  $[C_2H_4]$  and  $T$  are the post-shock relative particle velocity (m/s), the oxygen and ethylene concentrations (moles/l) and the temperature (K) behind a shock propagating at the C-J velocity of the respective ethylene-air mixture. These properties are calculated using the Gordon and McBride (1976) computer program assuming frozen chemistry and vibrationally-relaxed equilibrium conditions. The exponents  $a$  and  $b$  are taken from the proposed induction-time formula of Hidaka et al. (1974), but the pre-exponential factor  $k$  and the effective activation energy  $E$  are obtained by a two-parameter fit to the data from the three sets of field tests. The fit gives an effective activation energy of 37.2 kcal/mole which is considerably higher than the value of 27.5 kcal/mole reported by Hidaka et al. for the induction time. This suggests that factors in addition to the chemical induction time play a role in determining the detonation sensitivity of the mixture. Such factors are probably related to the three-dimensional structure of the wave.

### 3.3.3 Cell Width Measurements

A plot of cell width versus mixture composition appears in Figure 24. In the same manner as described in Chapter 2, cell sizes were determined by averaging individual cell widths or by identifying dominant diagonal bands of cells. The latter method could only be used occasionally with the field

test data due to the relatively small size of smoked plates employed for practical reasons. Oscillations on the pressure-time signatures were also used to estimate the transverse wave spacing. An interesting observation is that the width of the longitudinal plastic strips produced by a detonation in the bag is approximately equal to the cell width. A photograph illustrating the phenomenon is shown in Figure 25. These strips are thought to be produced by the piercing action of the triple points, followed by longitudinal shearing of the plastic wall material. This observation proved to be useful as a quick preliminary diagnostic tool since strips did not form in cases where transmission was unsuccessful. Also shown on the graph in Figure 24 are the cell size data reported by Borisov (1980), Bull et al. (1982), Knystautas et al. (1982, 1983) and Moen et al. (1981, 1983). The present results are in fair agreement with other measurements, although there is significant scatter in the data.

### 3.3.4 The $13\lambda$ Correlation - Difficulty Interpreting the Smoke Records

The solid line on the graph (Figure 24) corresponds to  $D_c/13$  with  $D_c$  as a function of  $\%C_2H_4$  described by the curve shown in Figure 23. The dashed line in the figure has been obtained from a two-parameter fit to the cell width data assuming the variation of  $\lambda$  with  $\%C_2H_4$  to conform with a standard induction-zone length formula similar to that given by Equation (3-1). Around stoichiometric composition (i.e., 6.54%  $C_2H_4$ ), the solid line overpredicts the cell size by about 15%, which is an acceptable discrepancy considering the scatter associated with cell measurements. However, at the lean end of the curves (i.e., around 4%  $C_2H_4$ ), the measured cell width is about half that predicted by  $D_c/13$  from the critical tube diameter data. The reason for this may be related to the difficulty in interpreting the smoke records. A photograph of one of the larger smoke records, together with a sketch illustrating the author's interpretation of the record, appears in Figure 26. The solid lines on the sketch denote what the author considers to be proper cell boundaries, while the dashed lines are intended to signify substructure. It is readily apparent from the figure that the interpretation of smoke records produced by fuel-air detonations at atmospheric pressure is very subjective. The difficulty is further increased by

the relatively small size of the smoked plates employed in the field tests for practical reasons. This precludes the identification of dominant diagonal bands consisting of more than three or four cells. As well, the cost of carrying out large-scale tests does not permit several experiments to be performed for a particular mixture composition as can be done in a laboratory environment.

The difficulty in interpreting the cellular structure is further emphasized by the comparison between the atmospheric fuel-air and low-pressure fuel-oxygen smoke records shown in Figure 27. It is not clear why the substructure appears to be much more dominant for the fuel-air detonation. One explanation is that the mechanics of writing on the smoked surface may simply be different at atmospheric and at low pressures. It is possible that at low pressures the substructure is not capable of eroding soot from the smoked plate, whereas at atmospheric pressure the threshold of "erosion ability" is exceeded by the substructure. Although a detailed investigation was not carried out, there is also some evidence from the plastic bag strips to support the notion of a threshold in erosion ability. It was observed that, for a given mixture, smaller strips were generally formed when a 1 mil thick polyethylene material was used in lieu of a heavier wall. That is, a threshold in "piercing ability" of the substructure was detected. In fact, the bag strip method for measuring cell widths was, for the most part, abandoned when bags manufactured from 1 mil thick wall material were employed.

Moen et al. (1983) provide an alternative explanation for why the substructure appears to be more dominant on smoke records from fuel-air detonations. These authors suggest that as the mixture is made less sensitive (i.e., as the cells are made larger) the cellular structure becomes increasingly unstable. It is thought that stability of the front may be maintained through a process in which the substructure becomes more and more intense, thus making identification of the controlling mode very difficult. Since there is already some evidence to indicate that primary transverse waves become stronger as the detonation becomes marginal (Edwards et al., 1970; Strehlow and Crooker, 1974), it is conceivable that the transverse

waves associated with higher modes (i.e., substructure) could also increase in strength, perhaps becoming more capable of writing on the smoked surface. An observation which does not lend support to this philosophy is that no apparent trend of increasing substructure dominance with decreasing mixture sensitivity could be detected from the smoke records. At least visually, all of the records from the ethylene-air tests appear to exhibit about equal presence of secondary structure.

In accordance with the above arguments, it is quite possible that the substructure may have been mistakenly identified as primary structure for lean ethylene-air compositions, resulting in the cell width data falling short of the  $D_c/13$  line by a factor of about two at the lean end of the curves. Note that the cell size data of Knystautas et al. (1982, 1983), obtained from numerous experiments under laboratory conditions in tubes up to 300 mm in diameter, are in somewhat better agreement with the prediction. If the data of these authors are increased by an additional 10% to account for the difference in ambient pressures at DRES and at McGill, agreement between their data and the prediction is fair. Thus, the possibility that the  $13\lambda$  correlation is valid for ethylene-air mixtures covering a wide range of off-stoichiometric compositions cannot be ruled out.

Similar critical tube experiments by Moen et al. (1983) using acetylene-, ethylene-, ethane- and propane-air systems showed that, at stoichiometric composition,  $D_c/\lambda$  varied between 11.7 (acetylene-air) and 15.4 (ethylene-air). For off-stoichiometric acetylene-air compositions, the correlation was seen to hold over a wide range of sensitivity. In the case of lean propane-air mixtures, the ratio  $D_c/\lambda$  was seen to depart considerably from 13 as for lean ethylene-air mixtures, but in this instance was less than 13 by a factor of about two, suggesting that twice the controlling cell size may have been measured. In other words, the primary structure may have been mistaken for secondary structure. The recent large-scale test results reported by Guirao et al. (1982) using hydrogen-air mixtures and tubes up to 1.21 m in diameter also confirm that the correlation is valid over a wide range of sensitivity. It is quite possible that Benedick et al. (1983) have fallen victim to a similar interpretation error in their recent experiments



to determine the critical conditions for transmission from a two-dimensional slit to an unconfined region. Although it was originally concluded that the critical channel width  $W_c$  was about three cell widths for detonations in  $H_2$ -air and  $C_2H_4$ -air mixtures, these authors now suspect that the primary structure may have been mistaken as substructure, and that the critical channel width is more likely about  $6\lambda$ . Judging from all of the available data, the  $13\lambda$  correlation linking the cell width and the critical tube diameter probably holds for fuel-air mixtures as well as it does for fuel-oxygen mixtures, provided the cellular structure is properly interpreted.

### 3.4 Summary

Large-scale tests on the transmission of planar detonation from circular tubes of 0.31 m, 0.45 m and 0.89 m diameter to spherical detonation in large plastic bags simulating an unconfined environment (Figure 18) have shown that critical reignition of the diffracted wave occurs near the tube axis at about the location where the rarefaction has penetrated the entire detonation core (Figure 21). High-speed cinematographic records confirm that the details of the reignition and subsequent processes by which the wave becomes globally reestablished are as proposed in Chapter 2, based on smoke-record observations of low-pressure fuel-oxygen detonations.

The variation of the critical tube diameter  $D_c$  with mixture composition determined in the present experiments (Figure 23) is consistent with the data of both Moen et al. (1983) for a 1.83 m diameter tube and Jenssen (1983) for a 0.35 m diameter tube. It was also found that transmission from a tube of 0.31 m diameter is not possible for any ethylene-air mixture.

The cell widths  $\lambda$  obtained in the present tests (Figure 24) show that the  $13\lambda$  correlation linking  $D_c$  and  $\lambda$ , as first proposed by Mitrofanov and Soloukhin (1965) for fuel-oxygen systems, is approximately valid for ethylene-air mixtures near stoichiometric composition. When the cell width inferred from  $D_c/13$  is compared with that from a least-squares fit to the cell size data, the former is found to exceed the latter by only 15%. This

difference is less than the scatter associated with the cell width measurements. For lean compositions (i.e.,  $\sim 4\% \text{ C}_2\text{H}_4$ ), the same comparison reveals a discrepancy of about 100%. That is, the  $D_c/13$  line overpredicts the cell width by a factor of about two. It is quite possible that this is the result of having mistakenly identified the substructure as the controlling primary structure, bearing in mind the relatively small size of the smoked plates used in the field tests and the difficulty in discriminating between the substructure and the primary structure on smoke records produced by fuel-air detonations at atmospheric pressure (Figure 26). This claim is supported by the fact that, when the independent cell width measurements of Knystautas et al. (1982, 1983) are used in conjunction with the present critical tube diameters, the correlation is fair over the entire range of composition for which data are available.

Similar difficulties in interpreting the smoke records for lean propane-air detonations were encountered by Moen et al. (1983), but these authors may have identified the primary structure as substructure. Likewise, Benedick et al. (1983) may have incorrectly interpreted the structure produced by  $\text{H}_2$ -air and  $\text{C}_2\text{H}_4$ -air detonations in their experiments on the transmission from a two-dimensional channel to an unconfined space. Consequently, great care must be exercised in the interpretation of smoke records appropriate to fuel-air mixtures. Judging from the present results, those of Guirao et al. (1982) for hydrogen-air mixtures, and those of Moen et al. (1983) for acetylene-, ethylene-, ethane- and propane-air mixtures, the  $13\lambda$  correlation is likely valid for the less sensitive fuel-air mixtures. Thus, the nature of the critical balance between the global rate of chemical reaction and the rate of gasdynamic expansion, proposed in Chapter 2 to be associated with a spherical wave having a radius of about  $11.5\lambda$ , appears to be the same for fuel-oxygen and fuel-air detonations.

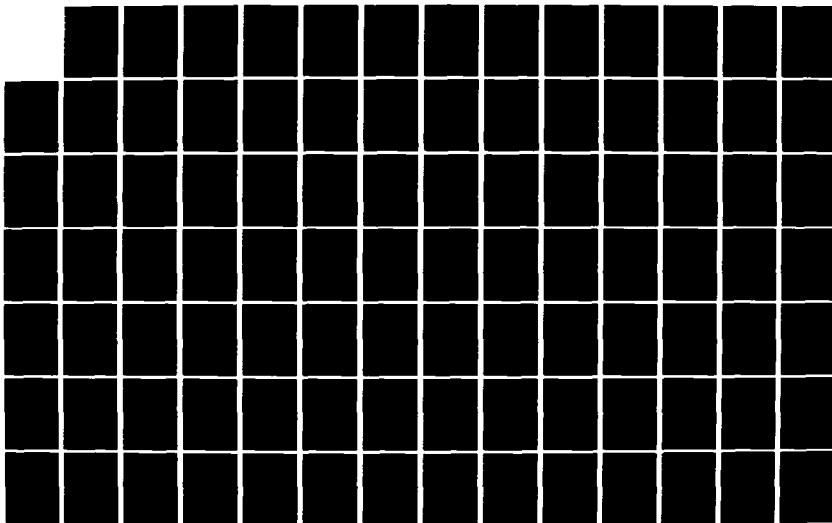
AD-A162 631

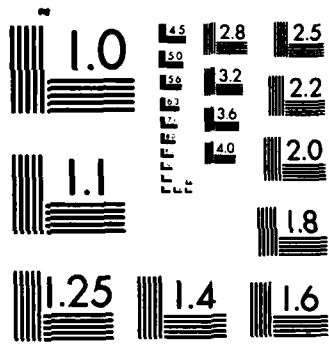
THE INFLUENCE OF INITIAL AND BOUNDARY CONDITIONS ON  
GASEOUS DETONATION WAVES(U) DEFENCE RESEARCH  
ESTABLISHMENT SUFFIELD RALSTON (ALBERTA) S B MURRAY  
SEP 85 DRES-SR-411 F/G 1974

2/4

UNCLASSIFIED

NL





MICROCOPY RESOLUTION TEST CHART  
NATIONAL BUREAU OF STANDARDS-1963-A

#### 4.0 THE INFLUENCE OF YIELDING CONFINEMENT ON LARGE-SCALE ETHYLENE-AIR DETONATIONS\*

##### 4.1 Introduction

In the previous two chapters, the critical conditions for transmission of detonation from one geometry to another were investigated. It was proposed that the critical condition in all cases was dictated by the same balance between the rate of gasdynamic expansion and the rate at which the reaction progresses in the cellular detonation front. This balance was expressed in terms of the ratio between the wave front curvature, which characterizes the rate of growth of the front (i.e., the gasdynamic expansion), and the cell size which characterizes the global reaction rate. A major diagnostic tool in these studies was the smoked surface which records the time-integrated history of triple-point motion at the front. Smoke records, however, provide no direct information about the history of the particles after they have entered the diverging front. Thus, the details of the expansion are not revealed. A configuration which is ideal for the study of the post-shock reacting flow is one involving the propagation of a wave in a tube having walls which yield under the influence of the high detonation pressure. Such a configuration has many advantages. First, the severity of the expansion can be regulated by varying the confining wall density and, hence, its acceleration under the influence of the gases inside the tube. Second the trajectory of the wall should be readily visible. Therefore, the expansion of the post-shock "stream tube" should be easy to quantify. Finally, in contrast to transmission problems, the global flow aft of the frontal shock is steady to an observer sitting on the shock, provided the tube is of constant cross section. This facilitates easy diagnosis and analysis. It is, of course, recognized that the flow is

---

\*The material described in this chapter has been presented at and accepted for publication under the same title in the proceedings of the Ninth International Colloquium on Dynamics of Explosions and Reactive Systems, held in Poitiers, France, July 1983. Authors: Murray, S.B. and Lee, J.H. Preliminary results were presented at the Spring Technical Meeting of the Combustion Institute (Canadian Section), held in Banff, Canada, May 1982.

locally three-dimensional and nonsteady. By "globally steady" it is meant that the time-averaged quantities at a specified location relative to the shock are constant. This approach is akin to the use of mean properties in the analysis of turbulent flow.

Investigations involving the interaction between gaseous detonation and yielding boundaries have been carried out by many researchers, but none have had the present purpose in mind. Sommers (1961) employed a cellophane wrap to separate an explosive mixture from a higher density confining inert gas but (wrongly) concluded that the presence of any solid boundary, no matter what its thickness, provides "infinite" confinement to detonations. Later, Dabora and colleagues (1963, 1965), realizing that this was not the case, calculated the thickness of, and manufactured thin membranes for the purpose of separating the explosive and boundary gases. However, these authors were specifically interested in the thickness of membranes which would not influence the post-shock expansion. Their objective was strictly to minimize diffusion at the explosive/inert interface. Vasiliev et al. (1972) have used cellophane tubes in an effort to identify the location of the sonic plane. More recently, the French have employed yielding tubes in shock and detonation studies, but they were more concerned with the dynamic response of the wall material (Brossard and Charpentier, 1976; Brossard and Renard, 1981; Aminallah, 1982). Bazhenova et al. (1981) have employed a variety of plastic detonation tubes in their study of heat transfer and boundary layer effects in the wake of the wave. Tarasenko (1974a, 1974b) has investigated the motion of metal walls confining high-explosive cylindrical charges and the influence of this motion on the rate of reaction. However, this author has not drawn quantitative conclusions due to the lack of knowledge about the thermodynamic properties, the rate of reaction and the equation of state for solid-phase explosives.

This chapter reports on the results of a large-scale study on the transmission of ethylene-air detonations from a rigid tube to a series of yielding polyethylene tubes of various wall thickness. Reinitiation of the wave exiting the rigid tube is seen to occur via the formation of reignition nuclei in the vicinity of the yielding tube wall. By calculating the motion

of the wall and making appropriate assumptions about the form of the kinetic rate equation and about the stability of detonation, it has been possible to identify the magnitude of the controlling chemical kinetic length in detonative propagation. The critical conditions for transmission appear to correlate well with the fractional increase in the area of a stream tube of particles entering the front, where such increase is evaluated over the proposed controlling chemical length.

#### 4.2 Experimental Details

The yielding wall tests were carried out using the same large-scale facility in which the critical tube diameter tests were conducted, but with minor changes. A photograph of the test section is shown in Figure 28. It consists of a round steel tube 7.82 m in length and 0.89 m in diameter, connected to one of several seamless, extruded, polyethylene tubes of the same diameter and about 10 m long. Tubes with three nominal wall thicknesses were investigated (1, 5 and 10 mil where a mil is 0.0254 mm). The corresponding measured area densities are given in Table I. These polyethylene tubes were supported by steel hoops 1.5 m apart. Ethylene gas (CP grade, 99.5% pure  $C_2H_4$ ) was again used as a test fuel. Particular care was exercised in calibrating the infrared analyzer and in monitoring the fuel concentration in this series of experiments so that the error was less than  $\pm 0.05\% C_2H_4$ .

In some of the tests, direct initiation of detonation at the ignition end of the tube was achieved using high-explosive PETN charges mounted on a plywood backing. In other tests, a sensitive slug of detonable mixture was used instead of a high-explosive charge. This slug was created by flowing oxygen and acetylene into a 0.89 m diameter plastic liner 1.5 m long, as shown in Figure 29. The sensitive mixture was separated from the test gas by a 1 mil thick polyethylene diaphragm placed over the end of the tube. Spark ignition of the sensitive mixture led to a detonation wave which, in turn, initiated detonation of the test mixture upon passing through the diaphragm.

As in the large-scale diffraction experiments, both piezoelectric pressure transducers (PCB 113A24) and ionization-gap probes were positioned along the tube. Probes were also mounted in each of the bag support hoops (see Figure 28) so that the detonation pressure and velocity could be measured in the yielding tube. The support hoops were made as small as possible to minimize their influence on the wave propagation. In addition to the two cameras employed in the critical tube diameter tests, a ruggedized "Fastax" (~5,000 frames per second) camera was mounted in a protective shelter (Figure 29) at the downstream end of the yielding tube so that it was looking through a plexiglass window along the axis of propagation. Also housed in the shelter was a microwave Doppler system (10.25 GHz) which was used in an effort to measure the velocity history of the ionized reaction front. It proved to be impractical in the present tests because the motion of other objects such as the yielding walls, the polyethylene diaphragm and the plywood end cap resulted in a signal which was difficult to interpret. Finally, 350 mm by 500 mm smoked plates were mounted near the exit end of the rigid tube in order to record the equilibrium cellular structure representative of the mixture.

A total of 17 tests were carried out.

#### 4.3 Experimental Results and Discussion

##### 4.3.1 Cell Width Measurements

All detonation velocities and pressures in the steel tube were within  $\pm 5\%$  of the corresponding C-J values, confirming that equilibrium propagation was established prior to the wave encountering the change in boundary conditions. Equilibrium propagation was further confirmed from smoke records. Cell measurements from these experiments are included along with those from the critical tube diameter tests in the graph of Figure 24. The same means of collection and interpretation of cell size data as described in Chapter 3 were applied. Most of the data from plastic strips shown in Figure 24 were obtained from the yielding tube tests since transmission from a rigid tube to a yielding tube of the same dia-



meter appeared to produce more uniform strips. A discussion about the difficulty in measuring cells appropriate to fuel-air detonations has already been presented in the previous chapter and will not be reiterated here. For the purpose of the correlations carried out in this chapter, the  $D_c/13$  line shown in Figure 24 will be assumed to describe the variation of the cell width with fuel concentration. Up to this point in the thesis, when the cell length  $L_c$  has been required in an analysis, the cell width-to-length ratio of 0.6 generally cited in the literature (e.g., Strehlow, 1970; Lee and Ramamurthi, 1976) has been used. However, the collection of measured aspect ratios presented in Figure 30 show that a higher value ( $\sim 0.7 - 0.8$ ) appears to be more appropriate for the ethylene-air system at atmospheric pressure. This observation is in agreement with the recent one by Bull et al. (1982) for stoichiometric hydrogen-air and acetylene-air mixtures, also at atmospheric pressure. In both cases, an aspect ratio near 0.7 was found to be appropriate. Consequently, in any future correlations applicable to fuel-air mixtures, the value of 0.7 will be used.

#### 4.3.2 High-Speed Cinematography of the Transmission and Propagation Phenomena

The contributions of this study centre around high-speed cinematographic records of detonation in the yielding tube which show the existence of a transient reinitiation phase followed by a steady propagation phase. These are discussed in detail below.

##### The Transient Reinitiation Phase

When the wave first emerges from the rigid tube, the head of the expansion propagates inward at sonic velocity  $C_{C-J}$  in the burned gases. This is felt over the entire front before it has moved a distance of about  $V_{C-J}R/C_{C-J}$  from the exit, where  $R$  is the tube radius. Since a typical value for  $V_{C-J}/C_{C-J}$  from equilibrium calculations is approximately 2, the distance in question is about one tube diameter. If the detonation wave does not act

to overcome the disturbance before travelling a distance of this order, it will be quenched. In the diffraction study, it was seen that, for transmission to an unconfined region, reinitiation occurs via the formation of reignition nuclei or "hot spots" near the edge of the detonation core. These evolve into expanding "detonation bubbles" which eventually coalesce to form a spherically diverging wave. Transmission of this type was found to be possible from the 0.89 m diameter tube for an ethylene concentration of 5.05%, corresponding to a cell width  $\lambda_s$  of about 68 mm. For transmission to a yielding tube, the gasdynamic gradients are milder so that reinitiation should be possible for less sensitive mixtures (i.e.,  $\lambda_s/\lambda < 1$ ) than that required for transmission to an unconfined medium. This is confirmed by the high-speed cinematographic records. A sequence from one such record is shown in Figure 31. In this case, transmission to a yielding tube having a 10 mil wall thickness is seen to be successful for a  $C_2H_4$  concentration of only 4.15%; that is, for a relative sensitivity  $\lambda_s/\lambda$  of only 0.41. In fact, there is no obvious reinitiation mechanism apparent in this sequence, indicating that conditions are well removed from criticality.

A distinct reinitiation mechanism is observed as the confinement is reduced or as the mixture is made less sensitive. Figure 32 shows a similar sequence of frames for transmission to a tube having a 5 mil wall thickness ( $\lambda_s/\lambda = 0.49$ ). The events in the sequence will be described with the aid of the schematic diagrams shown in Figure 33. The first frame shows the planar wave (P) just prior to exiting the rigid tube. In the second frame, a dark annular band (A) surrounding a luminous unattenuated circular core (C) is apparent. The inner boundary of the band marks the location of the head of the expansion (H) as it advances radially inward. A ring of luminous patches (L), bounded on the outside by the yielding wall and on the inside by the dark band, is seen to have formed in the wake of the expansion, indicating that a reinitiated wave has evolved from a locus of reignition centres (R) near the tube wall.

By the third frame of Figure 32, the renewed annular detonation has expanded transversely (T) inward, converging on the tube axis. The final frame shows a reestablished, more or less planar wave. This mode of super-

critical reinitiation is similar to that for transmission to an unconfined volume in that the number of reignition centres increases, while their location moves toward the tube exit as the mixture is made more sensitive.

Reignition near the boundary may be due to several factors. First, it may be induced by reflection of transverse wave remnants from the wall. Second, a thicker layer of shocked but unreacted gas exists near the wall since the expansion is initially most severe there. Thus, a minimum volume prerequisite for reignition is more likely to be satisfied. Third, a higher temperature may exist near the wall due to the presence of "X"-shaped compression waves behind the curved shock front (Fay and Opel, 1958; Edwards et al., 1963). Finally, small ripples or other irregularities in the polyethylene surface may give rise to localized shock reflections and thus hot spots.

Critical transmission to a yielding tube having a 1 mil wall thickness ( $\lambda_s/\lambda = 0.76$ ) is shown in the film sequence of Figure 34. In the first frame, a locus of reignition centres can be seen along part of the periphery of the tube. A small circular core of unattenuated planar wave can also be seen, although much of it is obscured by light emitting from the tube. In the second frame, a pair of circumferentially sweeping detonation waves has formed in the preheated gas behind the frontal shock. The rarefaction has also arrived at the axis so that a luminous central core is no longer visible. By the third frame, the reinitiated waves have swept over three quarters of the cross section but have fallen behind the front. Following the collision between these waves (Frame 4), the resulting overdriven detonation quickly catches up to the front to complete the reestablishment process. An end-on view showing the collision between two such sweeping waves appears in Figure 35. As in the supercritical case, there are similarities between this type of critical reinitiation and that observed for transmission to an unconfined region. As criticality is approached, for example, reignition occurs at fewer random and isolated locations. Another similarity is the formation of transversely sweeping waves which eventually engulf the decoupled front.

A side-on view of the above described critical reinitiation sequence, but at a much higher framing rate of approximately 18,000 frames per second, is shown in Figure 36. From this angle, it is apparent that the wave begins to curve upon entering the yielding tube. The curvature process begins at the edge and progresses inward. A similar observation was noted by Sommers and Morrison (1962) for the case of an oxyhydrogen detonation emerging from a confined channel into a column of detonable gas bounded by an inert gas. The trend of increasing curvature reverses in about the ninth frame of the sequence in which it is evident that the two reinitiated waves at the top and bottom of the tube are sweeping circumferentially toward one another and toward the camera. The collision between these waves occurs in the fifteenth frame, after which the resulting overdriven wave in the preconditioned mixture catches up to and coalesces with the front. The catch-up phase is complete by about the thirtieth frame.

Histories of the centreline axial velocity and global radius of curvature of the luminous reaction front, obtained from the cinematographic record, are shown in Figure 37. Measurements were taken with the aid of a "Telecomputing Corporation TELEREADDEX" film reader. Errors in velocity are due strictly to the difficulty in resolving the somewhat fuzzy outline of the front. Errors in the radius of curvature are due more to the subjectiveness in selecting a radius which best describes the mean curvature. Repeated measurements indicated a  $\pm 10\%$  variation to be typical. Initially, both the velocity and the radius of curvature decrease. These parameters approach a local minimum at about the time reignition nuclei are first observed. The subsequent sweeping of the reinitiated waves is accompanied by an increase in the radius of curvature and an approximately steady axial velocity. Such behavior is reminiscent of the so-called "quasi steady regime" observed in studies on direct initiation (e.g., Bach et al., 1969; Edwards et al., 1978). During the catch-up period which follows, the reaction front is asymmetrical and discontinuous, rendering curvature measurements unreliable. The velocity profile exhibits regular oscillations which dampen out as the reinitiated wave coalesces with the original front.

Similar oscillations have been noted in the high-explosive initiation studies by Bull et al. (1978) for ethylene-air mixtures and by Elsworth et al. (1983) for  $C_2H_6-O_2-N_2$  mixtures. The former authors have proposed that these "gallops" are indicative of the reaction zone attempting to couple with the shock front. The explanation provided by Ul'yanitskii (1980) may provide more insight into the phenomenon. This author claims that a "flash" can occur in the induction region between a shock wave and a decoupled reaction zone, leading to an overdriven detonation wave which catches up to the shock and drives it ahead. Perhaps it is possible that recoupling does not succeed on the first gallop and that subsequent attempts take place. This would explain the existence of several cycles.

If the velocity oscillations observed in the present tests are due to the above described mechanism, it should be possible to estimate the location behind the shock at which reinitiation occurs. For this purpose, the minimum of each velocity oscillation is assumed to correspond to the instant at which flashing occurs. The crest of each oscillation is assumed to be related to the period when recoupling is momentarily successful, prior to the reaction zone dropping back of the shock again. If the reinitiated wave in the decoupled region is considered to travel at the C-J velocity in the oncoming precompressed mixture, a simple calculation reveals that reignition occurs at a distance of  $1.3L_c$  behind the shock. This observation is consistent with an earlier one in Chapter 2. Recall that the distance between the diffracted wall shock and decoupled reaction zone was always about one cell length at the moment the transversely sweeping reinitiated detonation wave arrived at the back wall following spontaneous reinitiation. An interpretation of this observation was that reestablishment of the wave could not take place if the reaction zone fell behind the shock by more than one characteristic chemical kinetic distance.

The radius of curvature at which reignition occurs in the present tests (i.e.,  $\sim 5L_c$ ) is somewhat smaller than that observed in the case of transmission to an unconfined volume. One reason for this may be that the reaction front is more curved than the shock front due to more extensive shock/reaction zone decoupling near the edge of the yielding tube. Another

reason, in accordance with earlier discussion, may be that a favourable local perturbation exists in the vicinity of the tube wall. In fact, the cinematographic sequence of Figure 38, showing unsuccessful transmission, suggests that reignition would have taken place centrally and at a larger radius had such a perturbation been absent. In the second frame of the sequence, a ring of reignition nuclei are seen in the neighbourhood of the wall. However, by the third frame, these begin to diminish in luminosity as a second group of nuclei evolve near the axis where the gasdynamic gradients are milder. But these fade away as did the first nuclei. This cinematographic sequence suggests that, in cases of successful transmission, the usual spontaneous mode of reinitiation would probably occur at the expected critical spherical radius if the formation of reignition nuclei around the periphery could somehow be suppressed.

The critical conditions for transmission under various degrees of confinement are summarized in Figure 39 and in Table I. The case of transmission to an unconfined region is included for comparison. The dashed curve in Figure 39 will be discussed in a later subsection. The cell widths in Table I are based on the  $D_c/13$  line shown in Figure 24.

#### The Steady Propagation Phase

Velocity and pressure measurements confirm that propagation following reestablishment is steady at near C-J conditions as long as the mixture is considerably more sensitive than the critical one. The front is slightly curved and exhibits no time-averaged changes in either the luminosity or the scale of the cellular structure. Well above criticality, propagation is uninfluenced by the support hoops. However, as the mixture sensitivity for critical transmission is approached, the reestablished wave becomes very sensitive to perturbations such as the hoops. Figure 40 (a later continuation of the sequence shown in Figure 34) shows a wave encountering a hoop 3.4 tube diameters from the exit. Quenching is seen to occur around the periphery, followed by the formation of reignition nuclei which evolve into a renewed detonation front, in exactly the same manner as observed during transmission. This perturbation/recovery sequence repeats itself at each

hoop. It would appear that recovery from a noncritical perturbation is identical to supercritical reinitiation during transmission. Therefore, it is likely that recovery from a critical perturbation is identical to critical reinitiation during transmission. In this context, a test for critical transmission to a given confinement may be equivalent to determining the limiting perturbation that can be imposed on a wave propagating in that confinement; that is, to determining the propagation limits. Thus, the requirements for initiation (i.e., for transmission) and for propagation under a given set of boundary conditions may indeed be the same. This is certainly true on the scale of the cellular structure since propagation of the wave is possible through what appears to be an ongoing series of critical reinitiations at the end of successive cells.

In order to demonstrate that the critical conditions determined in the present tests represent the propagation limits and are not simply an artifact of the particular initiation source employed (i.e., the linear detonation tube), an additional test was carried out at the mixture composition required for critical transmission to one of the yielding tubes (4.15%  $C_2H_4$  for the 5 mil wall thickness), but using a disc of high-explosive PETN for an initiation source as shown in Figure 41. The mass of PETN employed was several times the mass required for critical initiation of spherical detonation. The cinematographic records showed that the wave failed suddenly upon encountering the first support hoop, having successfully propagated some 15 tube diameters. Therefore, we can conclude that the critical conditions do indeed represent the propagation limits.

The results in Table I show that, as the wall density tends to zero, the critical diameter for propagation in a free column of gas tends to the familiar critical tube diameter for transmission to an unconfined region. This result is in contrast to those of Vasiliev (1980) which suggest that the critical diameter of a free column is some 2 to 8 times the critical diameter for transmission. It is quite possible that the larger column diameter observed by Vasiliev is due to a turbulent interface between the test mixture and the surrounding air caused by the rapid withdrawal of the walls containing the test mixture. The only circumstance under which

Vasiliev's claim would be true is if the inert gas bounding the detonable column is of considerably lower density than the column itself. Conversely, it is suspected that the critical diameter for propagation in a free column could actually be reduced below the critical diameter for transmission if the inert boundary gas surrounding the column is of higher density than the explosive mixture. Some evidence of this has recently been noted in the field tests at Sandia (Guirao et al., 1982). Propagation in a hydrogen-air column surrounded by air was found to be possible for significantly fewer cells across the diameter than expected. This was attributed, in part, to the confinement effect of the higher density boundary gas.

The support hoops proved to be valuable in revealing additional information about detonation waves propagating under near limit conditions. In the case of the 1 mil wall thickness, the critical cell length (i.e.,  $L_C \approx 129$  mm) gives an effective hoop spacing of  $11.7L_C$  which allows the perturbed wave plenty of time to recover before a subsequent disturbance is encountered. In Figure 40, recovery would appear to be complete somewhere between the third and fourth frames. That is, between  $3.9L_C$  and  $7.6L_C$  downstream of the disturbance. As the tube wall thickness is increased to 10 mil, the critical cell length increases to 313 mm. The effective hoop spacing therefore decreases to about  $4.8L_C$  which apparently does not permit sufficient time for recovery between hoops. This is illustrated by the cinematographic sequence of Figure 42 in which each pair of frames ("a" and "b") shows the wave prior to, and subsequent to traversing a hoop. In short, each successive interaction degenerates the wave until it becomes a low-mode spinning detonation by the end of the tube (not shown in the figure). The velocity profile deduced from the film records shows both intense oscillations and a decreasing mean velocity over the 10 m length. This wave has been perturbed to extinction. The reason why a hoop spacing of about  $5L_C$  is critical can be understood from the velocity profile shown in Figure 37. The profile illustrates that, following a disturbance, reignition nuclei materialize at a distance of about  $5L_C$  downstream of the disturbance. This suggests that failure can be induced by perturbing the wave a second time, prior to the birth of reignition nuclei following an initial disturbance.



#### 4.3.3 Estimating the Magnitude of the Controlling Chemical Length

For a given gasdynamic field (i.e., a specified polyethylene wall thickness), it is possible to estimate the order of magnitude of the controlling chemical kinetic length in detonative propagation by making some assumptions about the form of the kinetic rate equation and about the stability of detonation. Since only the correct order of magnitude is sought, many simplifying assumptions will be made and a quasi one-dimensional approach will be taken.

##### A Criterion for Criticality

Bearing in mind that reignition appears to be favoured near the boundary, a criterion for criticality should logically be applied to particles near the tube wall which enter the shock and are subjected to an immediate expansion. Rather than committing ourselves to a specific chemical kinetic time (i.e., the one-dimensional induction time, the cell transit time, etc.), the controlling chemical kinetic time will simply be assumed of the usual form:

$$\tau = k [O_2]^a [C_2H_4]^b \exp(E/RT), \quad (4-1)$$

where  $\tau$  is in seconds and  $[O_2]$ ,  $[C_2H_4]$  and  $T$  are the oxygen and ethylene concentrations (moles/l) and the temperature (K) behind a shock propagating at the C-J velocity of the respective ethylene-air mixture. As in Chapter 3, these properties are calculated using the Gordon and McBride (1976) computer program assuming frozen chemistry and vibrationally-relaxed equilibrium conditions. The exponents  $a$  and  $b$  are taken from the proposed induction-time formula of Hidaka et al. (1974). However, instead of using Hidaka's value for the activation energy  $E$ , the value of 37.2 kcal/mole obtained from the curve fit to the critical tube diameter data (Chapter 3) is used.

The conditions for sustained propagation will be twofold. First, a particle must complete its chemical residence. That is,  $\int_0^t \tau^{-1}(t) dt$  must

reach unity at some time during the expansion. The second condition is a failure criterion, similar to the one advanced by Shchelkin (1959), which simply proposes that the chemical-gasdynamic coupling will not persist if the relevant chemical kinetic time increases by an amount on the order of itself; that is, if  $\Delta\tau \cong \tau$ . Hence, for a given particle thermodynamic history (i.e., a given wall thickness), the pre-exponential factor  $k$  can be varied until the chemical time is found for which the above integral reaches unity just prior to the failure criterion being satisfied. In his original work, Shchelkin was concerned with the growth of instabilities caused by the difference between the pressures in the post-shock and post-reaction zones. It was hypothesized that the hot but low-pressure combustion products, upon impinging on the higher pressure post-shock mixture, could cause expansion of the latter. The lower temperature of the expanded gas would then result in an increase in its induction time. In the present investigation, we are not concerned with the expansion resulting from the burned gases interacting with the shocked mixture, but rather with the expansion due to side relief.

#### The Particle Thermodynamic History

The particle thermodynamic history will be calculated by first determining the wall trajectory as it accelerates radially outward in the wake of the passing shock. We will consider a perfect, inviscid gas where the heat transfer to the wall and the skin friction are negligible. The coupling between the gasdynamics and the chemistry will be ignored. Resistance by the wall to motion will be due to inertia alone, material strength being ignored. This assumption is warranted since calculations show that, even at the yield strength of polyethylene, the heaviest wall is capable of exerting only a negligible counterpressure in comparison with the pressure driving the wall outward. Loss of the wall's integrity (tearing, for example) will be assumed to occur at later times than are of interest here. Since the wall trajectory does not vary with time to an observer attached to the shock, this is a globally steady, two-dimensional problem with rotational symmetry. It can thus be transformed into the unsteady, one-dimensional problem of an accelerating cylindrical piston. This approach is valid for small flow deflections and is identical to that used in computing hypersonic

flow over slender bodies. Dabora (1963) has used this approach previously with good success in a similar analysis. The radial position of the wall a distance  $x$  behind the shock in the real two-dimensional problem will be the same as that of the cylindrical piston after time  $x/V_{C-J}$ , as shown in Figure 43.

The one-dimensional piston motion will be calculated by the method first proposed by Meyer (1958). This author presents a means of solving the conservation equations, in characteristic form, applied to the particles immediately in front of, and behind the piston. For the present analysis, three modifications to Meyer's original formulation are required. These include: i) eliminating the reflected shock in his head-on impact problem and instead beginning with a quiescent high-pressure reservoir of equilibrium conditions consistent with those behind a C-J shock, ii) allowing for different ratios of specific heats  $\gamma$  on either side of the wall, and iii) adding an integral term to account for cylindrical divergence. Details of the analysis are given in Appendix B. The modified equation for the wall motion is:

$$\frac{du_r}{dt} = \frac{1}{m/A} \left\{ p_2 \left[ \frac{p_2 - \int_0^t \frac{c_b u_r}{r} dt - u_r}{p_2} \right]^{2\gamma_2/(\gamma_2 - 1)} - p_1 \left[ \frac{Q_1 - \int_0^t \frac{c_a u_r}{r} dt + u_r}{Q_1} \right]^{2\gamma_1/(\gamma_1 - 1)} \right\} \quad (4-2)$$

where  $m/A$  is the surface density of the wall material,  $u_r$  and  $r$  are the particle radial velocity and position,  $p$  is pressure,  $\gamma$  is the ratio of specific heats and  $c$  is sonic velocity. Subscripts 1 and 2 correspond to the initial low-pressure (atmospheric air ahead of the piston) and high-pressure (post-shock) states, respectively. Subscripts a and b refer to conditions immediately ahead of and behind the piston, respectively. The Riemann invariants  $P_2$  and  $Q_1$  are given by  $2c_2/(\gamma_2 - 1)$  and  $2c_1/(\gamma_1 - 1)$ . The above equation must be integrated numerically for  $u_r(t)$ .

It is not possible to resolve the wall motion at small distances behind the shock on the present photographic records. However, the motion can be resolved at much later times. As a check on the method, the trajectories

measured from film records were compared with those calculated using detonation parameters rather than post-shock parameters. As shown in Figure 43, even at ten tube radii behind the front, the measured radial position of the wall differs from the predicted one by only  $\pm 9\%$ . This gives us confidence in the early-time solution. A further check on the method was made by comparing the wall motion, as its density tends to zero, to the trajectory of a contact surface in a bursting cylinder problem. The latter was calculated (Thibault, 1983) using the flux-corrected transport computer code first developed by Boris (1976). For initial reservoir conditions corresponding to the detonation products of a stoichiometric ethylene-air mixture, Figure 44 shows that the two calculated trajectories differ by only 8% at a distance of seven tube radii behind the shock.

It must be borne in mind that the particle in the real problem does not experience as severe an expansion as indicated by the piston analysis since the particle is convected along with the shock rather than being fixed to the wall. This amounts to scaling the calculated results by a factor of  $V_{C-J}/u_s$  in time where  $u_s$  is the particle velocity relative to the shock.

#### Results of the Calculations

The calculated thermodynamic history of a particle at the edge of a tube having a 10 mil wall thickness is shown in Figure 45. The particle radial velocity and the post-shock pressure and temperature are plotted against normalized time  $t/\tau_0$  at the top of the figure. Here,  $\tau_0$  is the characteristic chemical kinetic time (based on the initial post-shock conditions) of a mixture which satisfies the criteria for sustained propagation outlined previously. This time was arrived at by varying the pre-exponential factor  $k$  until the value was found for which  $\int_0^t \tau^{-1}(t) dt \rightarrow 1$  as  $t \rightarrow 2\tau_0$ . The procedure is summarized graphically in the lower part of the figure where progress through reaction  $\int_0^t \tau^{-1}(t) dt$  is plotted against normalized time  $t/\tau_0$  for a range of assumed controlling chemical kinetic times (i.e., for different values of  $k$ ). For small chemical times, the

particle undergoes reaction before it is aware of an expansion, while for large chemical times, the expansion is so severe that the particle barely begins reacting. There is but one chemical kinetic time which satisfies the criteria for sustenance.

A summary of the calculations for the three severities of expansion investigated is shown in Table II. Columns 3 through 6 list the initial post-shock conditions as calculated by the Gordon-McBride (1976) chemical equilibrium computer code. Column 8 shows that the pre-exponential factors which satisfy the criteria for sustenance differ by only  $\pm 10\%$  about a mean value of  $2.21 \times 10^{-11}$  s·mole/l. This confirms the similarity of the chemical-gasdynamic dependence over the range of characteristic chemical kinetic times and gasdynamic expansion times investigated. Furthermore, as shown in column 9, the controlling chemical kinetic length is seen to be on the order of the cell length  $L_c$ . Intuitively, this makes sense since the very existence of detonation is due to a cyclic phenomenon characterized by precisely this streamwise length. Hence, our Shchelkin-like criterion may imply that, if a particle reacts after falling "out of phase" by an additional cycle, the periodic cellular mechanism breaks down. This is consistent with our earlier observation (Chapter 2) that the cell size approximately doubles prior to recovering from near critical perturbations.

#### 4.3.4 The "Stream Tube" Area Increase as a Means of Quantifying the Chemical-Gasdynamic Competition

Although the correlation described in Section 4.3.3 allowed the controlling chemical kinetic length scale to be identified, a fairly involved calculation of the particle thermodynamic history was required for a relatively simple geometry, even after neglecting many important details (e.g., the influence of the heat release on the thermodynamic profiles). The usefulness of such an approach for predicting critical conditions in situations of practical interest is therefore very limited. Rather than computing a detailed particle thermodynamic history for use in the kinetic rate equation, a more simplified means of expressing the chemical-gasdynamic competition is to evaluate the increase  $\xi$  in the cross-sectional area of a

"stream tube" of particles entering the front, as these particles migrate rearward of the shock through some appropriate chemical kinetic distance. This idea has been advanced by many investigators in the past (e.g., Jones, 1947; Fay, 1959; Dabora, 1963) but has not met with much success due to the difficulty in specifying the chemical kinetic length over which the area increase should be evaluated. Fay (1959), for example, suggested the use of either the "gross" thickness of the front, deduced from Schlieren photographs, or the mixture "relaxation" distance obtained from the one-dimensional chemical kinetic calculations of others (e.g., those of Kistiakowsky and Kydd, 1954). Since these early attempts, the universal cellular character of detonation has been revealed so that a reasonably well defined and measurable chemical kinetic length scale is now known to exist. With this in mind, and considering the results of the analysis in the previous section, the cell length  $L_C$  would appear to be a sensible choice for the characteristic chemical kinetic length. Perhaps, with this knowledge, the stream tube area concept warrants renewed consideration.

According to Fay (1959), the subsonic flow in a globally steady reaction zone adjusts so that each stream tube experiences the same fractional increase in area between the frontal shock and any streamwise location to the rear of the shock. In the case of the present yielding wall configuration, this means that the fractional increase in the area of each annular stream tube is equal to the fractional increase in the area of the yielding tube itself. Using the computed wall trajectories, the critical increases  $\xi$  in stream tube area for the 1, 5 and 10 mil polyethylene wall thicknesses are calculated to be 17.6%, 22.3% and 23.2%, respectively, evaluated over a particle path length equal to  $L_C$ . These calculations are summarized in Table III. It should be noted from the table that, for this purpose, the detonation parameters rather than the shock parameters have been used to calculate the wall trajectories. Having identified the controlling chemical kinetic length to be on the order of  $L_C$  from the correlation described in Section 4.3.3, the use of detonation parameters was felt to be warranted because these more closely reflect the average conditions existing within a region of that magnitude. The fact that the critical area increases  $\xi$  are all near 20% is encouraging evidence that the stream tube area concept,

incorporating the cell length as the relevant chemical kinetic distance, may be a viable means of describing the competition between the chemical energy release and the gasdynamic expansion occurring within the front.

If the 20% critical area increase continues to hold true as the wall density tends to zero, calculations of the above described type reveal that the minimum column diameter for unconfined propagation is about  $10\lambda$  (for  $\lambda/L_c = 0.7$ ). This compares with a critical diameter of about  $11\lambda$  if the contact surface trajectory computed numerically by Thibault (1983) is used instead (see Figure 44). These calculations support the earlier qualitative observation that, as the wall density tends to zero, the critical diameter for propagation in a cylindrical column approaches the critical diameter for transmission to an unconfined region. Similar calculations, covering the entire range of yielding wall densities  $m/A$ , are responsible for the dashed curve shown in Figure 39.

#### A Check on the Stream Tube Criterion Using Tapered Yielding Tubes

Experiments involving transmission to constant diameter yielding tubes suffer the drawback that several tests must be carried out in order to identify a single critical condition. This inconvenience could be avoided if either the mixture composition, the thickness of the yielding wall or the diameter of the yielding tube could be varied in the direction of propagation. Although the first two possibilities are difficult to implement from a practical point of view, the third option can be incorporated by simply tapering the yielding tube so that the relative expansion becomes more severe with increasing distance from the rigid tube exit. It was postulated that the behavior of the wave at any point along the tapered tube would not be unlike that in a constant area tube of the same local diameter as long as the taper was slight. By "slight" it is meant that the decrease in the tube area due to taper is small in comparison with the increase in area due to the outward motion of the wall. Four such tests were carried out in the field facility; two involving 5 mil thick polyethylene walls and two involving 10 mil thick polyethylene walls. Each tube was tapered from 0.89 m to 0.46 m in diameter over a 10 m length. Cinematography revealed that the

location of failure was not easy to identify because the failure process was a gradual one characterized by a gross spinning motion of the front, which increased in scale and accelerated as quenching was approached (somewhat like the sequence shown in Figure 42). Nonetheless, careful examination of the luminous front showed that, at a relatively well defined location prior to the commencement of spinning, there appeared reignition nuclei which formed repeatedly near the edges of the tube. Assuming the chemical-gasdynamic balance to be in jeopardy for the tube diameter corresponding to the earliest appearance of these reignition centres, the critical fractional increases in stream tube area have been calculated and are summarized in Table IV. The area increase  $\xi_m$  due to wall motion has been computed assuming constant local diameter. From this increase has been subtracted the area change  $\xi_t$  due to the reacting particles being convected down a converging duct. Note that the area decrease due to taper is an order of magnitude smaller than the area increase due to side relief, thereby confirming the "slight taper" assumption discussed above. In all but the third case shown in the table, the critical net area increase is seen to be very near the 20% increase noted earlier for tests involving constant diameter tubes. Inadvertently, the experiment involving a 10 mil wall thickness and an ethylene concentration of 3.80% was done with a lower fuel concentration than intended so that failure occurred immediately after the wave emerged from the rigid tube. In this case, the critical area increase could not be identified, but only an upper bound specified.

#### Other Support for the Stream Tube Criterion

Indirect evidence that the critical area increase of about 20% suggested above may apply more universally can be drawn from the recent field test data of Moen et al. (1983) on the methane-air system at stoichiometric composition. High-speed cinematography showed that transmission from a 1.83 m diameter rigid tube to a yielding polyethylene tube of the same diameter and having a nominal 6 mil wall thickness ( $m/A = 0.135 \text{ kg/m}^2$ ) was near critical, with failure occurring some two to three diameters from the rigid tube exit. Assuming the 20% critical area increase to hold, a calculation of the yielding wall trajectory indicates a cell length of



376 mm to be appropriate. If the cell aspect ratio of 0.7 found to be valid for ethylene-air mixtures is used for the stoichiometric methane-air mixture, the implied cell width  $\lambda$  is 263 mm. This value is in good agreement with that of  $280 \pm 30$  mm determined by Moen et al. (1983) from smoked plates and plastic strip measurements, and with that of  $310 \pm 50$  mm predicted by Bull et al. (1982) using a correlation between the cell size and the initiation energy.

Further indirect support for the existence of a critical 20% increase in stream tube area evaluated over the cell length can be drawn from the experience of Guirao et al. (1982) in their attempt to determine the critical hydrogen-air mixtures for transmission from tubes of 0.91 m and 1.21 m diameter. Initially, these authors assumed that the critical composition for transmission to an unconfined medium would be approximately equal to that for transmission to a polyethylene tube (100  $\mu$ m thick walls) of the same diameter. In other words, it was thought that the walls would have little influence on the transmission process. However, the field tests showed that transmission was possible for mixtures having cell widths about twice as large as had been anticipated (Lee, 1982). Although these tests were subsequently redone using larger diameter bags to simulate the unconfined region, the original data are of interest for the present purpose. If the 20% critical stream tube area increase is assumed to be valid, and if the density of the polyethylene used in the Sandia tests is the same as that of the material used in the present study, calculations of the type described above give critical cell lengths of 216 mm and 268 mm for transmission from tubes of 0.91 m and 1.21 m diameter, respectively. Assuming the cell aspect ratio  $\lambda/L_c$  of 0.7 observed by Bull et al. (1982) for stoichiometric hydrogen-air to hold for off-stoichiometric compositions, the implied cell widths are 151 mm and 188 mm. These cell widths are 2.15 times and 2.02 times greater than those required for transmission to an unconfined region (assuming  $\lambda = D_c/13$  to be valid). The calculations therefore substantiate the experimental observations.

#### 4.4 Summary

Large-scale tests on the transmission of lean ethylene-air detonations from a rigid tube to yielding polyethylene tubes of the same diameter (Figure 28) have shown that reinitiation of the emerging wave is via a circular locus of reignition nuclei which form in the vicinity of the yielding tube wall (Figure 32). These nuclei give rise to detonation bubbles which reestablish the wave globally by sweeping transversely through the gas bounded by the decoupled shock wave and the reaction zone. In the critical case, this reinitiation phenomenon is not unlike the one observed in tests to determine the critical initiation energy in that both are characterized by a critical radius of wave front curvature, a quasi steady regime in velocity and a "galloping" behavior which may be indicative of the reaction zone attempting to couple with the shock front as proposed by Bull et al. (1978). Following near critical transmission to a given polyethylene tube, the wave is seen to be very sensitive to boundary induced perturbations and, in particular, to the thin steel hoops used to support the tube (Figure 40). Cinematographic records show that a wave, once disturbed, can be quenched if it is perturbed a second time before reinitiation has commenced following the initial disturbance (Figure 42). For this reason, a critical hoop spacing of about five cell lengths appears to exist.

A simple correlation has been done to estimate the order of magnitude of the controlling chemical kinetic length in detonative propagation. The first step in the analysis is to compute the post-shock thermodynamic history of a particle adjacent the tube wall since reignition appears to be favoured there. For this purpose, the wall motion is considered to be analogous to that of a cylindrical piston accelerating radially outward under the influence of the high-pressure, post-shock mixture (Figure 43). The piston motion is calculated using a variation of the approximate method proposed by Meyer (1958). Concerning the energy release, the controlling chemical kinetic time  $\tau$  is assumed to be of the standard form:

$$\tau = k [O_2]^a [C_2H_4]^b \exp(E/RT), \quad (4-1)$$

so that in a nonsteady gasdynamic field the particle completes its chemical residence when  $\int_0^t \tau^{-1}(t) dt + 1$ . If it is further stipulated that this must occur before the chemical kinetic time increases by an amount on the order of itself (i.e., a Shchelkin-like failure criterion), there is but one pre exponential factor  $k$  which satisfies the dual criterion for sustenance. For the three different polyethylene wall thicknesses investigated, the pre-exponential factors emerging from the analyses are found to be nearly equal (Table II), thus confirming the similarity of the critical chemical-gasdynamic balance over the range of chemical kinetic and gasdynamic expansion times involved. Furthermore, the analyses give controlling chemical kinetic lengths which are of the same magnitude as the experimentally observed critical cell lengths.

A simplified means of quantifying the chemical-gasdynamic competition is via the "stream tube" area increase, as first proposed by Jones (1947). In this approach, the increase is evaluated in the cross-sectional area of a stream tube of particles entering the front, as these particles migrate rearward from the shock through some appropriate chemical kinetic distance. Assuming the cell length  $L_c$  to be the appropriate chemical kinetic length, as suggested by the results from the above described correlation, the critical fractional increases  $\xi$  in the stream tube area are found to be about 20% for the three polyethylene wall thicknesses employed (Table III). This value is confirmed by the results from four additional tests involving transmission to tapered polyethylene tubes of continuously decreasing diameter (Table IV). For these experiments, it was possible to identify the failure diameter from cinematographic records.

Indirect evidence that the critical area increase of 20% may apply more universally can be drawn from the results of other investigators. For example, Moen et al. (1983) have found that transmission from a 1.83 m diameter rigid tube to a polyethylene tube (density of wall material  $m/A = 0.135 \text{ kg/m}^2$ ) of the same diameter is near critical for a mixture of stoichiometric methane and air. Assuming the 20% critical area increase to

be valid, calculations of the present type indicate a cell width of 263 mm to be appropriate. This value is in good agreement with that of  $280 \pm 30$  mm measured by Moen et al. (1983) from smoked plates and plastic bag strips. It also agrees with the cell width of  $310 \pm 50$  mm estimated by Bull et al. (1982) using a correlation based on critical initiation energy data. Additional support for the stream tube criterion is provided by the observations of Guirao et al. (1982). These authors, in their attempt to determine the critical tube diameter for hydrogen-air mixtures, initially studied transmission from rigid tubes of 0.91 m and 1.21 m diameter to polyethylene tubes ( $m/A = 0.088 \text{ kg/m}^2$ ) of like diameter. Assuming the 20% critical area increase to again be valid, the present calculations show that transmission should be possible for cells 2.15 and 2.02 times larger, respectively, than those required for transmission from the same tubes to an unconfined volume. This factor of approximately two in critical cell size was indeed noted experimentally (Lee, 1983), thus adding credibility to the notion of a universal 20% critical stream tube area increase, evaluated over a particle path length of  $L_c$  relative to the shock.

Both the experimental results and the calculations show that, as the density of the yielding wall tends to zero, the critical diameter for propagation in a "free" column of gas tends to about  $10\lambda$ ; i.e., it approaches the familiar critical tube diameter for transmission to an unconfined region (Figure 39). This result is in disagreement with the observation by Vasiliev that the critical diameter for propagation in a free column is some 2 to 8 times that for transmission to an unconfined space. It is thought that the larger column diameter observed by Vasiliev is due to a turbulent interface between the test mixture and the surrounding air which reduces the effective diameter of the column.

## 5.0 THE INFLUENCE OF YIELDING CONFINEMENT ON THE VELOCITY OF PROPAGATION OF GASEOUS DETONATION WAVES\*

### 5.1 Introduction

In the previous chapter, it was proposed that the critical condition for sustained propagation could be expressed in terms of a maximum tolerable stream tube area increase  $\xi$ , evaluated over a distance equal to the cell length  $L_c$ . Owing to the perturbing nature of the thin steel hoops supporting the yielding tube, a steadily propagating wave could not be observed except under conditions well removed from criticality. Consequently, phenomena which are generally characteristic of propagation under supercritical but near limit conditions were not studied. One such phenomenon is the velocity deficit. Numerous investigations have revealed that detonation waves propagate at a velocity  $V$  somewhat below the theoretical value  $V_{C-J}$  when conditions are more favourable than the critical ones.

Velocity deficits were first studied in connection with the design of high-explosive cylindrical charges. Jones (1947), for example, advanced a theory which proposed that the deficit resulting from radial expansion in the reaction zone of the wave is proportional to the reaction-zone length and inversely proportional to the charge diameter. Later, Sommers (1961) and Sommers with Morrison (1962) attempted to gain some insight into the interaction between a condensed-explosive charge and a compressible boundary (i.e., the charge casing) by studying the analogous problem of a gaseous column of explosive mixture bounded by a compressible inert gas. Dabora (1963) measured velocity deficits in a similar apparatus and proposed a simple theory to relate the deficit to the increase in the flow area within the

---

\*The bulk of the material in this chapter was presented and well received at the Paul Vieille Scientific Meeting, held at the Centre de Recherches du Bouchet, Vert-le-Petit, France, 26 - 27 September, 1984. A paper has also been submitted for presentation at the Tenth International Colloquium on Dynamics of Explosions and Reactive Systems, to be held in Berkeley, California in August of 1985. Authors: Murray, S.B. and Lee, J.H.

reaction zone. However, as was the case in attempting to quantify the critical conditions (Chapter 4), the choice of an appropriate "reaction-zone" length over which to evaluate the area increase was not an obvious one.

Another scenario in which velocity deficits have been measured extensively is that involving detonations propagating in tubes with nonyielding walls. Deficits have been measured in smooth round tubes covering a large range of diameters and mixture compositions (Mooradian and Gordon, 1951; Kistiakowsky et al., 1952a, 1952b; Manson and Guénoche, 1957; Edwards et al., 1963; Brochet, 1966; Pujol, 1968; Renault, 1972). Similar investigations have been carried out using smooth tubes of rectangular cross section (Edwards et al., 1963; Boisleve, 1970; Renault, 1972). Shchelkin (1947) and Kistiakowsky et al. (1952b) have measured velocity deficits in tubes having walls which were roughened by the installation of helical spirals into the tube. It has been customary for experimenters to plot the propagation velocity against the reciprocal of the characteristic transverse dimension of the tube, and to extrapolate to infinite tube size in order to estimate the velocity of the wave in an unconfined space.

Along theoretical lines, the problem of velocity deficits has been addressed by many investigators (e.g., Zel'dovich, 1940; Tsugé, 1971; Dove et al., 1974). Fay (1959) has been most successful in this regard. This author proposed that, in a tube with nonyielding walls, the stream line divergence within the reaction zone is a result of the negative displacement thickness (in shock-fixed coordinates) associated with the growth of viscous boundary layers on the walls of the tube.

In the previous chapter, it was remarked that the past lack of success with the stream tube area concept was due to our inability to identify the relevant chemical kinetic length scale in detonative propagation. It was demonstrated that, when the cell length was chosen to be the characteristic chemical distance, the stream tube area concept was quite successful in the quantification of the critical chemical-gasdynamic balance. The contributions of the study to be described in this chapter centre around smoke record observations and velocity deficit measurements in a detonation tube

of square cross section, consisting of a combination of rigid and yielding walls. The gasdynamic expansion is regulated by varying the density and, to a larger extent, the number of yielding walls. The results show that the stream tube area increase, based on the cell length, is as successful a concept for describing the phenomenon of velocity deficits as it is in quantifying the critical conditions.

## 5.2 Experimental Details

The apparatus illustrated in Figure 46 and photographed in Figure 47 consists of three components: 1) an initiator section, 2) a linear detonation tube, and 3) a test section. The initiator section is a hollow steel cylinder, 492 mm in length, filled with a detonation sensitive mixture of equimolar oxygen and acetylene at atmospheric pressure. Following spark ignition of this mixture, the resulting detonation transmits through an open ball valve to the test mixture in the adjacent linear tube. The valve separates the mixtures until moments before ignition. The transmitted wave in the square tube (62 mm by 62 mm) is allowed to equilibrate over a 1640 mm length before emerging into one of three interchangeable test sections (Figures 46b to 46d). Each test section has been manufactured from square tubing similar to that noted above. In one case, a single steel wall has been milled from the tube leaving a three-sided channel open at the top. In a second case, a pair of parallel walls has been removed. In yet a third case, three walls have been machined away leaving rigid confinement on only one side. Having removed one or more of the steel walls, the remaining structure has been appropriately reinforced as illustrated in Figure 46.

In preparation for an experiment, each rigid boundary which has been removed is replaced by one of five thin yielding materials. These materials include a paraffin coated paper (A), a common variety of stationery paper (B), a polyethylene plastic and two types of high-strength acetate plastic (A and B) often used in the making of shock tube diaphragms. The measured surface density of each material is given in Table V. In most of the experiments, the paraffin coated paper or one of the acetate plastics was employed. Since the investigation was carried out in the laboratory, the

test section had to be enclosed within a protective vessel. A large diameter cylindrical pipe mounted on a trolley was used for this purpose (see Figure 47).

The test mixture was stoichiometric oxygen and acetylene with nitrogen dilution (i.e.,  $2C_2H_2+5O_2+5\beta N_2$  with  $3.5 < \beta < 6.5$ ) at atmospheric pressure. The flow rate of each gaseous component was monitored by measuring, with a manometer, the pressure drop across a small bore capillary tube. A bubble tube technique was employed to calibrate the flow system. At least five volumes of the apparatus were flushed through with the test mixture once the correct individual flow rates were established.

A series of nine piezoelectric pressure transducers (PCB 113A24) were positioned along the apparatus. Signals from four such transducers (two in the linear tube and two in the test section) were displayed on a pair of oscilloscopes. An additional transducer in the linear tube was used to trigger the oscilloscopes and to start a series of time interval counters having nanosecond resolution. Signals from the four remaining transducers in the test section were used to stop the time interval counters. The measured times of arrival enabled the mean wave velocities between neighbouring transducers to be calculated. The other diagnostic technique was the smoked plate, made by applying a thin layer of soot to a white enamelled metal sheet. This sheet was subsequently positioned on one of the nonyielding walls of the test section, as shown in Figures 46b to 46d.

The experimental procedure was simply to carry out a series of "GO" - "NO-GO" tests for a given set of boundary conditions until the critical mixture composition for successful propagation was identified. Additional tests were then conducted with more sensitive mixtures in order to determine the velocity deficits under supercritical conditions.

A total of 50 experiments were carried out.



### 5.3 Experimental Results and Discussion

#### 5.3.1 Cell Width Measurements

Pressure measurements and velocities deduced from the transducers in the linear tube showed that an equilibrium C-J detonation existed prior to the wave encountering the change in boundary conditions. Equilibrium propagation was further confirmed by the smoke records located just prior to the exit from the rigid tube to the test section. A plot of the cell width  $\lambda$  versus the mixture composition, expressed in terms of the dilution ratio  $\beta = [N_2]/[O_2]$ , appears in Figure 48. Included on the graph are the cell widths measured from the smoked plates used to line one of the nonyielding walls of the test section. In cases where transmission and subsequent propagation were successful, there was no noticeable difference between the scale of the cellular structure in the rigid tube and in the test section. The data for compositions near acetylene-air (i.e.,  $\beta = 3.76$ ) are in good agreement with the direct measurements of cell size by Knystautas et al. (1982), Bull et al. (1982) and Moen et al. (1983). Estimates of the cell width based on the  $13\lambda$  correlation and the critical tube diameter measurements of Knystautas et al. (1982), Freiwald and Koch (1963), Zeldovich et al. (1956) and Moen et al. (1983) are included for off-stoichiometric compositions. The line through the data is a prediction based on the assumption that the cell width  $\lambda$  varies with the mixture composition in accordance with a standard induction-zone length expression of the form:

$$\lambda = k u_s [O_2]^a [C_2H_2]^b \exp(E/RT) \quad (5-1)$$

where  $\lambda$  is in meters and  $u_s$ ,  $[O_2]$ ,  $[C_2H_2]$  and  $T$  are the post-shock particle velocity relative to the shock (m/s), the oxygen and acetylene concentrations (moles/l) and the temperature (K) behind a shock propagating at the C-J velocity of the respective  $C_2H_2-O_2-N_2$  mixture. All post-shock properties are calculated using the Gordon and McBride (1975) computer program assuming frozen chemistry and vibrationally-relaxed equilibrium conditions. Exponents  $a$  and  $b$  are taken from the proposed induction-time formula of

White (1967). However, instead of using White's activation energy of 17.3 kcal/mole, the value of 27.5 kcal/mole suggested by Bjerketvedt et al. (1981) has been adopted. Using this higher activation energy, these authors were successful in predicting the variation of the critical tube diameter with dilution ratio for compositions ranging between acetylene-oxygen and acetylene-air. With a reference cell width of  $\lambda = 9.5$  mm at  $\beta = 3.76$ , the pre-exponential factor  $k$  can be evaluated and used to predict the cell width over the entire range of  $\beta$ . The reference cell width of 9.5 mm represents an average of the values reported by Knystautas et al. (1982), Bull et al. (1982) and Moen et al. (1983) for the stoichiometric acetylene-air mixture.

As shown in Figure 48, the prediction describes the trend of the data quite well over the entire range of compositions for which data are available. This is a bit surprising in view of the fact that Bjerketvedt et al. (1981) used post-shock temperatures based on constant gamma, whereas the present correlation employs vibrationally-relaxed post-shock states (i.e., lower temperatures). The curve in the figure will be used as a reference for the cell width in the correlations to be described later. When the cell length  $L_c$  is required, the aspect ratio  $\lambda/L_c$  of 0.7, apparent from the data of Bull et al. (1982) for stoichiometric acetylene-air, will be assumed to hold for the more highly diluted  $C_2H_2-O_2-N_2$  mixtures used in the present experiments.

### 5.3.2 The Transmission Phenomenon

In the study involving the transmission of ethylene-air detonations from a rigid circular tube to yielding polyethylene tubes of the same diameter (Chapter 4), an initial transient reinitiation phase followed by a steady propagation phase were both observed. Figure 49 shows a comparison between the reinitiation phenomenon proposed from the cinematographic records from the large-scale experiments and that evident from the smoke records in the present laboratory study. The smoke record shown in the figure was situated on the side wall of a channel having three rigid boundaries and a yielding top (i.e., the test section shown in Figure 46b). There is clear evidence on the record that reinitiation (R) took place near

the yielding boundary, leading to an overdriven detonative Mach stem which decayed in strength while growing in height. This renewed detonation front (L) expanded transversely inward (T) until it occupied the entire cross section of the channel a distance of about 2.3 channel widths from the exit. The smoke record confirms that the essential details of the reinitiation phenomenon are as proposed from the cinematographic records.

### 5.3.3 Critical Conditions for Propagation

Figure 50 consists of a collection of smoke records from the side wall of a channel consisting of three rigid walls and a yielding top. The records appear in order of decreasing mixture sensitivity from top (A) to bottom (I). The direction of propagation is from left to right. The first six records, for  $4.25 < \beta < 6.13$ , show successful propagation of the wave from one end of the test section to the other without any apparent cell size gradient in either the transverse or longitudinal directions. The absence of a longitudinal gradient in cell size suggests that the wave has quickly adjusted to the newly imposed boundary conditions and has resumed propagating in an equilibrium fashion. The lack of a transverse gradient in cell size may be evidence to support the hypothesis of Fay (1959) that the flow in the subsonic region adjusts so that each stream tube experiences the same fractional increase in cross-sectional area between the frontal shock and any streamwise location aft of the shock. Another point of interest is that there is no measurable difference between the scale of the cellular structure observed in the rigid tube and that observed in the test sections. Thus, the structure of the frontal shock complex appears to be independent of the severity of the post-shock expansion, provided sustained propagation is possible. This is consistent with the fact that, for a diverging detonation wave where the post-shock expansion is continuously decreasing in severity with increasing radius, multiplication of cells occurs at a rate required to maintain the equilibrium cell size.

The records labelled G through I in Figure 50, for  $6.25 < \beta < 6.50$ , show that the wave is not capable of coping with the expansion once the global rate of reaction drops below some critical rate; that is, once the

detonation cell exceeds some critical size. From the figure, it would appear that smoke record G corresponds to the critical conditions. Note that the failure process is characterized by an approximate doubling of the cell size. A similar observation was noted in the earlier study (Chapter 2) on the transmission of planar detonation from a rigid tube to cylindrical detonation expanding radially outward between a pair of parallel plates. In that investigation, the cell size was seen to approximately double prior to the wave recovering from a near critical disturbance or prior to the onset of critical reinitiation. If the cell length  $L_c$  is considered to be the controlling chemical kinetic length associated with the front, the above noted observation supports the hypothesis of Shchelkin (1959) that the front loses stability if the relevant chemical kinetic time increases by an amount on the order of itself.

Having identified the critical mixture composition and the corresponding cell length  $L_c$ , the critical stream tube area increase  $\xi$  can be evaluated in a manner similar to that described in the previous chapter. The only difference is that the geometry is not axisymmetric as it was in the large-scale experiments. For the purpose of evaluating the area increase, each yielding wall is assumed to be displaced laterally outward so that it remains parallel to its initial orientation. Corner effects are ignored. As in Chapter 4, the wall trajectory is obtained by first transforming the real, two-dimensional, steady-flow problem into one involving the unsteady, one-dimensional motion of a piston. Meyer's (1958) approximate method is again used to obtain the distance-time history of the piston.

A summary of the calculations appears in Table V. For a single yielding wall, the results for the paraffin coated paper (A) and both acetates (A and B) reveal critical fractional area increases slightly below the value of about 20% noted from the large-scale experiments. An insufficient number of tests was carried out to determine the critical conditions for a single yielding wall made of either polyethylene or paper (B). For two yielding walls made of acetate (A), the critical area increase  $\xi$  is again close to 20%. However, for experiments involving two or three yielding walls consisting of paper (A), the calculated area increases are well below 20%.

With this wall material, it was noted that the critical conditions were not repeatable from one test to the next. Furthermore, the outcome was seen to be dependent on the elapsed time between the termination of flowing gas and the initiation procedure, suggesting that diffusion through the wall material was likely the problem. This suspicion was confirmed from the smoke records which showed that the actual cell size was considerably larger than the anticipated one based on the known gas flow rates and the reference graph of cell width versus dilution ratio shown in Figure 48. Using the actual cell size instead of that corresponding to the assumed mixture composition, the calculations for these two cases have been redone. The results, which appear in the table as bracketed quantities, are in better agreement with those from the other experiments.

Note that, for a yielding wall density tending to zero, the test section illustrated in Figure 46b (i.e., yielding confinement on the top only) could be used to determine the minimum thickness for propagation in a cloud sitting on the ground. Equivalently, the minimum thickness of a detonable layer of gas bounded by air on both the top and the bottom could be determined using the test section pictured in Figure 46c (i.e., yielding confinement on two parallel sides). This approach assumes, of course, that jetting at the corners is negligible. Although experiments of these types were not carried out, the likely results can be predicted by the same kind of calculation used to estimate the critical diameter for propagation in a cylindrical column surrounded by air (Chapter 4). When this is done for the stoichiometric acetylene-air mixture, the critical thickness of a cloud sitting on the ground is found to be about  $2.5\lambda$  (for  $\lambda/L_c = 0.7$ ). This result is consistent with the observation by Dabora (1963) that the minimum thickness of an oxyhydrogen layer in a three-sided channel bounded on the top by nitrogen is about 4.7 mm at atmospheric pressure. Using the cell width of 1.65 mm inferred from the  $13\lambda$  correlation and the critical tube diameter data of Matsui and Lee (1979), the minimum cloud thickness evaluates to  $2.8\lambda$ .

### 5.3.4 The Behavior of the Wave Under Supercritical Conditions

#### Velocity Deficits and the Stream Tube Area Increase

Under supercritical conditions, the wave propagates the length of the test section at a velocity  $V$  lower than the theoretical velocity  $V_{C-J}$ . That is, it propagates with a velocity deficit  $\Delta V/V_{C-J} = (V_{C-J} - V)/V_{C-J}$ . Figure 51 shows experimentally measured velocity deficits from the present tests plotted against the corresponding calculated increases in the stream tube area  $\xi$ , evaluated over one cell length. Open symbols denote the deficits determined from oscilloscope traces, while shaded symbols signify the deficits based on measurements from the time interval counter. The scatter in the data is due partly to errors in the measurement of the elapsed times, particularly for the cases involving oscilloscope traces. The scatter may also be due to the three-dimensional pulsating nature of the front which could introduce variations in the elapsed time between neighbouring transducers. The curve through the data is based on Dabora's (1963) version of Fay's (1959) "nozzle" analysis. Briefly, the conservation equations are solved for flow through a quasi one-dimensional reaction zone with heat addition and area increase. The gas is assumed to be calorically and thermally perfect, and the heat release is assumed to be the same whether there exists an area change or not. If the pressure prevailing throughout the reaction zone is assumed to be close to the C-J pressure, the analysis gives the following expression for the velocity deficit:

$$\frac{\Delta V}{V_{C-J}} = 1 - \left[ \frac{(1 - v)^2}{(1 - v)^2 + \gamma_2^2 (2v - v^2)} \right]^{1/2} \quad (5-2)$$

where  $v = \xi/(1 + \gamma_2)/(1 + \xi)$ . Here,  $\gamma_2$  is the ratio of specific heats of the detonation products. A detailed description of Dabora's velocity deficit analysis is given in Appendix C.

The curve plotted in Figure 51, corresponding to Equation (5-2) and a typical value of  $\gamma_2 = 1.2$ , is seen to describe the trend of the present data

quite well. If we had chosen a smaller characteristic chemical kinetic length (e.g., the induction-zone length) over which to calculate the area increase due to the motion of the yielding walls, the data would have fallen well below Dabora's (1963) theoretical line. On the other hand, had we selected the hydrodynamic thickness of the wave [i.e.,  $\sim 2 - 4$  cell lengths according to Edwards et al. (1976b)] over which to compute the area increase, the data would have sat well above Dabora's curve. From this observation, we can draw the important conclusion that the three-dimensional, nonsteady cellular front can be treated satisfactorily in a one-dimensional sense if it is assumed to have an effective thickness of  $L_C$ . In essence, the good correlation between the data and the theoretical curve is independent evidence that our selection of  $L_C$  as the controlling chemical kinetic length in detonative propagation is probably correct.

It should be noted that the existence of an area increase implies a deficit in other detonation parameters as well (e.g., the C-J pressure, temperature, etc.). These parameters are important in the present study because the motion of the yielding walls depends on them. An iterative approach must be taken in order to arrive at the area increase and the sonic conditions which are interconsistent. This approach has been adhered to in the computations carried out in Chapters 4 and 5. The calculation of these "modified" sonic conditions is described in Appendix C.

#### Velocity Deficits Reported by Other Investigators

Figure 52 shows a similar plot of  $\Delta V/V_{C-J}$  versus  $\xi$  for the data reported by several other authors. These data cover a wide range of mixture composition, initial mixture pressure, geometry and mechanism responsible for the expansion. Included are the data of Edwards et al. (1963), Brochet (1966) and Renault (1972) for deficits resulting from viscous boundary layers in rigid circular tubes. Also shown are the related data of Boisleve (1970) and Renault (1972) for boundary layer growth in rigid tubes of rectangular cross section. For the above configurations, the boundary layer displacement thickness  $\delta^*$  estimated by Fay (1959) using Gooderum's (1958) boundary layer correlation has been used:

$$\delta^* = 0.22x^{0.8} (\mu_e/\rho_1 u_1)^{0.2} \quad (5-3)$$

where  $\rho_1$  and  $u_1$  are the density and the velocity of the gas entering the front, and  $\mu_e$  is the dynamic viscosity of the gas at the edge of the boundary layer a distance  $x$  behind the front. The viscosity, assumed to be that corresponding to the C-J temperature, was taken from West and Astle (1979). When data were not available for the temperature range of interest, the viscosity was estimated by fitting a curve of the form suggested by Sutherland [e.g., see Chapman and Cowling (1970)] to the available data and subsequently extrapolating to the temperature required.

The results from Dabora (1963) shown in Figure 52 are for a rectangular column of gas bounded rigidly on three sides and by an inert compressible gas on the remaining side. For the purpose of calculating the stream tube area increases, the explosive/inert interface deflection angles computed by Dabora have been used. The influence of boundary layer growth on the three confining walls has also been accounted for using the displacement thickness correlation described above. It should be noted that the data of this author have been reprocessed so that the deficits are now quoted with respect to the theoretical velocity rather than to the measured velocity in a tube of the same dimensions but with no side relief. In fact, two velocity deficits have been deduced from each of Dabora's data points; one related to only the boundary layer growth in the rigid channel, and the other related to the compressibility of the inert boundary gas in conjunction with boundary layer growth on the rigid walls.

The cell sizes required for the above described calculations have been obtained from various sources. Those for low-pressure stoichiometric  $C_3H_8-O_2$  and  $C_2H_4-O_2$  mixtures, and for the stoichiometric  $H_2-O_2$  mixture at atmospheric pressure, have been deduced from the  $13\lambda$  correlation using the critical tube diameter data of Matsui and Lee (1979). The  $13\lambda$  correlation has also been employed to estimate the cell size for the stoichiometric  $C_3H_8-O_2-N_2$  system at one atmosphere, but using the critical tube diameter



data reported by Knystautas et al. (1982). To the author's knowledge, no cell size data are available for off-stoichiometric  $H_2-O_2$  mixtures at atmospheric pressure. However, estimates have been made based on the stoichiometric  $H_2-O_2$  cell size and the assumption that the ratio of the cell size to the induction-zone length is independent of composition. For this purpose, the induction-time formula of Schott and Kinsey (1958) has been used:

$$\log_{10} (\tau [O_2]) = -10.647 + 3966/T \quad (5-4)$$

where  $\tau$  is in seconds and  $[O_2]$  and  $T$  are the post-shock oxygen concentration (moles/l) and the temperature (K), respectively.

When the velocity deficit data reported by Boislevé (1970) and Renault (1972) were initially plotted, it was found that the intercept did not pass

through zero as the area increase  $\xi$  tended to zero. In the plot of Figure 52, these data have been shifted downward by a fixed amount (on the order of one percent as shown in the inset tables of Figure 52) deemed necessary in order to recover the intercept. It is felt that this procedure can be justified in terms of the experimental error. In fact, the results reported by these two authors for identical mixtures in identical tubes differ by about one percent.

As was the case in Figure 51, the theoretical line given by Dabora (1963) describes the trend of the data quite well with the cell length  $L_c$  assumed to be the relevant chemical kinetic length. The limiting area increase of about 20% apparent from the figure is also in good agreement with that observed in the present small-scale and large-scale (Chapter 4) tests, suggesting that our philosophy may have universal application.

The maximum velocity deficit apparent in both Figures 51 and 52 is about 10%. Edwards et al. (1979), in their diffraction study using low-pressure oxyacetylene mixtures, attempted to relate the existence of a maximum 10% velocity deficit to the Shchelkin (1959) instability criterion.

According to Shchelkin, if an increase  $\Delta\tau$  occurs in the relevant steady-state chemical kinetic time  $\tau$  such that

$$\Delta\tau > \tau, \quad (5-5)$$

then the front loses stability and fails. If  $\tau$  is assumed to be of the form

$$\tau = k\rho^{-1} \exp(E/RT), \quad (5-6)$$

(which it has been throughout the thesis) where  $k$  is a kinetic rate factor, with  $\rho$  and  $T$  the post-shock density and temperature, respectively, then the Rankine-Hugoniot relations for a normal shock can be combined with the above expression for the chemical kinetic time to obtain

$$\frac{\Delta\tau}{\tau} = -2 \frac{\Delta M}{M} \left\{ \frac{2 + (\gamma-1)M^2 (E/RT)}{2 + (\gamma-1)M^2} \right\}. \quad (5-7)$$

Assuming typical values for the activation energy  $E$  of 80 kJ per mole,  $T = 2000$  K and  $M = M_{C-J} \cong 6$ , these authors showed that the inequality becomes

$$\frac{\Delta M_{C-J}}{M_{C-J}} < -0.1. \quad (5-8)$$

Thus, if the velocity of the plane detonation falls below the C-J value by about 10%, the wave fails. Although the activation energy is generally higher and the Mach number and temperature lower for fuel-air mixtures, the result given by Equation (5-8) is found to be approximately true for these mixtures as well. The analysis is therefore consistent with the present data.

### 5.3.5 Limitations of the Stream Tube Approach

A final point of interest was noted by the author while plotting (Figure 52) the velocity deficit data of Brochet (1966) for propagation in rigid circular tubes of various diameter. It was observed that the maximum

reported deficit for any given tube became smaller as the tube diameter became larger. Upon closer examination of the data, it was evident that the limiting deficit corresponded to the condition of single-head spin. Different limiting deficits for different sizes of tube can be explained in terms of the following argument. Consider single-head spin in a tube of diameter  $D$  in which the displacement thickness of the boundary layer is  $\delta^*$  a distance  $L_c$  aft of the shock. Now, if both the tube diameter and the cell length are doubled so that the mode number of the detonation remains unchanged (i.e., still single-head spin), it will be noted that  $\delta^*$  does not double but rather increases by a factor of only 1.74 since  $\delta^*$  varies as  $x^{0.8}$  for the turbulent boundary layer. This means that the fractional increase in the stream tube area, evaluated over one cell length, is smaller for the large tube; i.e., only 87% of what it is for the small tube. Thus, a correspondingly smaller velocity deficit will exist. Note that, for the case of an accelerating wall, the opposite is true since  $\delta^*$  varies approximately as  $x^2$ . A possible consequence of the nonlinear growth of the boundary layer may be that one of two physical mechanisms govern the propagation limit in rigid tubes. For large tubes, in which the influence of boundary layers is minimal, the limit is due to the loss of stability in the coupling between the spin structure and the tube walls. For small tubes, in which boundary layers become increasingly important, there exists a maximum rate of gasdynamic expansion for which the chemical reaction can be sustained, regardless of the detonation mode number.

#### 5.4 Summary

The laboratory study described in this chapter involved the propagation of stoichiometric  $C_2H_2-O_2-N_2$  detonations in square tubes (62 mm by 62 mm) consisting of a combination of rigid (steel) and yielding (paper or plastic) walls (Figures 46 and 47). The rate of gasdynamic expansion imposed on the wave was controlled by varying both the number of walls which were allowed to yield (1, 2 or 3) and the density of the yielding wall material. The global rate of chemical reaction was regulated by adjusting the nitrogen-to-oxygen ratio  $\beta$  and thus the cell size characteristic of the nonsteady, three-dimensional detonation front (Figure 48). Smoked plates running the

full length of the test section (attached to one of the rigid walls) were used to determine the success or the failure of propagation (Figure 50). Detonation velocities were deduced from the times of arrival of the wave at the pressure transducer locations along the test section. From these velocities, the deficits  $\Delta V/V_{C-J}$  under supercritical conditions were calculated.

As was the case in Chapter 4, the fractional increase  $\xi$  in the area of the post-shock "stream tube", evaluated over a distance of one cell length  $L_C$  relative to the shock, was used to quantify the competition between the rates of gasdynamic expansion and chemical reaction. The stream tube area increase was again estimated by calculating the trajectories of the yielding walls, under the influence of the passing wave, using the method first proposed by Meyer (1958). Two important conclusions have been drawn from the data. First, the critical conditions for propagation appear to be characterized by a fractional increase of about 20% in the stream tube area (Table V). This conclusion is in agreement with the results from Chapter 4 for ethylene-air detonations propagating in large-scale yielding polyethylene tubes of circular cross section. Second, the measured velocity deficit  $\Delta V/V_{C-J}$  appears to be a unique function of the stream tube area increase  $\xi$  under supercritical conditions (Figure 51). Furthermore, the theoretical relation between the velocity deficit and the expansion occurring within the reaction zone of the wave, as derived by Dabora (1963) using the quasi one-dimensional "nozzle" analysis of Fay (1959), is seen to describe the present correlation between  $\Delta V/V_{C-J}$  and  $\xi$  quite well. This is independent evidence that the effective one-dimensional thickness of the detonation front is indeed about one cell length.

For the test section with three rigid walls and a yielding boundary on top, calculations show that the critical channel height becomes about  $2.5\lambda$  as the density of the yielding wall material tends to zero (assuming the 20% maximum stream tube area increase continues to hold in the limit of a vanishing wall). This result is substantiated by the data of Dabora (1963) which reveal that the critical thickness of an oxyhydrogen layer (stoichiometric composition at atmospheric pressure) bounded by nitrogen is about

2.8λ. This would be the approximate thickness required for a cloud sitting on the ground to be detonable.

When the velocity deficits reported by many other investigators for a wide range of conditions are analyzed in light of the present philosophy, all of the data are found to collapse onto a single curve (Figure 52). Included in the analysis are the data of Edwards et al. (1963), Brochet (1966) and Renault (1972) for deficits resulting from boundary layer growth in rigid circular tubes. Also included are the related data of Boislevé (1970) and Renault (1972) from experiments in rigid tubes of rectangular cross section. The results of Dabora (1963) for a rectangular column of gas bounded rigidly on three sides and by an inert compressible gas on the remaining side are seen to be consistent with the present philosophy as well. The good agreement among the data, bearing in mind the many different experimental configurations and techniques employed, suggests that the stream tube concept, incorporating a relevant chemical distance on the order of the cell length, may have universal application in the description of supercritical detonation phenomena.

The velocity deficit data of Brochet (1966) for propagation in rigid circular tubes have demonstrated that failure can occur for a stream tube area increase less than 20% if the cell size approaches the transverse dimension of the test volume. In other words, the stream tube approach breaks down when the intricate details of the interaction between the structure and the boundaries become important (i.e., when the phenomenon of acoustic coupling becomes significant).

## 6.0 DIRECT INITIATION OF DETONATION IN ETHYLENE-AIR MIXTURES\*

### 6.1 Introduction

The geometries studied in Chapters 4 and 5 were of a type such that the flow aft of the shock was globally steady when viewed in shock-fixed coordinates. This means that the gasdynamic expansion imposed on each stream tube of particles entering the front was invariant with time. In the case of a diverging wave front this is not true; the severity of the expansion is a decreasing function of the shock radius  $R_S$ . For a small radius, the post-shock stream tube undergoes a more rapid expansion than it does at a relatively larger radius. Thus, the competition between the gasdynamic expansion and the chemical reaction is a function of  $R_S/\Delta$ , where  $\Delta$  is some distance which characterizes the rate of reaction [e.g., as shown by Sichel (1965)]. Along these lines, the reactive blast wave calculations by Bach et al. (1971) have been successful in demonstrating that the critical radius  $R_S^*$  for the initiation of a spherical oxyacetylene detonation is about 8.2 reaction-zone lengths  $\Delta$ . In keeping with our earlier conclusion that the effective reaction-zone length is approximately equal to the cell length  $L_C$ , it is likely that there exists a critical normalized shock radius  $R_S^*/L_C$  beyond which the gasdynamic expansion is mild enough for the reaction zone to always remain coupled with the shock. In this context, the role of the initiation source may simply be to support the wave until such time that self-sustenance is possible.

This chapter reports on the results of a large-scale test series to determine the critical energy for direct initiation of spherical detonation in ethylene-air mixtures. The measured critical energies are found to be in good agreement with those reported by others, and with those predicted by a modified version of Lee and Ramamurthi's (1976) "kernel" theory in which the critical shock radius  $R_S^*$  has been chosen to be consistent with the concept

---

\*The experimental results described in this chapter have been published in the proceedings of the Seventh International Symposium on Military Applications of Blast Simulation, held in Medicine Hat, Alberta, 13 - 17 July, 1981. Authors: Murray, S.B., Moen, I.O., Gottlieb, J.J., Lee, J.H., Coffey, C.G. and Remboutsikas, D.

of a maximum stream tube area increase. When the model is applied to other detonative systems, the predicted variation of critical energy with composition is seen to describe the experimental results of many investigators in a satisfactory way.

## 6.2 Experimental Details

The tests were performed in plastic bags 10 m long with a cross-sectional area of 1.83 m by 1.83 m, constructed by wrapping 3.5 mil thick polyethylene sheet around a rectilinear lattice frame assembled from extruded aluminum tubing and cast aluminum corner fixtures. The frame was supported in a manner such that one side of the test section was always in contact with the ground surface. The ignition end of the bag was covered by a square sheet of 7 mm thick plywood having a circular central hole in which the initiator charge was mounted. The opposite end of the bag was sealed by drawing the polyethylene material into a neck around the fuel flow line and securing it with nylon cord. Schematic diagrams of the test facility and the bag construction are shown in Figures 53 and 54, with selected photographs of the apparatus included in Figure 55.

The desired gas mixture was prepared by continuous flow of regulated quantities of ethylene (CP grade, 99.5% pure) and bottled dry air through a specially designed mixing chamber. Flow rates were controlled by dual-stage, industrial regulators and monitored by standard, ball-type rotameters. The supply mixture was distributed throughout the bag by means of a perforated plastic tube aligned down the central axis of the bag. Homogeneity of the test mixture was achieved through convection and diffusion. The compositions of the supply mixture and the test mixture at three positions in the bag were examined at regular intervals using an infrared analyzer which was calibrated in the manner described in Chapter 3. One gas sampling port was located at each end of the bag (close to the axis), with a third port positioned about half way down the bag (near the periphery). Uniformity of the mixture composition prior to ignition was always within  $\pm 0.1\%$   $C_2H_4$ . Typically, gas filling was carried out in two stages. In the first stage, a supply mixture having twice the fuel concentration ultimately

desired was flowed at the maximum possible rate of 250 liters per minute for approximately 20 minutes. Subsequently, in stage two, the composition of the supply mixture was adjusted to that desired in the bag. Since fine tuning of the composition was done by trial and error, overall flow times were variable, ranging from 70 to 180 minutes. The average flow time was about 90 minutes.

The initiator charges consisted of circular discs of high-explosive Dupont "Detasheet" (density of 1.58 kg/m<sup>2</sup> with 63% PETN and 7% NC). Initiation of detonation in the charge was achieved by a standard No. 12 electric detonator mounted near the centre of the charge. The initiator energy was varied by using discs of different mass W. The equivalent mass of tetryl is approximately 0.98W (Bull, 1979).

Three types of instrumentation were used to record the details of the initiation and propagation in the bag. A high-speed "Hycam" camera with framing rates between 1000 and 7000 frames per second was used to obtain a cinematographic record of each event. The time of arrival of the wave at various positions along the axis of the bag was monitored by nine ionization-gap probes mounted on a rod down the centre of the bag. The signals from these probes were recorded on magnetic tape using an analogue recorder (Ampex FR1300). The positions of the ionization-gap probes are shown in Figure 54. Also shown in this figure are the positions of eight pressure transducers (PCB 113A24) which were housed in explosion-proof boxes fastened to the lattice frame members. Pressure signals from six transducers were recorded on magnetic tape using a 7 channel analogue recorder (Racal Thermionic Store 7D). Signals from the other two transducers were displayed on an oscilloscope (Tektronix 7623A). Proper timing of the events was accomplished by having the camera activate the firing circuit for the detonator. The time of ignition (det zero) was also recorded on magnetic tape as a reference.

A total of 11 experiments were carried out.



### 6.3 Experimental Results and Discussion

#### 6.3.1 High-Speed Cinematography of the Initiation Phenomenon

Selected frames from a high-speed cinematographic record, showing unsuccessful initiation of detonation in an ethylene-air mixture with 6.40%  $C_2H_4$ , are included in Figure 56. Failure of the hemispherical blast wave from a 9 g Detasheet charge to initiate detonation is clearly seen. Successful initiation of the same mixture, but with a larger 18 g charge, is shown in Figure 57. The first few frames of this latter sequence show the initiation of a detonation wave which grows in a spherical manner until the bag boundaries are reached. The subsequent propagation of a slightly curved detonation wave extending over the entire cross section of the bag can be seen in the later frames. This detonation wave propagates at a constant velocity near the C-J value of 1820 m/s. Similar direct initiation and subsequent propagation at a constant velocity were observed in all ethylene-air mixtures near the stoichiometric composition (i.e., near 6.54%  $C_2H_4$  in  $C_2H_4$ -air).

#### 6.3.2 Velocity Deficits and Oscillations

At a leaner concentration of 3.90%  $C_2H_4$ , strong periodic oscillations in velocity were observed. A comparison of the propagation velocities measured at various positions in the bag for detonation waves in mixtures containing 6.40%  $C_2H_4$  and 3.90%  $C_2H_4$  is provided in Figure 58. The top profile, for 6.40%  $C_2H_4$ , shows the velocity increasing monotonically from a local minimum to a velocity very near the C-J value. The reason why a velocity deficit is not observed in the propagation phase is probably because the relative stream tube area increase  $\xi$  is very small. When a calculation of the type described in Chapter 5 is carried out, assuming yielding boundaries ( $m/A = 0.077 \text{ kg/m}^2$ ) on three sides of the square cross section, the area increase  $\xi$  is found to be about 0.95% over the small cell length (i.e., ~ 50 mm) characteristic of mixtures near stoichiometric composition. The corresponding velocity deficit  $\Delta V/V_{C-J}$  given by Dabora's (1963) theory is less than 1% which, in practical terms, cannot be discerned using the present diagnostic techniques.

The bottom velocity profile in Figure 58, corresponding to an ethylene concentration of 3.90%, exhibits large excursions in velocity which appear to dampen out as the wave approaches the end of the bag. Although difficult to establish with any precision, it would appear that the resultant velocity becomes steady somewhere in the range of 1450 - 1500 m/s. If this was the case, the observed velocity is in good agreement with that predicted from the calculations. For the cell length of 313 mm characteristic of this mixture (see Figure 24), the computed stream tube area increase  $\xi$  is 14.3%. The corresponding velocity deficit from Dabora's (1963) theory is 7.9%, giving a propagation velocity of 1480 m/s, which lies in the middle of the above noted range.

The mechanism responsible for the oscillations in velocity is not understood. One possibility is that the "galloping" behavior is the result of an interaction between the wave and the boundaries, similar to that observed in the experiments of Chapter 4. Recall that in these earlier tests, a detonation wave propagating at the critical stream tube area increase of 20% could be quenched if it was perturbed at the boundary by obstacles spaced about  $5L_c$  apart. In the present initiation experiment, the area increase  $\xi$  of 14.3% is less than the critical one. Furthermore, the 1220 mm spacing between the lattice frame members gives an effective obstacle spacing of  $3.9L_c$ , which is smaller than the critical spacing noted in Chapter 4. In fact, when additional calculations are carried out to determine the cell length that would be necessary for  $\xi$  to achieve a value of 20%, the corresponding effective hoop spacing is seen to reduce to  $2.9L_c$ . Thus, it would appear that the mechanism responsible for the excursions in velocity described in Chapter 4 is, in all likelihood, not at work here.

The results from the recent initiation experiments conducted by Elsworth et al. (1983) may provide another explanation. These authors used tetryl charges to determine the critical energy for direct initiation of spherical detonation in subatmospheric  $C_2H_6-O_2-N_2$  mixtures. Using radially aligned smoked plates and streak photography, they were able to show that, for a mixture having a characteristic detonation cell length of 40 mm, the reaction front galloped for several cycles in the critical energy regime.

The first acceleration of the reaction front commenced at a distance of about 275 mm (i.e.,  $R_s \cong 6.9L_c$ ) from the charge centre. This behavior was attributed to a process called "flashing" by Ul'yanitskii (1980), in which a flame appears in the induction region between the separated shock and the reaction zone following spontaneous ignition of the post-shock mixture. It is possible that the first gallop marks the radial position at which the gasdynamic expansion becomes mild enough for the shock wave and the reaction zone to remain coupled without the assistance of the initiator charge.

Bull et al. (1978) reported a similar galloping behavior during critical initiation in stoichiometric ethylene-air mixtures. Using microwave interferometry, a minimum in velocity was observed at a radial position of about 320 mm, followed by a series of velocity oscillations during a rapid acceleration of the reaction front toward the C-J velocity. Using a cell length of 47 mm (see Figure 24) the radius  $R_s$  at which acceleration of the front and "attempts to couple" commenced is  $6.8L_c$ , which is in good agreement with the result of Elsworth et al. (1983).

In the present initiation experiment with 3.90%  $C_2H_4$  in  $C_2H_4$ -air, the radius at which the minimum in velocity occurred is about 3100 mm or  $9.9L_c$ . Although this value is somewhat larger than those deduced from the data of both Elsworth et al. (1983) and Bull et al. (1978), we have no way of knowing just how close conditions were to the critical ones, since only a single initiator charge mass was investigated for the mixture composition in question. Elsworth et al. have reported that galloping is possible, for a given charge mass, over a narrow range of mixture compositions near the critical one. Hence, it is possible that the galloping phenomenon evident in Figure 58 is a slightly supercritical case of the reaction zone attempting to couple once the initiating shock wave decays to some critical velocity around the C-J value. This occurs at a radius somewhat larger than the critical one.

### 6.3.3 The Critical Energy for Direct Initiation

A summary of the critical energy results is shown in Figure 59. The present field test data are in good agreement with the results of Bull et al. (1978, 1979a) and Pfortner (1977), and with the recent, unpublished data of Elsworth [as cited by Donato (1982)] obtained from experiments in a closed detonation chamber. The results of Hikita et al. (1975) are in fair agreement with both the present and other available data.

#### Wave Front Curvature and the Stream Tube Area Increase

In Chapters 4 and 5, it was concluded that a detonation wave will be self-sustained provided the gasdynamic expansion is mild enough so that the reaction zone can remain coupled with the frontal shock complex. Quantitatively, the condition for sustenance was that the increase in the cross-sectional area of a "stream tube" of particles entering the shock front could not exceed 20% at the time such particles had migrated one cell length rearward of the shock. Now in the present case of a diverging spherical wave, the gasdynamic expansion becomes less severe with increasing radius. Thus, it should be possible to identify the shock radius for which the critical chemical-gasdynamic balance is realized. Consider an expanding wave of radius  $R_s$  and surface area  $k_j R_s^j$  where  $j = 0, 1$  or  $2$  and  $k_j = 1, 2\pi$  or  $4\pi$  for planar, cylindrical or spherical geometries, respectively. Assuming that C-J conditions prevail throughout the reaction zone, the particles entering the shock migrate rearward a distance  $L_c$  in time  $\Delta t = L_c / C_{C-J}$ . But during this period, these particles achieve a radius of  $R_s + U_{C-J} \Delta t$ . Therefore, the relative increase in the area of the particle surface (i.e., the relative stream tube area increase) is

$$\xi = \frac{[R_s + (U_{C-J}/C_{C-J})L_c]^j - R_s^j}{R_s^j} \quad (6-1)$$

Noting that  $U_{C-J}/C_{C-J} = \rho_{C-J}/\rho_0 - 1$  and rearranging Equation (6-1) gives the normalized shock radius in terms of the area increase  $\xi$ . That is,

$$\frac{R_S}{L_C} = \frac{[\rho_{C-J}/\rho_0 - 1]}{[(1 + \xi)^{1/j} - 1]} \quad (6-2)$$

For the limiting area increase  $\xi$  of 0.2 and a typical value for  $\rho_{C-J}/\rho_0$  of 1.8, the above equation gives critical radii of  $R_S^* = 4L_C$  and  $R_S^* = 8.4L_C$  for  $j = 1$  and  $j = 2$ , respectively. In this context, we could look upon the role of the initiation charge as keeping conditions above C-J conditions until such time that the wave attains a radius for which the expansion is mild enough so that the reaction zone remains coupled with the shock. It should be noted that  $R_S^*$  becomes zero for  $j = 0$ . This simply reflects the fact that the stream tube area increase for planar geometry is not a result of the front diverging. As discussed in depth in Chapters 4 and 5, the expansion occurring within the reaction zone of a wave propagating in a constant diameter duct is brought about by much different mechanisms (e.g., boundary layer growth, compressible or yielding boundaries, etc.).

The calculated minimum spherical radius of  $8.4L_C$  is entirely consistent with the earlier observation (Chapter 2) from the critical tube diameter experiments. Recall that critical reignition was seen to occur behind an approximately spherical shock wave of radius  $11.5\lambda$ . It also ties in well with the streak photographic observations by Elsworth et al. (1983) and the interferometry results of Bull et al. (1978) which reveal that the reaction zone races ahead once it achieves a radius of  $6.8 - 6.9L_C$ . In Chapter 4, it was estimated that the reaction front lagged behind the shock front by a distance of approximately  $1.3L_C$  at the moment it was seen to accelerate in an attempt to couple with the shock. Assuming the same to be true in the initiation experiments, the critical shock radius would be about  $8.1 - 8.2L_C$ .

There also exists some evidence to support the calculated critical cylindrical radius of  $4L_C$  noted above. Recall from Chapter 2 that the minimum radius for which a cylindrical wave appeared to be self-sustained was approximately  $0\lambda$ . In these earlier experiments, the role of the reflected shock may have been similar to that of the initiator charge in the present tests; namely, to support the wave until self-sustenance becomes possible. The cylindrical initiation experiments carried out by Lee et al. (1974)

provide additional support. These authors measured the distance-time trajectory of the shock front during critical initiation by an exploding wire in low-pressure (100 Torr) stoichiometric oxyacetylene mixtures. When compared to that of a shock wave in air (produced by the same discharge of energy), the trajectories were seen to depart rather distinctly at a radius of about 5 mm. Assuming this departure to be associated with the rapid acceleration of the front following critical reignition, and using a cell length of 1.3 mm inferred from the critical tube diameter data of Matsui and Lee (1979), the critical radius would be about  $3.8L_c$ .

#### The "Kernel Theory" in Light of the Stream Tube Criterion

Knowing the critical radius required for self-sustained detonation in a given geometry, it is possible to calculate the minimum energy for direct initiation. The following derivation is very similar to the one presented by Lee and Ramamurthi (1976) in their attempt to evaluate the minimum size of a detonation "kernel". Consider a rapid and localized deposition of energy  $E_s(t)$  into a combustible mixture. At any point in time, the conservation of total energy enclosed by the shock wave gives

$$E_s(t) + \int_0^{R_s(t) - \Delta} \rho Q k_j r^j dr = \int_0^{R_s(t)} \left\{ \frac{\rho U^2}{2} + \frac{P}{\gamma - 1} \right\} k_j r^j dr \quad (6-3)$$

where  $Q$  is the chemical energy per unit mass,  $\rho$ ,  $U$ ,  $P$  and  $\gamma$  have their usual meaning, and  $\Delta$  is the relevant reaction-zone length. The first term on the left-hand side of the equation denotes the energy deposited by the source up to time  $t$ , while the second term represents the chemical energy released through combustion. The sum of the source and the chemical energies goes into both the kinetic and the internal energies of the gas bounded by the shock wave of radius  $R_s(t)$  [i.e., the integral on the right-hand side of the equation]. In Equation (6-3), we have neglected the initial internal energy of the gas

$$\int_0^{R_s(t)} \rho_0 e_0 k_j r^j dr$$

since it is negligibly small in comparison with the chemical energy released through combustion. Making a straightforward transformation to dimensionless variables  $\psi$ ,  $\phi$ ,  $f$  and  $\zeta$ , we may write

$$E_s(t) = \rho_0 k_j R_s^{j+1} \left\{ \dot{R}_s^2 I - Q \int_0^{1 - \Delta/R_s} \psi \zeta^j d\zeta \right\} \quad (6-4)$$

where  $\psi = \rho/\rho_0$ ,  $\phi = U/\dot{R}_s$ ,  $f = P/\rho_0 \dot{R}_s^2$ ,  $\zeta = r/R_s(t)$  and  $I$  is the dimensionless energy integral

$$I = \int_0^1 \left\{ \frac{\psi \phi^2}{2} + \frac{f}{\gamma - 1} \right\} \zeta^j d\zeta. \quad (6-5)$$

As noted by Lee and Ramamurthi (1976), the integral given by Equation (6-5) is not particularly sensitive to the details of the flow distributions, provided the boundary values are the same. The value of  $I$  calculated by the strong shock similarity solution, the power law density profile method and the similarity solution for a sub C-J detonation are almost identical and match the asymptotic value of  $I$  given by Equation (6-4) when  $R_s(t) \rightarrow \infty$  and  $E_s(t)$  becomes negligibly small; that is,

$$I = \frac{Q}{(j+1)M_{C-J}^2 C_0^2}. \quad (6-6)$$

In keeping with our earlier observations that the reaction front lags behind the shock front by a distance approximately equal to the cell length just prior to critical reignition,  $\Delta$  in Equation (6-4) will be set equal to  $L_c$ . The mass integral in that equation can then be evaluated by writing

$$\int_0^{1 - L_C/R_S} \psi \zeta^j d\zeta = \int_0^1 \zeta^j d\zeta - \int_{1 - L_C/R_S}^1 \psi(\zeta, M_S) \zeta^j d\zeta. \quad (6-7)$$

Since the density ratio across the shock  $\rho_S/\rho_0$  is fairly high, most of the mass is concentrated in the vicinity of the shock itself. We may therefore assume the density profile in the post-shock region to be of a power law form:

$$\psi(\zeta, M_S) = \psi(1, M_S) \zeta^{q(M_S)}, \quad (6-8)$$

where the exponent  $q(M_S)$  is determined from the mass integral to be

$$q(M_S) = (j + 1)[\psi(1, M_S) - 1] \quad (6-9)$$

so that the total mass enclosed by the shock is conserved at all times. Substituting Equations (6-6) through (6-9) into (6-4) gives

$$E_C = \frac{\rho_0 k_j R_S^{j+1} Q}{(j + 1)} \left\{ \left[ \frac{M_S}{M_{C-j}} \right]^2 + \frac{\rho_S}{\rho_0} \left[ \frac{j+1}{q+j+1} \right] \left[ 1 - \left( 1 - \frac{L_C}{R_S} \right)^{q+j+1} \right] - 1 \right\}. \quad (6-10)$$

Equation (6-10) can be used to predict the critical energy for direct initiation once the critical shock Mach number  $M_S^*$  has been specified. Several experimental observations may be useful in this regard. Edwards et al. (1979), for example, have examined the centreline velocity of a detonation wave diffracting from a channel under critical conditions and found from streak photographs that it dips to about  $0.6M_{C-j}$  before the reinitiated front begins to accelerate. Ungut et al. (1983) have carried out a similar study on the diffraction of ethane-air and propane-air detonations from a circular tube. In their tests, the minimum centreline velocity, measured using a multibeam laser Schlieren time-of-arrival system, was found to vary between  $0.5M_{C-j}$  and  $0.7M_{C-j}$ . In the critical initiation experiments conducted by Elsworth et al. (1983), the velocity profile along a radius from the charge was examined by streak photography, laser Schlieren anemometry and microwave Doppler velocimetry. The minimum velocity was seen



to lie in the range from  $0.6M_{C-J}$  to  $0.8M_{C-J}$  prior to the front reinitiating itself.

The three studies mentioned above reveal quite a variation in the minimum velocity of the front. A more appropriate criterion for selecting the critical Mach number may be established by appealing to the similarity between the critical reignition process in initiation and transmission problems and that which occurs on a smaller scale toward the end of an individual detonation cell. Detailed experiments by Strehlow and Crooker (1974) and by Libouton et al. (1981) have shown that the Mach number of the shock wavelet in the cell drops to about  $0.7M_{C-J}$  prior to the explosive recoupling of the reaction front with the wavelet. This value lies in the range of minimum Mach numbers observed in the initiation and transmission studies.

Apart from the selection of the reaction-zone thickness, the present formulation differs from the original kernel theory in two ways: i) the critical radius  $R_S^*$  is drawn from observations about the maximum stream tube area increase, rather than being arbitrarily defined as the radius for which the source and chemical energies are equal, and ii) the critical Mach number  $M_S^*$  is that observed during critical reignition at the end of a detonation cell, rather than that which yields a post-shock temperature representing the auto-ignition limit for the mixture. The changes to the original kernel theory spelled out above essentially remove the "static" balance condition advocated by Lee and Ramamurthi (i.e., that the source and chemical energies be equal) and replace it with a balance condition which is more representative of the "dynamic" competition ongoing within the cellular front.

The solid line through the data in Figure 59 is based on Equation (6-10) with  $R_S^* = 8.4L_C$  and  $M_S^* = 0.7M_{C-J}$ . The Gordon and McBride (1976) chemical equilibrium computer program has been used once again for evaluating the detonation parameters. The cell length  $L_C$  is based on the criti-

cal tube diameter measurements presented in Chapter 3. Although the curve describes the trend of the data rather well, particularly for lean compositions, it represents only 37% of the energy given by Equation (6-10). That is, the equation overpredicts the required energy by a factor of about 2.7.

#### Other Models for the Critical Energy

Also shown in Figure 59 is a theoretical curve based on Lee and Matsui's (1976) "work" model. These authors reduced the critical tube diameter  $D_c$  to an equivalent critical energy  $E_c$  by assuming that the energy delivered to the gas in the unconfined region is via the compression work done by the interface separating the expanding combustion products in the tube and the quiescent gas in the larger volume. Their analysis gives

$$E_c = \frac{\pi P_{C-J} U_{C-J}}{24 C_{C-J}} D_c^3 \quad (6-11)$$

However, as with Equation (6-10), the required energy for direct initiation is overpredicted. The curve shown in Figure 59 represents only 17% of the energy given by the model. More recently, Lee and coworkers (1981, 1982) have proposed a "surface energy" model for the prediction of the critical energy. Essentially, the model assumes that the smallest patch of detonation wave which will successfully transform into a spherically expanding detonation is that corresponding to the cross-sectional area of the critical tube. By equating this area to the surface area of a blast sphere, a critical radius is first identified. Strong blast theory is then used to estimate the energy required to give a C-J strength shock at this critical radius. The model yields the expression:

$$E_c = \frac{2196}{16} \pi \gamma_0 P_0 I_{M_{C-J}}^2 \lambda^3 \quad (6-12)$$

which is depicted by the dashed curve in Figure 59. This model has the advantage of not requiring a constant of proportionality in order for the

theory to describe the experimental data. It should be noted that Equations (6-10) and (6-12) are very similar. For a given geometry, the second term inside the curly brackets of Equation (6-10) is essentially constant. Setting  $M_{C-j}^2 \cong Q/C_0^2 I(j+1)$ , and using the definition of the speed of sound and the perfect gas law, Equation (6-10) can be transformed into Equation (6-12) with only the numerical constant being different.

Figure 60 is a summary of available initiation energy data for fuel-air mixtures at atmospheric pressure. All of the points on the graph are direct measurements except that for the stoichiometric methane-air mixture. The initiation energy of 22 kg is an extrapolated value based on experiments employing diluted methane-oxygen mixtures. The four curves through the data for the fuels  $H_2$ ,  $C_2H_2$ ,  $C_2H_4$  and  $C_3H_8$  are based on Equation (6-10). The critical tube diameter correlations reported by Moen et al. (1983) have been used to infer the cell lengths. The constants of proportionality (values of  $k$  on the graph) required to make Equation (6-10) describe the experimental results show that the measured energies are between 14% and 58% of the predicted ones, depending on the fuel. This means that, with  $k = 0.29$ , it is possible to predict the initiation energy to within a factor of about two using Equation (6-10). There does not appear to be a trend in the value of  $k$  with the relative sensitivity of the fuel, suggesting that other factors may play a role in determining the absolute sensitivity. The recent observations on transmission by Edwards et al. (1981b) and by Moen et al. (1983) give rise to speculation that the cell regularity may be important in this regard.

### 6.5 Summary

This chapter reports on the results of a field investigation to determine the critical energy for direct initiation of ethylene-air mixtures in large plastic bags simulating an unconfined region (Figure 55). The initiator energy was varied by adjusting the mass of high-explosive PETN charges. Pressure transducers and ionization-gap probes (Figure 54) showed that, in the critical energy regime, the wave "galloped" for several cycles

in a manner similar to that observed in the critical energy experiments of others [i.e., those of Bull et al., (1978) using  $C_2H_4$ -air mixtures, and those of Elsworth et al. (1983) using  $C_2H_6$ - $O_2$ - $N_2$  mixtures. These gallops (Figure 58) are attributed to a process known as "flashing" in which reignition occurs in the post-shock induction region, leading to an overdriven wave which catches up to and coalesces with the runaway frontal shock (Ul'yanitskii, 1980). The radius at which the first gallop occurs is found to be close to the critical radius of  $R_S^* \cong 8.4L_C$  for a spherical detonation wave, based on the 20% maximum tolerable stream tube area increase  $\xi$  noted in Chapters 4 and 5. This observation suggests that the role of the initiator charge may simply be to maintain the wave until the gasdynamic expansion becomes mild enough for the reaction zone to remain coupled with the shock once it decays to some critical Mach number.

The "kernel" theory, as originally formulated by Lee and Ramamurthi (1976), has been reworked in an effort to predict more successfully the critical energy for direct initiation. Assuming the detonation cell length  $L_C$  to be the effective reaction-zone length, two modifications have been made to the theory. First, the critical radius  $R_S^*$  is based on the maximum 20% stream tube area criterion. This is in contrast to the original formulation in which the critical radius was arbitrarily defined as that for which the source and chemical energies are equal. Second, rather than choosing the critical Mach number  $M_S^*$  as that needed to yield a post-shock temperature above the auto-ignition limit, it has been set equal to the Mach number of  $0.7M_{C-3}$  observed during critical reinitiation at the end of an individual detonation cell. As with other models, the revised theory overpredicts the required energy. However, if a curve corresponding to 37% of the predicted energy is drawn through the data, the trend is well described (Figure 59). When the model is applied to other fuel-air systems (Figure 60), the same conclusion can be drawn except that a different constant of proportionality must be used for each fuel-air system (i.e., the measured energies are between 14% and 58% of the predicted ones). The reason for this is not clear, but it is suspected that the regularity of the cellular structure may play a role.

## 7.0 CONCLUSIONS AND RECOMMENDATIONS FOR FUTURE RESEARCH

### 7.1 Highlights of the Individual Experimental Studies

Before tying together the findings of the present work into a coherent picture of detonation behavior, the highlights of the individual experimental studies will be summarized.

#### Chapter 2: The Critical Conditions for the Transmission of Planar Detonation to Spherical or Cylindrical Detonation

- Laboratory-scale tests employing low-pressure oxyacetylene mixtures have shown that two modes of reinitiation are possible when a planar detonation wave emerges from a circular tube and transforms into a cylindrical wave expanding radially outward between a pair of parallel plates. When the plate spacing  $w$  is large in comparison with the cell width  $\lambda$ , "spontaneous reinitiation" commences in the vicinity of the head of the expansion with the formation of reignition nuclei at a distance of about  $11.5\lambda$  from the tube exit. For plate spacings between  $5.7\lambda$  and  $11.5\lambda$ , "reinitiation by reflection" takes place as reignition nuclei are born near the wall opposite the tube exit in the wake of the reflected wave. Transmission does not occur for plate spacings smaller than  $5.7\lambda$ .
- It has been found that the minimum radius of curvature for self-sustained cylindrical detonation in oxyacetylene mixtures is about  $6\lambda$ , while for spherical waves it is about  $11.5\lambda$  or approximately twice as large. Since the rate of post-shock gasdynamic expansion is proportional to the rate of growth of the expanding detonation surface  $A^{-1}dA/dR$  ( $= 1/R$  and  $2/R$  for cylindrical and spherical geometries, respectively), the difference in minimum radii by a factor of about two suggests that the critical conditions in both geometries are a consequence of the same chemical-gasdynamic competition occurring within the cellular detonation front.

- The requirement for the diffracted wave to exceed some minimum radius in order for the chemical processes to survive the gasdynamic expansion has been proposed to be the basis of the  $13\lambda$  correlation linking the critical tube diameter  $D_c$  and the cell width  $\lambda$ . Assuming that reignition cannot take place once the rarefaction wave arrives at the tube axis (a distance of 0.92 tube diameters from the exit, according to equilibrium calculations for oxyacetylene mixtures), the critical spherical radius  $R_s$  and the critical tube diameter  $D_c$  are related by  $R_s \cong 11.5\lambda = 0.92D_c$ ; that is,  $D_c \cong 12.5\lambda$ .
- Correlations have shown that the critical tube diameter for transmission to an unconfined region, the critical plate spacing for transmission to a cylindrical gap, the location of reignition for both types of transmission, and the distances travelled by the diffracted wall shocks during both types of reestablishment are all intimately linked to the cell size. These observations are convincing evidence that the controlling chemical kinetic length in detonative propagation is on the order of the cell dimensions.

### Chapter 3: Large-Scale Experiments on the Transmission of Planar Detonation to Spherical Detonation in Ethylene-Air Mixtures

- High-speed cinematography showing the transmission of planar detonation from circular tubes of 0.31 m, 0.45 m and 0.89 m diameter to large plastic bags simulating an unconfined environment has revealed that critical reignition occurs near the tube axis, behind an approximately spherical shock, at about the location where the rarefaction wave has penetrated the detonation core. Thus, the reinitiation process appears to be similar in both large-scale and small-scale transmission.
- Interpretation of the cellular structure produced on smoked plates by ethylene-air detonations has been found to be much more subjective than it is for low-pressure fuel-oxygen detonations. Differentiation between the primary and secondary structures is difficult and can easily result in an error by a factor of two in the reported cell size. Simi-

lar difficulties have been encountered by other investigators (e.g., Moen et al., 1983) for a variety of fuel-air mixtures.

- The  $13\lambda$  correlation linking the critical tube diameter  $D_c$  and the cell width  $\lambda$  is likely valid for fuel-air mixtures, judging from both the present and other available data [e.g., those of Guirao et al. (1982) and Moen et al. (1983)]. All discrepancies are consistent with the possibility that the structure may have been misinterpreted.

#### Chapter 4: The Influence of Yielding Confinement on Large-Scale Ethylene-Air Detonations

- Large-scale tests on the transmission of lean ethylene-air detonations from a rigid tube to yielding polyethylene tubes of the same diameter (0.89 m) have shown that reinitiation of the emerging wave is via a circular locus of reignition nuclei which form in the vicinity of the yielding tube wall. These nuclei give rise to detonation bubbles which reestablish the wave globally by sweeping transversely through the gas bounded by the decoupled shock and reaction zone. This reinitiation phenomenon is similar to that observed during the diffraction of a wave from a tube to an unconfined region in that the reignition nuclei decrease in number and move away from the tube exit as criticality is approached. In the critical case, this phenomenon is similar to the one observed in critical energy experiments. Both are characterized by a critical radius of wave front curvature, a quasi steady regime in velocity and a "galloping" behavior which may be indicative of the reaction zone attempting to couple with the shock front.
- A simple correlation has shown that the controlling chemical kinetic length in detonative propagation is approximately equal to the cell length  $L_c$ . For the purpose of the correlation, the post-shock thermodynamic history of a particle near the yielding tube wall (where reignition occurs) is calculated using the analogy of an accelerating cylindrical piston to model the wall motion. The relevant chemical kinetic time is assumed to be of the usual induction-time form, while

the stability of the chemical-gasdynamic coupling is considered to be described by a failure criterion similar to the one proposed by Shchelkin (1959). In addition to identifying the controlling chemical kinetic length scale, the correlation emphasizes the similarity of the critical chemical-gasdynamic balance for the different gasdynamic times (i.e., wall densities) and chemical kinetic times (i.e., mixture compositions) investigated.

- It has been shown that the critical conditions for propagation in a constant diameter yielding tube can be expressed in terms of a 20% increase in the cross-sectional area of a "stream tube" of particles entering the front, as such particles migrate rearward from the shock through the relevant chemical kinetic distance (i.e., the cell length  $L_c$ ). The 20% criterion is found to be equally valid in predicting the failure diameter for propagation in tapered yielding tubes, and in explaining the observations made by other investigators who employed yielding tubes [e.g., Moen et al. (1983) using methane-air mixtures and Guirao et al. (1982) using hydrogen-air mixtures].
- Both the experiments and the supporting calculations have shown that, as the wall density tends to zero, the critical diameter for propagation in an unconfined cylindrical column approaches the critical diameter for transmission from a rigid tube to an unconfined region. This is true, provided the gas which bounds the column has physical properties (i.e., density and sonic velocity) similar to those of the combustible mixture. This result is in disagreement with the claim by Vasiliev (1980) that the critical column diameter is some 2 - 8 times the minimum diameter for transmission.

Chapter 5:    The Influence of Yielding Confinement on the Velocity  
of Propagation of Gaseous Detonation Waves

- Laboratory-scale tests involving the propagation of stoichiometric  $C_2H_2-O_2-N_2$  detonations in square tubes consisting of a combination of rigid and yielding walls have shown that the stream tube area criterion



is successful in describing the critical conditions for propagation under a variety of boundary conditions. Regardless of the rate of gasdynamic expansion (varied primarily by changing the number of yielding walls) or the rate of chemical reaction (varied by adjusting the dilution ratio  $\beta = [N_2]/[O_2]$ ), the critical conditions were found to be consistent with a relative stream tube area increase of about 20%.

- For the case of a test section consisting of three rigid walls and a yielding top, the calculations show that, as the density of the yielding wall tends to zero, the critical channel height for stoichiometric acetylene-air bounded on top by air approaches  $2.5\lambda$  (assuming the 20% criterion to hold in the limit of a vanishing wall). Thus, the minimum thickness required for such a cloud sitting on the ground to be detonable is  $2.5\lambda$ . This result is in good agreement with the minimum thickness of  $2.8\lambda$  for stoichiometric oxyhydrogen bounded on top by nitrogen, deduced by the author from the experimental results of Dabora (1963).
- It has been found that, under supercritical conditions (i.e.,  $\xi < 20\%$ ), the measured velocity deficit  $\Delta V/V_{C-J}$  is a unique function of the stream tube area increase. In fact, having chosen the cell length  $L_C$  over which to evaluate the area increase, the measured velocity deficits are seen to be in good agreement with the theoretical relation derived by Dabora (1963) based on a quasi one-dimensional "nozzle" analysis. This observation is independent evidence that our selection of a one-dimensional length (i.e.,  $L_C$ ) to characterize the three-dimensional phenomenon is appropriate.
- When the velocity deficit data reported by several other investigators (e.g., Edwards et al., 1963; Dabora, 1963; Brochet, 1966; Boislevé, 1970; Renault, 1972) for a wide range of boundary conditions and mixture compositions are plotted in the above described manner (i.e.,  $\Delta V/V_{C-J}$  versus  $\xi$ ), all of the data are found to agree with Dabora's (1963) theoretical relation, suggesting some degree of universality in the behavior of detonation waves under supercritical conditions.

- Using the velocity deficit data reported by Brochet (1966) for propagation in rigid circular tubes of various diameter, the author has discovered that the stream tube philosophy breaks down once the cell dimensions approach the characteristic transverse dimension of the tube. This is true because another phenomenon - the coupling between the spin structure and the tube wall - becomes important. Thus, one of two mechanisms can govern the propagation limits; too severe a gasdynamic expansion, or the onset of single-head spin.

#### Chapter 6: Direct Initiation of Detonation in Ethylene-Air Mixtures

- Large-scale experiments on the direct initiation of ethylene-air mixtures using high-explosive charges have shown that the wave "gallops" for several cycles in the critical energy regime in a manner similar to that reported by both Elsworth et al. (1983) using  $C_2H_6-O_2-N_2$  mixtures and Bull et al. (1978) using ethylene-air mixtures. These gallops are thought to be the consequence of a process known as "flashing" (Ul'yanitskii, 1980) in which reignition occurs in the decoupled region, leading to an overdriven wave that catches up to and drives forward the decaying shock wave.
- The shock radius at which the first gallop occurs in both the present experiments and those of the other investigators is seen to be very close to the critical spherical radius of  $R_S \cong 8.4L_C$  estimated from the 20% stream tube area criterion. These observations imply that the role of the initiator charge may simply be to maintain the wave in the face of a severe gasdynamic expansion until it achieves a radius at which the shock/reaction zone coupling can survive on its own.
- The "kernel" theory, as originally formulated by Lee and Ramanurthi (1976), has been reworked in an effort to predict more successfully the critical energy for direct initiation. By setting the effective reaction-zone length equal to the cell length  $L_C$ , and using the critical spherical radius of  $8.4L_C$ , the modified theory is found to describe

the trend of the experimental data quite well, although it overpredicts the critical energy by a factor of about 2.7.

- The reworked theory is also found to describe satisfactorily the critical energy results reported in the literature for many other fuel-air mixtures. However, a different constant of proportionality between the theoretical and experimental energies is required for each fuel-air system. This observation suggests that factors in addition to the cell size are important in quantifying the absolute detonation sensitivity of combustible mixtures.

## 7.2 A Unified Description of Detonation Based on the Present Results

The experimental results presented in this thesis show that the behavior of a detonation wave under a given set of boundary conditions depends on an intimate competition between the post-shock rates of gasdynamic expansion and chemical energy release occurring within the cellular detonation front. The "stream tube" concept has been proposed as a simple and effective means of quantifying the **absolute** gasdynamic expansion. In essence, one ignores the nonsteady, three-dimensional nature of the front and considers only the increase in the area of an idealized, post-shock stream tube. In order to express the **relative** severity of the gasdynamic expansion, the rate of expansion must be compared with the rate of chemical energy release. The fractional stream tube area increase  $\epsilon$ , evaluated over some distance deemed to be characteristic of the overall rate of chemical reaction, is used for this purpose. The cell length  $L_c$  has been chosen as the relevant chemical kinetic distance based on detailed correlations revolving around the nature of the chemical-gasdynamic competition (see Chapters 2, 3 and 4). Although the stream tube approach is not new, the present study is novel in that it appeals to the cellular structure of the wave for the appropriate chemical kinetic length scale.

Given a particular combustible mixture, and hence a specific chemical kinetic length, the role of the physical boundaries in any scenario is to control the rate of gasdynamic expansion experienced by the particles entering the detonation front. An increase in the area of the post-shock stream tube can be brought about in one of two basic ways. The first possibility is that an interaction may take place between the post-shock flow and the boundaries surrounding the mixture, causing a divergence of the stream lines within the reaction zone. Several different types of interactions are possible. For example, the boundary material may compress under the influence of the high-pressure gases in the reaction zone. A divergence of the flow can also be brought about by the growth of viscous boundary layers on the walls confining the mixture. Another type of interaction, and the one studied thoroughly in the present thesis (see Chapters 4 and 5), involves confining walls which yield or accelerate under the influence of the high-pressure post-shock flow. In all cases, an increase is brought about in the area of the stream tube, even though the shock front may not experience a change in its area.

The large-scale experiments involving ethylene-air detonations in yielding polyethylene tubes (Chapter 4) showed that the critical stream tube area increase is about 20% over the relatively small range of chemical kinetic times (i.e., mixture compositions) and gasdynamic expansion times (i.e., yielding wall densities) investigated. However, the corresponding laboratory tests (Chapter 5), in which nitrogen-diluted stoichiometric oxy-acetylene detonations were observed in channels of square cross section, have provided evidence that the 20% criterion may apply more universally. In those tests, both the number of walls which were allowed to yield (1, 2 or 3) and the density of the wall material were varied in order to regulate the rate or severity of the expansion. In all tests, a critical  $\xi$  near 20% was observed.

It is of interest to note that the minimum diameter for propagation in an unconfined cylindrical column, and the minimum thickness for propagation in a cloud sitting on the ground, are simply limiting cases of the geometries investigated in Chapters 4 and 5, respectively, in which the

yielding wall density tends to zero. Although tests were not carried out for the case of zero wall density, the calculations revealed a minimum diameter for an unconfined cylindrical column of about  $10\lambda - 11\lambda$  for fuel-air mixtures. Similarly, the critical thickness of a layer sitting on the ground was computed to be about  $2.5\lambda - 3\lambda$ .

For mechanisms which induce a rather slow rate of expansion, such as the growth of viscous boundary layers on the inside surface of a duct, the cell length required in order to effect a stream tube area increase of 20% could be very large. So large, in fact, that the cell size may well exceed the tube dimensions. In this event, the above described critical chemical-gasdynamic balance would not be responsible for the propagation limit, but rather the onset of single-head spin.

The second basic means by which an increase can be brought about in the area of the post-shock stream tube is by virtue of the wave front diverging in a partially confined or unconfined space. In this case, the boundaries dictate the rates at which the detonation surface and, correspondingly, any surface of particles entering the front, are permitted to grow. Based on the critical  $\xi$  of 20% deduced from the yielding wall experiments, it is a simple matter to compute the radius of curvature  $R_s$  for which the critical chemical-gasdynamic balance is realized. This is done by simply analyzing the relative motion between the shock surface and a surface of particles entering the shock at any particular radius. For cylindrical and spherical geometries,  $R_s$  equates to  $4L_c$  and  $8.4L_c$ , respectively, assuming a critical  $\xi$  of 20% and a typical detonation density ratio of 1.8. At smaller radii, the gasdynamic expansion is too severe for the chemical-gasdynamic coupling to persist behind a C-J strength shock. The fact that the critical spherical radius is about twice the critical cylindrical radius is a reflection of the fact that the fractional rate of growth of the detonation surface area  $A^{-1}dA/dR$  is twice as large in spherical geometry as it is in cylindrical geometry for a given radius  $R$  (i.e.,  $2/R$  versus  $1/R$ ).

Knowing the minimum radius of curvature for self-sustained detonation in a given geometry, the critical conditions required for the transmission

of detonation begin to make sense. Consider, for example, the critical diameter  $D_c$  for the transmission of detonation from a circular tube to an unconfined region. Critical reignition of the approximately spherical diffracted wave is seen to occur at the location where the rarefaction wave converges on the tube axis (see Chapters 2 and 3). Using the experimentally observed critical tube diameter of  $13\lambda$  as a scale, the radius of the diffracted shock becomes  $8.2L_c$  (for  $\lambda/L_c = 0.7$ ) which is very nearly equal to the critical spherical radius of  $8.4L_c$  deduced from the stream tube criterion. Thus, the role of the linear detonation tube may simply be to provide a large enough initial area of detonation wave so that the diffracted shock can achieve the minimum spherical radius before the rarefaction quenches the last remaining portion of the wave still at C-J conditions.

If similar reasoning is applied to the case of a planar detonation wave transmitting from a two-dimensional channel to an unconfined space, the critical channel width  $w_c$  corresponding to a minimum cylindrical radius of  $4L_c$  is computed to be  $6.3\lambda$ . This value is about twice that reported by Benedick et al. (1983) and Liu et al. (1984). However, some concern does exist over whether the cellular structure recorded in those tests was interpreted correctly (Lee, 1983), suggesting that the actual cell sizes may, in fact, be half the reported ones. Thus, a critical channel width close to  $6\lambda$  cannot be ruled out. More direct support for the proposed minimum cylindrical radius of  $4L_c$  can be drawn from the present experiments involving the transformation of planar detonation in a circular tube to cylindrical detonation expanding radially outward between a pair of parallel plates (see Chapter 2). With this geometrical arrangement, the detonation wave emerging from the tube impacts the wall opposite the tube exit. The reflected shock wave acts to halt the incoming rarefaction and support the diverging wave until it achieves a radius at which self-sustained detonation is possible. Smoke records reveal that a cylindrically expanding wave is finally established at a radius of about  $4L_c$  in the critical limit.

The requirement for a minimum radius of curvature may also help to explain many of the observations about direct initiation. For example, both Bull et al. (1978) and Elsworth et al. (1983) observed "galloping" phenomena

in the critical energy regime during experiments on the direct initiation of spherical detonation using high-explosive charges. There is little doubt that the "flashing" process reported by Elsworth et al., in which reignition occurs between the shock and decoupled reaction zone, is a signal that the wave is not in need of further support from the initiation source. Bull et al. (1978) also attributed the oscillations in the velocity of the reaction front to repeated "attempts to couple". In both cases, acceleration of the reaction front was seen to occur at a radius of about seven cell lengths. Since the reaction zone trails the shock by a distance on the order of the cell length just prior to reestablishment of a wave under critical conditions (Chapters 2 and 4), these observations are consistent with the critical spherical shock radius of  $8.4L_c$  estimated from the stream tube criterion. Further support can be drawn from the velocity measurements obtained in the present tests on the direct initiation of ethylene-air mixtures (see Chapter 6). In one such test, acceleration of the shock front, accompanied by a series of velocity oscillations, was seen to occur when the shock reached a radius of  $9.9L_c$ . Since the conditions in this experiment were thought to be somewhat more favourable than the critical ones, the above noted radius is in agreement with the critical spherical radius deduced from the stream tube criterion. Using the proposed critical radius of  $8.4L_c$  to define the minimum size  $R_s^*$  of a detonation "kernel", the critical initiation energies have been predicted using the theory of Lee and Ramamurthi (1976) and found to be in reasonable agreement with the experimentally measured energies. This is true for both the ethylene-air mixtures used in the present tests and for the data reported by other experimenters for a range of different fuels.

Evidence from initiation experiments also exists to support the proposed critical cylindrical radius of  $4L_c$ . Lee et al. (1974) measured the distance-time trajectory of the initiating shock wave produced by an exploding wire in low-pressure oxyacetylene. When this trajectory was compared to that produced by the same discharge in an air medium, it was seen to depart from the latter at a radius of  $3.8L_c$ . It is likely that the front began to accelerate when self-sustenance became possible. All of the observations on

direct initiation of detonation support the idea that the role of the initiation source is simply to maintain the wave under specified adverse boundary conditions until such time that the post-shock gasdynamic expansion becomes mild enough for the shock/reaction zone complex to remain coupled on its own.

It would appear that the stream tube criterion is useful in clarifying the link between the critical conditions for initiation, propagation and transmission. It has been demonstrated that all of these critical conditions are a reflection of the same chemical-gasdynamic balance existing within the cellular detonation front. The concept has been successful in elucidating the link between many experimental parameters, including the critical tube diameter and the critical channel width for transmission of a planar wave to an unconfined region, the minimum diameter for propagation in an unconfined cylindrical column, and the minimum thickness for propagation in a cloud sitting on the ground. It has also been successful in interrelating the critical conditions for propagation under the influence of various expansion inducing mechanisms, including viscous boundary layers, compressible inert boundary gases, and yielding or moving boundaries.

The stream tube concept appears to be successful in describing the behavior of detonation waves under supercritical conditions as well. For values of  $\xi$  less than 20%, the measured velocity deficit  $\Delta V/V_{C-J}$  for propagation in square tubes consisting of a combination of rigid and yielding walls (Chapter 5) is seen to be a unique function of  $\xi$ . Furthermore, by choosing the cell length  $L_c$  over which to evaluate  $\xi$ , the relation between  $\Delta V/V_{C-J}$  and  $\xi$  is found to be in good agreement with the theoretical relation derived by Dabora (1963). This adds support to the claim that the relevant chemical kinetic thickness of the detonation front is approximately equal to the cell length. When the velocity deficit data reported by other investigators are processed in the above noted manner, they too are seen to be consistent with Dabora's theory. Included are deficits due to viscous boundary layer growth (e.g., Edwards et al., 1963; Dabora, 1963; Brochet, 1966; Boislevé, 1970; Renault, 1972) and deficits resulting from the compression of an inert boundary gas (e.g., Dabora, 1963). These observations suggest



that the behavior of detonation under supercritical conditions may be of a universal nature.

In a nutshell, the role of the "boundary conditions" is to govern the rate at which the post-shock particles are subjected to a gasdynamic expansion. If the rate of expansion is too rapid for the chemical processes to remain coupled with the shock, the wave will fail. The role of the "initial conditions" is to ensure that the wave is maintained in the presence of an adverse expansion until conditions become acceptable for it to survive on its own. A self-explanatory chart which helps to clarify the link between many different experimental investigations is presented in Figure 61.

### 7.3 Recommendations for Future Research

Having proposed a unifying theme which appears to explain satisfactorily the findings of many diverse experimental investigations, the author believes that an effort should now be directed toward clarifying, in a quantitative sense, the details of the stream tube criterion. Based on a few semi-quantitative observations, and the results of a relatively crude correlation (Chapter 4) in which many important physical details were ignored (e.g., the coupling between gasdynamic and chemical phenomena), the controlling chemical kinetic length in detonative propagation was concluded to be on the order of the cell size. Rather arbitrarily, the cell length  $L_c$  was chosen as the distance over which to evaluate the stream tube area increase  $\xi$ . We could just as easily have selected the cell width, or perhaps some multiple of the cell length, and simply arrived at a different fractional area increase to describe the critical conditions for sustenance. The fact remains that, to this point, there is very little direct physical evidence to support the claim that the controlling chemical kinetic length is precisely one cell length. What is required to clarify the issue is an experimental configuration which would allow us to i) clearly identify the streamwise location behind the shock beyond which a rarefactive disturbance will not influence the propagation, and ii) clearly identify the boundaries of the stream tube so that the critical fractional area increase  $\xi$  can be

measured. For ease of diagnosis and analysis, it would be attractive if the design was such that the flow aft of the shock is globally steady in shock-fixed coordinates.

An apparatus which may meet the above requirements is the variation of Dabora's (1963) test section sketched in Figure 62. Basically, it is a detonation tube of rectangular cross section, consisting of rigid top and bottom walls and a pair of parallel, photographically transparent side plates. A pair of dividing walls separate three equal velocity, parallel, laminar flows until they are allowed to interface in the test section. The bottom layer is an explosive gas. Confinement is provided on top by two layers of compressible inert gas (A and B). The apparatus would be constructed so that the widths of the gas columns,  $w_1$  and  $w_2$ , are independently adjustable. Care would have to be taken in the design to ensure that viscous boundary layer growth and spin structure/boundary coupling were not significant phenomena. The experimental procedure would be to first determine the critical column width  $w_1$  for propagation, given a particular explosive/inert gas combination and a ratio  $w_2/w_1$  which ensures that the top layer of inert gas (B) does not play a role in the outcome (i.e.,  $w_2 \gg w_1$ ). In essence, we would repeat the experiment carried out by Dabora. Having done so, the critical condition would then be monitored in subsequent tests as  $w_2$  is systematically decreased. Eventually, a configuration would be identified for which the disturbance created by the rarefaction wave in inert gas (A) would impinge on the gases in the reaction zone of the detonation wave and alter the critical condition for propagation. The strength of the rarefactive disturbance could be regulated by adjusting the properties (i.e., the density and the sonic velocity) of the two inert gases. Using Schlieren photography to observe the interaction between the reflected disturbance and the explosive/inert interface, the relevant chemical kinetic length and the corresponding critical stream tube area increase could be deduced. Pressure transducers or streak photography could be used to measure the velocity of propagation.

Impetus for the suggested experiments is provided, in part, by the observations of Tarasenko (1974b). This author investigated the influence

of an annular layer of water placed between a bare high-explosive cylindrical charge and a coaxial metal casing. He came to two important conclusions. First, for a given sensitivity of explosive and charge diameter, there existed a limiting thickness of water, beyond which the metal casing was of no consequence. Second, as the explosive was made less sensitive (i.e., as the reaction zone was made longer), the required water layer thickness was seen to increase. These observations suggested to Tarasenko that the limiting water layer thickness could be used to infer the reaction-zone length, but the idea was not pursued. In essence, what is proposed here is that the gaseous analogy to Tarasenko's problem be investigated, but with a rarefactive disturbance rather than a compressive one.

## 8.0 ORIGINALITY AND CONTRIBUTION TO KNOWLEDGE

Based on the findings of the nearly three hundred experiments carried out in five experimental apparatus, the author has made original contributions to knowledge by:

- i) providing for the first time a detailed description of the failure and reinitiation processes involved in the transformation of planar detonation from a circular tube to cylindrical detonation expanding radially outward between a pair of parallel plates. The author has identified two modes of reinitiation and proposed a correlation linking the critical plate separation for transmission  $w_c$  to the cell width  $\lambda$ ; i.e.,  $w_c \cong 5.7\lambda$ .
- ii) obtaining simultaneous measurements of the critical tube diameter and the cell size in large-scale experiments employing relatively insensitive ethylene-air mixtures. In doing so, the author has assisted in the evaluation of whether the  $13\lambda$  correlation, linking the critical tube diameter  $D_c$  to the cell width  $\lambda$ , is as valid for fuel-air mixtures as it is for the fuel-oxygen mixtures for which it was proposed.
- iii) successfully employing yielding boundaries to regulate the severity of the gasdynamic expansion imposed on the wave. This has been possible due to the relatively long chemical kinetic times characteristic of fuel-air mixtures. As a result, the author has provided a detailed description of the failure and reinitiation processes involved in the transmission of detonation from a rigid tube to one having yielding walls. Furthermore, he has proposed a criterion for criticality based on the competition between the rate of gasdynamic expansion and the rate at which energy is liberated within the cellular detonation front. When the author's criterion is applied to the results of many other investigators, it is found to describe successfully the critical conditions for propagation under a wide range of different boundary conditions and mixture

sensitivities, suggesting that the proposed critical chemical-gasdynamic balance may have universal implications.

- iv) measuring velocity deficits for propagation in a square channel consisting of a combination of rigid and yielding walls. The author has demonstrated that the conventional "stream line divergence" philosophy for the prediction of velocity deficits is valid, provided the nonsteady, three-dimensional, cellular detonation front is treated as an effective, one-dimensional reaction zone having a thickness equal to the cell length. Although the stream tube concept is not new, this is the first velocity deficit study which appeals to the cellular structure for the relevant chemical kinetic length scale. When the author's theory is applied to the results of many other investigators, it is found to describe successfully the observed velocity deficits for propagation under a wide range of boundary conditions and mixture sensitivities, suggesting that detonation behavior under supercritical conditions may be of a universal nature.
  
- v) showing that the critical conditions for a) initiation of detonation in various geometries, b) transmission of detonation from one geometry to another, and c) propagation of detonation under various boundary conditions, are all a result of the same critical chemical-gasdynamic balance being realized within the detonation front. This has been done by demonstrating that the increase in the area of the post-shock "stream tube", evaluated over a relevant chemical kinetic distance equal to the cell length, is the same in all cases.

The findings of this thesis have been presented in several international forums. The study on the transformation of planar detonation to cylindrical detonation (Chapter 2) has been reported in *Combustion and Flame* (1983). The results from the large-scale critical tube diameter experiments (Chapter 3) have been presented at the Nineteenth Symposium on Combustion in Haifa, Israel in 1982. The preliminary findings on the influence of yield-

ing confinement on large-scale ethylene-air detonations (Chapter 4) were described at the Spring Technical Meeting of the Combustion Institute (Canadian Section) in Banff, Canada in 1982. Final results have been published in the proceedings of the Ninth International Colloquium on Dynamics of Explosions and Reactive Systems, which was held in Poitiers, France in 1983. The velocity deficit results for propagation in square channels consisting of a combination of rigid and yielding walls (Chapter 5) were presented at the Paul Vieille Scientific Meeting, held in Vert-le-Petit, France in September of 1984. The experimental findings from the large-scale tests on the initiation of ethylene-air detonations (Chapter 6) have been published in the proceedings of the Seventh International Symposium on Military Applications of Blast Simulation, held in Medicine Hat, Canada in 1981. Finally, a paper summarizing the findings of the thesis has been submitted for presentation at the Tenth International Colloquium on Dynamics of Explosions and Reactive Systems, to be held in Berkely, California in the summer of 1985.

A report on the design and construction of the DRES large-scale fuel-air explosives (FAE) testing facility has been published internally at DRES as Suffield Memorandum No. 1051. Details of the facility, in conjunction with an overview of the DRES large-scale FAE research program, have been published in the proceedings of the International Conference on Fuel-Air Explosions, held in Montreal, Canada in 1981, and also as Suffield Memorandum No. 1053.

LIST OF REFERENCES

1. Abouseif, G. E. and Toong, T. Y. (1982) "On Direct Initiation of Gaseous Detonations". Combustion and Flame 45, 39.
2. Adams, T. G. (1972) "Experimental Investigation of the Interaction of a Detonation Wave with a Boundary Gas". Thesis, Michigan State University.
3. Adams, T. G. (1978) "Do Weak Detonation Waves Exist?" American Institute of Aeronautics and Astronautics 16, 1035.
4. Aminallah, M. (1982) "Effets d'une Onde de Choc Plane sur son Confinement Tubulaire Souple". Thèse, Université d'Orléans, France.
5. Atkinson, R., Bull, D. C. and Shuff, P. J. (1980) "Initiation of Spherical Detonation in Hydrogen/Air". Combustion and Flame 39, 287.
6. Bach, G. G., Knystautas, R. and Lee, J. H. (1969) "Direct Initiation of Spherical Detonations in Gaseous Explosives". Proceedings of the Twelfth Symposium (International) on Combustion, p. 853. The Combustion Institute.
7. Bach, G. G., Knystautas, R. and Lee, J. H. (1971) "Initiation Criteria for Diverging Gaseous Detonations". Proceedings of the Thirteenth Symposium (International) on Combustion, p. 1097. The Combustion Institute.
8. Barthel, H. O. (1972) "Reaction Zone - Shock Front Coupling in Detonations". Physics of Fluids 15, 43.
9. Barthel, H. O. (1974) "Predicted Spacings in Hydrogen-Oxygen-Argon Detonations". Physics of Fluids 17, 1547.

10. Bazhenova, T. V., Fokeev, V. P., Yu. Lobostov, Brossard, J., Bonnet, T., Brion, B. and Charpentier, N. (1981) "Influence of the Nature of Confinement on Gaseous Detonation". Progress in Astronautics and Aeronautics 75, 87.
11. Becker, R. (1936) "Uber Detonation". Z. Electroch. Bd. 42, 76, S. 457.
12. Belles, F. E. (1959) "Detonability and Chemical Kinetics: Prediction of Limits of Detonability of Hydrogen". Proceedings of the Seventh Symposium (International) on Combustion, p. 745. London: Butterworths.
13. Benedick, W. B. (1979) "High-Explosive Initiation of Methane-Air Detonations". Combustion and Flame 35, 89.
14. Benedick, W. B., Knystautas, R. and Lee, J. H. S. (1983) "Large Scale Experiments on the Transmission of Fuel-Air Detonations from Two-Dimensional Channels". Presented at the Ninth International Colloquium on Dynamics of Explosions and Reactive Systems (to be published).
15. Berthelot, M. (1881) "On the Velocity of Propagation of Explosive Processes in Gases". C. R. Hebd. Scéances Acad. Sci. 93, 18.
16. Berthelot, M. and Vieille, P. (1882) "On Explosive Waves". C. R. Hebd. Scéances Acad. Sci. 94, 101.
17. Bjerketvedt, D., Knystautas, R., Lee, J. H., Moen, I. O. and Rinnan, A. (1981) "Final Report on the Investigation of the Transmission of Detonations Through Orifices and Perforated Plates". Swacer Inc. Report, Montreal, Canada.
18. Bjerketvedt, D., Moen, I. O. and Jenssen, A. (1984) "Propagation of Fuel-Air Detonations Through Openings: Field Tests". Defence Research Establishment Suffield Memorandum SM-1143, Ralston, Alberta, Canada.



19. Boisleve, J.-N. (1970) "Propagation des Détonations dans des Mélanges Gazeux Contenus dans des Tubes de Section Rectangulaire". Thèse, Université de Poitiers, France.
20. Bone, W. A. and Townsend, P. T. A. (1927a) "Flame and Combustion in Gases". London: Longmans, Green.
21. Bone, W. A. and Townsend, P. T. A. (1927b) "Explosions and Gaseous Explosives". International Critical Tables, Vol. II, 172-195, published for the National Research Council. New York: McGraw-Hill.
22. Bone, W. A. and Frazer, N. D. (1930) "Photographic Investigation of Flame Movements in Gaseous Explosions" IV, V, VI. Philosophical Transactions of the Royal Society of London A230, 363.
23. Bone, W. A., Fraser, R. P. and Wheeler, W. H. (1935) "A Photographic Investigation of Flame Movements in Gaseous Explosions. VII. The Phenomenon of Spin in Detonations". Philosophical Transactions of the Royal Society of London A235, S. 29.
24. Boris, J. P. (1976) "Flux-Corrected Transport Models for Solving Generalized Continuity Equations". NRL Memorandum Report 3237.
25. Borisov, A. A. (1980) Private Communication.
26. Borisov, A. A. and Loban, S. A. (1977) "Detonation Limits of Hydrocarbon-Air Mixtures in Tubes". Fizika Goreniya i Vzryva 13, 729.
27. Brinkley, S. R. Jr. and Kirkwood, J. G. (1949) "On the Condition of Stability of the Plane Detonation Wave". Proceedings of the Third Symposium (International) on Combustion, p. 586. Baltimore: Williams and Wilkins.

28. Brochet, C. (1966) "Contributions à l'Étude des Détonations Instables dans les Mélanges Gazeux". Thèse, Université de Poitiers, France.
29. Brossard, J., Desbordes, D. and Manson, N. (1972) "Variation de la Célérité des Détonations Sphériques Divergentes dans les Mélanges Stricts Propane-Oxygène-Azote et Acétylène-Oxygène-Azote en Fonction de l'Abscisse Radiale: Influence de la Dilution en Inerte". C. R. Acad. Sci. Paris 274, 1198.
30. Brossard, J., Charpentier de Coysevox, N. (1976) "Effets d'un Confinement Souple sur la Détonation des Mélanges Gazeux". Acta Astronautica 3, 971.
31. Brossard, J. and Renard, J. (1981) "Mechanical Effects of Gaseous Detonations on a Flexible Confinement". Progress in Astronautics and Aeronautics 75, 108.
32. Bull, D. C. (1979) "Concentration Limits to the Initiation of Unconfined Detonation in Fuel/Air Mixtures". Transactions of the Institution of Chemical Engineers 57, 219.
33. Bull, D. C., Elsworth, J. E., Hooper, G. and Quinn, C. P. (1976) "A Study of Spherical Detonation in Mixtures of Methane and Oxygen Diluted by Nitrogen". Journal of Physics D: Applied Physics 9, 1991.
34. Bull, D. C., Elsworth, J. E. and Hooper, G. (1978) "Initiation of Spherical Detonation in Hydrocarbon/Air Mixtures". Acta Astronautica 5, 997.
35. Bull, D. C. and Elsworth, J. E. (1979a) "Concentration Limits to Unconfined Detonation of Ethane-Air". Combustion and Flame 35, 27.
36. Bull, D. C., Elsworth, J. E., McLeod, M. A. and Hughes, D. (1979b) "Initiation of Unconfined Gas Detonations in Hydrocarbon-Air Mixtures by

- a Sympathetic Mechanism". Proceedings of the Seventh International Colloquium on Dynamics of Explosions and Reactive Systems.
37. Bull, D. C., Elsworth, J. E., Shuff, P. J. and Metcalfe, E. (1982) "Detonation Cell Structures in Fuel/Air Mixtures". *Combustion and Flame* 45, 7.
  38. Campbell, A. W., Malin, M. E. and Holland, T. E. (1955) "Detonation in Homogeneous Explosives". Proceeding of the Second ONR Symposium on Detonation, p. 336. Office of Naval Research. United States Department of the Navy, Washington, D.C.
  39. Campbell, C. and Woodhead, D. W. (1927) "The Ignition of Gases by an Explosion Wave. Part I. Carbon Monoxide and Hydrogen Mixtures". *Journal of the Chemical Society*, p. 1572.
  40. Campbell, C. and Finch, A. C. (1928) "Striated Photographic Records of Explosion Waves. Part II. An Explanation of the Striae". *Journal of the Chemical Society* 131, 2094.
  41. Carlson, G. A. (1973) "Spherical Detonation in Gas-Oxygen Mixtures". *Combustion and Flame* 21, 383.
  42. Cassut, L. H. (1961) "Experimental Investigation of Detonation in Unconfined Gaseous Hydrogen/Oxygen/Nitrogen Mixtures". *Journal of the American Rocket Society* 31, 1123.
  43. Chapman, D. L. (1899) "On the Rate of Explosion in Gases". *Philosophical Magazine* 47, 90.
  44. Chapman, S. and Cowling, T. G. (1970) "The Mathematical Theory of Non-Uniform Gases". Third Edition, Cambridge University Press. London: Bentley House.

45. Cook, M. A. (1958) "The Science of High Explosives". New York: Reinhold.
46. Crooker, A. J. (1969) "Phenomenological Investigation of Low-Mode Marginal Planar Detonations". University of Illinois (Urbana) Technical Report AAE 69-2 (Ph.D. Thesis).
47. Crussard, L. and Jouguet, E. (1907a) "Sur les Ondes de Choc et Combustion, Stabilité de l'Onde Explosive". C. R. Acad. Sci. Paris 144, 560.
48. Crussard, L. (1907b) "Ondes de Choc et Onde Explosive". Bull. Soc. Industr. Min. St-Étienne 4e Serie, tome 6, p. 257.
49. Dabora, E. K. (1963) "The Influence of a Compressible Boundary on the Propagation of Gaseous Detonations". University of Michigan Technical Report U5170-1-T (Ph.D. Thesis).
50. Dabora, E. K., Nicholls, J. A. and Morrison, R. B. (1965) "The Influence of a Compressible Boundary on the Propagation of Gaseous Detonations". Proceedings of the Tenth Symposium (International) on Combustion, p. 817. The Combustion Institute.
51. Davenport, J. A. (1977) "A Survey of Vapour Cloud Incidents". Proceedings of the Eighty-Third National Meeting, AIChE, p. 54. Houston, Texas.
52. Denisov, Yu. N. and Troshin, Ya. K. (1959) "Pulsating and Spinning Detonation of Gaseous Mixtures in Tubes". Dokl. Akad. Nauk SSSR (Phys.-Chem. Sec.) 125, 110.
53. Desbordes, D. and Manson, N. (1981) "Influence of Walls on Pressure Behind Self-sustained 'Expanding Cylindrical' and 'Plane' Detonations in

- Gases". Presented at the Eighth International Colloquium on Dynamics of Explosions and Reactive Systems (to be published).
54. Dixon, H. B., Bower, J., Bradshaw, L., Dawson, B., Graham, E., Jones, R. H. and Strange, E. H. (1903) "On the Movement of Flame in the Explosion of Gases". Philosophical Transactions of the Royal Society of London A200, 315.
  55. Donato, M. (1982) "The Influence of Confinement on the Propagation of Near Limit Detonation Waves". Ph.D. Thesis, McGill University, Montreal, Canada.
  56. Döring, W. and Burckhardt, G. (1944) "Contributions to the Theory of Detonation". VDI Forschungsbericht No. 1939, 1944 (in German). English Translation: Brown University, Technical Report No. F-TS-1277-1A (GDAM A9-T46) Air Material.
  57. Dove, J. E. and Wagner, H. Gg. (1962) "A Photographic Investigation of the Mechanism of Spinning Detonation". Proceedings of the Eighth Symposium (International) on Combustion, p. 589. Baltimore: Williams and Wilkins.
  58. Dove, J. E., Scroggie, B. J. and Semerjian, H. (1974) "Velocity Deficits and Detonability Limits of Hydrogen-Oxygen Detonations". Acta Astronautica 1, 345.
  59. Dremin, A. N. and Trofimov, V. S. (1965) "On the Nature of the Critical Diameter". Proceedings of the Tenth Symposium (International) on Combustion, p. 839. The Combustion Institute.
  60. Duff, R. E. (1963) Discussion of Paper Presented by Manson et al. Proceedings of the Ninth Symposium (International) on Combustion, p. 469. New York and London: Academic Press.

61. Edwards, D. H. (1969) "A Survey of Recent Work on the Structure of Detonation Waves". Proceedings of the Twelfth Symposium (International) on Combustion, p. 819. The Combustion Institute.
62. Edwards, D. H., Jones, T. G. and Price, B. (1963) "Observations on Oblique Shock Waves in Gaseous Detonations". Journal of Fluid Mechanics 17, 21.
63. Edwards, D. H., Hooper, G., Job, E. M. and Parry, D. J. (1970) "The Behavior of the Frontal and Transverse Shocks in Gaseous Detonation Waves". Astronautica Acta 15, 323.
64. Edwards, D. H., Hooper, G. and Morgan, J. M. (1974) "A Study of Unstable Detonations Using a Microwave Interferometer". Journal of Physics D: Applied Physics 7, 242.
65. Edwards, D. H., Hooper, G. and Morgan, J. M. (1976a) "An Experimental Investigation of the Direct Initiation of Spherical Detonations". Acta Astronautica 3, 117.
66. Edwards, D. H., Jones, A. T. and Phillips, D. E. (1976b) "The Location of the Chapman-Jouguet Surface in a Multiheaded Detonation Wave". Journal of Physics D: Applied Physics 9, 1331.
67. Edwards, D. H. and Morgan, J. M. (1977) "Instabilities in Detonation Waves Near the Limits of Propagation". Journal of Physics D: Applied Physics 10, 2377.
68. Edwards, D. H., Hooper, G., Morgan, J. M. and Thomas, G. O. (1978) "The Quasi-Steady Regime in Critically Initiated Detonation Waves". Journal of Physics D: Applied Physics 11, 2103.

69. Edwards, D. H., Thomas, G. O. and Nettleton, M. A. (1979) "The Diffraction of a Planar Detonation Wave at an Abrupt Area Change". *Journal of Fluid Mechanics* 95, 79.
70. Edwards, D. H., Fearnley, P., Thomas, G. O. and Nettleton, M. A. (1981a) "Shocks and Detonations in Channels with 90° Bends". Proceedings of the First Specialists Meeting (International) of the Combustion Institute, p. 431. The Combustion Institute.
71. Edwards, D. H., Thomas, G. O. and Nettleton, M. A. (1981b) "Diffraction of Planar Detonation in Various Fuel-Oxygen Mixtures at an Area Change". *Progress in Astronautics and Aeronautics* 75, 341.
72. Edwards, D. H., Thomas, G. O. and Williams, T. L. (1981c) "Initiation of Detonation by Steady Planar Incident Shock Waves". *Combustion and Flame* 43, 187.
73. Eisen, C. L., Gross, R. A. and Rivlin, T. J. (1960) "Theoretical Calculations in Gaseous Detonation". *Combustion and Flame* 4, 137.
74. Elsworth, J. E., Shuff, P. J. and Ungut, A. (1983) "'Galloping' Gas Detonation in the Spherical Mode". Presented at the Ninth International Colloquium on Dynamics of Explosions and Reactive Systems (to be published).
75. Enig, J. W. and Petrone, F. J. (1970) "The Failure Diameter Theory of Dremin". Proceedings of the Fifth ONR Symposium on Detonation, p. 99. Office of Naval Research. United States Department of the Navy, Washington, D.C.
76. Erpenbeck, J. J. (1969) "Theory of Detonation Stability". Proceedings of the Twelfth Symposium (International) on Combustion, p. 711. The Combustion Institute.

77. Eyring, H., Powell, R. E., Duffey, G. H. and Parlin, R. B. (1949) "The Stability of Detonation". Chemical Reviews 45, 69.
78. Fay, J. A. (1952) "A Mechanical Theory of Spinning Detonation". Journal of Chemical Physics 20, 942.
79. Fay, J. A. (1959) "Two-Dimensional Gaseous Detonations: Velocity Deficit". Physics of Fluids 2, 283.
80. Fay, J. A. and Opel, G. (1958) "Two-Dimensional Effects in Gaseous Detonation Waves". Journal of Chemical Physics 29, 955.
81. Fickett, W. and Davis, W. C. (1979) "Detonation". Berkeley, Los Angeles and London: University of California Press.
82. Freiwald, A. and Koch, H. W. (1963) "Spherical Detonations of Acetylene-Oxygen-Nitrogen Mixtures as a Function of Nature and Strength of Initiation". Proceedings of the Ninth Symposium (International) on Combustion, p. 275. New York and London: Academic Press.
83. Fry, R. S. and Nicholls, J. A. (1974) "Blast Wave Initiation of Gaseous and Heterogeneous Cylindrical Detonation Waves". Proceedings of the Fifteenth Symposium (International) on Combustion, p. 43. The Combustion Institute.
84. Funk, J. W. and Murray, S. B. (1982) "The DRES Large-Scale Fuel-Air Explosives Testing Facility". Defence Research Establishment Suffield Memorandum SM-1051, Ralston, Alberta, Canada.
85. Funk, J. W., Murray, S. B., Moen, I. O. and Ward, S. A. (1982) "A Brief Description of the DRES Fuel-Air Explosives Testing Facility and Current Research Program". Proceedings of the International Conference on Fuel-Air Explosions, Montreal, Nov. 4-6, 1981, p. 565. SM Study No. 16, University of Waterloo Press, Ontario, Canada.



86. Glassman, I. (1977) "Combustion". New York: Academic Press.
87. Gooderum, P. B. (1958) "An Experimental Study of the Turbulent Boundary Layer on a Shock Tube Wall". NACA Technical Note No. 4243.
88. Gordeev, V. E. (1976) "The Cause of Multiplication of Discontinuities in a Detonation". Dokl. Akad. Nauk SSSR (Phys. Sec.) 226, 288.
89. Gordon, S. and McBride, B. I. (1976) "Computer Program for Calculation of Complex Chemical Equilibrium Compositions, Rocket Performance, Incident and Reflected Shocks and Chapman-Jouguet Detonations". NASA report SP-273.
90. Gross, R. A. and Oppenheim, A. K. (1959) "Recent Advances in Gaseous Detonation". Journal of the American Rocket Society 29, 173.
91. Guirao, C. M., Knystautas, R., Lee, J. H., Benedick, W. and Berman, M. (1982) "Hydrogen-Air Detonations". Proceedings of the Nineteen Symposium (International) on Combustion, p. 583. The Combustion Institute.
92. Hidaka, Y., Kataoka, T. and Suga, M. (1974) "A Shock-Tube Investigation in Ethylene-Oxygen-Argon Mixtures". Bulletin of the Chemical Society of Japan 47, 2166.
93. Hikita, T. et al. (1975) "A Report on the Experimental Results of Explosions and Fires of Liquid Ethylene Facilities". Safety Information Centre, Institution for Safety of High Pressure Gas Engineering, Tokyo, Japan.
94. Hirschfelder, J. O. and Curtiss, C. F. (1958a) "Theory of Detonations. I. Irreversible Unimolecular Reactions". Journal of Chemical Physics 28, 197.

95. Hirschfelder, J. O., Linder, B. and Curtiss, C. F. (1958b) "Theory of Detonations. II. Reversible Unimolecular Reaction". Journal of Chemical Physics 28, 1147.
96. Hirschfelder, J. O., Curtiss, C. F. and Barnett, M. P. (1959) "Theory of Detonations. III. Ignition Temperature Approximation". Journal of Chemical Physics 30, 470.
97. Hugoniot, H. (1887-1889) "Propagation du Mouvement dans les Corps". J. Éc. Polyt. Paris, 57e cahier, pp. 3-97, 58e cahier, pp. 1-125.
98. Jenssen, A. (1983) Private Communication.
99. Jones, H. (1947) "A Theory of the Dependence of the Rate of Detonation of Solid Explosives on the Diameter of the Charge". Proceedings of the Royal Society of London A189, 415.
100. Jouguet, E. (1905) "Sur la Propagation des Réactions Chimiques dans les Gaz". J. Math. Pures Appl. 6e Serie, tome 1, v. 60, fasc. 4, p. 347.
101. Jouguet, E. (1906) "Sur la Propagation des Réactions Chimiques dans les Gaz". J. Math. Pures Appl. 6e Serie, tome 2, v. 61, fasc. 1, p. 1.
102. Jouguet, E. (1917) "Mécanique des Explosifs". Encyclopédie Scientifique. Paris: Dion et Fils.
103. Jouguet, E. (1927) "La Théorie Thermodynamique de la Propagation des Explosions". Proc. 2nd Int. Congr. Appl. Mech., p. 12.
104. Kailasanath, K. and Oran, E. S. (1983) "The Relation Between Power and Energy in the Shock Initiation of Detonations. I. Basic Theoretical Considerations and the Effects of Geometry". Naval Research Laboratory Memorandum Report 5179. Washington, D. C.

105. Kirkwood, J. G. and Wood, W. W. (1954) "Structure of a Steady-State Plane Detonation Wave with Finite Reaction Rate". *Journal of Chemical Physics* 22, 1915.
106. Kistiakowsky, G. B., Knight, H. T. and Malin, M. E. (1952a) "Gaseous Detonations. V. Nonsteady Waves in CO-O<sub>2</sub> Mixtures". *Journal of Chemical Physics* 20, 994.
107. Kistiakowsky, G. B. and Kydd, P. H. (1952b) "Gaseous Detonations. III. Dissociation Energies of Nitrogen and Carbon Monoxide". *Journal of Chemical Physics* 20, 876.
108. Kistiakowsky, G. B. and Kydd, P. H. (1954) "The Reaction Zone in Gaseous Detonations". *Journal of Chemical Physics* 22, 1940.
109. Klug, C. and Simpson, S. (1982) "Investigations on the Diffraction of Gaseous Detonations". Internal Report. Defence Research Establishment Suffield, Ralston, Alberta, Canada.
110. Knystautas, R. and Lee, J. H. (1976) "On the Effective Energy for Direct Initiation of Gaseous Detonations". *Combustion and Flame* 27, 221.
111. Knystautas, R., Lee, J. H., Moen, I. O. and Wagner, H. Gg. (1978) "Direct Initiation of Spherical Detonation by a Hot Turbulent Gas Jet". Proceedings of the Seventeenth Symposium (International) on Combustion, p. 1235. The Combustion Institute.
112. Knystautas, R., Lee, J. H. and Moen, I. O. (1981) "Determination of Critical Tube Diameters for C<sub>2</sub>H<sub>4</sub>-Air and C<sub>2</sub>H<sub>4</sub>-Air Mixtures. II. Raufoss Field Experiments". Swacer Inc. Report, Montreal, Canada.
113. Knystautas, R., Lee, J. H. and Guirao, C. M. (1982) "The Critical Tube Diameter for Detonation Failure in Hydrocarbon-Air Mixtures". *Combustion and Flame* 48, 63.

114. Knystautas, R., Guirao, C., Lee, J. H. and Sulmistras, A. (1983) "Measurements of Cell Size in Hydrocarbon-Air Mixtures and Predictions of Critical Tube Diameter, Critical Initiation Energy and Detonability Limits". Presented at the Ninth International Colloquium on Dynamics of Explosions and Reactive Systems (to be published).
115. Kogarko, S. M. and Zeldovich, Ya. B. (1948) "Detonation of Gaseous Mixtures". Dokl. Akad. Nauk SSSR 63, 553.
116. Kogarko, S. M., Adushkin, V. V. and Lyamin, A. G. (1965) "Investigation of Spherical Detonation of Gas Mixtures". Combustion, Explosion and Shock Waves 2, 22.
117. Kyong, W. H. (1972) "A Theoretical Study of Spherical Gaseous Detonation Waves". Ph.D. Thesis, McGill University, Montreal, Canada.
118. Lafitte, P. (1923) "Sur la Formation de l'Onde Explosive". C. R. Acad. Sci. Paris 176, 1392.
119. Lafitte, P. (1924) "Sur la Propagation de l'Onde Explosive". C. R. Acad. Sci. Paris 179, 1394.
120. Lafitte, P. F. (1938) "Flames of High-Speed Detonation". Science of Petroleum 4, 2995.
121. Le Chatelier, H. (1900) "Sur le Développement et la Propagation de l'Onde Explosive". C. R. Acad. Sci. Paris 130, 1755.
122. Lee, J. H. (1972) "Gasdynamics of Detonations". Astronautica Acta 17, 455.
123. Lee, J. H. S. (1977) "Initiation of Gaseous Detonation". Annual Review of Physical Chemistry 28, 75.

124. Lee, J. H. S. (1983) Private Communication.
125. Lee, J. H. and Lee, B. H. K. (1965) "On Cylindrical Imploding Shock Waves". Proceedings of the Fifth International Shock Tube Symposium, p. 501. The American Physical Society.
126. Lee, J. H. S., Lee, B. H. K. and Knystautas, R. (1966) "Direct Initiation of Cylindrical Gaseous Detonations". Physics of Fluids 9, 221.
127. Lee, J. H., Soloukhin, R. I. and Oppenheim, A. K. (1969) "Current Views on Gaseous Detonation". Astronautica Acta 14, 565.
128. Lee, J. H., Knystautas, R. and Guirao, C. M. (1974) "Critical Power Density for Direct Initiation of Unconfined Gaseous Detonations". Proceedings of the Fifteenth Symposium (International) on Combustion, p. 53. The Combustion Institute.
129. Lee, J. H. and Ramamurthi, K. (1976) "On the Concept of the Critical Size of a Detonation Kernel". Combustion and Flame 27, 331.
130. Lee, J. H. and Matsui, H. (1977) "A Comparison of the Critical Energies for Direct Initiation of Spherical Detonations in Acetylene-Oxygen Mixtures". Combustion and Flame 28, 61.
131. Lee, J. H. S. and Moen, I. O. (1980) "The Mechanism of Transition From Deflagration to Detonation in Vapour Cloud Explosions". Progress in Energy and Combustion Science 6, 359.
132. Lee, J. H., Knystautas, R., Guirao, C. M., Benedick, W. B. and Shepard, J. (1981) "Hydrogen-Air Detonations". Proceedings of the Second International Workshop on the Impact of Hydrogen on Water Reactor Safety, p. 583.

133. Lee, J. H. S., Knystautas, R, and Guirao, C. M. (1982) "On the Link Between Cell Size, Critical Tube Diameter, Initiation Energy and Detonability Limits". Proceedings of the International Conference on Fuel-Air Explosions, Montreal, Nov. 4-6, 1981, p. 157. SM Study No. 16, University of Waterloo Press, Ontario, Canada.
134. Levin, V. A. and Markov, V. V. (1976) "Detonation with Concentrated Underwater Energy". Fluid Dynamics USSR 9, 754.
135. Lewis, B. and Friaf, J. B. (1930) "Explosions in Detonating Gas Mixtures. I. Calculation of Rates of Explosion in Mixtures of Hydrogen and Oxygen and the Influence of Rare Gases". Journal of American Chemistry 52, 3905.
136. Lewis, B. and von Elbe, G. (1961) "Combustion, Flames and Explosions of Gases". New York and London: Academic Press.
137. Libouton, J.-C. and van Tiggelen, P. J. (1976) "Influence of the Composition of the Gaseous Mixture on the Structure of Detonation Waves". Acta Astronautica 3, 759.
138. Libouton, J.-C., Dormal, M. and van Tiggelen, P. J. (1981) "Reinitiation Process at the End of the Detonation Cell". Progress in Astronautics and Aeronautics 75, 358.
139. Litchfield, E. L., Hay, M. H. and Forshey, D. R. (1962) "Direct Electrical Initiation of Freely Expanding Gaseous Detonation Waves". Proceedings of the Ninth Symposium (International) on Combustion, p. 282. New York and London: Academic Press.
140. Liu, Y. K., Lee, J. H. and Knystautas, R. (1984) "Effect of Geometry on the Transmission of Detonation Through an Orifice". Combustion and Flame 56, 215.

141. Lu, P.-L. (1968) "The Structure and Kinetics of  $H_2$ -CO- $O_2$  Detonations". Ph.D. Thesis, University of Michigan.
142. Lundstrom, E. A. and Oppenheim, A. K. (1969) "On the Influence of Non-Steadiness on the Thickness of the Detonation Wave". Proceedings of the Royal Society of London A310, 463.
143. Mach, E. and Sommer, J. (1877) "Uber die Fortpflanzungsgeschwindigkeit von Explosionsschallwellen. Akademie der Eissenschaften, Wien.-Naturw.-Klasse Sitzungsberichte Teil II, p. 101.
144. Mallard, E. and Le Chatelier, H. (1881) "On the Propagation Velocity of Burning of Gaseous Explosive Mixtures". C. R. Hebd. Scéances Acad. Sci. 93, 145.
145. Mallard, E. and Le Chatelier, H. (1883) "Recherches Expérimentales et Théoriques sur la Combustion des Mélanges Gazeux Explosifs". Ann. Mines 8, 274.
146. Manson, N. (1946) "On the Structure of So-Called Helical Detonation Waves in Gaseous Mixtures". C. R. Hebd. Scéances Acad. Sci. 222, 46.
147. Manson, N. and Ferrié, F. (1953) "Contribution to the Study of Spherical Detonation Waves". Proceedings of the Fourth Symposium (International) on Combustion, p. 486. Baltimore: Williams and Wilkins.
148. Manson, N. and Guénoche, H. (1957) "Effect of the Charge Diameter on the Velocity of Detonation Waves in Gas Mixtures". Proceedings of the Sixth Symposium (International) on Combustion, p. 631. New York: Reinhold.
149. Manson, N., Brochet, Ch., Brossard, J. and Pujol, Y. (1963) "Vibratory Phenomena and Instability of Self-Sustained Detonations in Gases".

- Proceedings of the Ninth Symposium (International) on Combustion, p. 461. New York and London: Academic Press.
150. Martin, L. and Lee, J. H. (1982) Private Communication.
151. Matsui, H. and Lee, J. H. (1976) "Influence of Electrode Geometry and Spacing on the Critical Energy for Direct Initiation of Spherical Gaseous Detonations". *Combustion and Flame* 27, 217.
152. Matsui, H. and Lee, J. H. (1979) "On the Measure of the Relative Detonation Hazards of Gaseous Fuel-Oxygen and Air Mixtures". Proceedings of the Seventeenth Symposium (International) on Combustion, p. 1269. The Combustion Institute.
153. Meyer, R. F. (1958) "The Impact of a Shock on a Movable Wall". *Journal of Fluid Mechanics* 3, 309.
154. Mitrofanov, V. V. and Soloukhin, R. I. (1965) "The Diffraction of Multifront Detonation Waves". *Soviet Physics-Doklady* 9, 1055.
155. Moen, I. O. (1982) Private Communication.
156. Moen, I. O., Donato, M., Knystautas, R. and Lee, J. H. (1981) "The Influence of Confinement on the Propagation of Detonation Near the Detonability Limits". Proceedings of the Eighteenth Symposium (International) on Combustion, p. 1615. The Combustion Institute.
157. Moen, I. O., Thibault, P. A., Funk, J. W., Ward, S. A. and Rude, G. M. (1983) "Detonation Length Scales for Fuel-Air Explosives". Presented at the Ninth International Colloquium on Dynamics of Explosions and Reactive Systems (to be published).



158. Moen, I. O., Bjerketvedt, D., Jenssen, A. and Thibault, P. A. (1984) "Transition to Detonation in a Large Fuel-Air Cloud". Submitted to Combustion and Flame as a Short Communication.
159. Mooradian, A. J. and Gordon, W. E. (1951) "Gaseous Detonation. I. Initiation of Detonation". Journal of Chemical Physics 19, 1166.
160. von Neumann, J. (1942) "Theory of Detonation Waves". John von Neumann, Collected Works 6.
161. Nicholls, J. A. et al. (1962a) "The Feasibility of a Rotating Detonation Wave Rocket Motor". University of Michigan Quarterly Report U5179-1-P.
162. Nicholls, J. A. et al. (1962b) "The Feasibility of a Rotating Detonation Wave Rocket Motor". University of Michigan Quarterly Report U5179-2-P.
163. Nicholls, J. A. et al. (1963) "The Feasibility of a Rotating Detonation Wave Rocket Motor". University of Michigan Quarterly Report U5179-3-P.
164. Nolan, M. E. (1973) "A Simple Model for the Detonation Limits of Gas Mixtures". Combustion Science and Technology 7, 57.
165. Oppenheim, A. K. (1961) "Development and Structure of Plane Detonation Waves". Fourth AGARD Colloquium on Combustion and Propulsion, p. 186.
166. Oppenheim, A. K. (1970) "Introduction to Gasdynamics of Explosions". New York: Springer-Verlag Wien.
167. Oppenheim, A. K. and Rosciszewski, J. (1963) "Determination of the Detonation Wave Structure". Proceedings of the Ninth Symposium (International) on Combustion, p. 424. New York and London: Academic Press.

168. Oppenheim, A. K., Smolen, J. J., Kwak, D. and Urtiew, P. A. (1970) "On the Dynamics of Shock Intersections". Proceedings of the Fifth ONR Symposium on Detonation, p. 119. Office of Naval Research. United States Department of the Navy, Washington, D.C.
169. Oppenheim, A. K. and Soloukhin, R. I. (1973) "Experiments in Gasdynamics of Explosions". Annual Review of Fluid Mechanics 5, 31.
170. Oran, E. S., Boris, J. P., Young, T., Flanigan, M., Burks, T. and Picone, M. (1981) "Numerical Simulations of Detonations in Hydrogen-Air and Methane-Air Mixtures". Proceedings of the Eighteenth Symposium (International) on Combustion, p. 1641. The Combustion Institute.
171. Parsons, G. H., Vanta, E. B., Collins, P. M. and Bearley, J. (1973) "Techniques for Investigation of Unconfined Fuel-Air Detonations". AFATL-TR-73-230. Air Force Armament Laboratory, Eglin AFB, Florida.
172. Patch, R. W. (1961) "Prediction of Composition Limits for Detonations of Hydrogen-Oxygen-Diluent Mixtures". Journal of the American Rocket Society 31, 46.
173. Pförtner, H. (1977) Private Communication as cited by Bull (1979).
174. Pförtner, H., Schneider, H., Drenchan, W. and Koch, C. (1983) "Flame Acceleration and Pressure Build-Up in Free and Partial Confined Hydrogen-Air Clouds". Presented at the Ninth International Colloquium on Dynamics of Explosions and Reactive Systems (to be published).
175. Pujol, Y. (1968) "Contribution à l'Étude des Détonations par la Méthode Inverse". Thèses, Université de Poitiers, France.
176. Ramamurthi, K. (1976) "On the Blast Initiation of Gaseous Detonation". Ph.D. Thesis, McGill University, Montreal, Canada.

177. Renault, G. (1972) "Propagation des Détonations dans des Mélanges Gazeux Contenus dans des Tubes de Section Circulaire et de Section Rectangulaire: Influence de l'État de la Surface Interne des Tubes". Thèse, Université de Poitiers, France.
178. Rinnan, A. (1982) "Transmission of Detonation Through Tubes and Orifices". Proceedings of the International Conference on Fuel-Air Explosions, Montreal, Nov. 4-6, 1981, p. 553. SM Study No. 16, University of Waterloo Press, Ontario, Canada.
179. Rivan, M. and Sokolik, A. (1936) " Les Limites d'Explosivité des Melanges Gazeux". Acta Phys.-Chem. URSS Tome 4, No. 2, 301.
180. Rybanin, S. S. (1969) "Theory of Detonation in Rough Tubes". Fizika Goreniya i Vzryva 5, 395.
181. Saint-Cloud, J. P., Guerraud, Cl., Brochet, C. and Manson, N. (1972) "Some Properties of Very Unstable Detonations in Gaseous Mixtures". Astronautica Acta 17, 487.
182. Schott, G. L. (1965) "Observations of the Structure of Spinning Detonations". Physics of Fluids 8, 850.
183. Schott, G. L. and Kinsey, J. H. (1958) "Kinetic Studies of Hydroxyl Radicals in Shock Waves. II. Induction Times in the Hydrogen-Oxygen Reaction". Journal of Chemical Physics 29, 1177.
184. Shchelkin, K. I. (1940) "Effects of Roughness on the Surface in a Tube on Origination and Propagation of Detonation in Gases". Soviet Physics J.E.T.P. 10, 823.
185. Shchelkin, K. I. (1947) "Detonation of Gases in Rough Tubes". Zh. Technich. Fiz. 17, 613.

186. Shchelkin, K. I. (1959) "Two Cases of Unstable Combustion". Soviet Physics J.E.T.P. 9, 146.
187. Shchelkin, K. I and Troshin, Ya. K. (1965) "Gasdynamics of Combustion". Baltimore: Mono Book.
188. Sichel, M. (1965) "A Hydrodynamic Theory for the Interaction of a Gaseous Detonation with a Compressible Boundary". University of Michigan Technical Report 05170-2-T.
189. Sichel, M. A. (1977) "A Simple Analysis of the Blast Initiation of Detonations". Acta Astronautica 4, 409.
190. Soloukhin, R. I. and Ragland, K. W. (1969) "Ignition Processes in Expanding Detonations". Combustion and Flame 13, 295.
191. Sommers, W. P. (1961) "The Interaction of a Detonation Wave with an Inert Boundary". Ph.D. Thesis, University of Michigan.
192. Sommers, W. P. and Morrison, R. B. (1962) "Simulation of Condensed-Explosive Detonation Phenomena with Gases". Physics of Fluids 5, 241.
193. Steel, G. B. and Oppenheim, A. K. (1966) "Experimental Study of the Wave Structure of Marginal Detonations in a Rectangular Tube". University of California, Berkely, Report AS66-4.
194. Strehlow, R. A. (1968) "Gas Phase Detonations: Recent Developments". Combustion and Flame 12, 81.
195. Strehlow, R. A. (1969) "The Nature of Transverse Waves in Detonations". Astronautica Acta 14, 539.
196. Strehlow, R. A. (1970) "Multi-Dimensional Detonation Wave Structure". Astronautica Acta 15, 345.

AD-A162 631

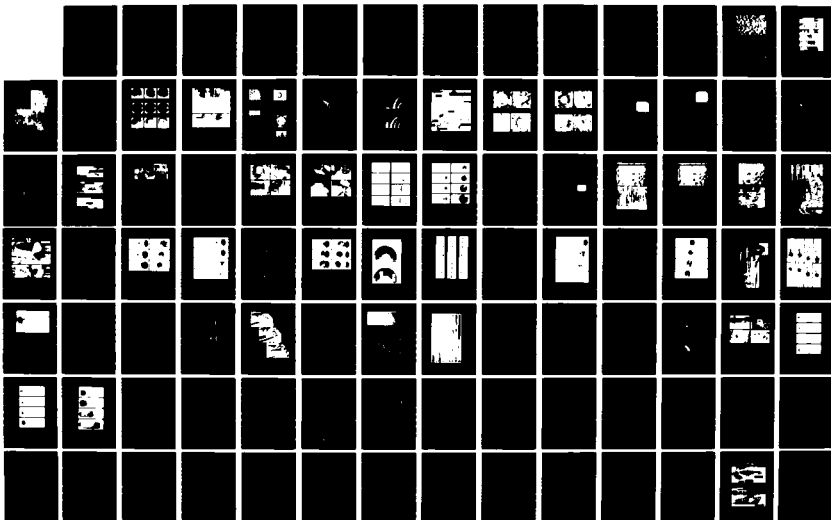
THE INFLUENCE OF INITIAL AND BOUNDARY CONDITIONS ON  
GASEOUS DETONATION WAVES(U) DEFENCE RESEARCH  
ESTABLISHMENT SUFFIELD RALSTON (ALBERTA) S B MURRAY  
SEP 85 DRES-SR-411

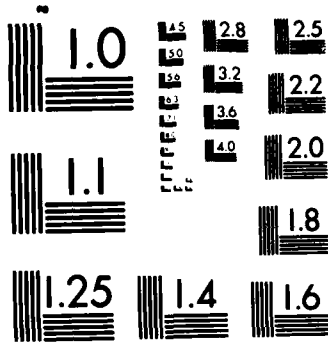
3/4

UNCLASSIFIED

F/G 19/4

NL





MICROCOPY RESOLUTION TEST CHART  
NATIONAL BUREAU OF STANDARDS-1963-A

197. Strehlow, R. A. and Cohen, A. (1962) "Initiation of Detonation". *Physics of Fluids* 5, 97.
198. Strehlow, R. A., Liaugminas, R., Watson, R. H. and Eymen, J. R. (1967) "Transverse Wave Structure in Detonations". *Proceedings of the Eleventh Symposium (International) on Combustion*, p. 683. The Combustion Institute.
199. Strehlow, R. A. and Biller, J. R. (1969) "On the Strength of Transverse Waves in Gaseous Detonations". *Combustion and Flame* 13, 577.
200. Strehlow, R. A. and Engel, C. D. (1969) "Transverse Waves in Detonations: II. Structure and Spacing in  $H_2-O_2$ ,  $C_2H_2-O_2$ ,  $C_2H_4-O_2$  and  $CH_4-O_2$  Systems". *American Institute of Aeronautics and Astronautics* 7, 492.
201. Strehlow, R. A., Adamczyk, A. A. and Stiles, R. J. (1972) "Transient Studies on Detonation Waves". *Astronautica Acta* 17, 509.
202. Strehlow, R. A. and Crooker, A. J. (1974) "Structure of Marginal Detonation Waves". *Acta Astronautica* 1, 303.
203. Subbotin, V. A. and Mitrofanov, V. V. (1980) "Mechanism of Detonation Re-establishment at Abrupt Expansion of Front". *Lavrent'yev Institute of Hydrodynamics, Siberian Branch of the USSR Academy of Sciences, Novosibirsk, USSR. Report.*
204. Sulmistras, A., Moen, I. O. and Thibault, P. A. (1984) "Laboratory Studies on Transmission Through Openings". *Internal Report. Defence Research Establishment Suffield, Ralston, Alberta, Canada.*
205. Takai, R., Yoneda, K. and Hikita, T. (1974) "Study of Detonation Wave Structure". *Fifteenth Symposium (International) on Combustion*, p. 69. The Combustion Institute.

206. Taki, S. and Fujiwara, T. (1981) "Numerical Simulation of Triple Shock Behavior of Gaseous Detonation". Proceedings of the Eighteenth Symposium (International) on Combustion, p. 1671. The Combustion Institute.
207. Tarasenko, N. N. (1974a) "Investigation of the Motion of the Wall of a Tube Under the Action of the Detonation Products of an Internal Charge of Explosive". Fizika Goreniya i Vzryva 10, 737.
208. Tarasenko, N. N. (1974b) "Effect of the Casing on the Detonation Rate of Mixed Explosives". Fizika Goreniya i Vzryva 10, 598.
209. Taylor, G. I. (1950) "The Formation of a Blast Wave by a Very Intense Explosion". Proceedings of the Royal Society of London A201, 159.
210. Thibault, P. A. (1982) Private Communication.
211. Thibault, P. A. (1983) Private Communication.
212. Thomas, G. A. and Edwards, D. H. (1983) "Simulation of Detonation Cell Kinematics Using Two-Dimensional Reactive Blast Waves". Journal of Physics D: Applied Physics 16, 1881.
213. Tsugé, S. (1971) "The Effect of Boundaries on the Velocity Deficit and the Limit of Gaseous Detonations". Combustion Science and Technology 3, 195.
214. Ul'yanitskii, V. Yu. (1979) "Closed Model of Direct Initiation Taking Account of Instability. II. Nonpoint Initiation". Fizika Goreniya i Vzryva 16, 79
215. Ul'yanitskii, V. Yu. (1980) "Role of 'Flashing' and Transverse Wave Collisions in the Evolution of a Multifrontal Detonation-Wave Structure". Fizika Goreniya i Vzryva 17, 127.



216. Ungut, A., Shuff, P. J. and Eyre, J. A. (1983) "Initiation of Unconfined Gaseous Detonation by Diffraction of a Detonation Front Emerging from a Pipe". Presented at the Ninth International Colloquium on Dynamics of Explosions and Reactive Systems (to be published).
217. Urtiew, P. A. (1976) "Idealized Two-Dimensional Detonation Waves in Gaseous Mixtures". *Acta Astronautica* 3, 187.
218. Urtiew, P. A. and Tarver, C. M. (1981) "Effects of Cellular Structure on the Behavior of Gaseous Detonation Waves Under Transient Conditions". *Progress in Astronautics and Aeronautics* 75, 370.
219. Vanta, E. B., Parsons, G. H. and Collins, P. M. (1973) "Detonability of Propylene Oxide/Air and n-Propyl Nitrate/Air Mixtures". AFATL-TR-73-3. Air Force Armament Laboratory, Eglin AFB, Florida.
220. Vasiliev, A. A. (1980) "Gas Detonation of a Free Mixture Column". Lavrent'yev Institute of Hydrodynamics, Siberian Branch of the USSR Academy of Sciences, Novosibirsk, USSR. Report.
221. Vasiliev, A. A. (1982) "Geometric Limits of Gas Detonation Propagation". *Fizika Goreniya Vzryva* 18, 132.
222. Vasiliev, A. A., Gavrilenko, T. P. and Topchian, M. E. (1972) "On the Chapman-Jouguet Surface in Multi-headed Gaseous Detonations". *Astronautica Acta* 17, 499.
223. Vasiliev, A. A. and Nikolaev, Yu. (1978) "Closed Theoretical Model of a Detonation Cell". *Acta Astronautica* 5, 983.
224. Voitsekhovskii, B. V., Mitrofanov, V. V. and Topchian, M. E. (1963) "Structure of a Detonation Front in Gases". English Translation: Wright-Patterson AFB Report TD-MT-64-527, 1966.

225. Wagner, H. Gg. (1963) "Reaction Zone and Stability of Gaseous Detonations". Proceedings of the Ninth Symposium (International) on Combustion, p. 454. New York and London: Academic Press.
226. Weast, R. C. and Astle, M. J. (1979) "CRC Handbook of Chemistry and Physics". Boca Raton, Florida: CRC Press.
227. Westbrook, C. K. (1982) "Chemical Kinetics of Hydrocarbon Oxidation in Gaseous Detonations". Combustion and Flame 46, 191.
228. Westbrook, C. K. and Urtiew, P. A. (1982) "Chemical Kinetic Predictions of Critical Parameters in Gaseous Detonations". Proceedings of the Nineteenth Symposium (International) on Combustion, p. 615. The Combustion Institute.
229. White, D. R. (1961) "Turbulent Structure of Gaseous Detonation". Physics of Fluids 4, 465.
230. White, D. R. (1967) "Density Induction Times in Very Lean Mixtures of  $D_2$ ,  $H_2$ ,  $C_2H_2$  and  $C_2H_4$  with  $O_2$ ". Proceedings of the Eleventh Symposium (International) on Combustion, p. 147. The Combustion Institute.
231. Whitham, G. B. (1957) "A New Approach to Problems of Shock Dynamics. Part I. Two-Dimensional Problems". Journal of Fluid Mechanics 2, 145.
232. Williams, F. A. (1976) "Quenching Thickness for Detonations". Combustion and Flame 26, 403.
233. Wolanski, P., Kauffman, C. W., Sichel, M. and Nicholls, J. A. (1981) "Detonation of Methane-Air Mixtures". Proceedings of the Eighteenth Symposium (International) on Combustion, p. 1651. The Combustion Institute.

234. Wood, W. W. and Kirkwood, J. G. (1954) "Diameter Effect in Condensed Explosives. The Relation between Velocity and Radius of Curvature of the Detonation Wave". *Journal of Chemical Physics* 22, 1920.
235. Zeldovich, Ya. B. (1940) "On the Theory of the Propagation of Detonation in Gaseous Systems". *Soviet Physics J.E.T.P.* 10, 542.
236. Zeldovich, Ya. B. (1940-1944) "*Zh. Eksp, Teor. Fiz.* 10, 542 [English Translation National Committee for Aeronautics Technical Memorandum No. 1261, November 1950, 90pp.]; (1944) "Theory of Combustion and Detonation of Gases". Academy of Sciences of the USSR, Institute of Chemical Physics [English Translation: Tech. Rept. No. F-TS-1226-1A(GDAM A9-T-45), Air Material Command, Wright-Patterson AFB, May 1949, 118 pp.]
237. Zeldovich, Ya. B., Kogarko, S. M. and Simonov, N. N. (1956) "An Experimental Investigation of Spherical Detonation of Gases". *Soviet Physics: Technical Physics* 1, 1689.
238. Zeldovich, Ya. B. and Kompaneets, A. S. (1960) "Theory of Detonation". New York and London: Academic Press.

**TABLE I. Critical conditions for transmission from a rigid tube of 0.89 m diameter to various yielding tubes and to an unconfined region.**

Nominal tube wall thickness $t$ mil	Measured wall surface density $m/A$ $\text{kg/m}^2$	Critical $\text{C}_2\text{H}_4$ concentration %	Critical cell width $\lambda$ mm	Ratio of tube diameter to cell width $D/\lambda$
0	0.0	5.05	68.5	13.0
1	0.0242	4.70	90.3	9.9
5	0.124	4.15	165.0	5.4
10	0.220	3.90	219.0	4.1

**TABLE II. Initial post-shock conditions and results from calculations to determine the relevant chemical length scale associated with detonative propagation.**

(1) Nominal wall thickness t mil	(2) Critical C <sub>2</sub> H <sub>4</sub> concentration %	(3) Detonation velocity V <sub>C-J</sub> m/s	(4) Relative particle velocity u <sub>s</sub> m/s	(5) Temperature ratio across shock T <sub>s</sub> /T <sub>0</sub>	(6) Pressure ratio across shock P <sub>s</sub> /P <sub>0</sub>
1	4.70	1696	289.2	4.92	28.86
5	4.15	1637	287.0	4.70	26.80
10	3.90	1606	285.7	4.58	25.76

(7) Nominal wall thickness t mil	(8) Critical cell length L <sub>c</sub> mm	(9) Pre- exponential factor k × 10 <sup>11</sup> s · mole / l	(10) Particle travel during reaction 2τ <sub>0</sub> u <sub>s</sub> /L <sub>c</sub>
1	129	1.99	0.71
5	236	2.43	0.86
10	313	2.33	0.88
Average, %		2.21 ± 10	0.80 ± 11

TABLE III. Calculated stream tube area increases for the constant diameter yielding tube configurations.

Nominal wall thickness $t$ mil	Critical $C_2H_4$ concentration %	Detonation velocity $V_{C-J}$ m/s	Temperature ratio $T_{C-J}/T_0$	Pressure ratio $P_{C-J}/P_0$	Critical cell length $L_C$ mm	Critical stream tube area increase $\xi$ %
1	4.70	1696	8.75	15.7	129	17.6
5	4.15	1637	8.20	14.5	236	22.3
10	3.90	1606	7.92	13.9	313	23.2

**TABLE IV. Calculated stream tube area increases for the tapered yielding tube configurations.**

(1) Nominal wall thickness $t$ mil	(2) Critical $C_2H_4$ concentration %	(3) Detonation velocity $V_{C-J}$ m/s	(4) Detonation temperature ratio $T_{C-J}/T_o$	(5) Detonation pressure ratio $P_{C-J}/P_o$	(6) Critical cell length $L_c$ mm
5	4.25	1649	8.31	14.75	199
5	4.35	1661	8.42	14.97	177
10	3.80	1594	7.80	13.69	368
10	4.00	1619	8.03	14.18	276

Nominal wall thickness $t$ mil	(7) Apparent failure diameter $D$ (mm)	(8) Area increase due to wall motion $\xi_m$ %	(9) Area decrease due to taper $\xi_t$ %	(10) Net critical stream tube area increase $\xi = \xi_m - \xi_t$ %
5	810	21.4	1.6	19.8
5	610	19.3	1.9	17.4
10	> 890	< 30.9	< 2.6	< 28.3
10	760	24.3	2.4	21.9

**TABLE V. Summary of critical conditions for propagation of  $C_2H_2-O_2-N_2$  detonations in square channels with various rigid/yielding wall combinations.**

Number of yielding sides	Yielding wall material	Density of yielding wall m / A kg/m <sup>2</sup>	Critical dilution ratio $\beta$	Critical cell length $L_c$ mm	Critical fractional area increase $\xi$ %
1	acetate A	0.0381	6.25	53.1	16.6
1	acetate B	0.0351	6.25	53.1	17.3
1	paper A	0.0372	6.13	50.0	15.4
1	paper B	0.0616	—	—	—
1	polyethylene	0.0831	—	—	—
2	acetate A	0.0381	5.75	41.3	21.8
2	paper A	0.0372	~4.90 (5.80)	~26.0 (42.9)	~10.0 (22.8)
3	paper A	0.0372	~4.50 (5.30)	~20.7 (32.9)	~10.9 (22.7)



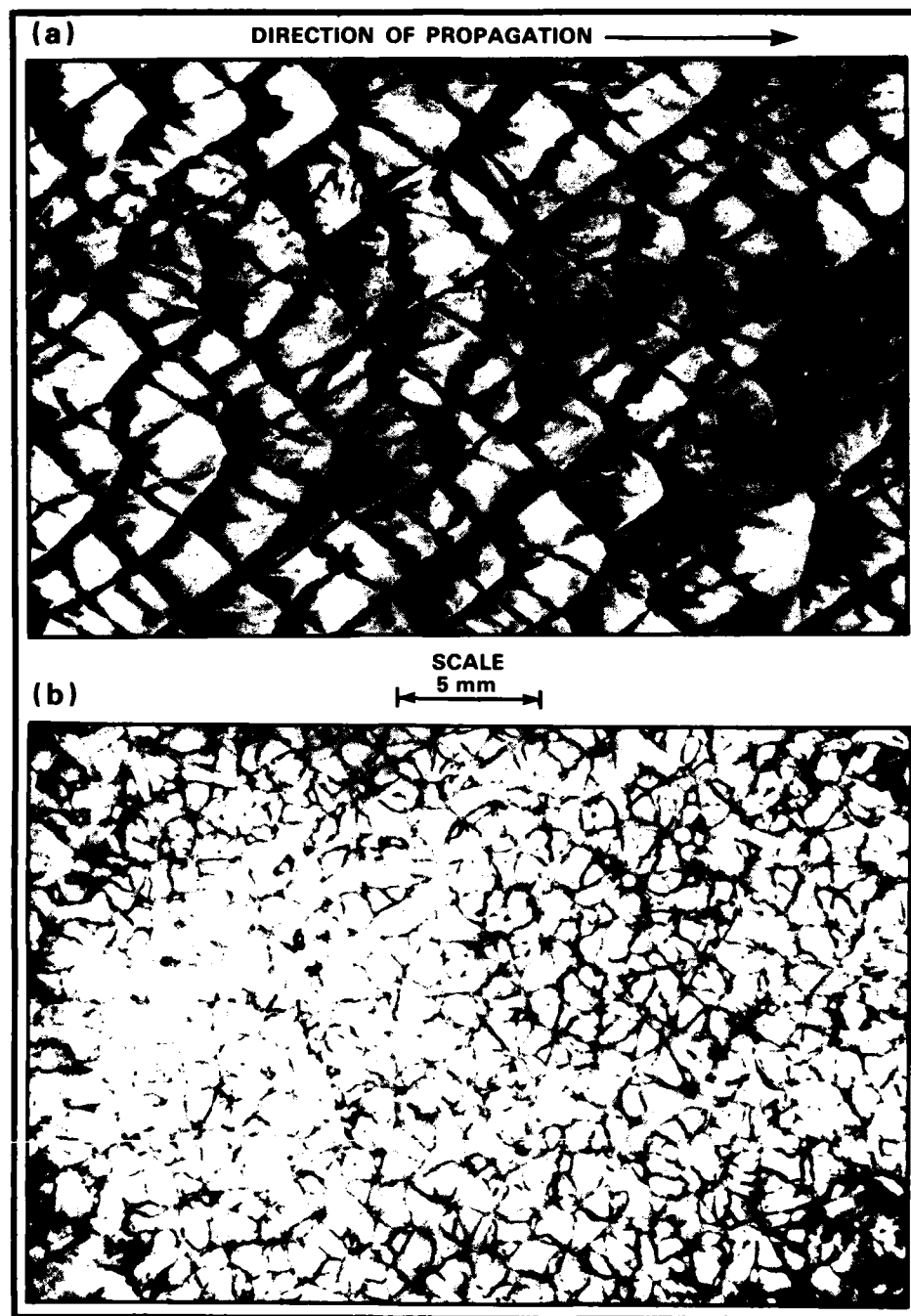


Figure 1

Smoke records produced by a detonation wave in low-pressure (24 Torr) equimolar oxyacetylene showing the cellular structure recorded on a wall (a) parallel to the direction of propagation and (b) normal to the direction of propagation.

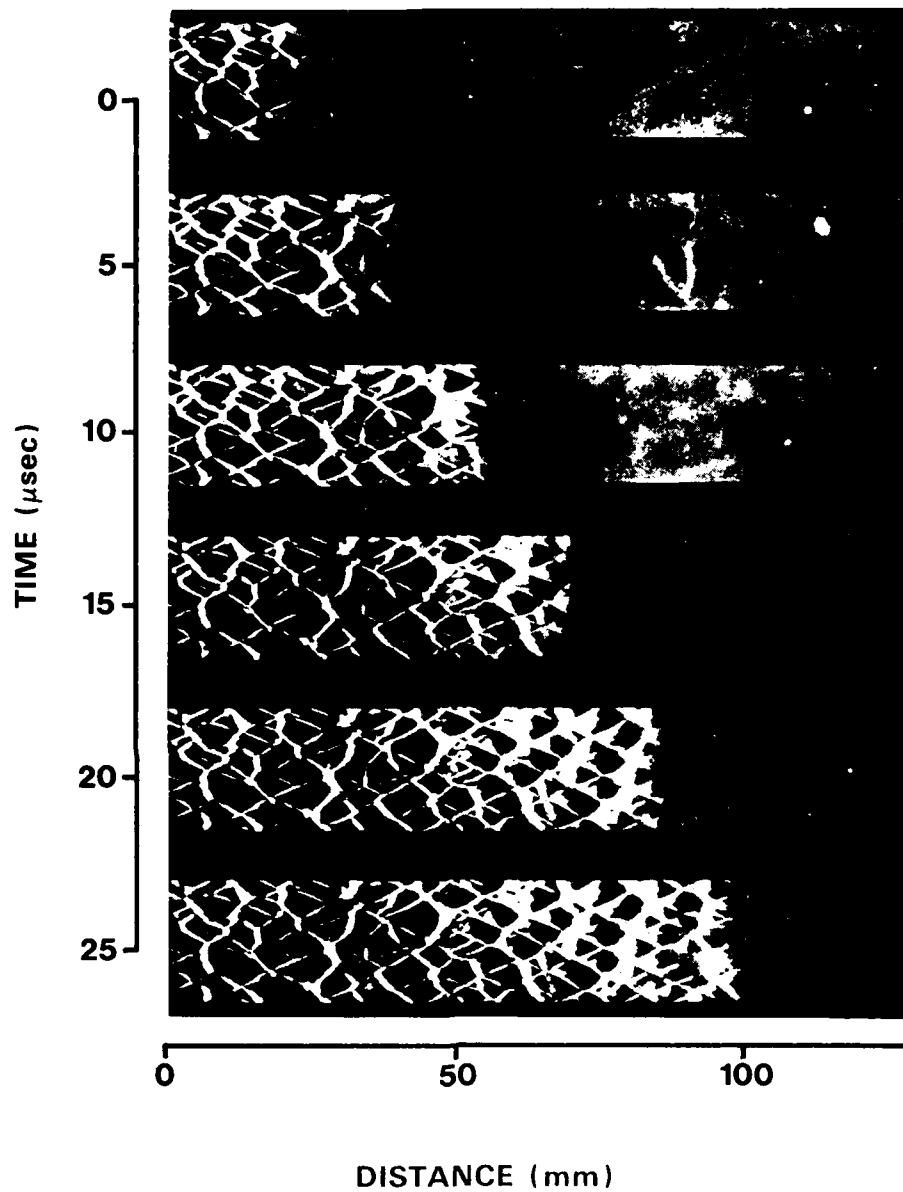


Figure 2

Stroboscopic laser-shadow photographs of a detonation wave propagating in a hydrogen-oxygen mixture.

From Lee *et al.* (1969).

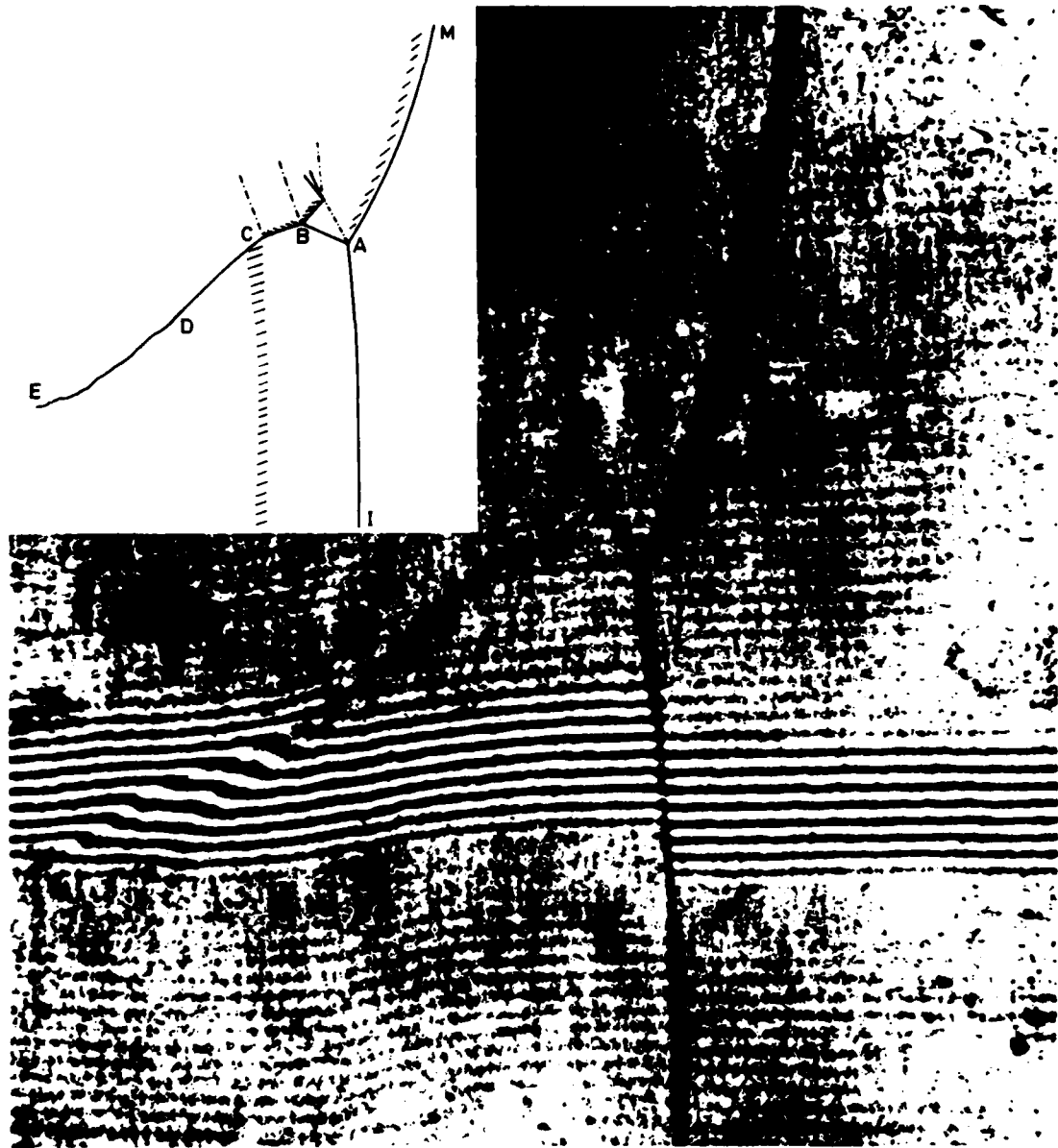


Figure 3

Schlieren interferogram and interpretive sketch showing details of the double Mach reflection associated with the cellular structure of a detonation wave. From Edwards *et al.* (1970).

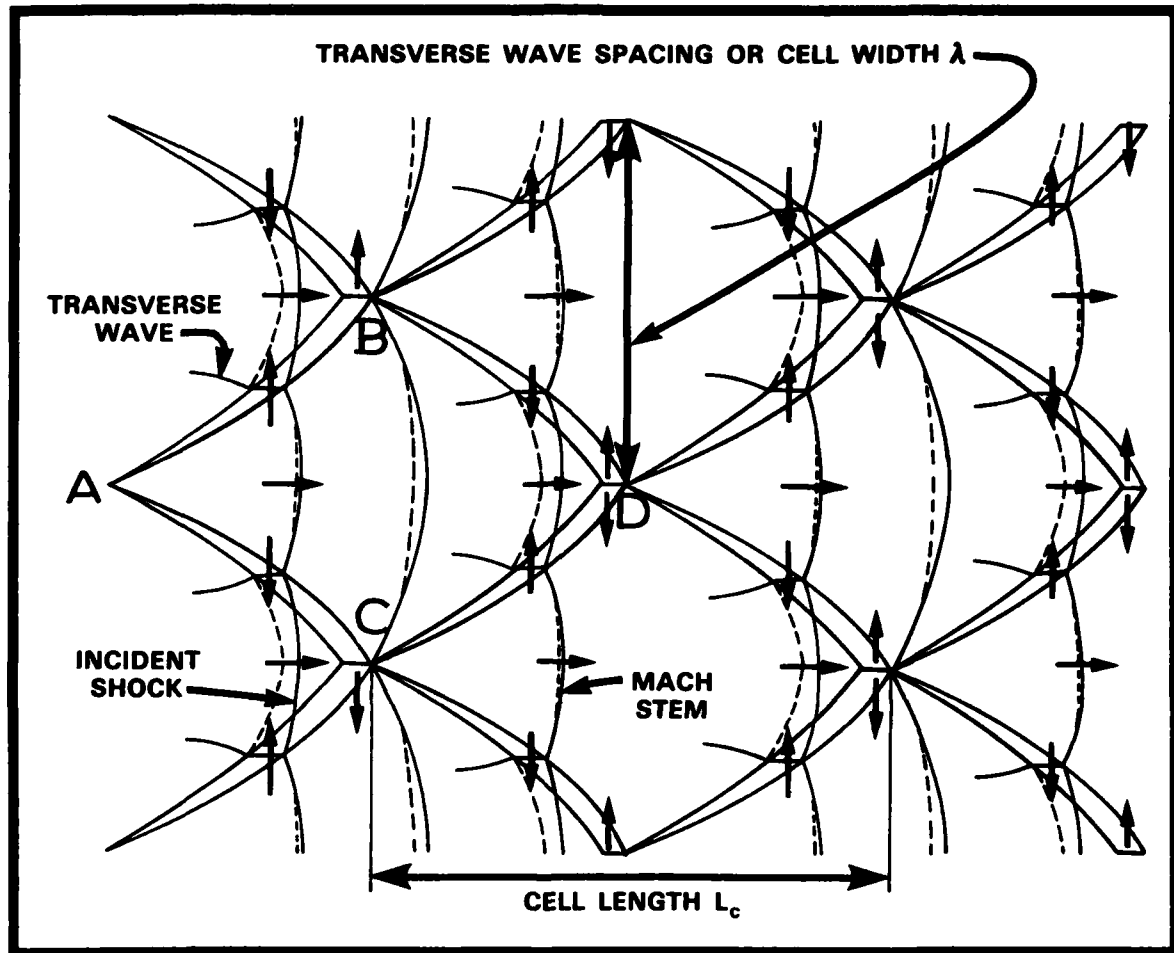
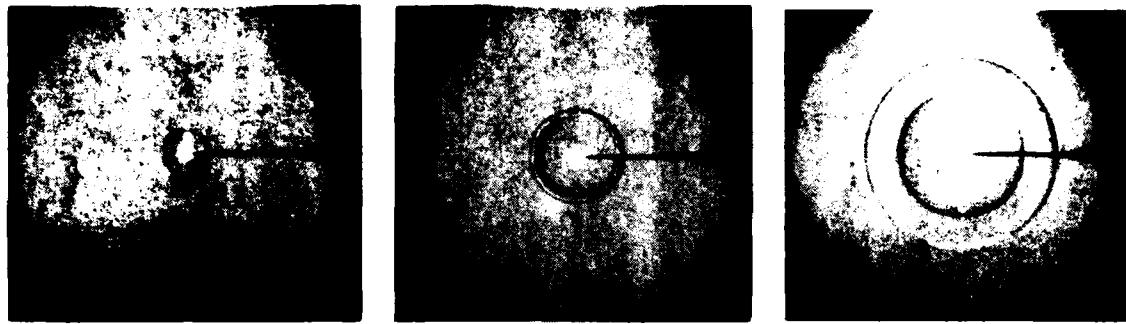
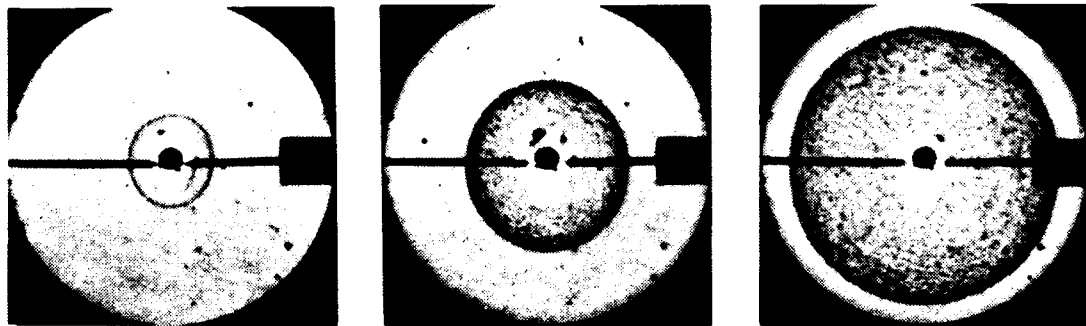


Figure 4

Sketch illustrating the cyclic nature of detonative propagation.  
Solid lines denote triple-point trajectories while broken lines  
signify zones of heat release.

1.6  $\mu$ s8.0  $\mu$ s32.3  $\mu$ s

a. SUBCRITICAL: 80 TORR  $2C_2H_2 + 5O_2$ ; IGNITER: LASER SPARK

6.0  $\mu$ s12.5  $\mu$ s23.0  $\mu$ s

b. SUPERCRITICAL: 120 TORR  $H_2 + Cl_2$ ; IGNITER: ELECTRICAL SPARK

6.5  $\mu$ s14.4  $\mu$ s20.3  $\mu$ s

c. CRITICAL: 100 TORR  $2C_2H_2 + 5O_2$ ; IGNITER: LASER SPARK

Figure 5

Spark Schlieren photographs of a spherical detonation illustrating (a) the subcritical, (b) supercritical and (c) critical regimes of direct initiation. From Lee (1977).

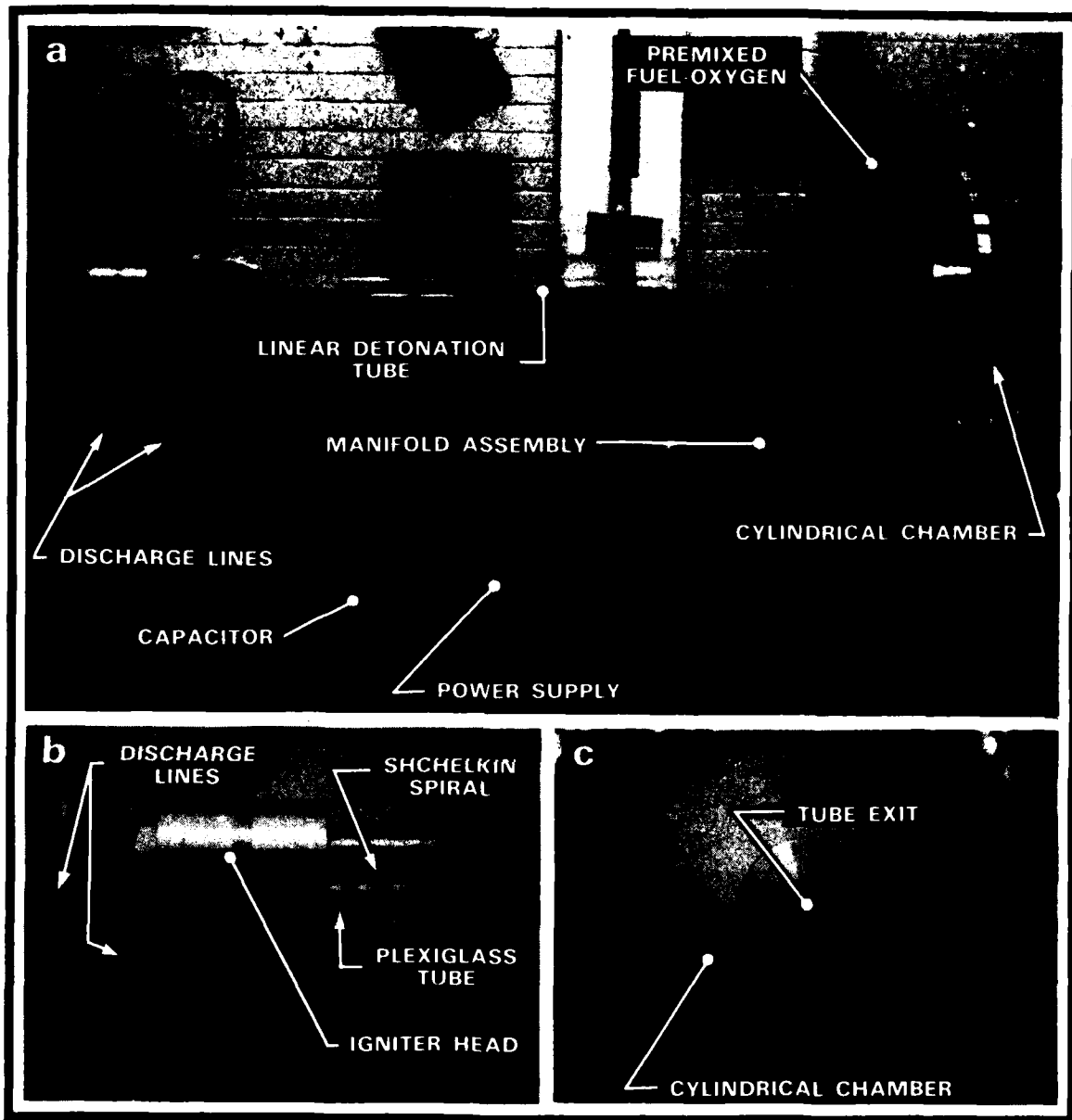


Figure 6

Photographs of apparatus used to investigate the transformation of planar detonation to cylindrical or spherical detonation:

- (a) general side view,
- (b) details of ignition end of tube, and
- (c) front view of cylindrical chamber.

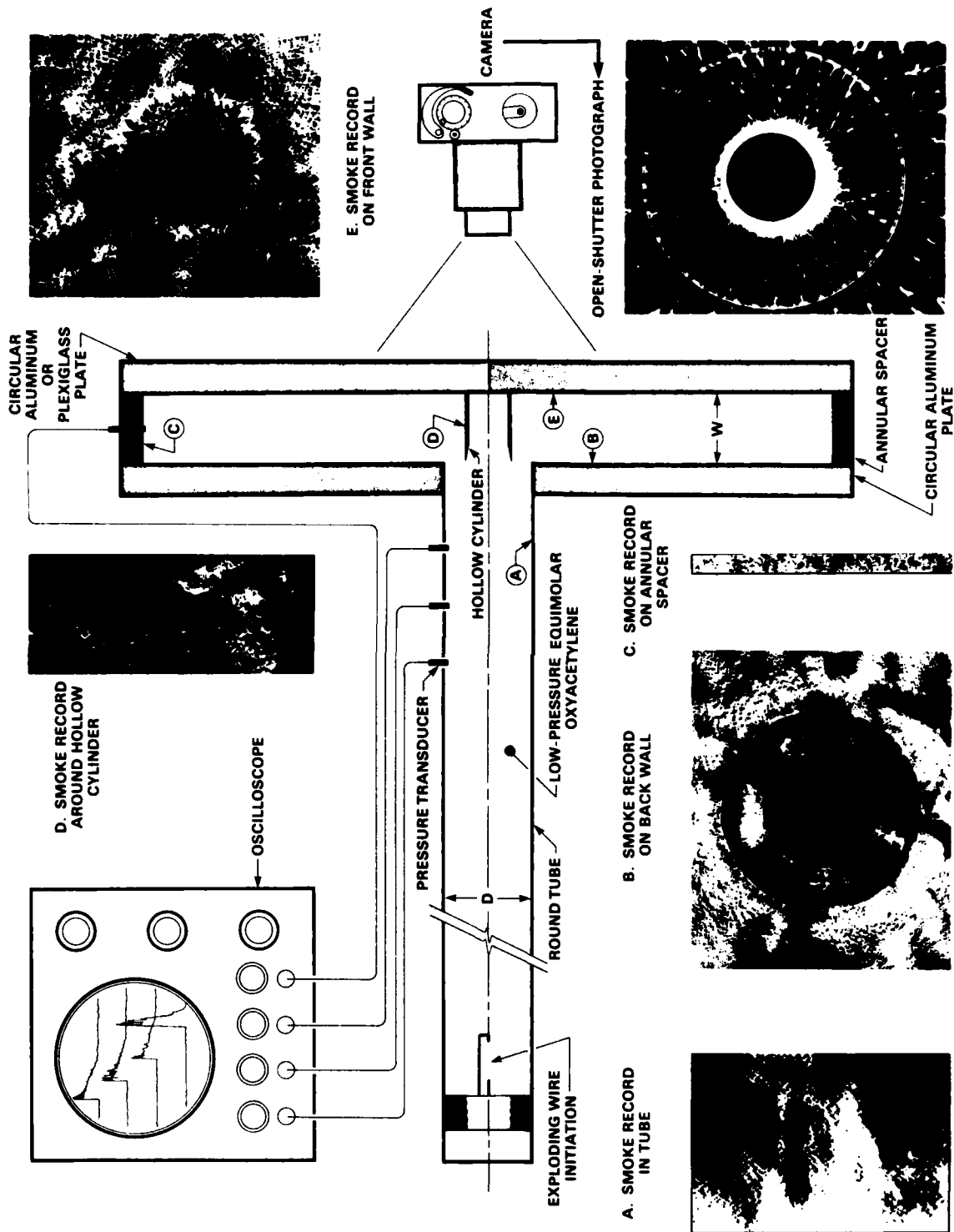


Figure 7

Schematic diagram of apparatus and diagnostic techniques used to study the transformation of planar detonation to cylindrical or spherical detonation.

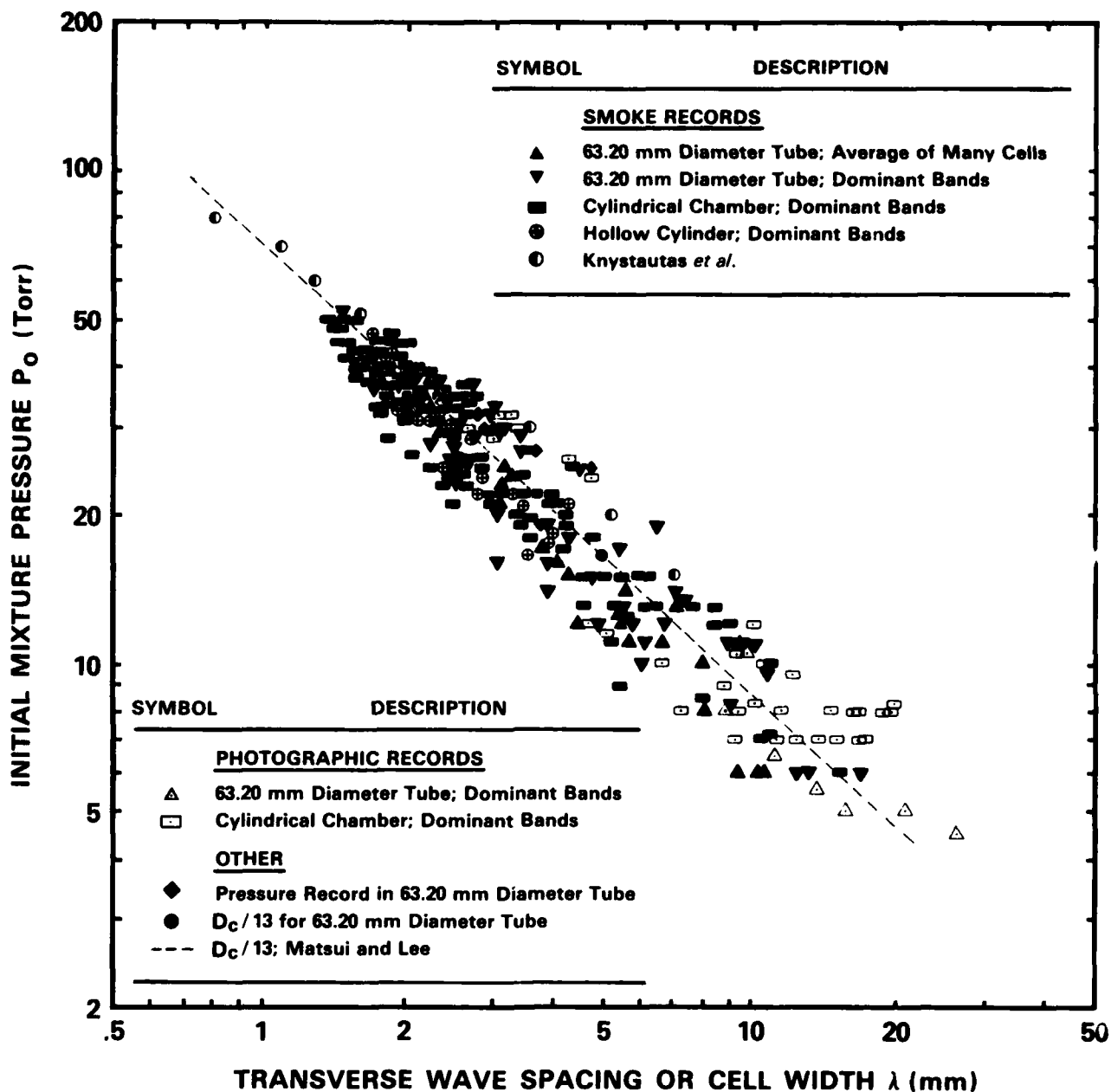


Figure 8

Transverse wave spacing or cell width versus initial mixture pressure for equimolar oxyacetylene mixtures. Matsui and Lee (1979), Knystautas *et al.* (1982).



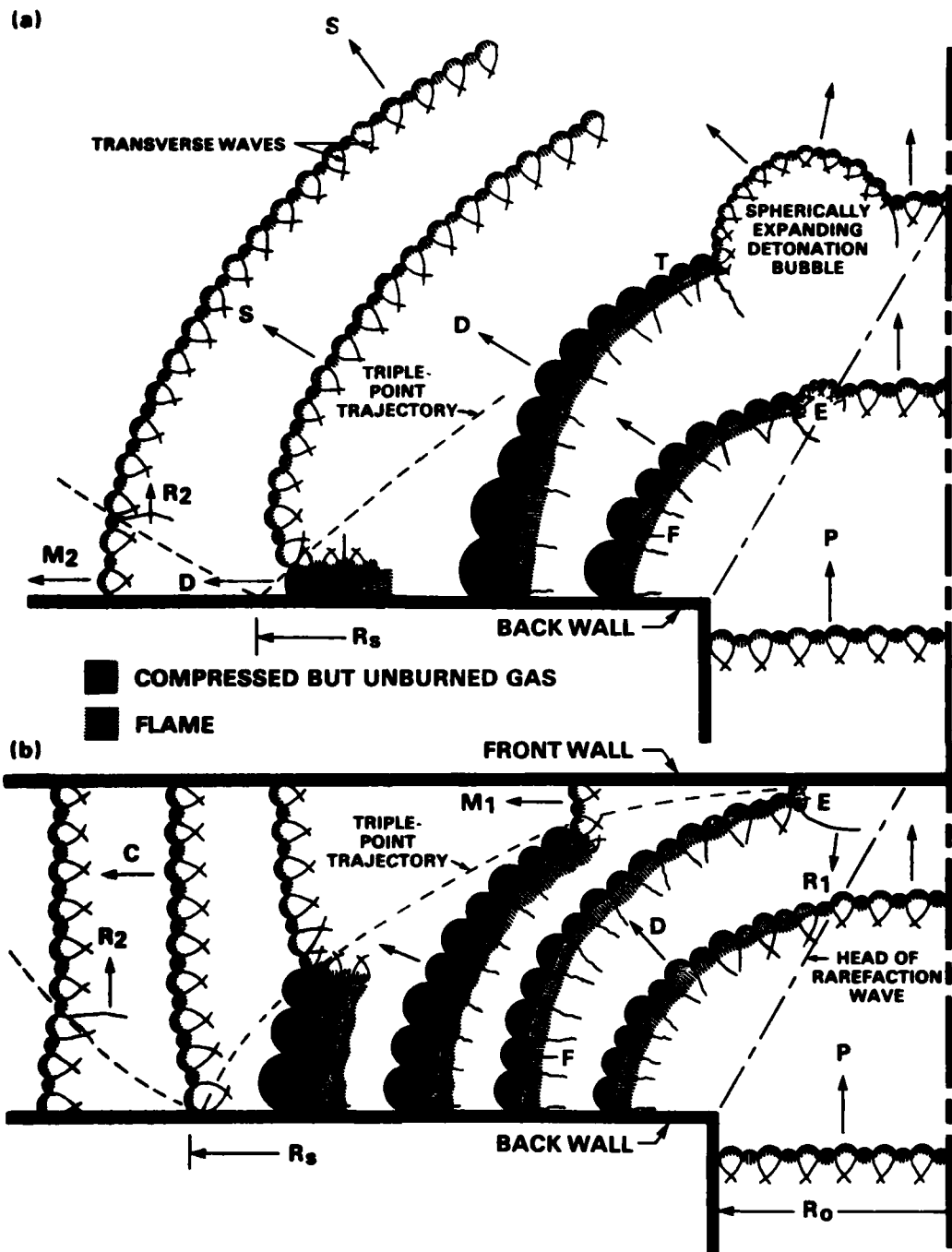


Figure 9

Schematic diagrams of (a) the spontaneous reinitiation mechanism (top), and (b) the process of reinitiation by reflection from a wall (bottom).

P – Planar detonation wave; C – Cylindrical detonation wave;  
 S – Spherical detonation wave; D – Diffracted shock wave;  
 R – Reflected shock wave; M – Detonative Mach stem;  
 F – Flame; T – Transversely propagating detonation wave;  
 E – Reinitiation nucleus.

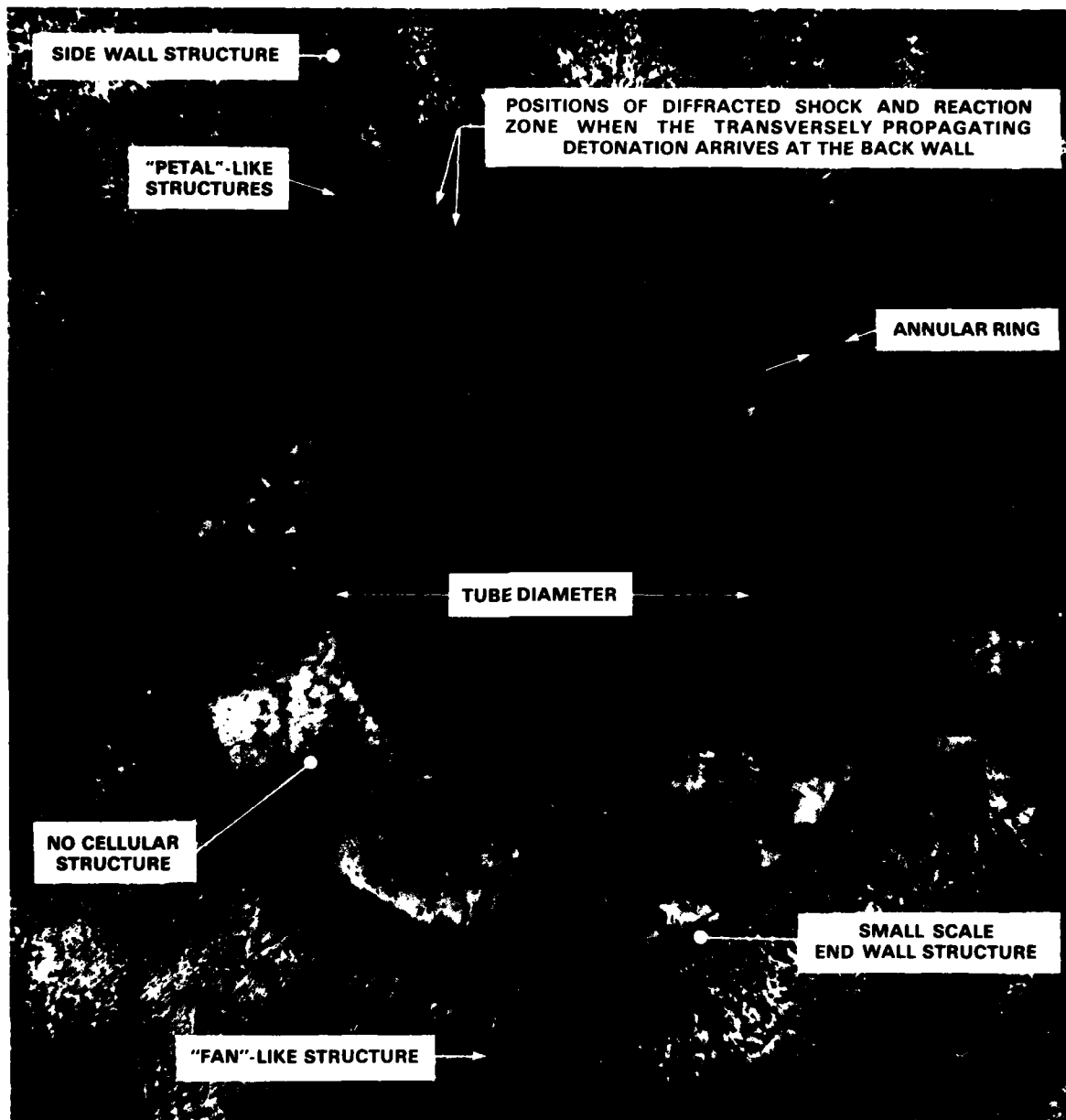
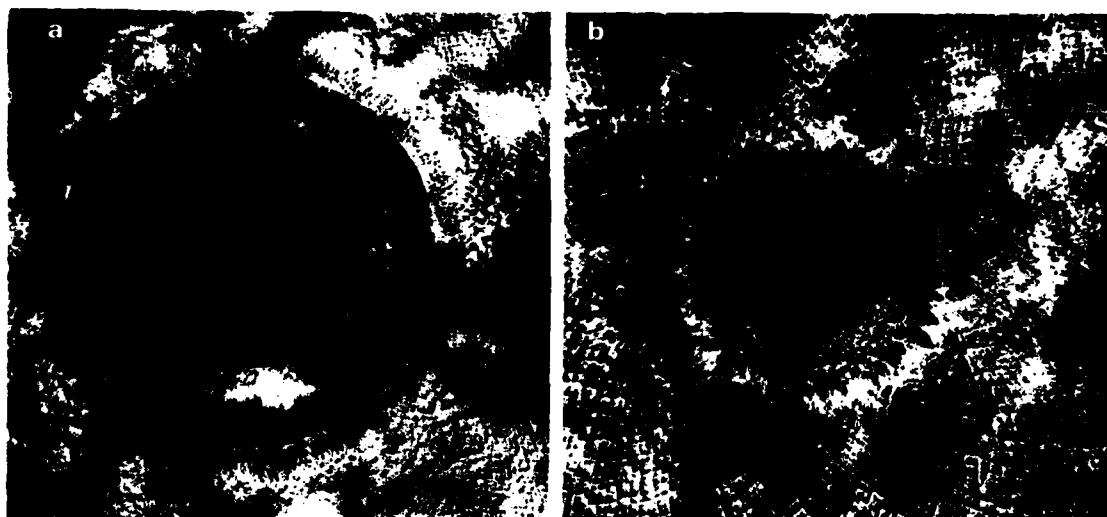


Figure 10

Smoke record from the back wall showing features of the annular ring formed during the spontaneous reinitiation process.

(1)  $P_0 = 40$  Torr  $D/\lambda \cong 34$



(2)  $P_0 = 19$  Torr  $D/\lambda \cong 15$

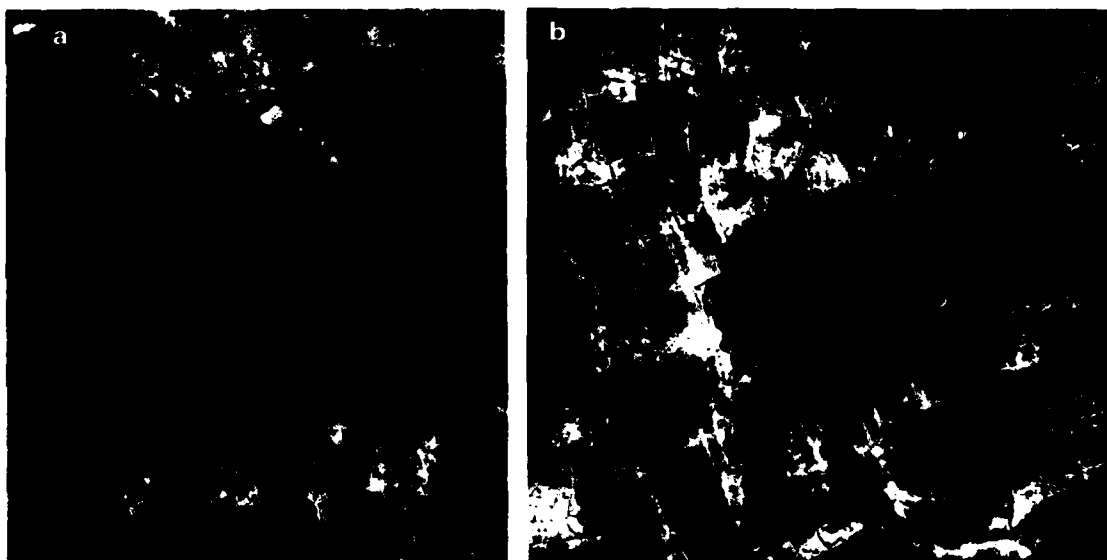


Figure 11

Collection of smoke records from the back wall (a) and front wall (b) of the cylindrical chamber for a plate separation of  $w/D = 0.391$ . Reinitiation by reflection enabled supercritical transmission in (1) and (2). Critical transmission is shown in (3). Failure to transmit is seen in (4).

(3)  $P_0 = 16$  Torr  $D/\lambda \cong 13$



(4)  $P_0 = 14$  Torr  $D/\lambda \cong 11$

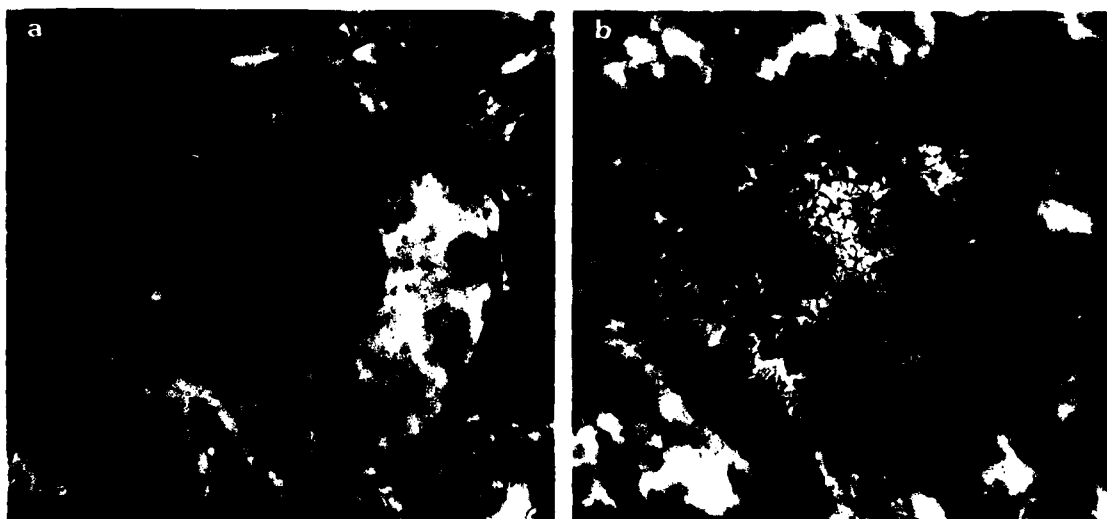


Figure 11 (Cont'd)

Collection of smoke records from the back wall (a) and front wall (b) of the cylindrical chamber for a plate separation of  $w/D = 0.391$ . Reinitiation by reflection enabled supercritical transmission in (1) and (2). Critical transmission is shown in (3). Failure to transmit is seen in (4).

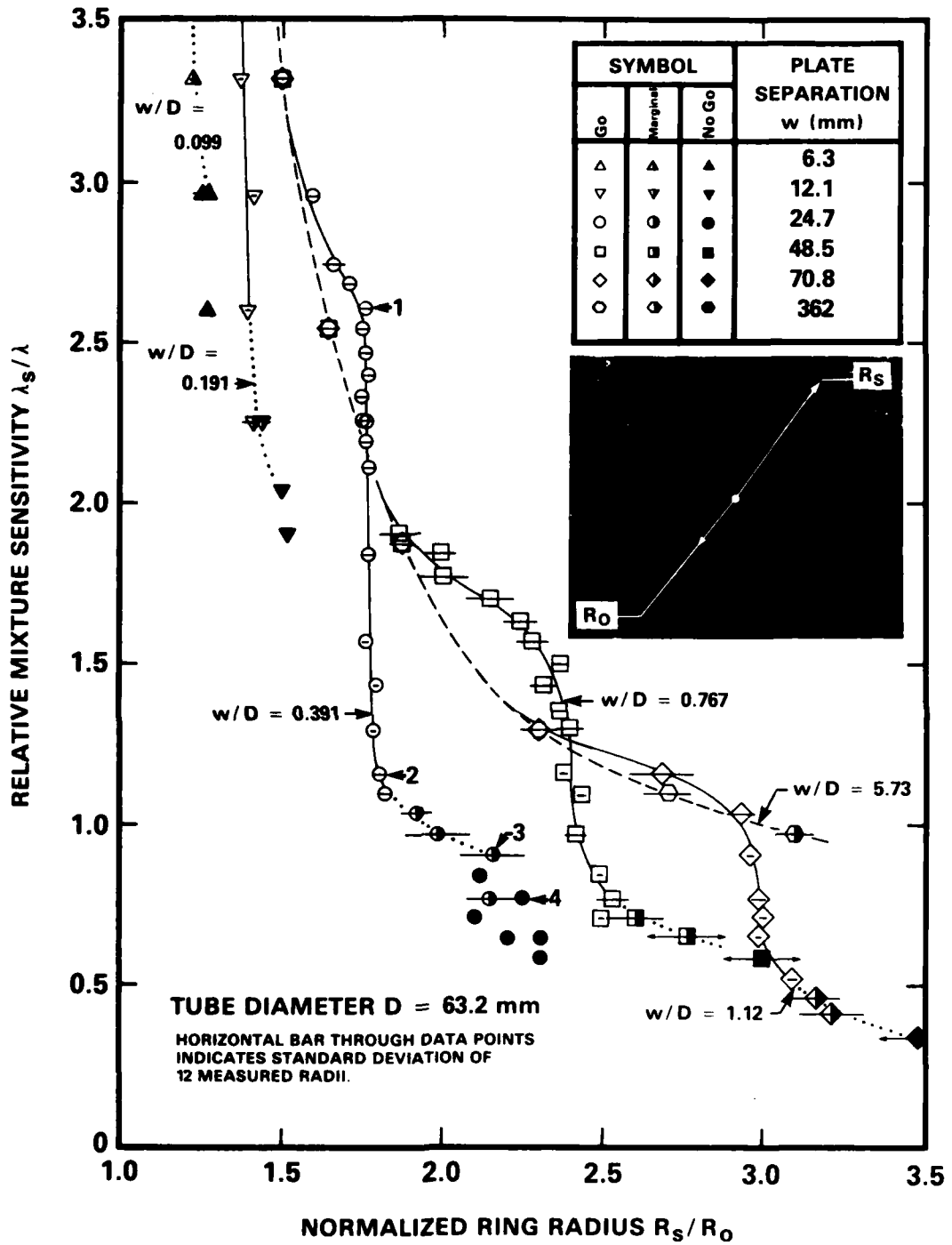


Figure 12

Normalized ring radius ( $R_s/R_0$ ) versus relative mixture sensitivity ( $\lambda_s/\lambda$ ).

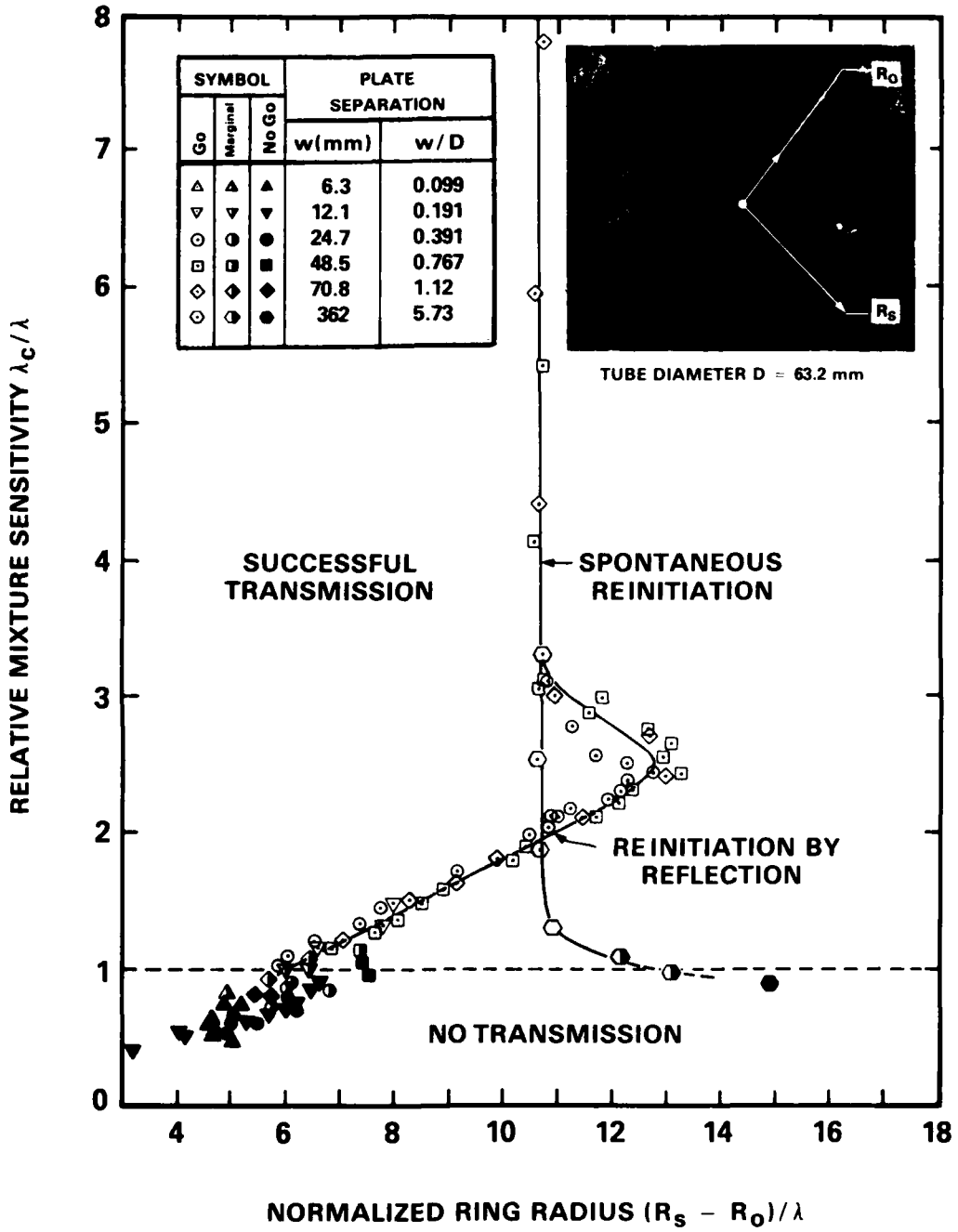


Figure 13

Normalized ring radius  $(R_s - R_o)/\lambda$  versus relative mixture sensitivity  $(\lambda_c/\lambda)$ .

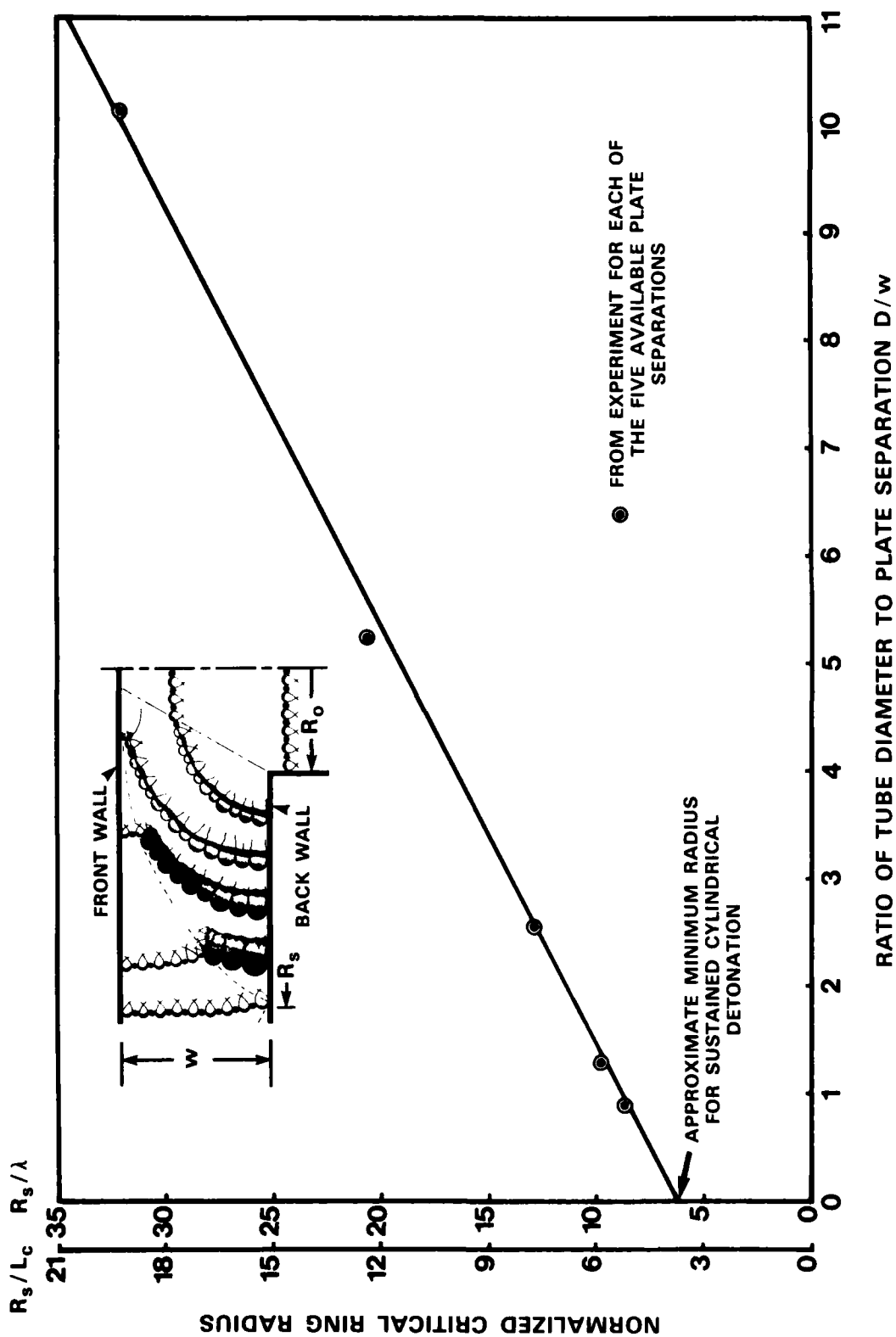


Figure 14

Normalized critical ring radius versus ratio of tube diameter to plate separation  $D/w$ .

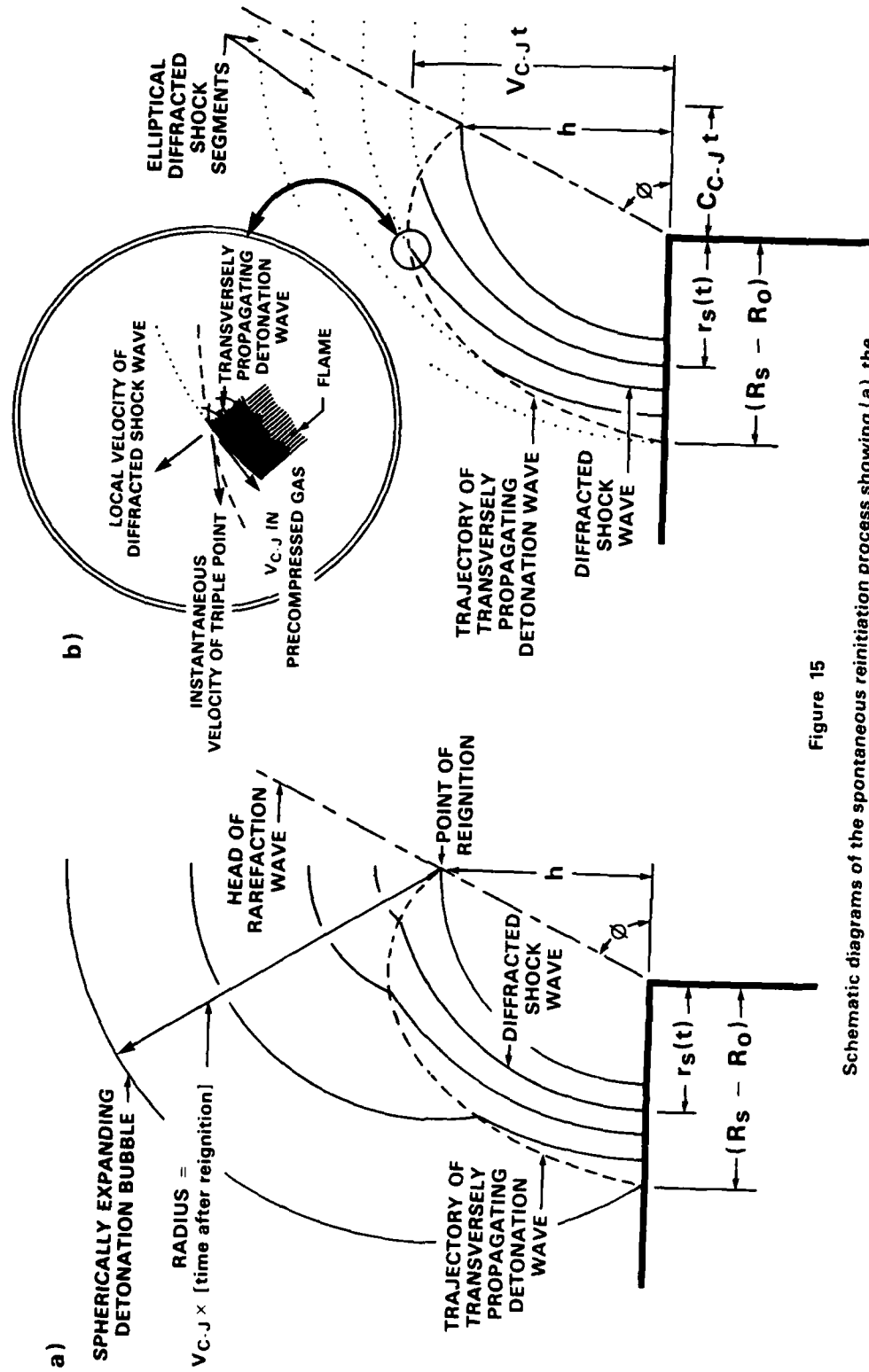


Figure 15

Schematic diagrams of the spontaneous reignition process showing (a) the spherical detonation bubble model, and (b) the transversely propagating detonation model used to calculate the axial location of reignition at a distance  $h$  downstream of the tube exit.



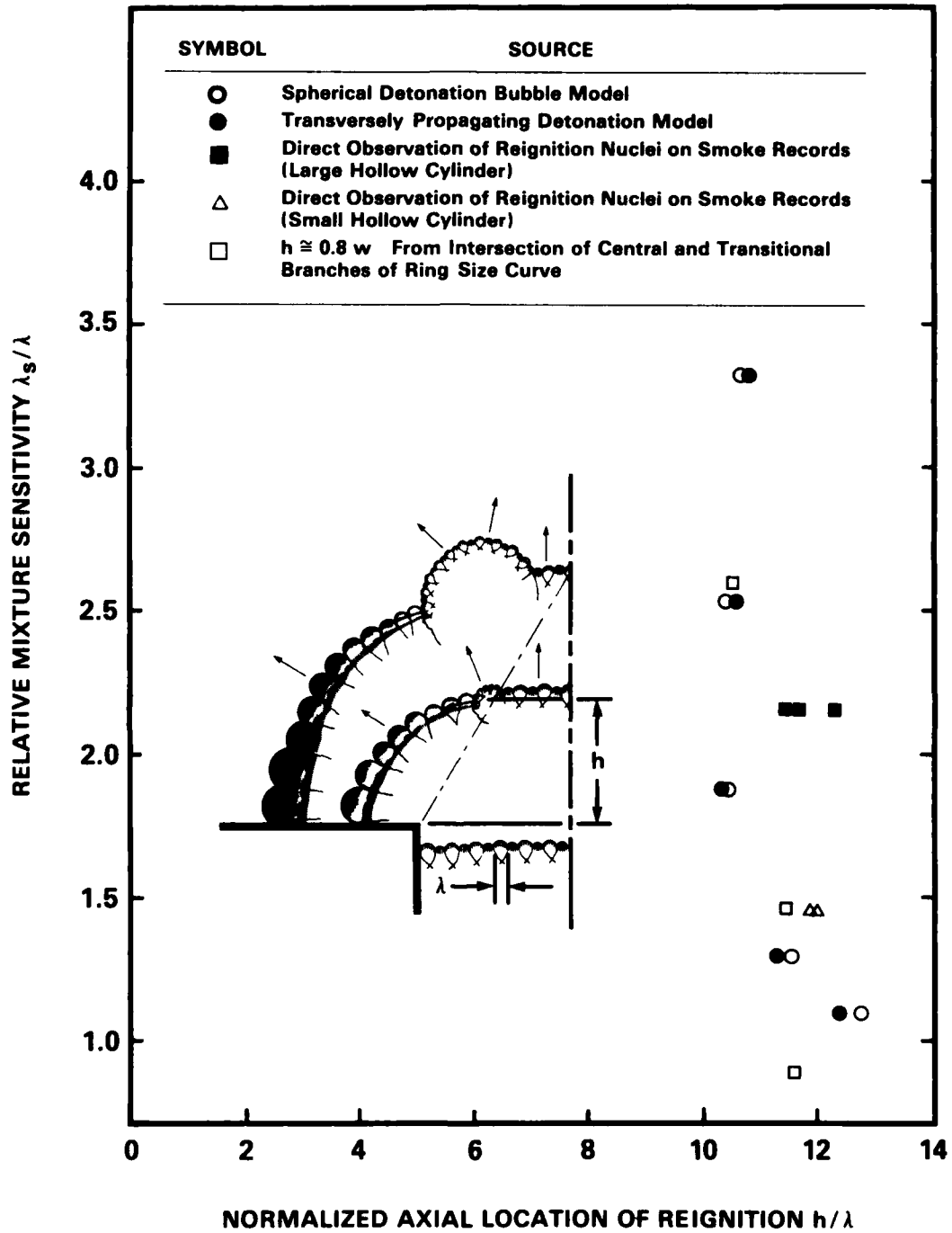
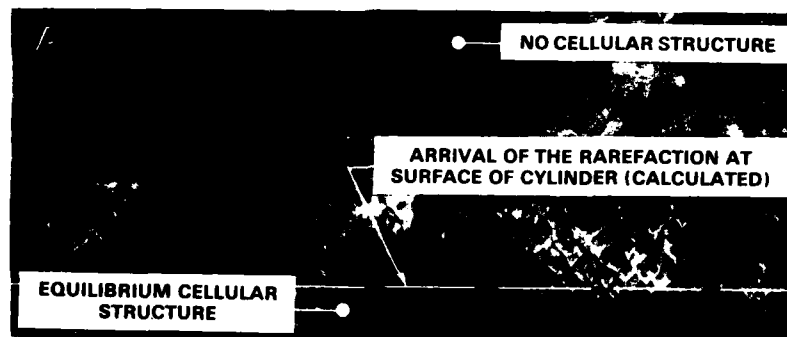


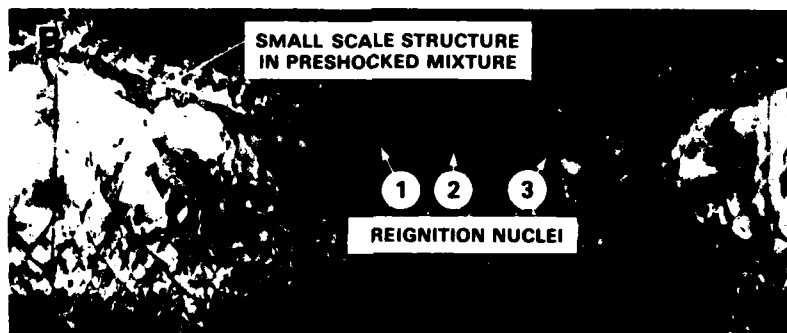
Figure 16

Normalized axial location of reignition versus relative mixture sensitivity for spontaneous reinitiation.

$P_0 = 32.5$  Torr



$P_0 = 33.5$  Torr



$P_0 = 50$  Torr

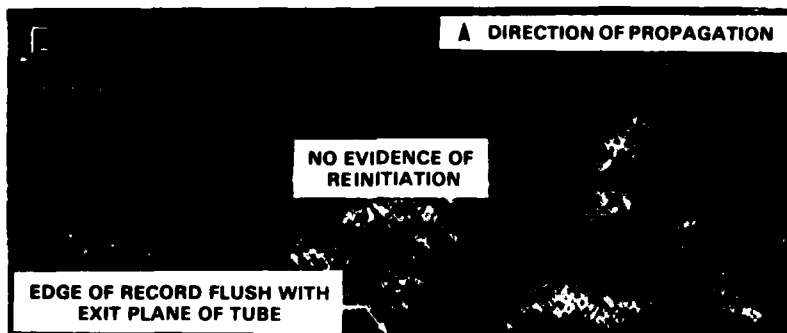


Figure 17

Collection of smoke records from the outer surface of the thin-walled hollow cylinder ( $d_0/D = 0.804$ ) showing (a) failure to transmit, (b) formation of reignition nuclei during critical transmission, and (c) supercritical transmission.

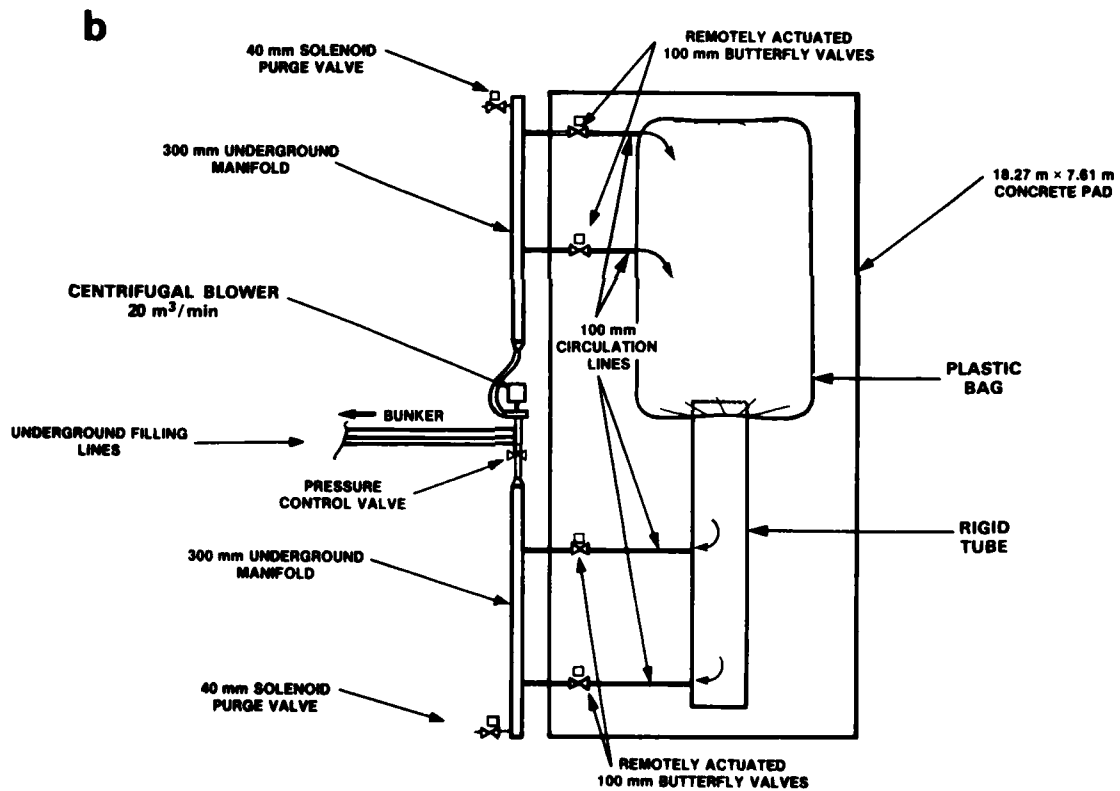
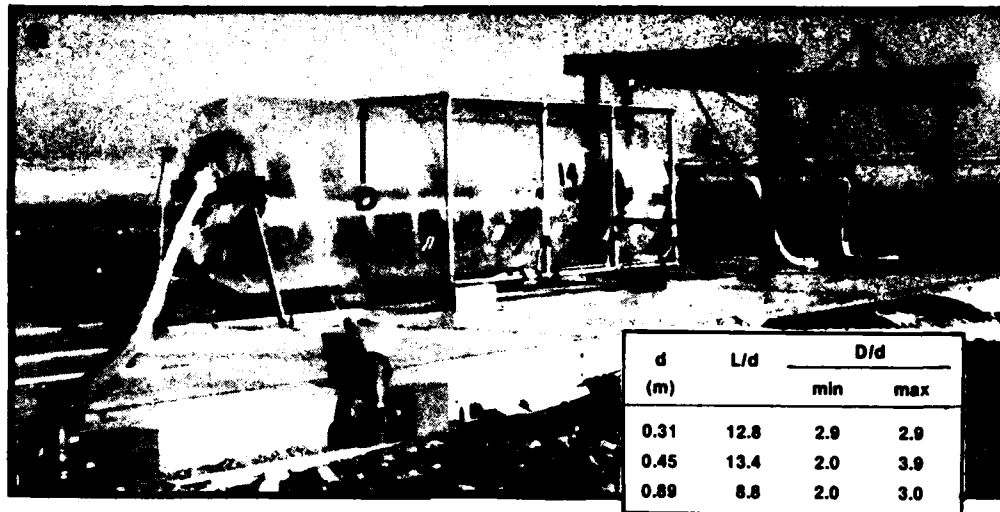


Figure 18

- a) Photograph showing large-scale experimental configuration for critical tube diameter test. A rigid tube of 0.45 m diameter and plastic bag of 1.75 m diameter are pictured.
- b) Schematic diagram showing details of the gas mixing system.

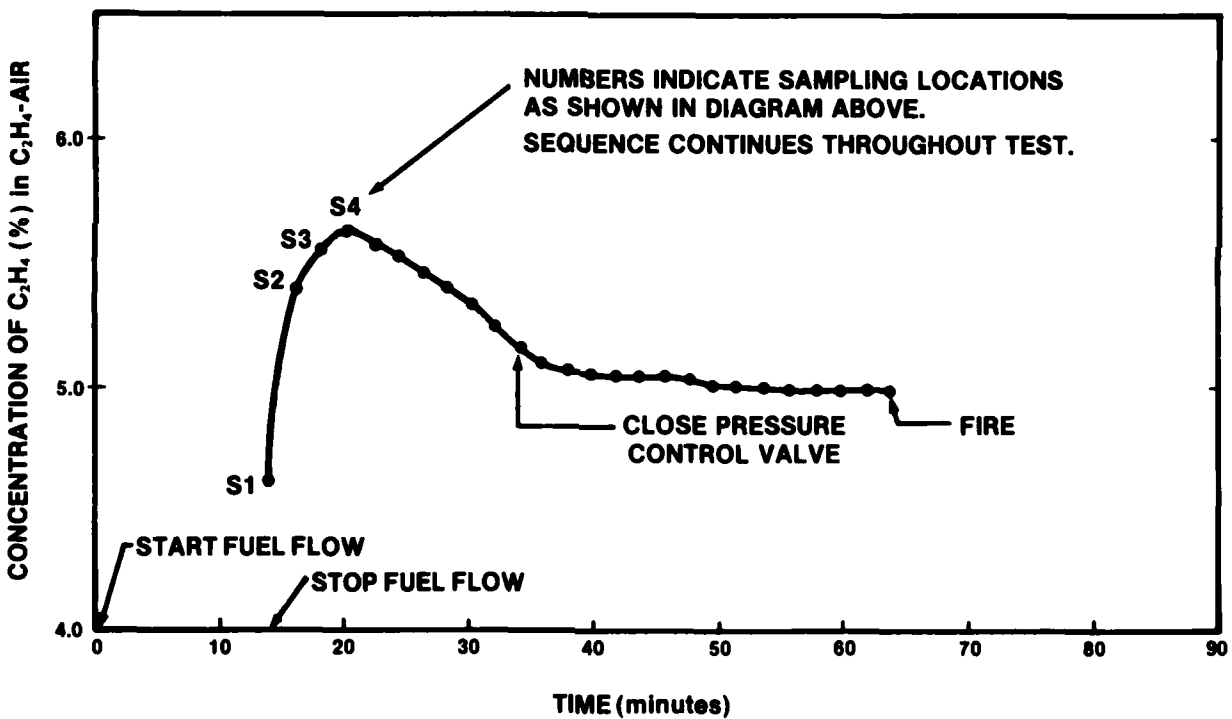
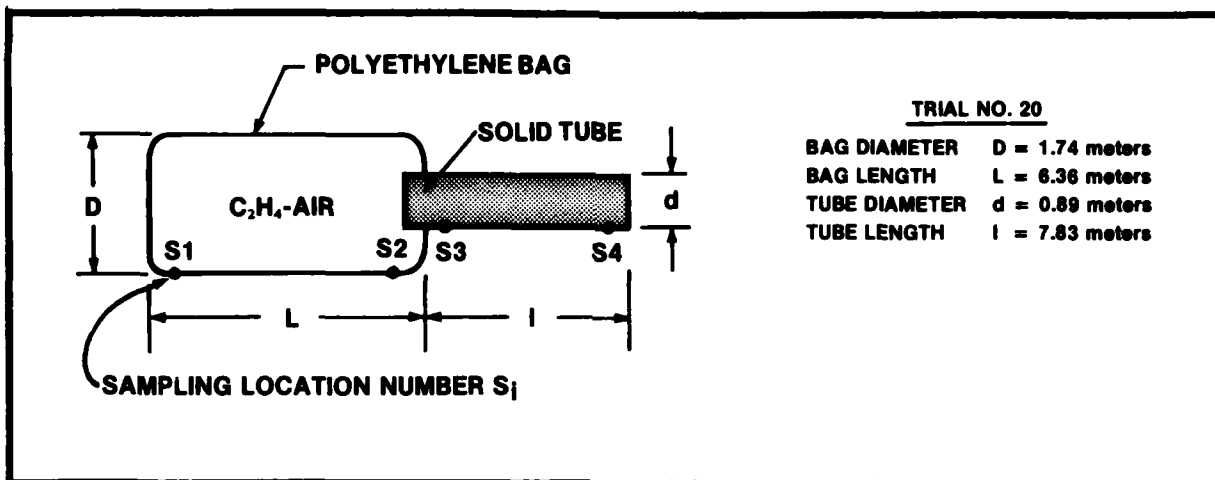


Figure 19

Fuel concentration (% C<sub>2</sub>H<sub>4</sub> in C<sub>2</sub>H<sub>4</sub>-air) versus time (minutes) for a typical critical tube diameter experiment.



Figure 20

Selected photographs of the experimental facility showing:

- a) the exit end of the tube with bag attached,
- b) the centrifugal blower used for recirculating the test gas,
- c) the interior of the gas flow and analysis van, and
- d) the interior of the instrumentation van.

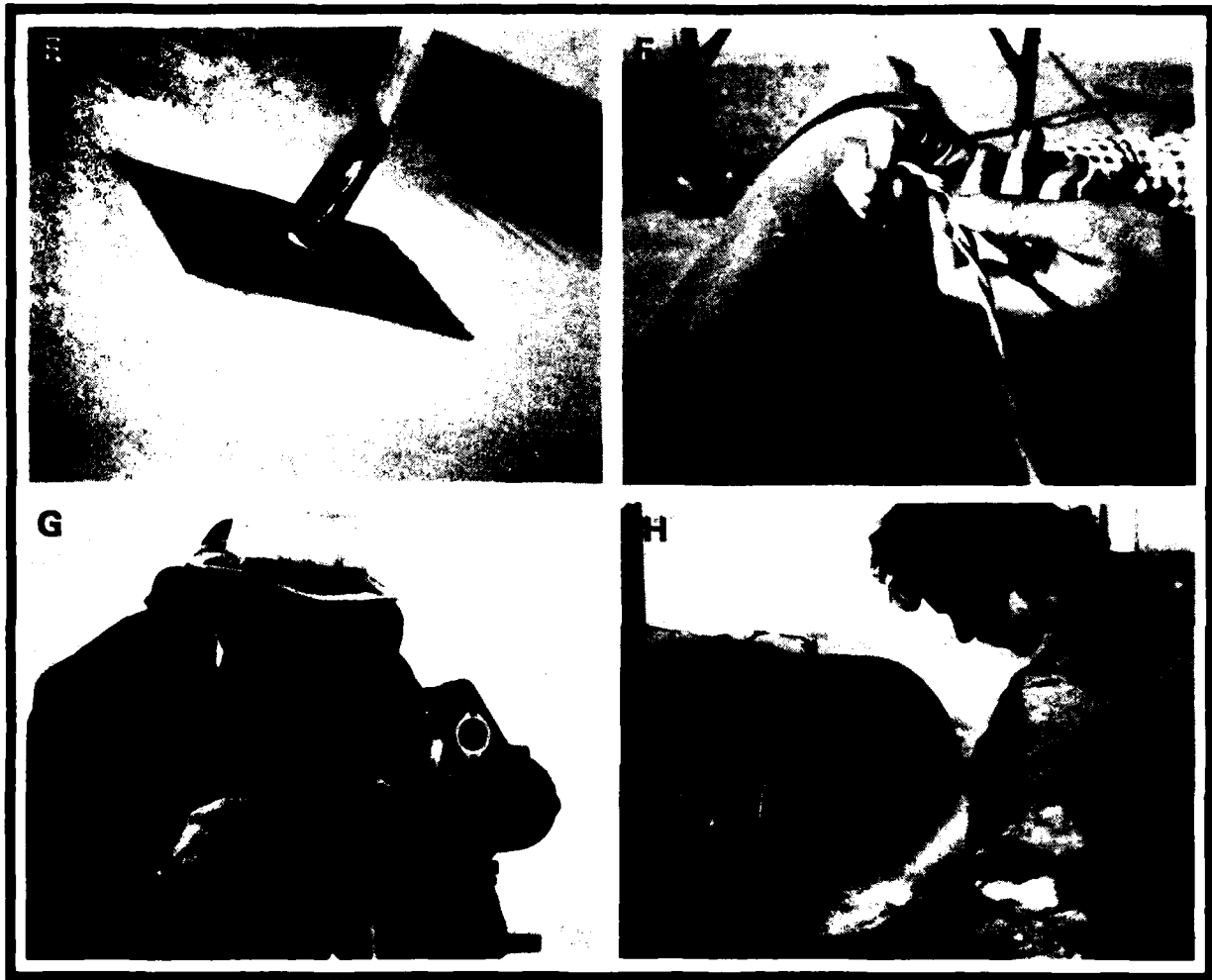


Figure 20 (cont'd)

Selected photographs of the experimental facility showing:

- e) gas sampling port installed in plastic bag,
- f) installation of ionization-gap probe into rigid tube,
- g) loading of film into high-speed camera, and
- h) installation of smoked foil into rigid tube.

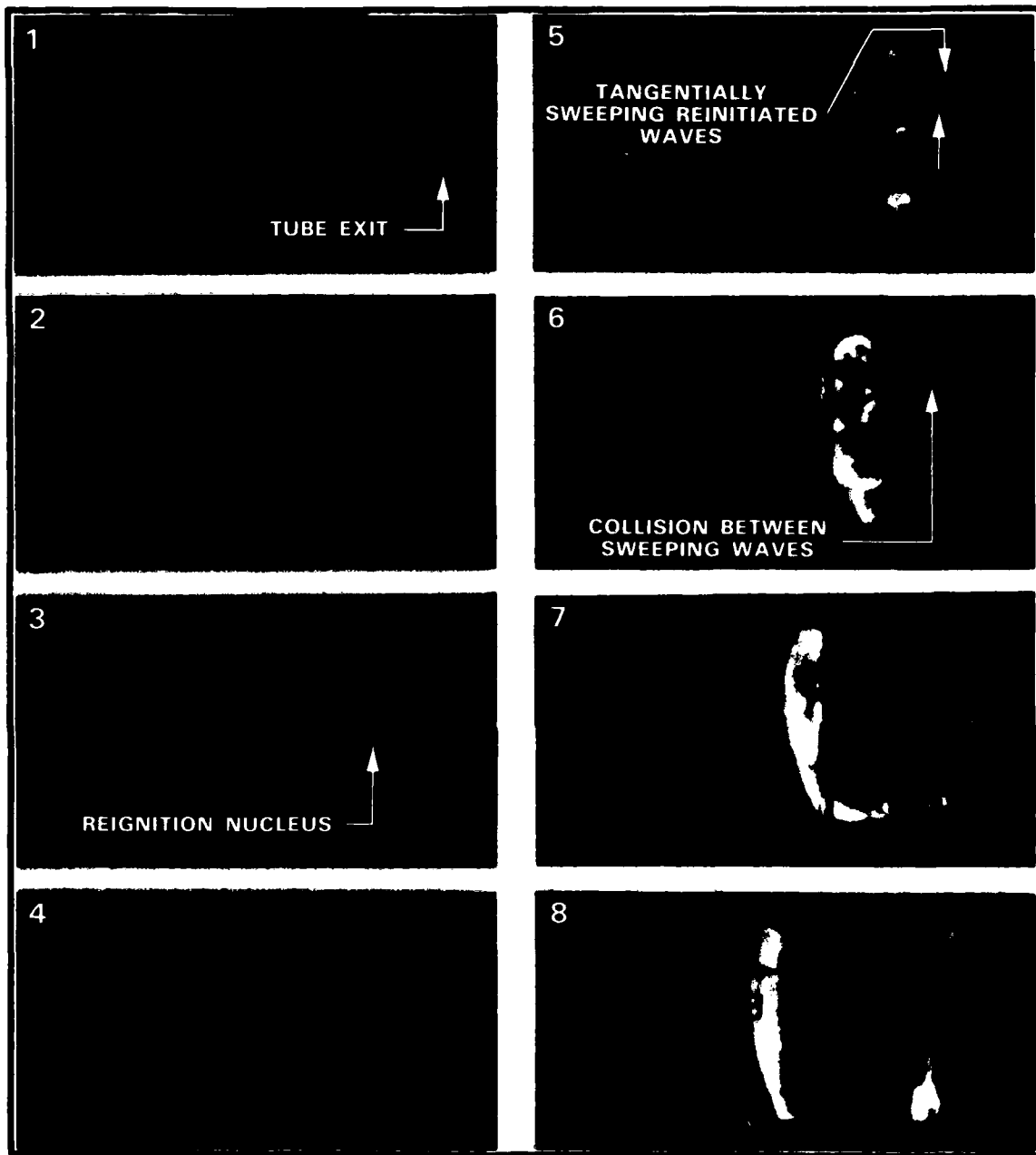


Figure 21

Selected frames from a high-speed cinematographic record showing near critical transmission of detonation from a rigid tube of 0.89 m diameter to a large gas bag simulating an unconfined environment (approximately 0.2 ms between frames).

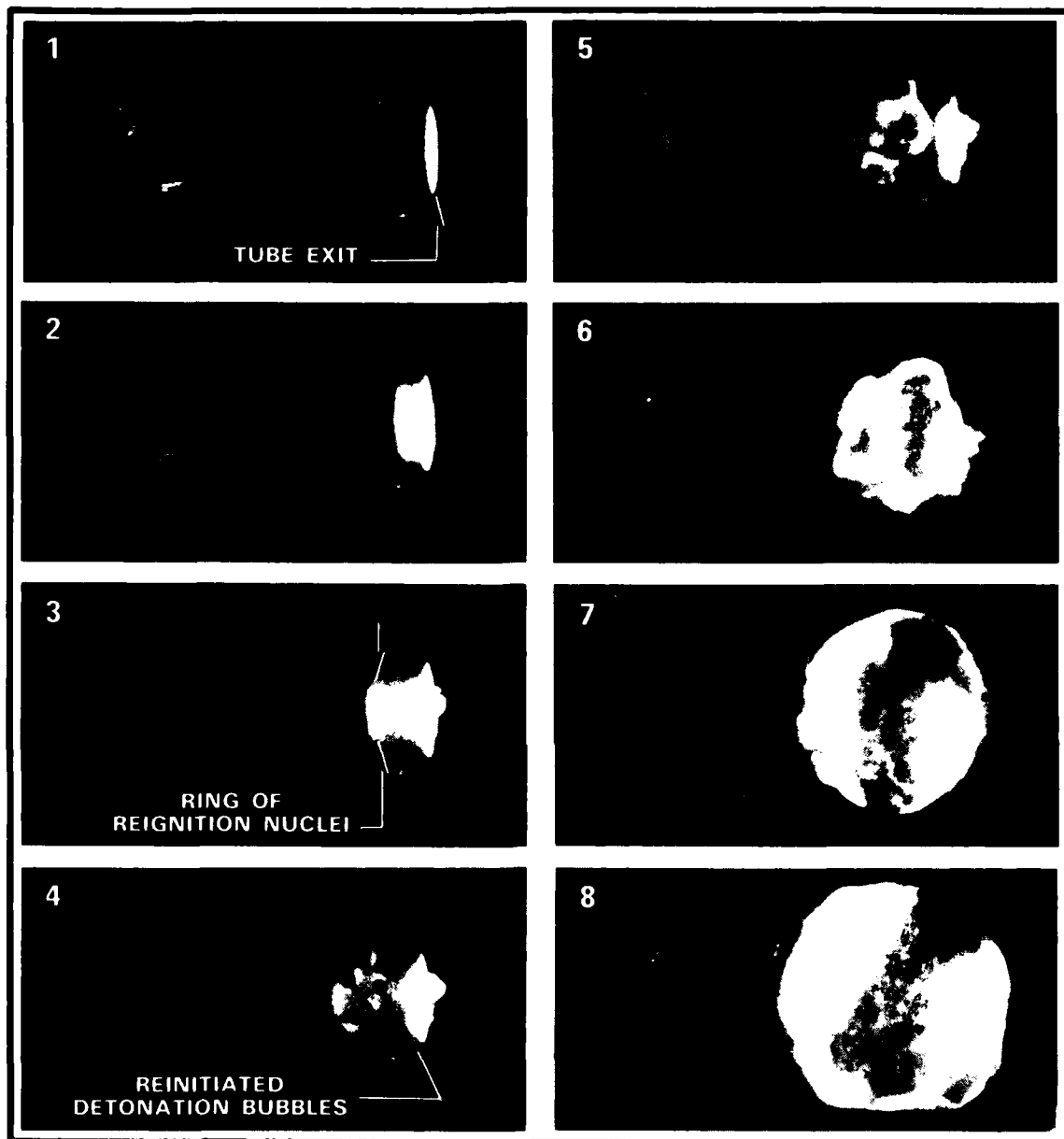


Figure 22

Selected frames from a high-speed cinematographic record showing supercritical transmission of detonation from a rigid tube of 0.89 m diameter to a large gas bag simulating an unconfined environment (approximately 0.2 ms between frames).



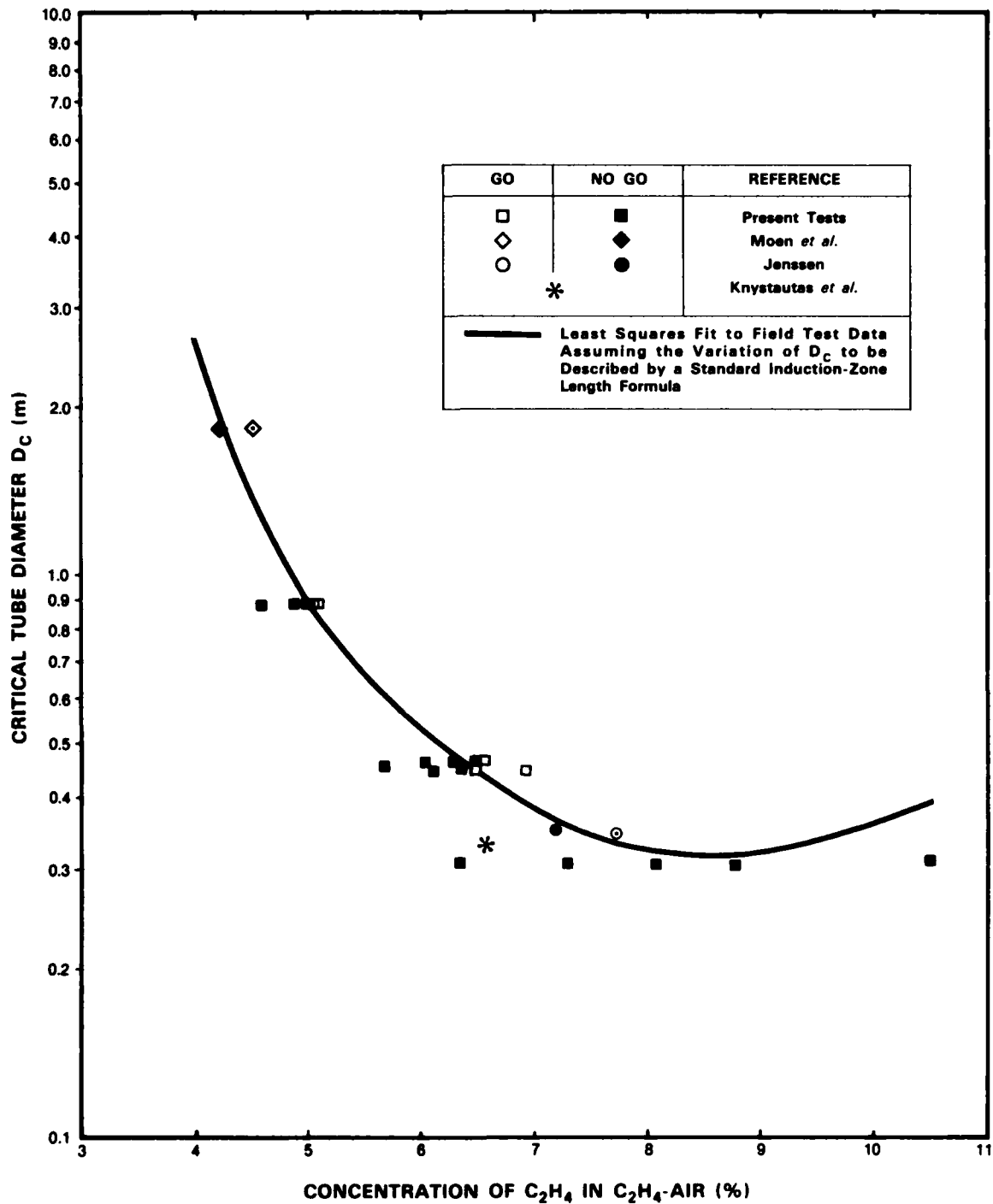


Figure 23

Critical tube diameter versus fuel concentration for the ethylene-air system at atmospheric pressure. Knystautas *et al.* (1982), Jenssen (1983), Moen *et al.* (1983).

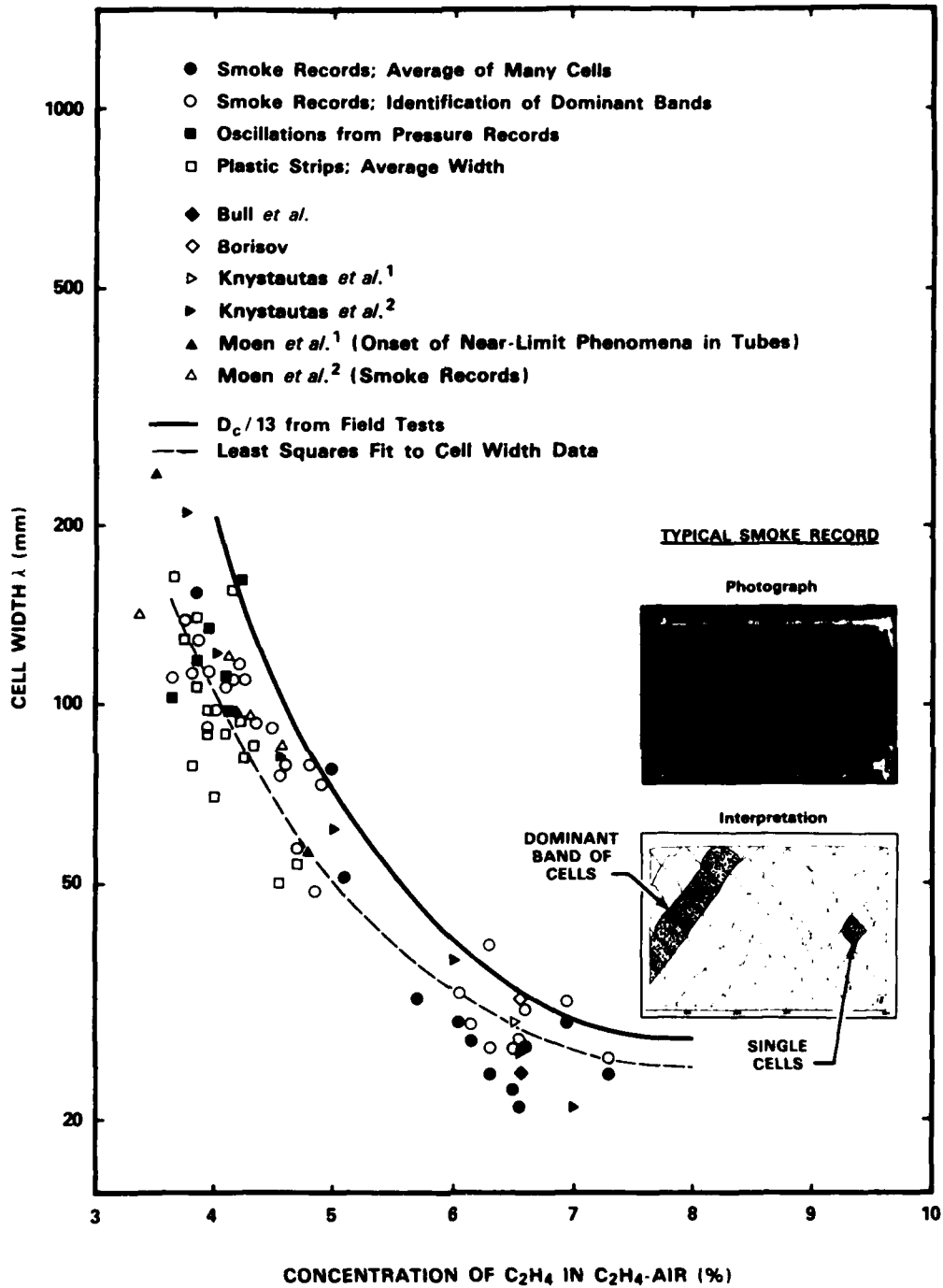


Figure 24

Detonation cell width versus fuel concentration for the ethylene-air system at atmospheric pressure. Borisov (1980), Moen *et al.*<sup>1</sup> (1981), Bull *et al.* (1982), Knystautas *et al.*<sup>1</sup> (1982), Knystautas *et al.*<sup>2</sup> (1983), Moen *et al.*<sup>2</sup> (1983).

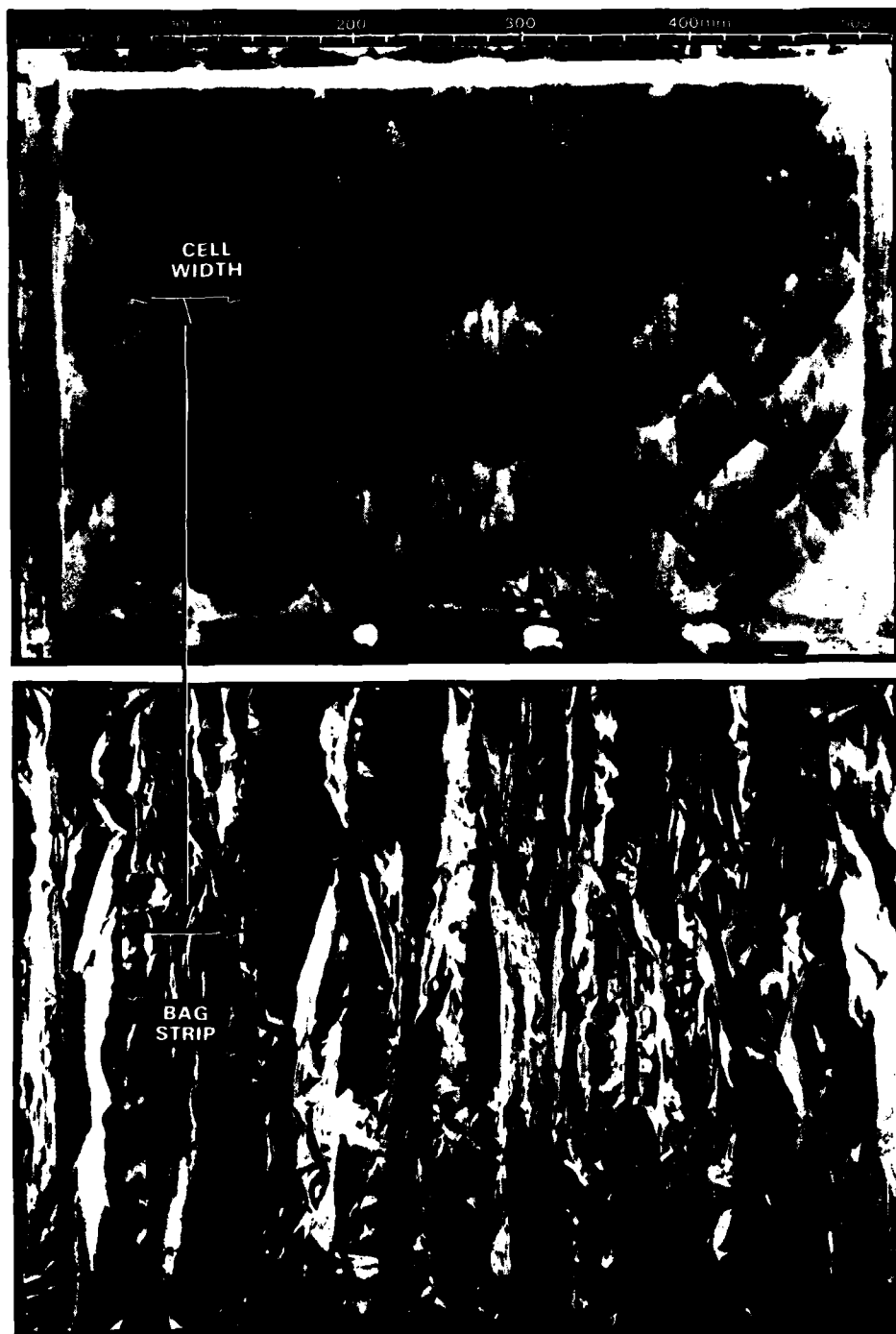


Figure 25

Comparison between the cellular structure recorded on a smoked plate (top) and the plastic strips produced by an ethylene-air detonation propagating in a plastic bag (bottom).

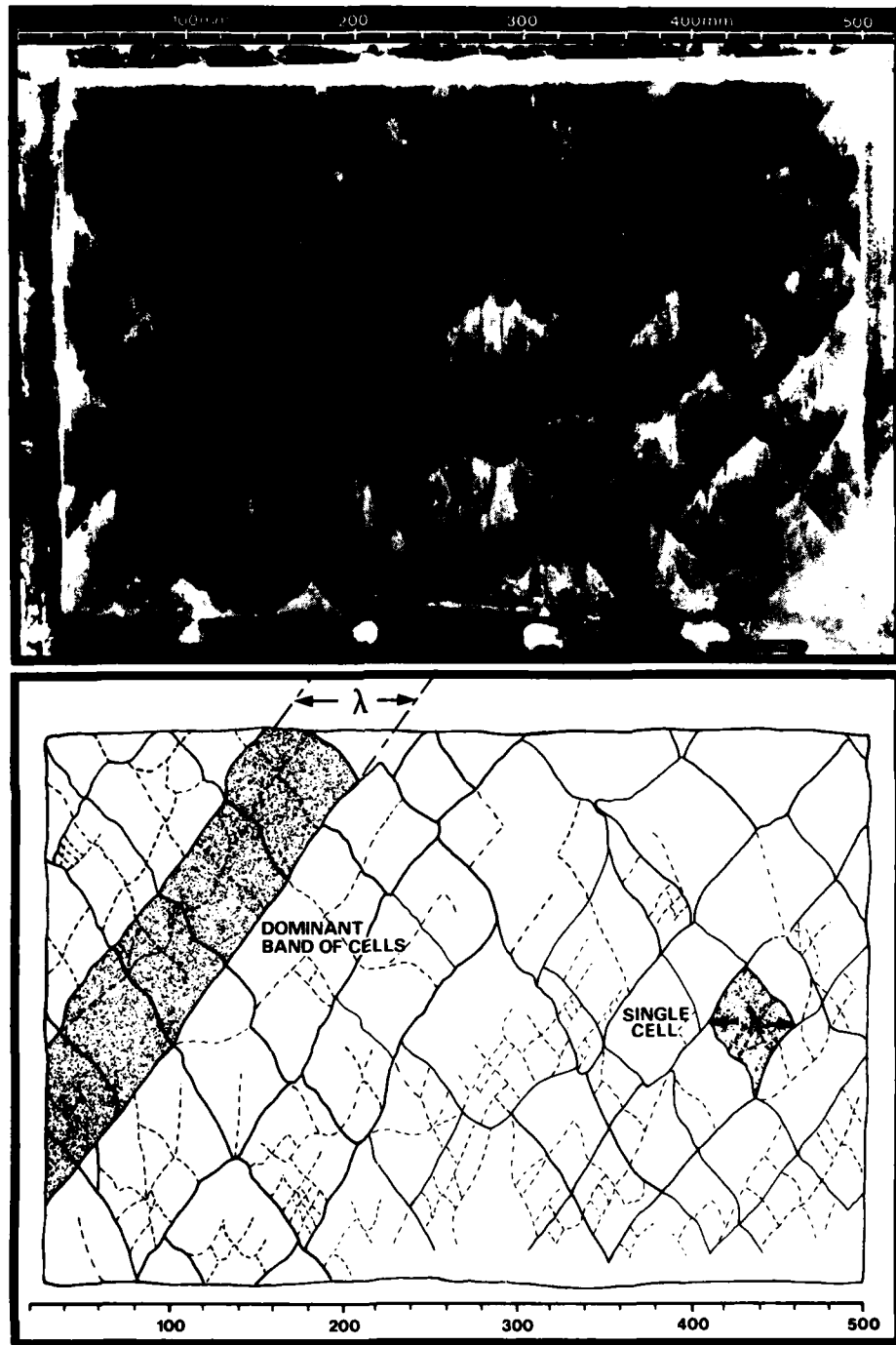


Figure 26

Photograph of a smoked plate produced by an ethylene-air detonation (top) and the author's interpretation of the cellular structure (bottom).

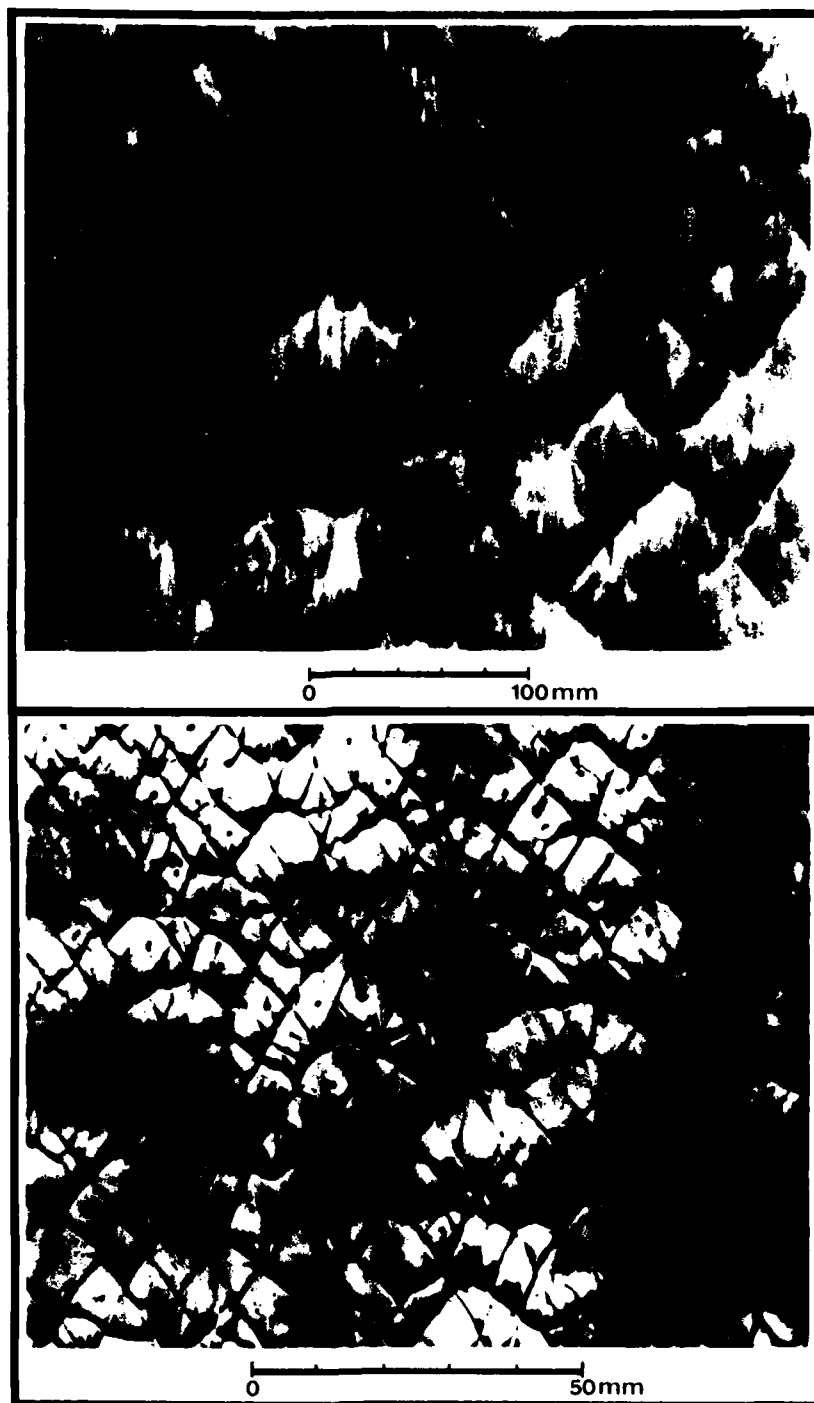


Figure 27

Photographs of smoke records showing the difference between the cellular structure of a fuel-air detonation at atmospheric pressure (top) and a fuel-oxygen detonation at low pressure (bottom).

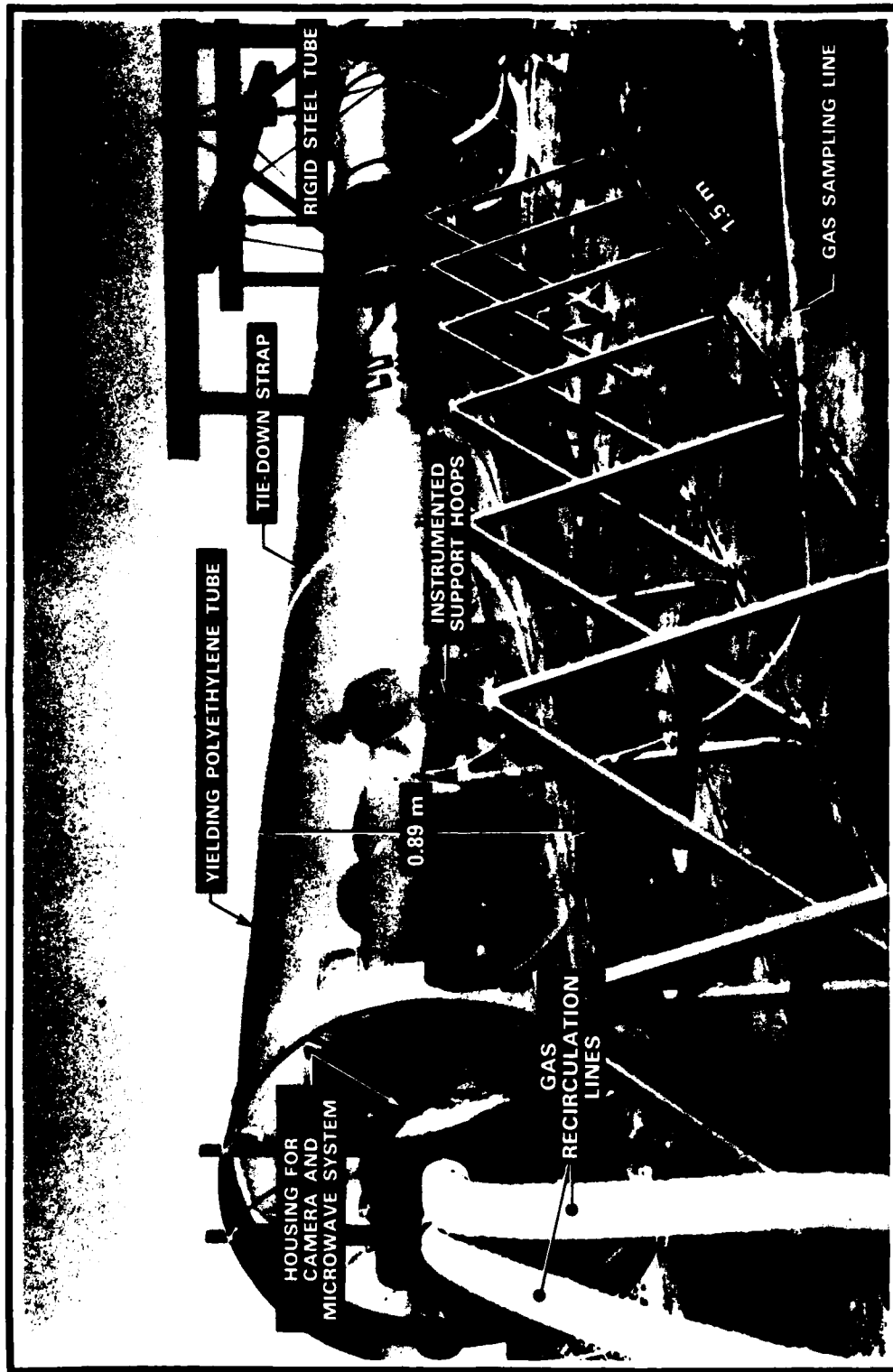


Figure 28

Large-scale field facility showing rigid/yielding tube combination prior to testing.

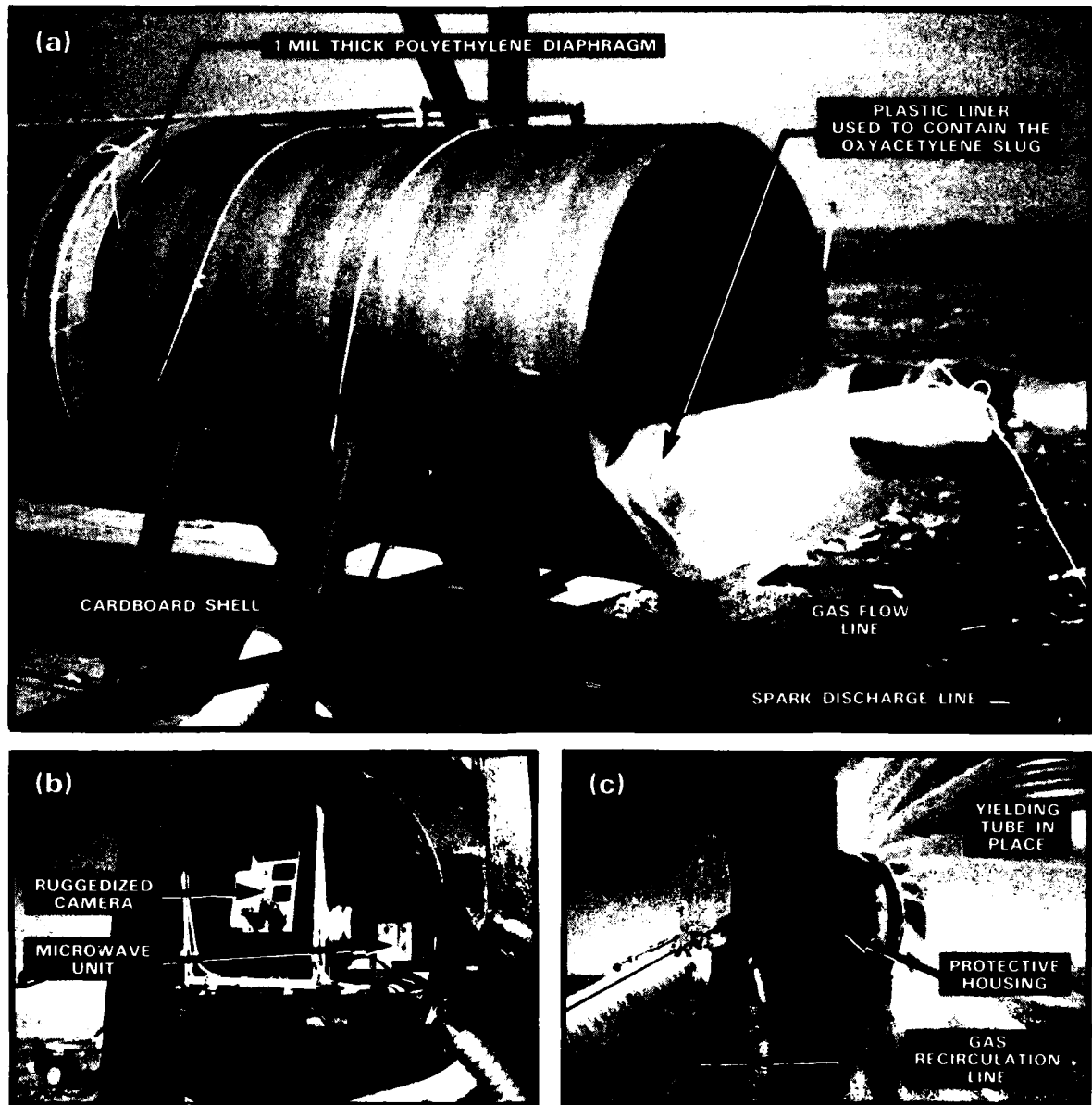


Figure 29

Photographs showing (a) the initiation scheme employing an oxyacetylene slug, (b) an interior view of the protective housing showing the camera and microwave unit, and (c) the yielding tube attached to the protective housing at the downstream end of the test section.

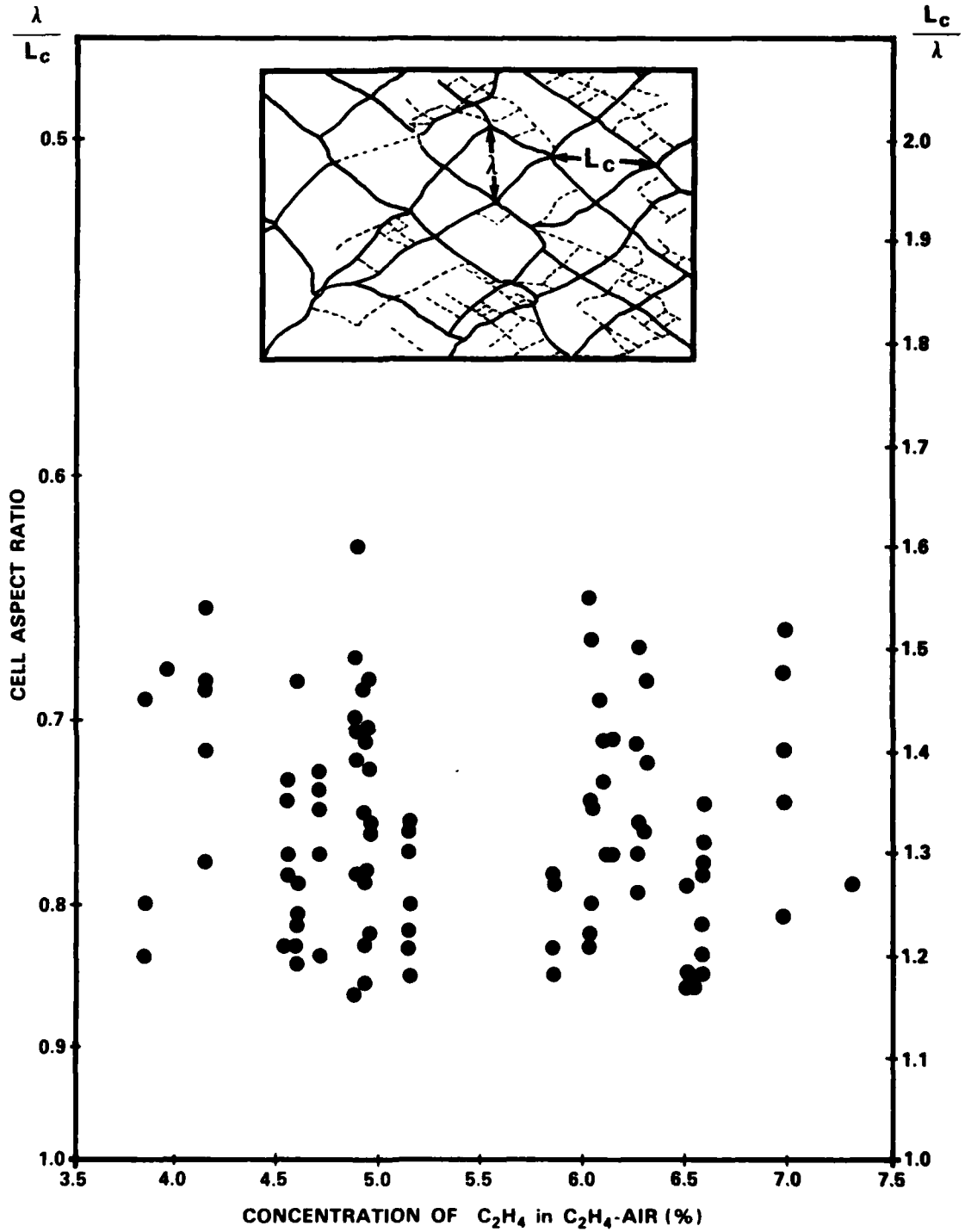


Figure 30

Measured cell aspect ratios for the C<sub>2</sub>H<sub>4</sub>-air system at atmospheric pressure.



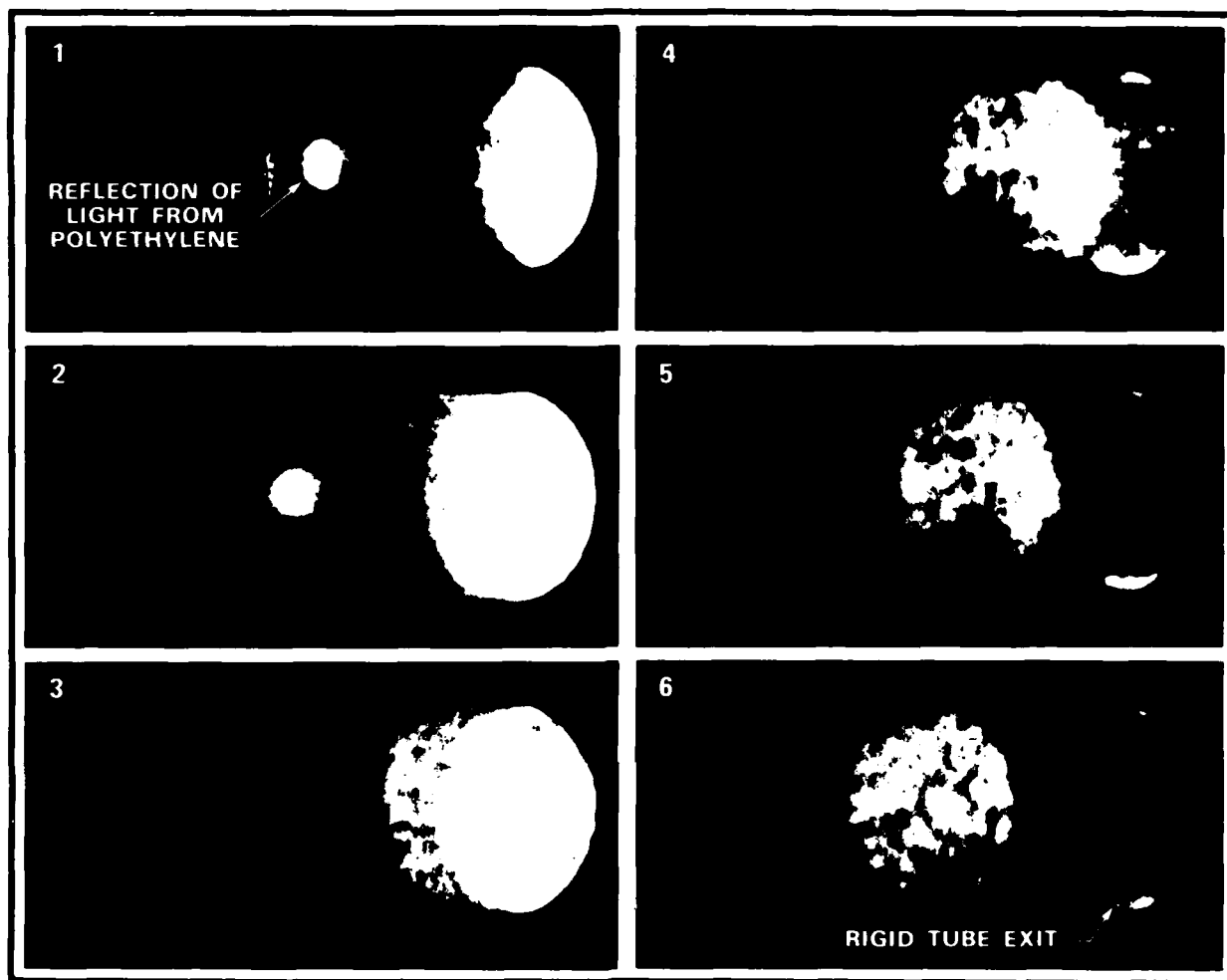


Figure 31

Cinematographic sequence showing supercritical transmission to a yielding tube of nominal 10 mil wall thickness and 0.89 m diameter. The gas mixture is 4.15%  $C_2H_4$  in  $C_2H_4$ -air. Elapsed time between frames is approximately 0.2 ms.

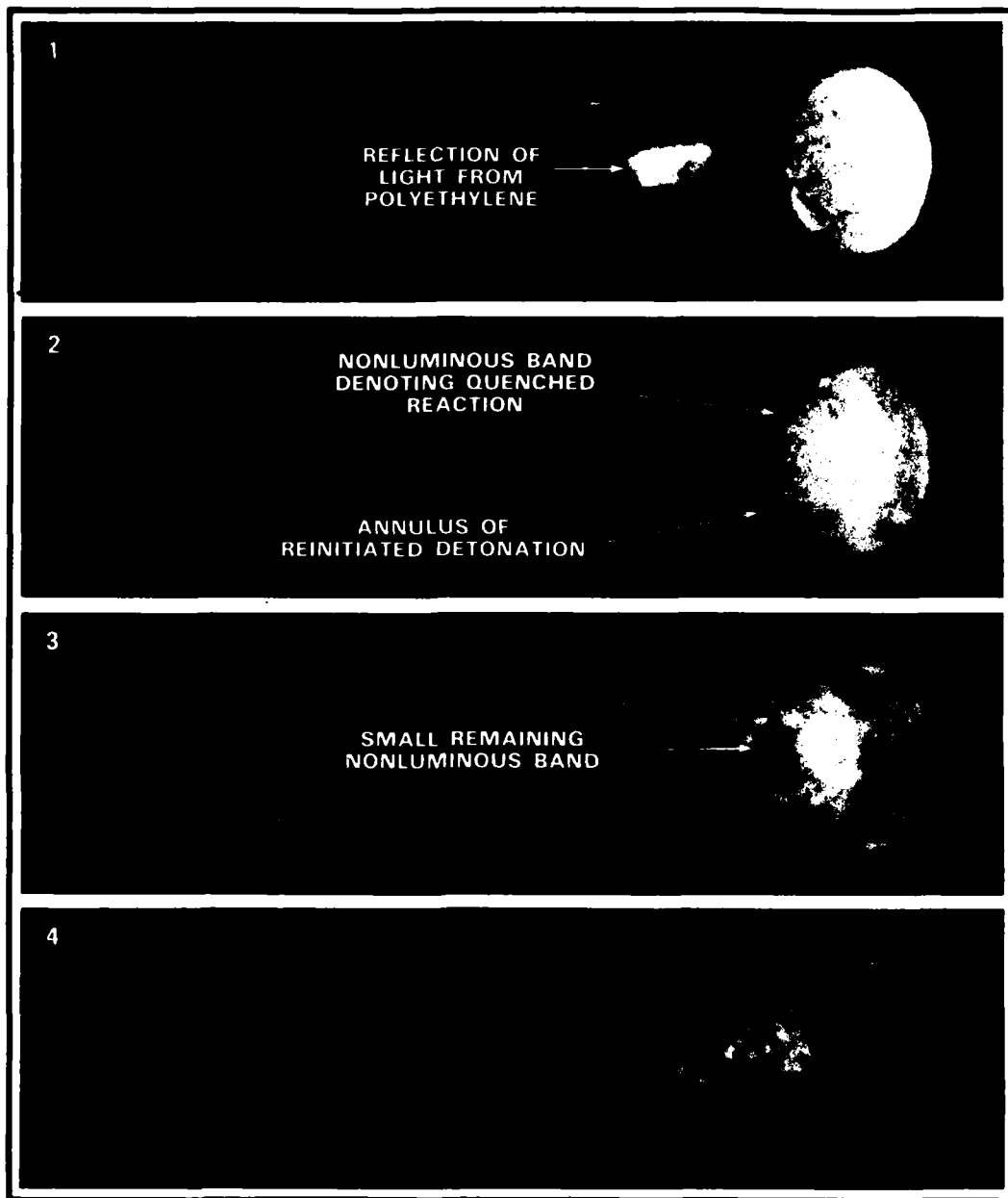


Figure 32

Cinematographic sequence showing transmission to a yielding tube of nominal 5 mil wall thickness and 0.89 m diameter. The mixture of 4.25%  $C_2H_4$  in  $C_2H_4$ -air is slightly more sensitive than the critical one (4.15%  $C_2H_4$ ) for this wall thickness. Elapsed time between frames is approximately 0.2 ms.

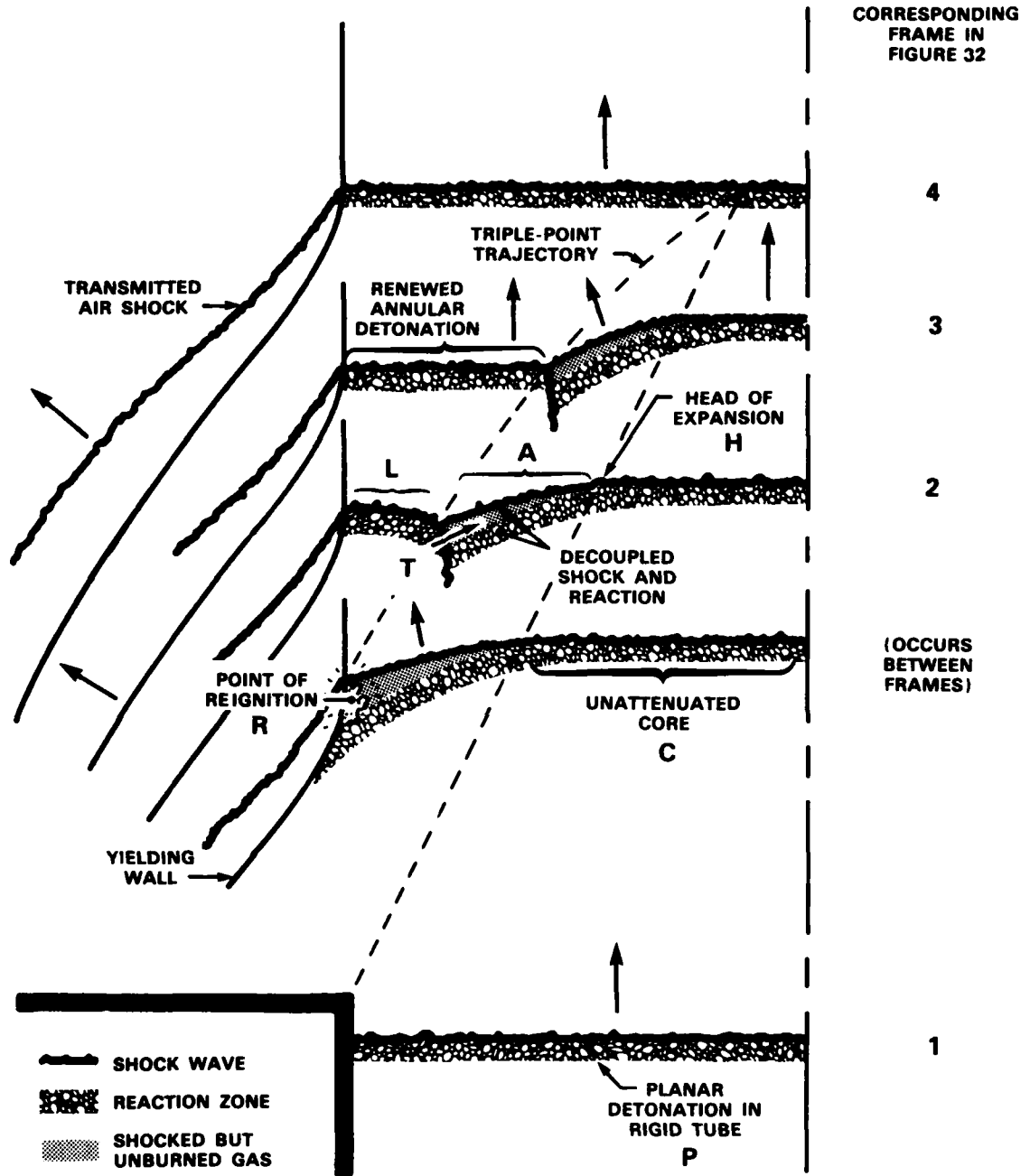


Figure 33

Schematic diagrams showing details of the reinitiation process typical of transmission to a tube with yielding walls.

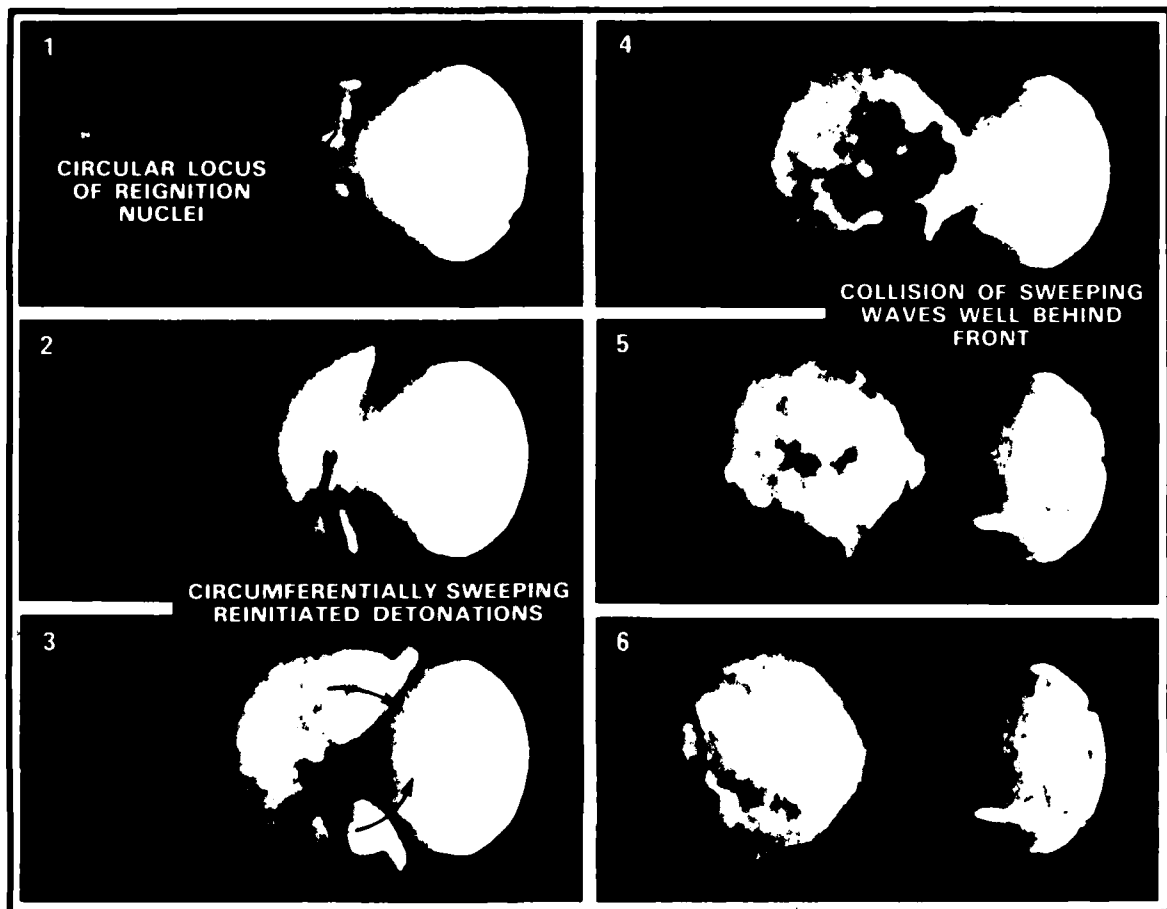


Figure 34

Cinematographic sequence showing critical transmission to a yielding tube of nominal 1 mil wall thickness and 0.89 m diameter. The gas mixture is 4.70%  $C_2H_4$  in  $C_2H_4$ -air. Elapsed time between frames is approximately 0.2 ms.

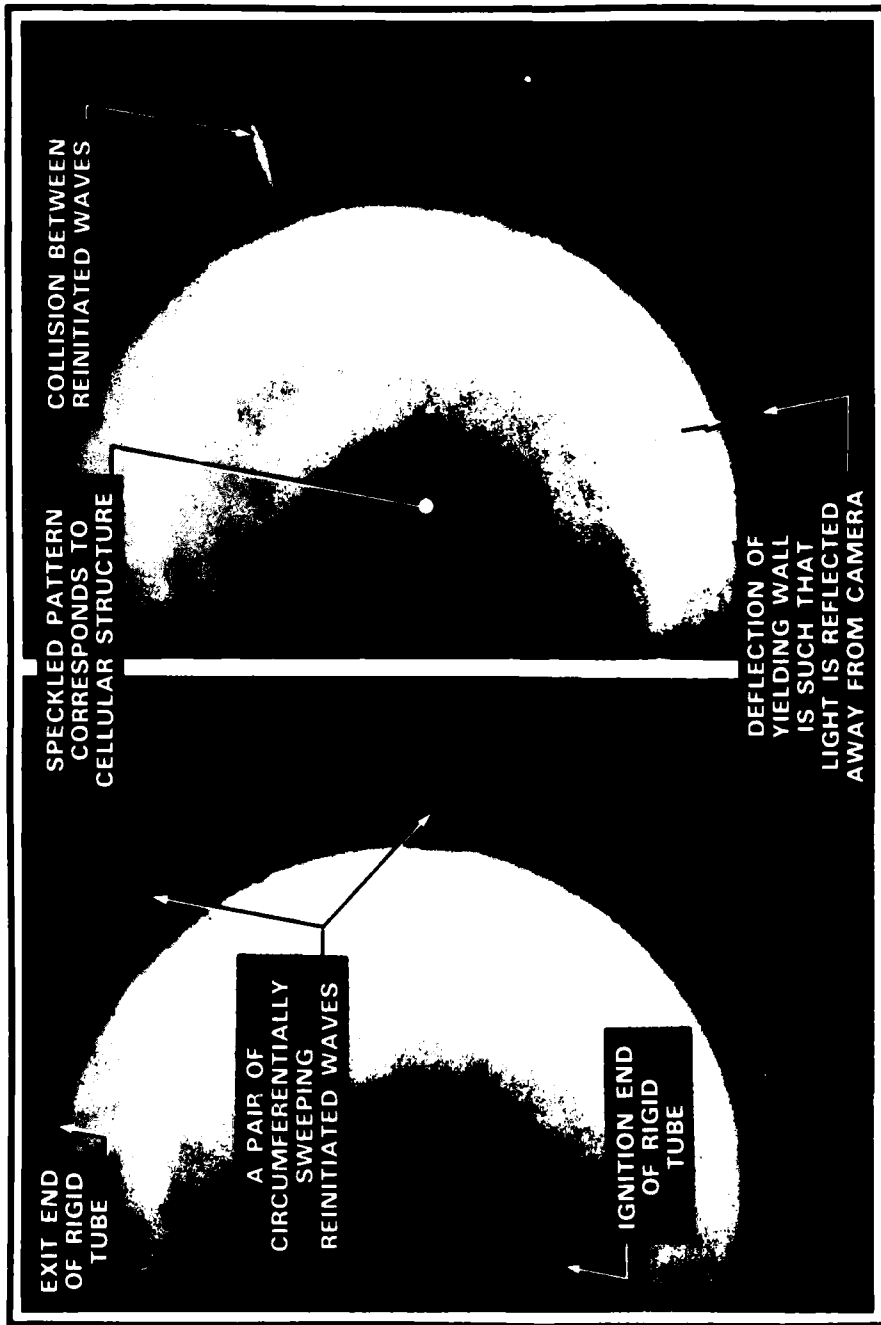


Figure 35

Cinematographic sequence looking along the axis of propagation. Transmission of detonation is to a yielding tube of nominal 6 mil wall thickness and 1.83 m diameter. The gas mixture is 6.45% C<sub>3</sub>H<sub>8</sub> in C<sub>3</sub>H<sub>8</sub>-air. Elapsed time between frames is approximately 0.06 ms.

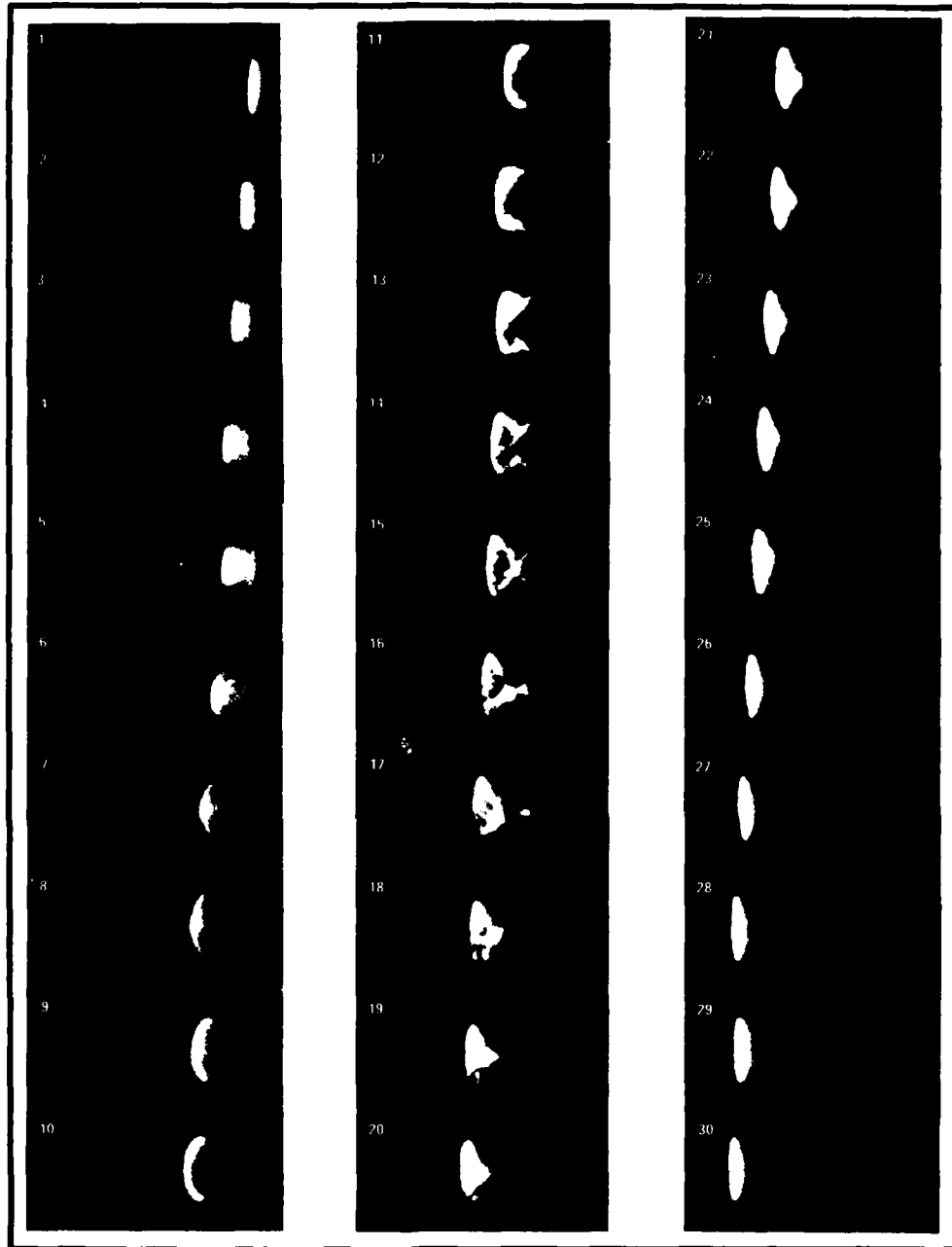


Figure 36

Cinematographic sequence showing critical transmission to a yielding tube of nominal 1 mil wall thickness and 0.89 m diameter. The gas mixture is 4.70%  $C_2H_4$  in  $C_2H_4$ -air. Elapsed time between frames is approximately 0.06 ms. Frame 9 – first occurrence of reignition nuclei; frame 15 – collision between sweeping waves; frame 30 – catch-up phase complete.

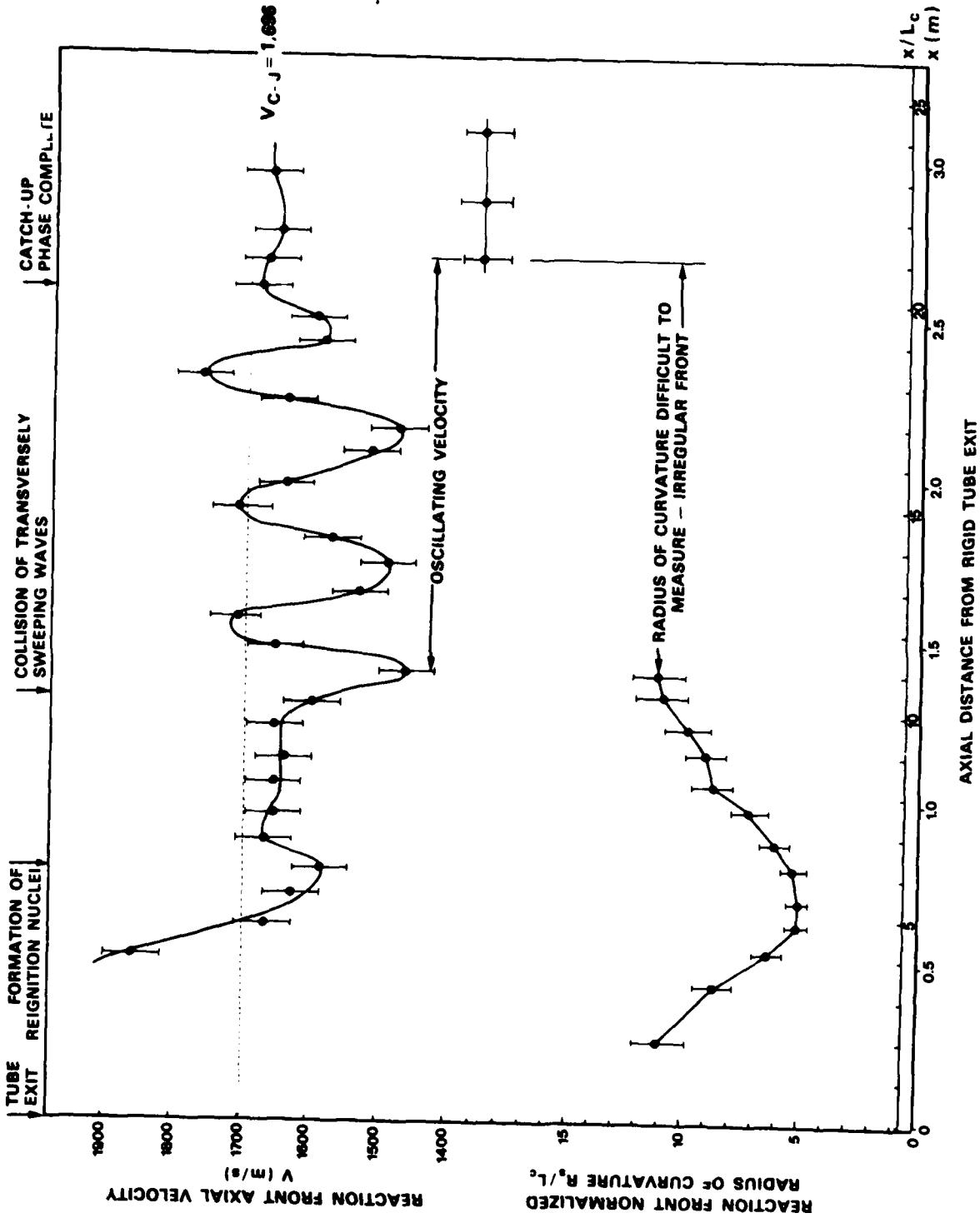


Figure 37

Reaction front axial velocity and normalized radius of curvature as a function of axial distance from the rigid tube exit as measured from cinematographic records.

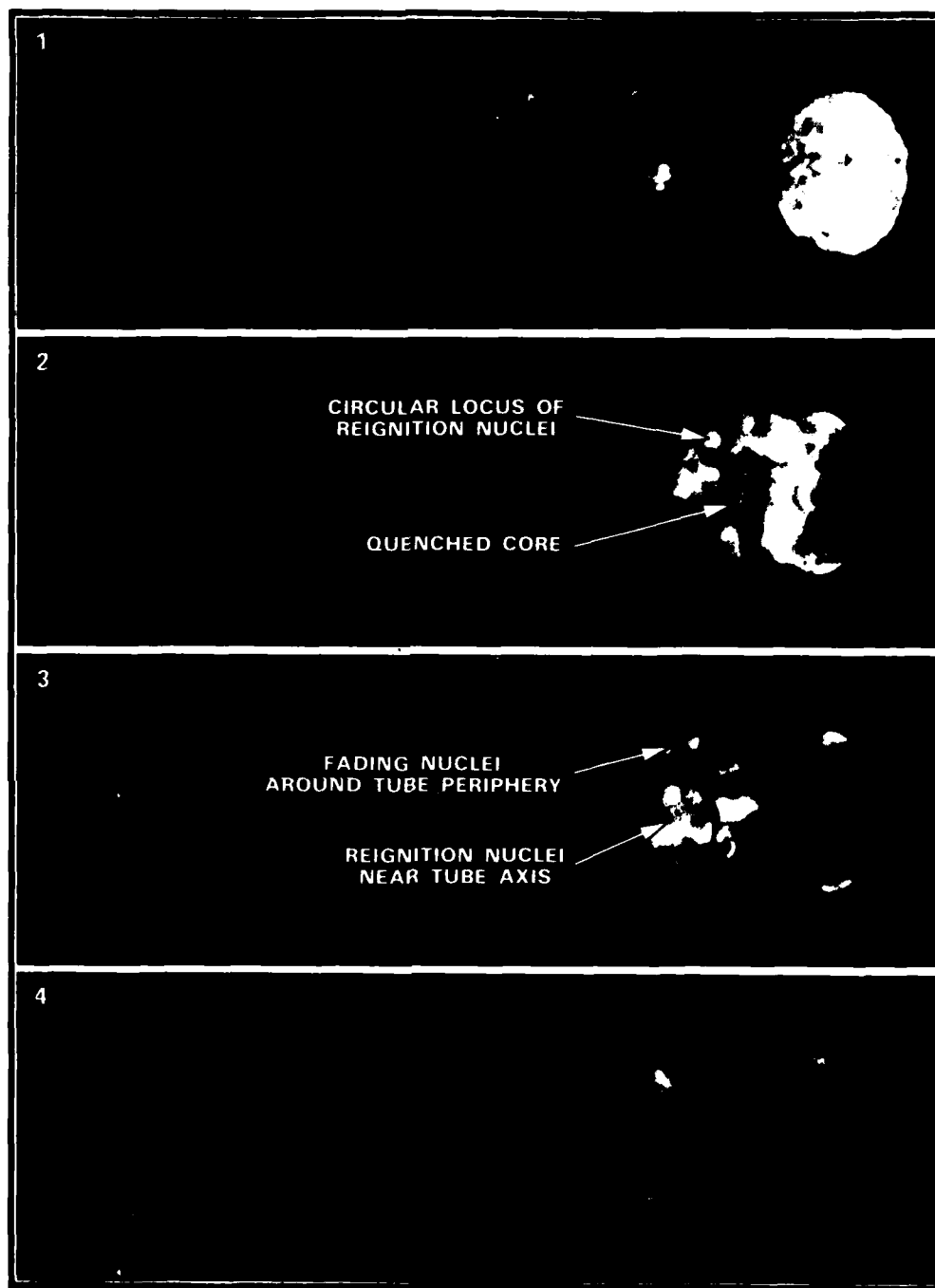


Figure 38

Cinematographic sequence showing subcritical transmission to a yielding tube of nominal 5 mil wall thickness and 0.89 m diameter. The gas mixture is 3.95%  $C_2H_4$  in  $C_2H_4$ -air. Elapsed time between frames is approximately 0.4 ms.



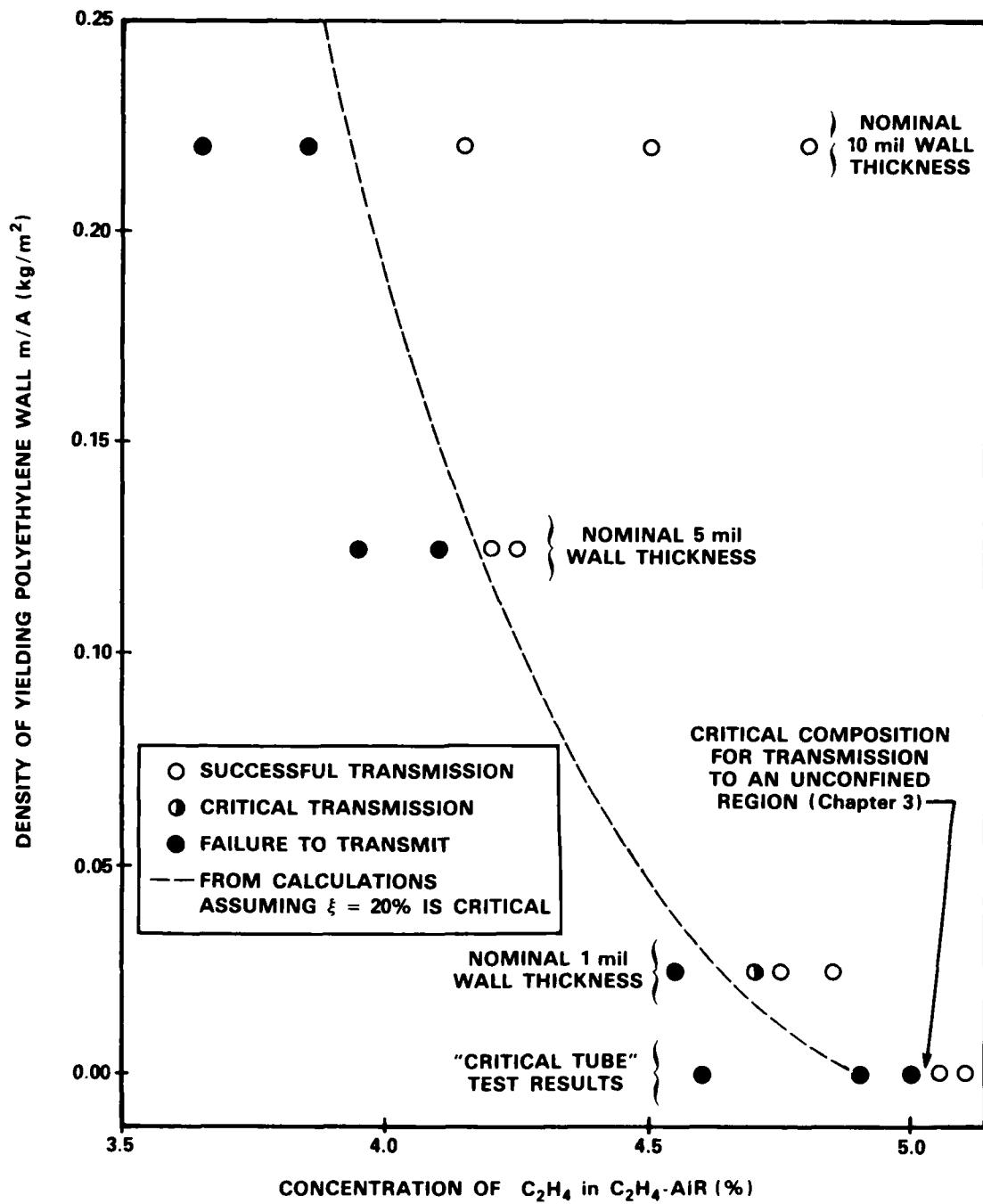


Figure 39

Summary of test results for transmission of detonation from a rigid tube of 0.89 m diameter to yielding polyethylene tubes having various wall thicknesses.

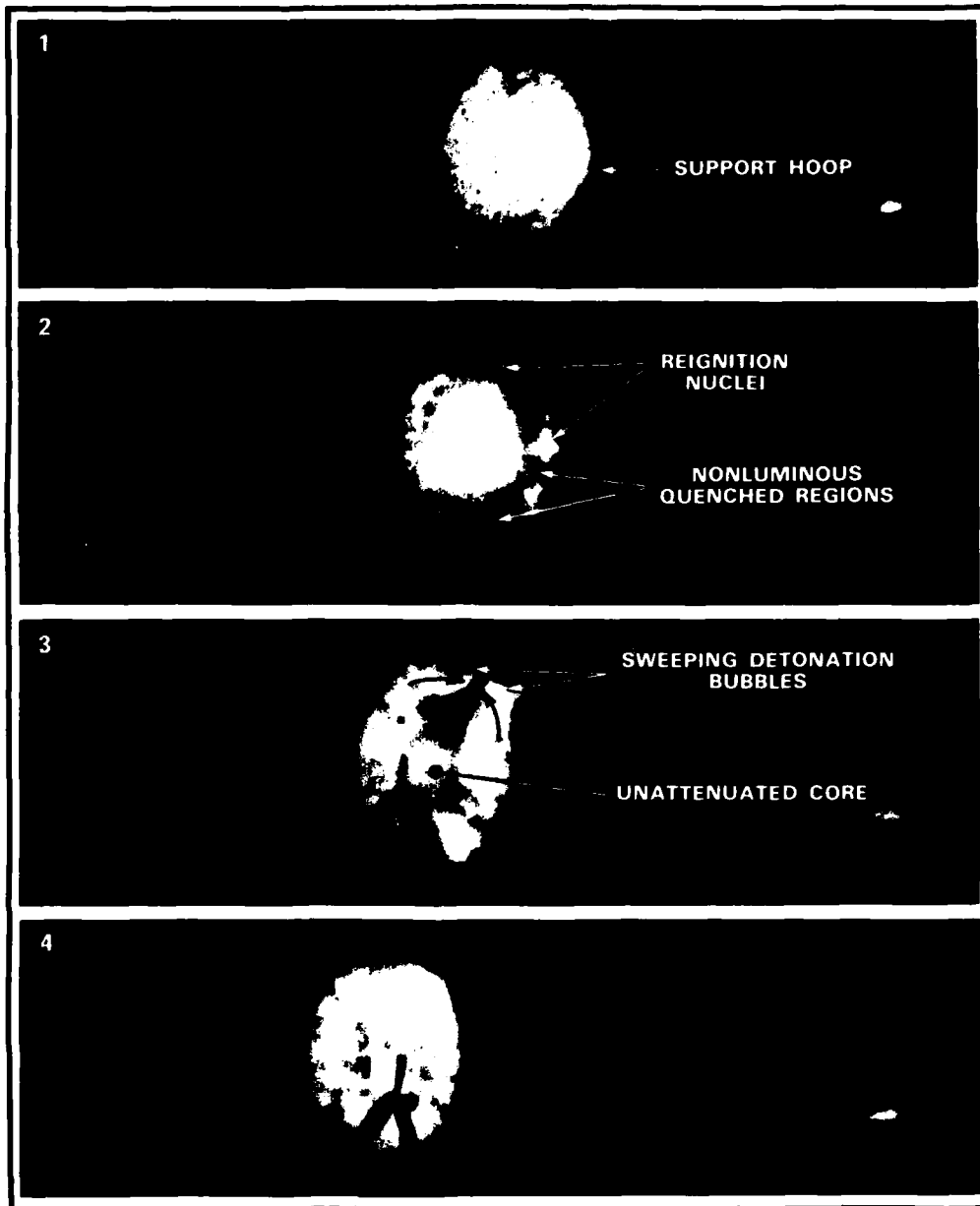


Figure 40

Cinematographic sequence showing recovery of a detonation wave perturbed at the boundary. The perturbing obstacles are a steel hoop along the bottom and a heavy piece of tape along the top of the periphery. The mixture is 4.70%  $C_2H_4$  in  $C_2H_4$ -air. Elapsed time between frames is approximately 0.2 ms.

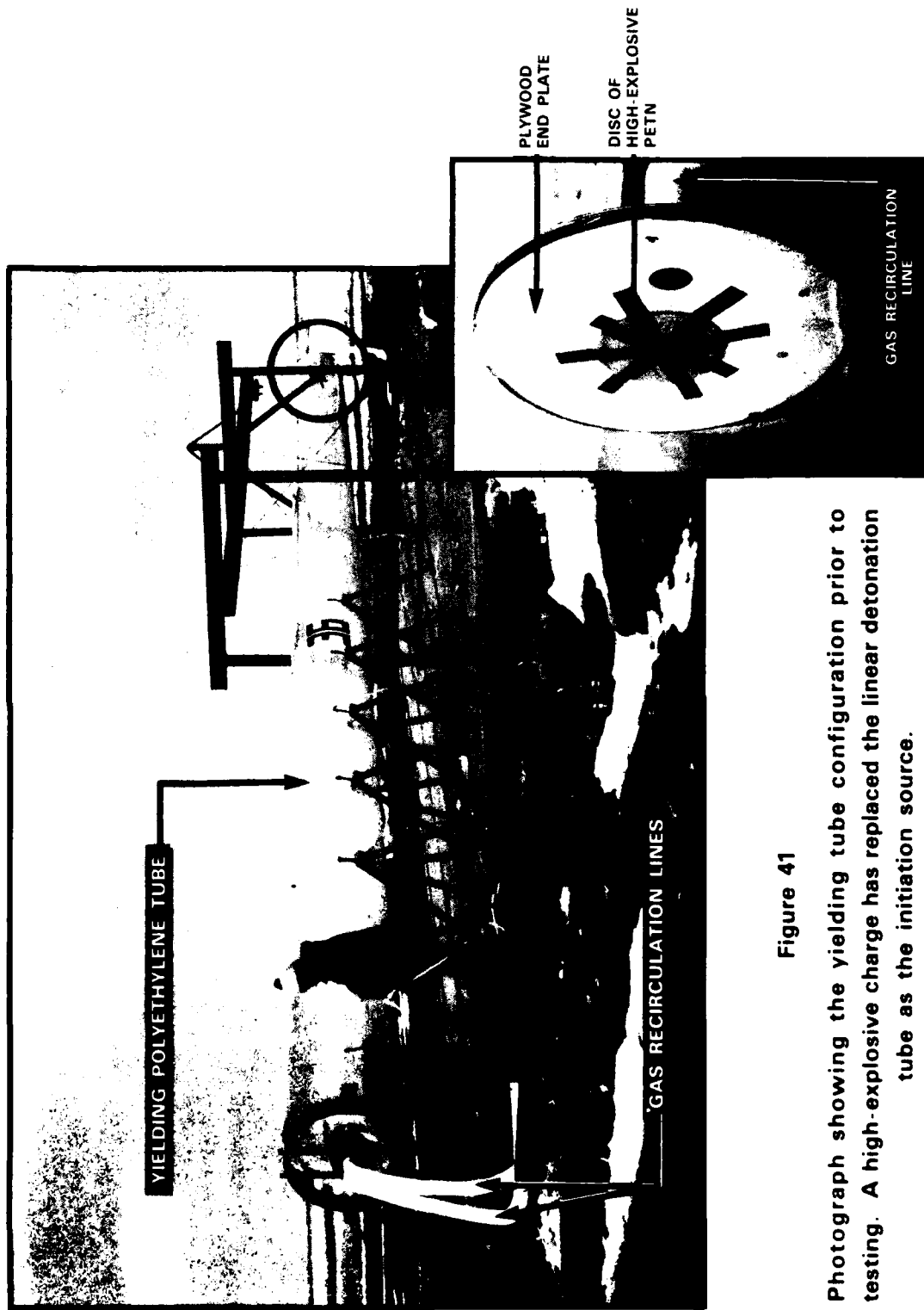


Figure 41

Photograph showing the yielding tube configuration prior to testing. A high-explosive charge has replaced the linear detonation tube as the initiation source.

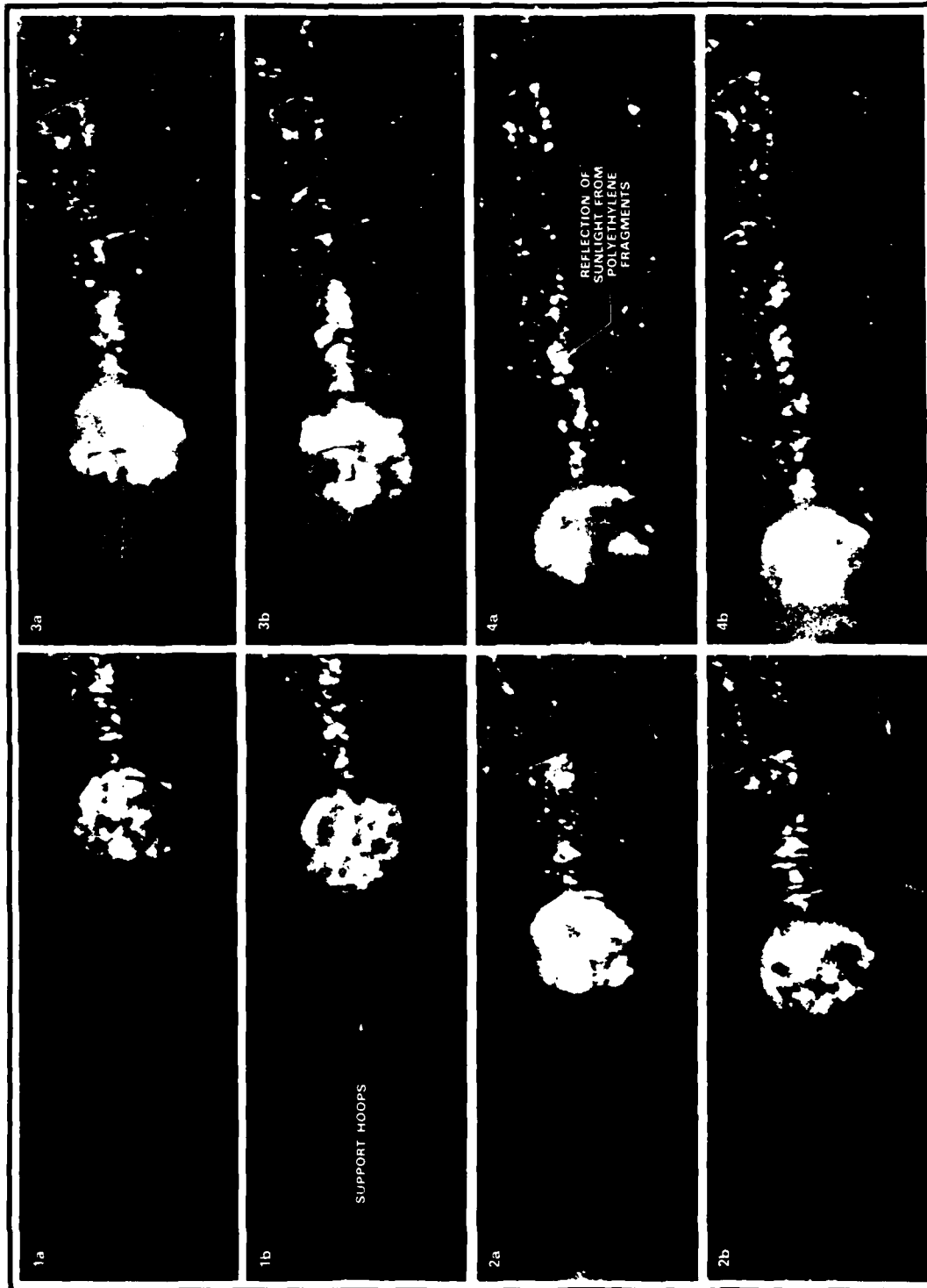


Figure 42

Cinematographic sequence showing gradual failure of detonation induced by a series of perturbing obstacles around the periphery of a tube of nominal 10 mil wall thickness. The gas mixture is 3.90%  $C_2H_4$ -air. Each pair of frames shows the wave (a) prior to, and (b) subsequent to traversing a hoop. Elapsed time between "a" and "b" frames is approximately 0.2 ms.

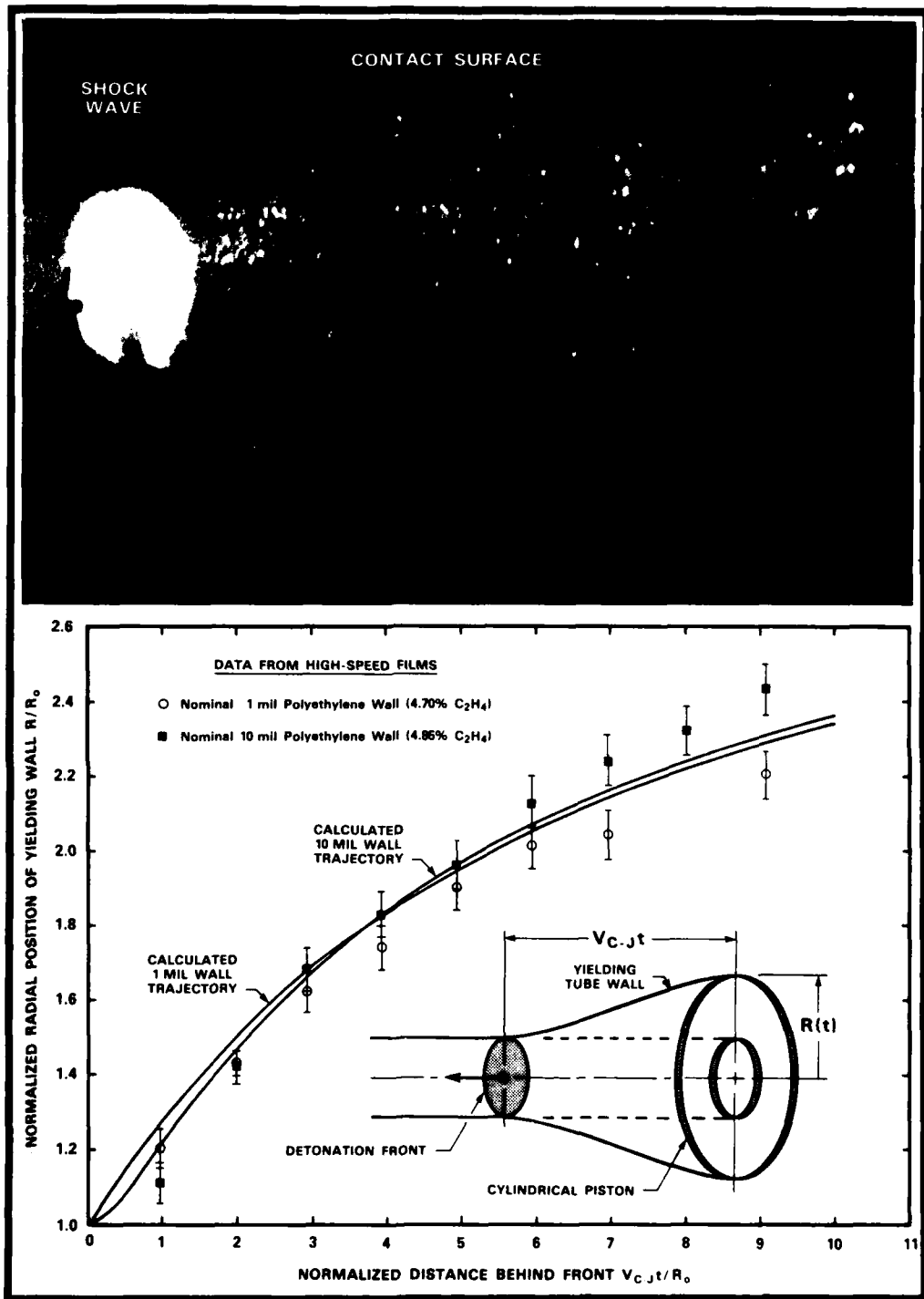


Figure 43

Comparison between measured wall trajectories and those calculated using a cylindrical piston analogy.

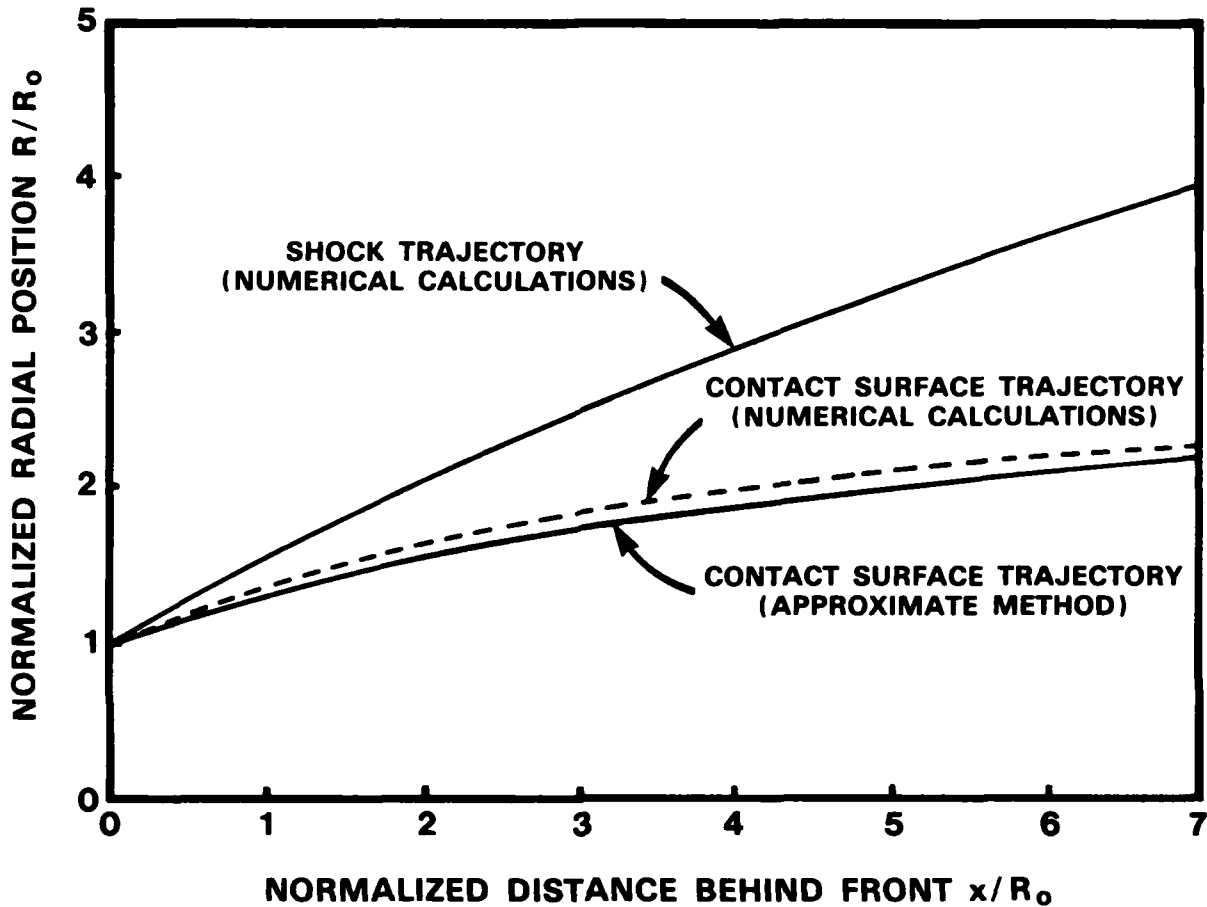


Figure 44

Comparison between calculated contact surface trajectories from a bursting cylinder. Initial conditions inside the cylinder correspond to the detonation products of stoichiometric ethylene-air.

Approximate method is due to Meyer (1958).

Numerical calculations are due to Thibault (1983).

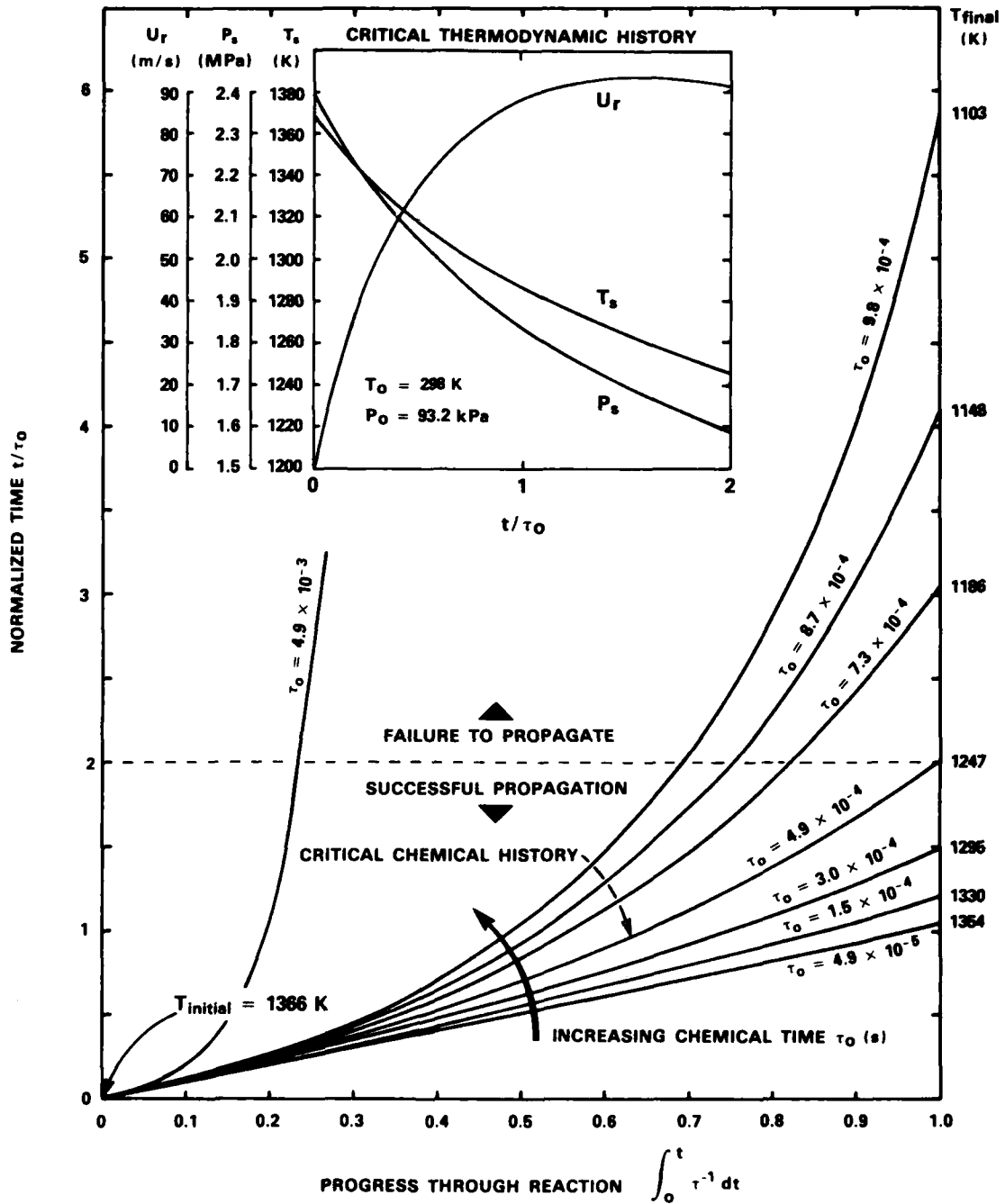
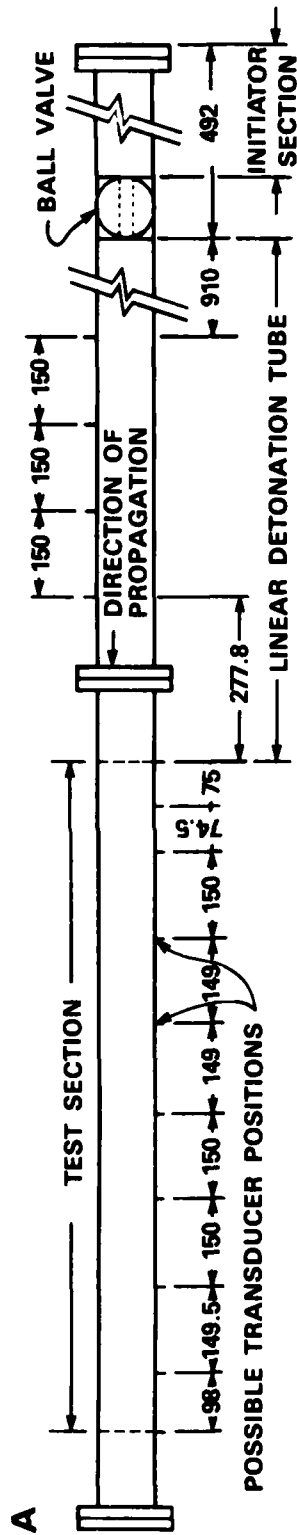


Figure 45

Chemical histories (bottom plot) for various assumed controlling chemical times,  $\tau_0$ , given the expansion corresponding to the 10 mil thick polyethylene wall. The critical particle thermodynamic history is shown in the inset at the top left of the figure.



\* ALL DIMENSIONS ARE IN MILLIMETERS

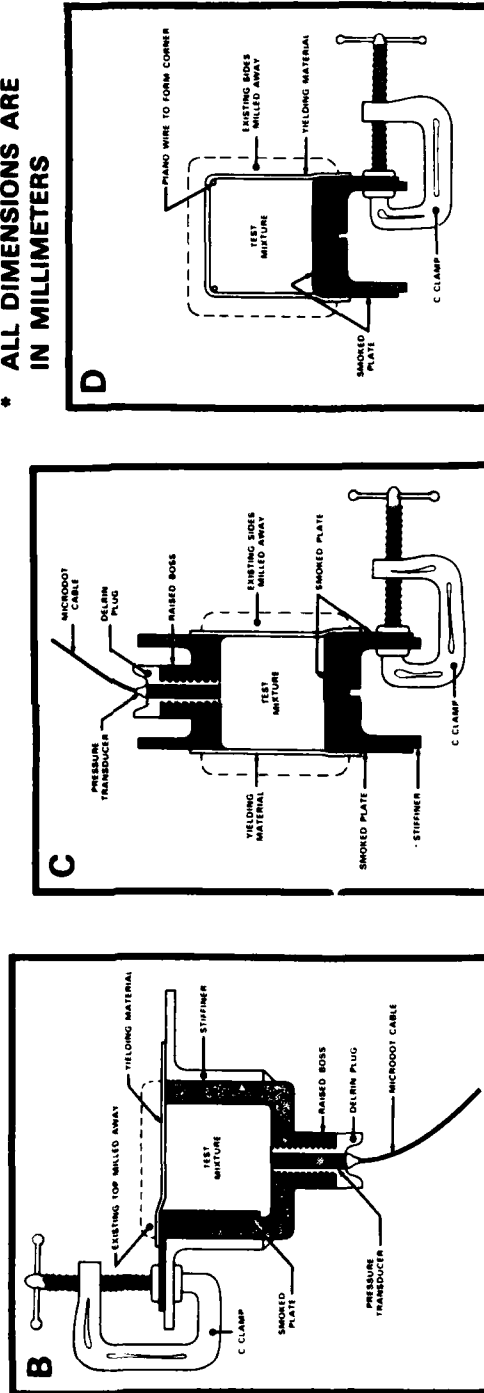


Figure 46

Apparatus used to investigate the phenomenon of velocity deficits in the presence of yielding confinement. Illustrated at the top (A) is the overall configuration of the test facility. Details of the test sections with one, two and three yielding walls are shown in (B), (C) and (D), respectively.



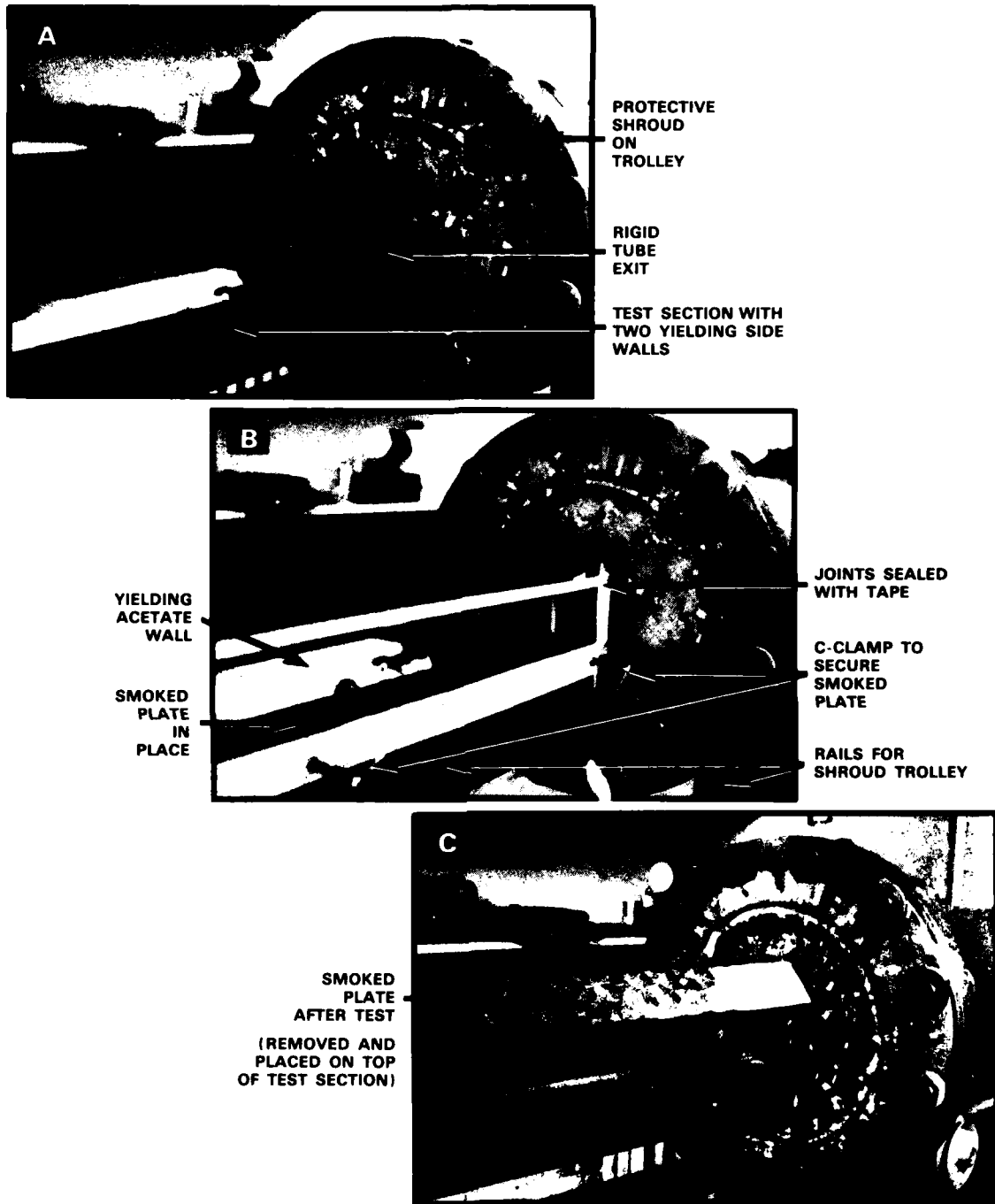


Figure 47

Photographs showing (A) the test section prior to being prepared for testing, (B) after preparation for an experiment, and (C) after completion of a test.

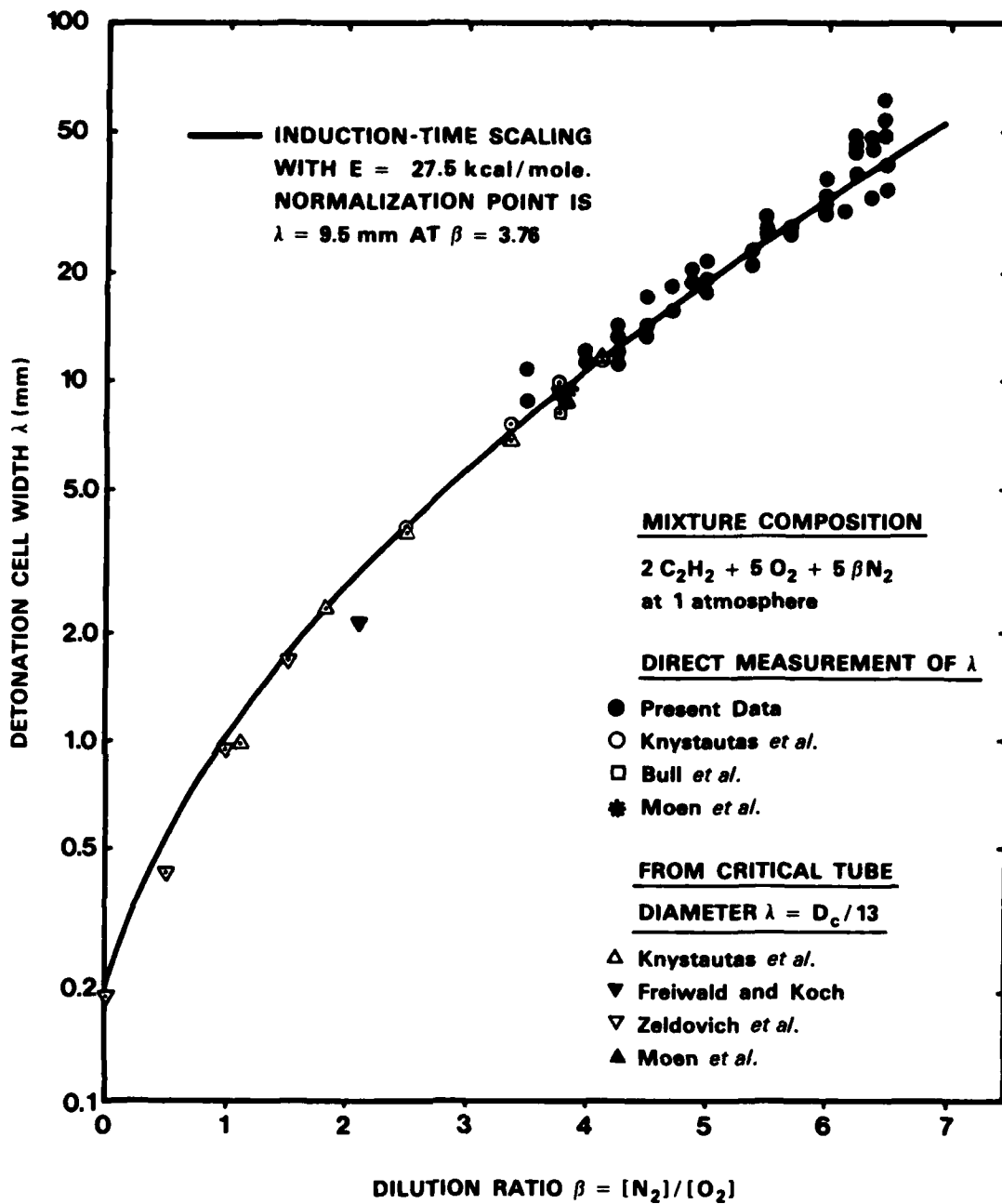


Figure 48

Cell width versus mixture composition for stoichiometric oxycetylene with nitrogen dilution at atmospheric pressure. Zeldovich *et al.* (1956), Freiwald and Koch (1963), Bull *et al.* (1982), Knystautas *et al.* (1982), Moen *et al.* (1983).

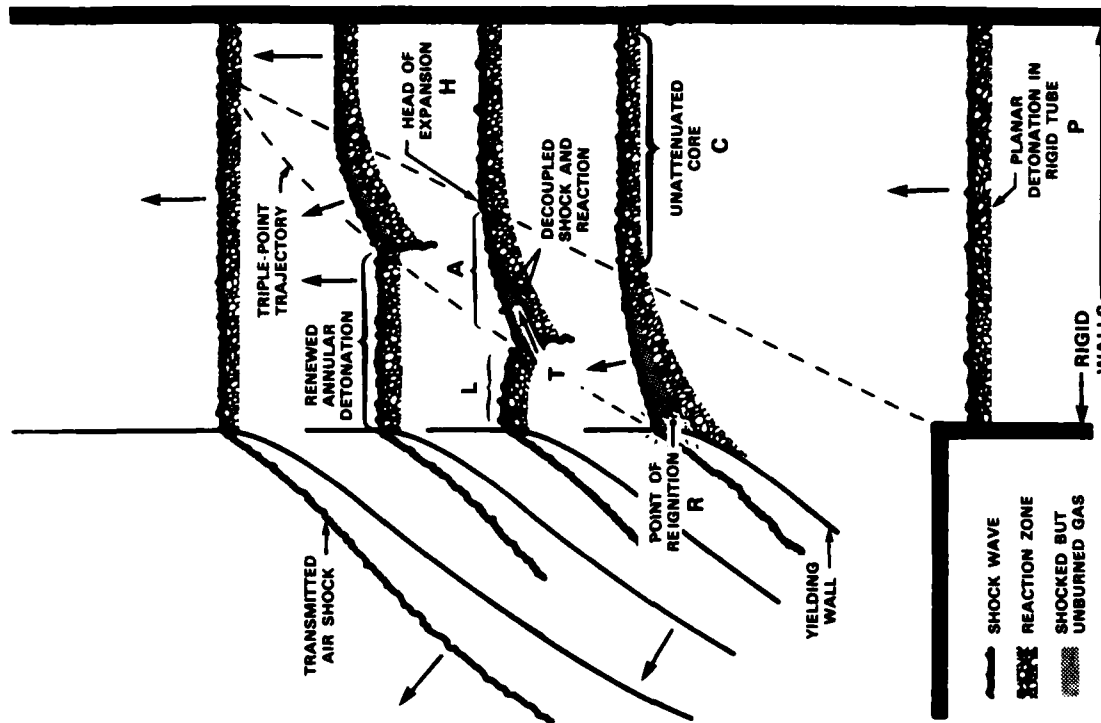
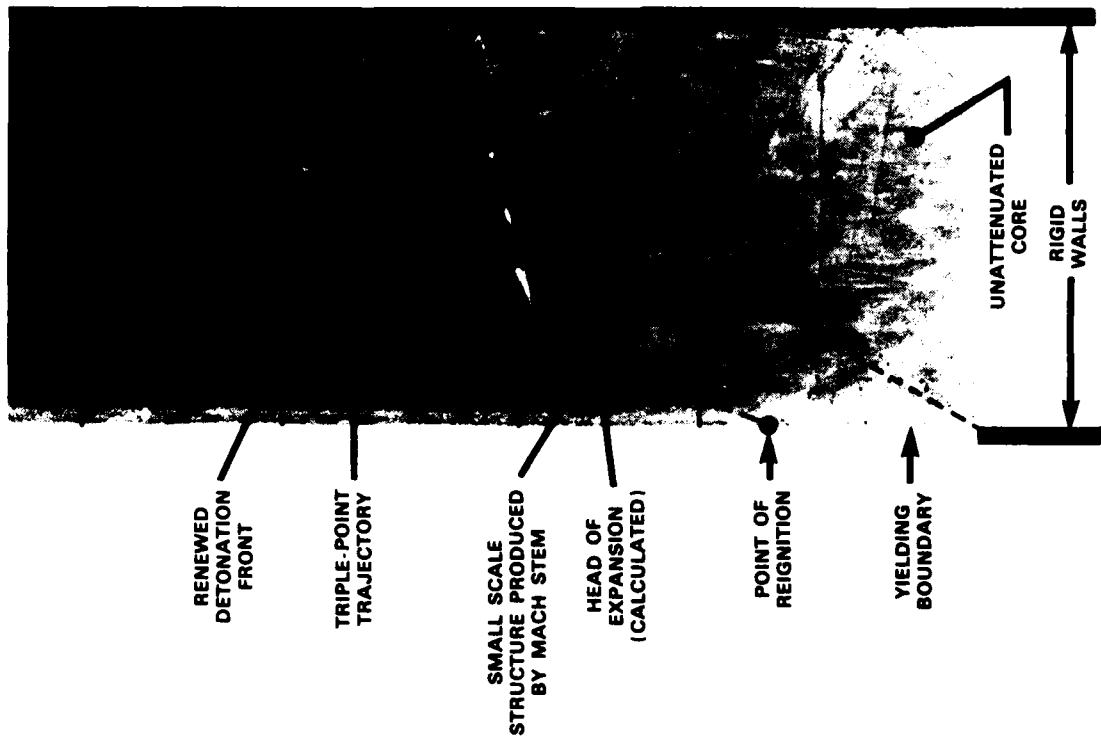


Figure 49

Comparison between the reinitiation phenomenon proposed from cinematographic records of large-scale transmission (left) and that evident from smoke records in laboratory experiments (right).

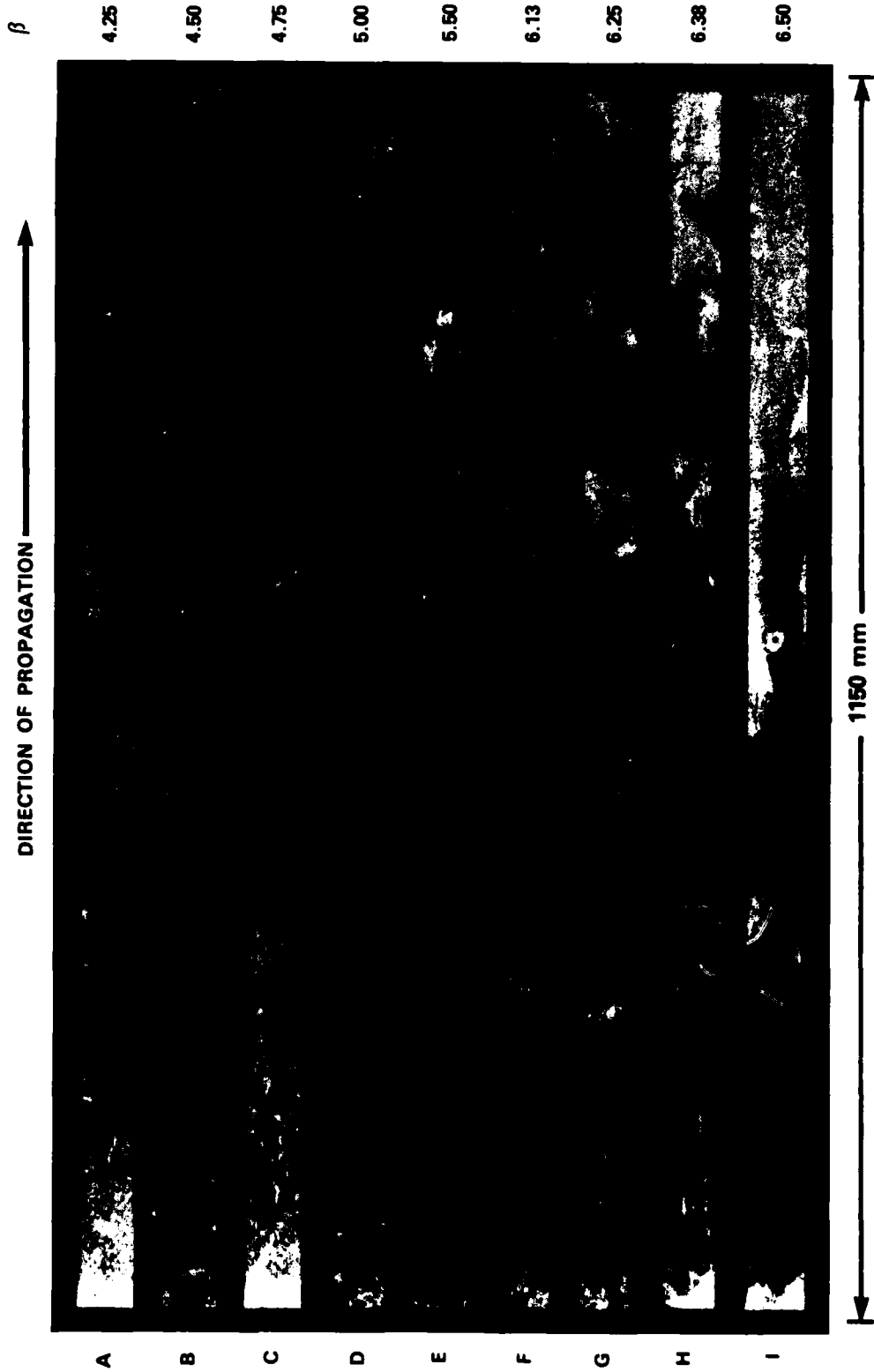


Figure 50

A series of smoke records from the side wall of a channel having three rigid walls and a yielding acetate top. The mixture is  $2\text{C}_2\text{H}_2 + 5\text{O}_2 + 5\beta\text{N}_2$  at atmospheric pressure. Records appear in order of decreasing sensitivity from top (A) to bottom (I).

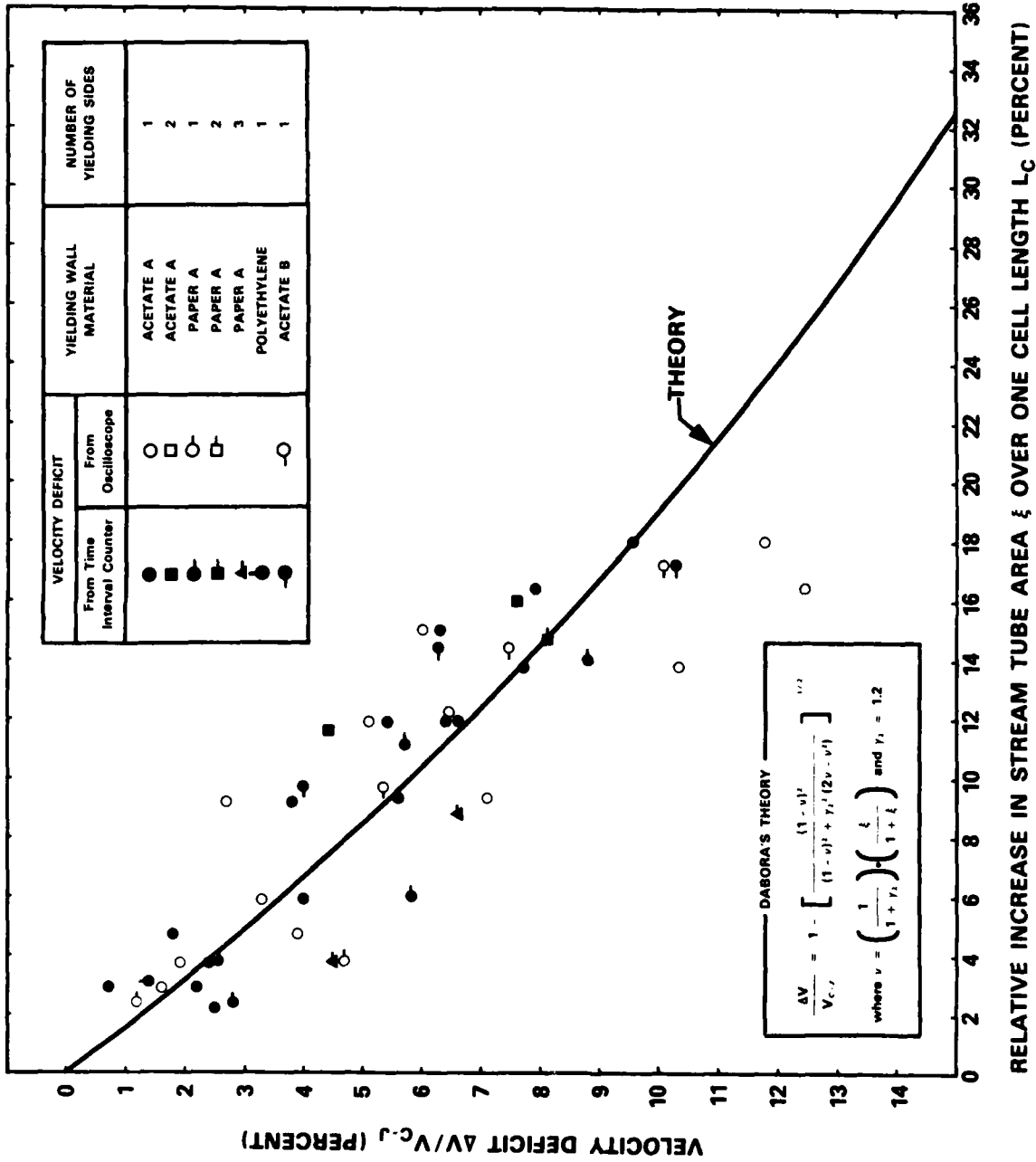


Figure 51

Experimentally measured velocity deficit  $\Delta V/V_{c,j}$  versus the calculated increase in stream tube area  $\xi$  over one cell length  $L_c$ . The data are from tests in channels with yielding walls. The theoretical line is due to Dabora (1963).

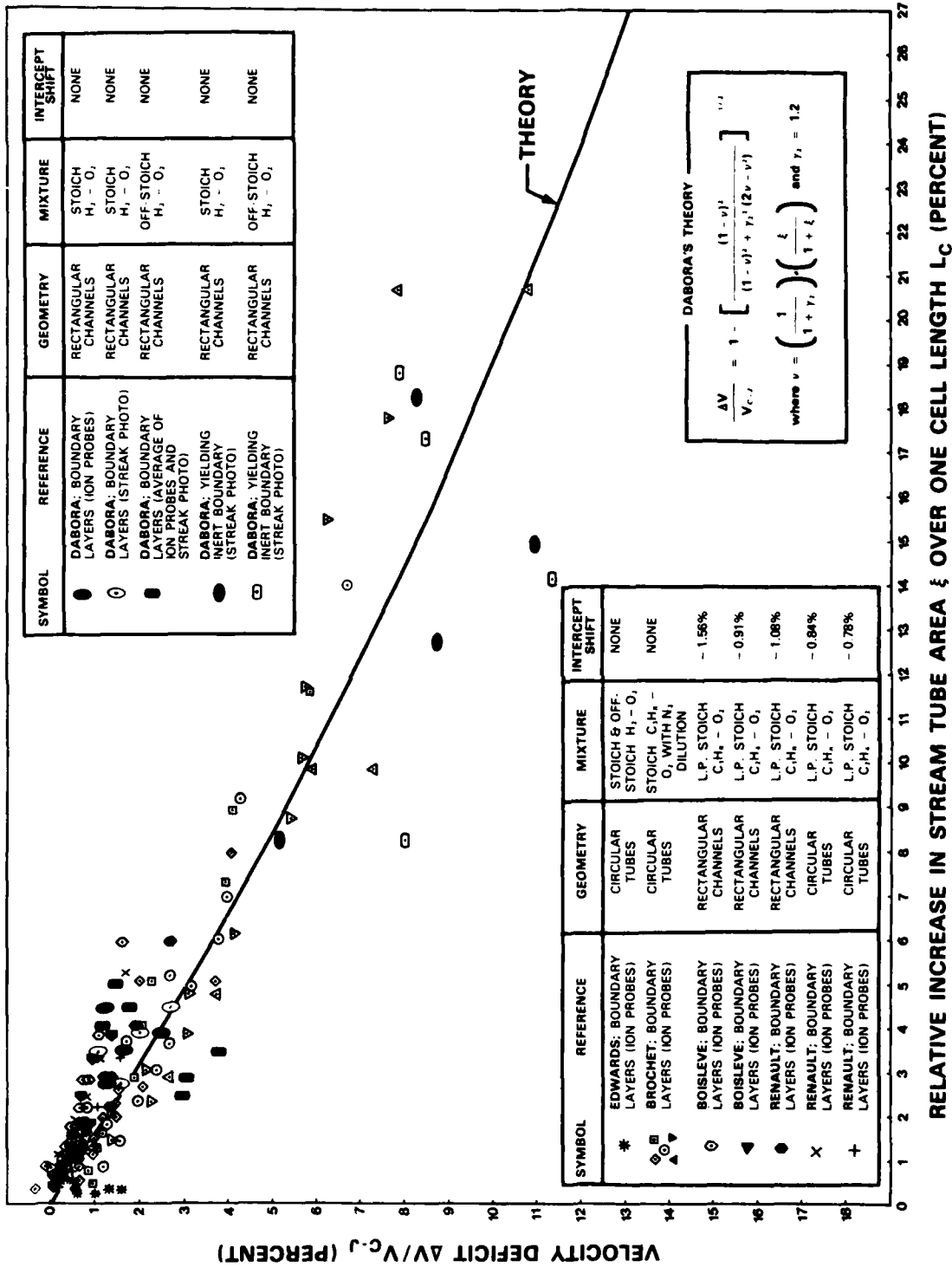


Figure 52

Experimentally measured velocity deficit  $\Delta V/V_{c,j}$  versus the calculated increase in stream tube area  $\xi$  over one cell length  $L_c$ . The data are due to Dabora (1963), Edwards et al. (1963), Brochet (1966), Boisleve (1970) and Renault (1972). The theoretical line is due to Dabora (1963).

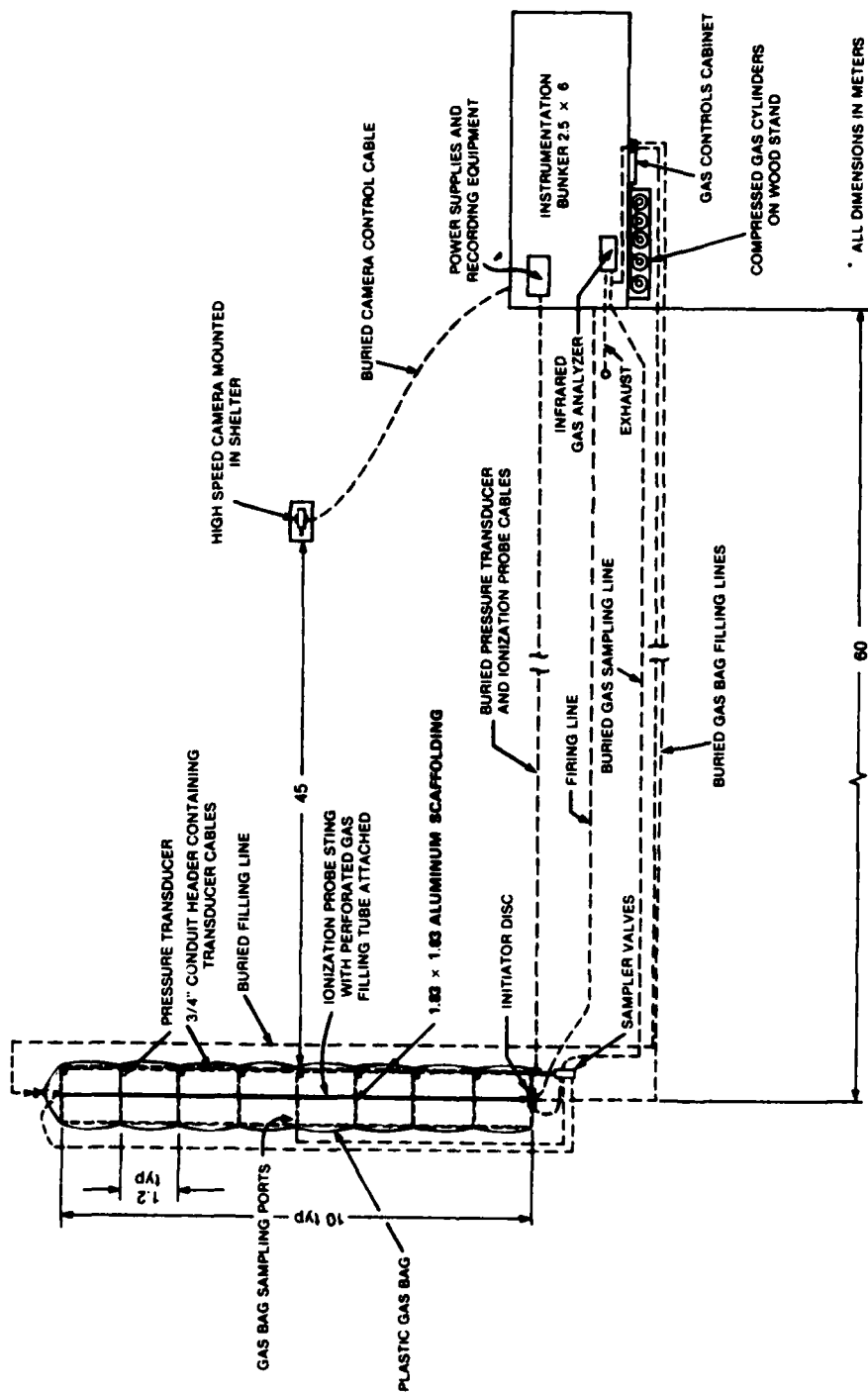


Figure 53

General layout of field facility used to determine the critical energy for direct initiation of ethylene-air mixtures.

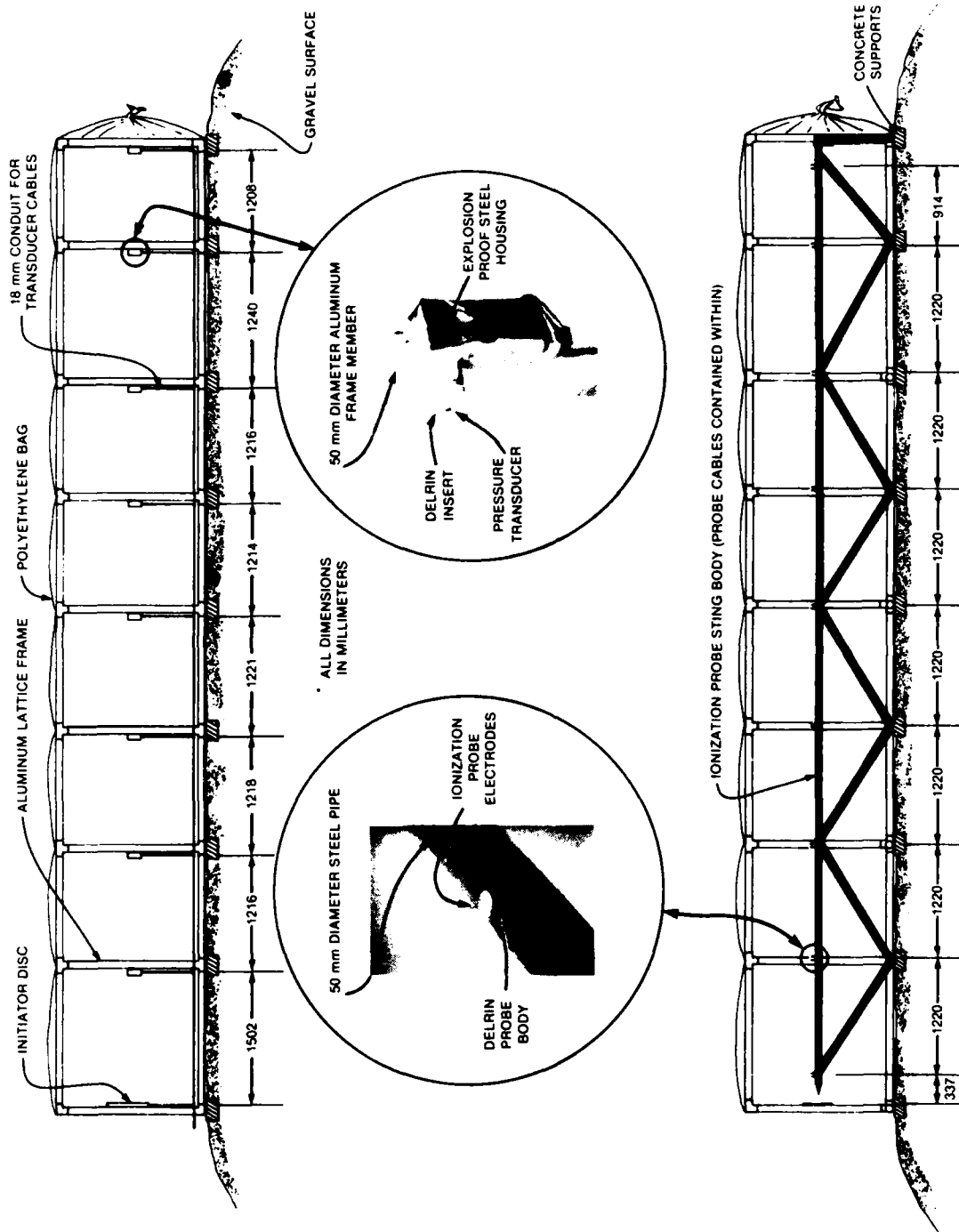


Figure 54

Schematic diagrams of the test section showing the location of pressure transducers (top) and ionization-gap probes (bottom).





**Figure 55**

**Photographs showing the configuration of the gas bag test section:**

- A) Exterior of bag ready for testing**
- B) Interior of bag showing ionization probe  
sting, pressure transducers and circular  
hole cut in ignition end**
- C) Ignition end of bag showing installed  
initiator disc**
- D) Far end of bag showing fuel flow line.**

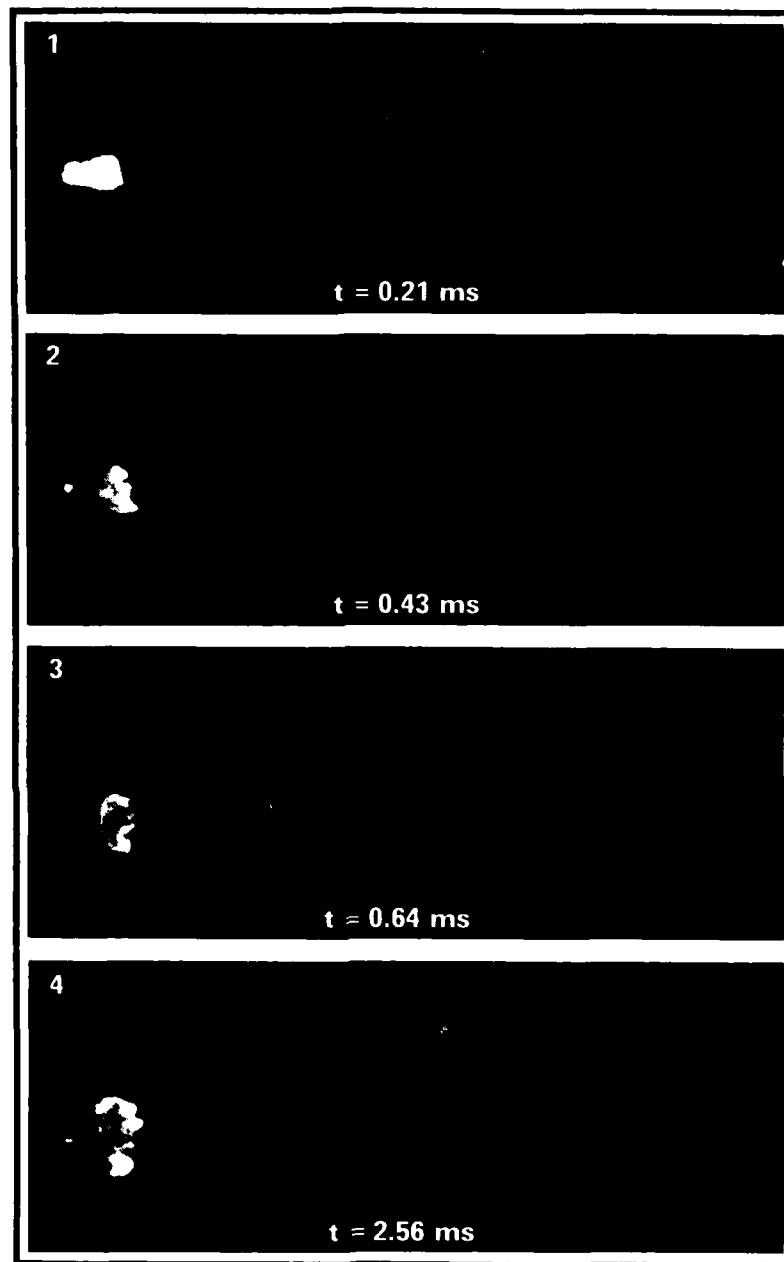


Figure 56

**Selected frames from a cinematographic record showing unsuccessful initiation of detonation. The gas mixture is 6.40%  $\text{C}_2\text{H}_4$  in  $\text{C}_2\text{H}_4$ -air. The initiator charge is 9 grams of Detasheet.**

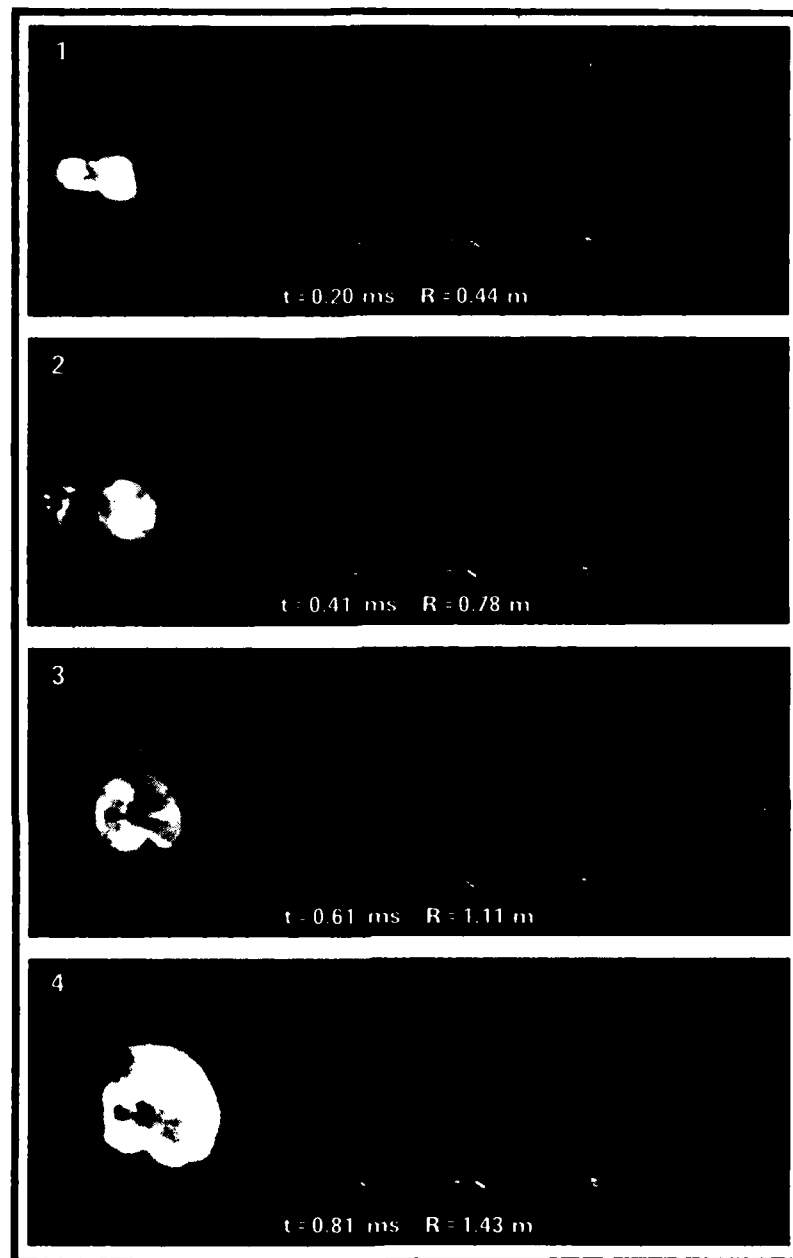


Figure 57

**Selected frames from a cinematographic record showing successful initiation of detonation. The gas mixture is 6.40%  $\text{C}_2\text{H}_4$  in  $\text{C}_2\text{H}_4$ -air. The initiator charge is 18 grams of Detasheet.**

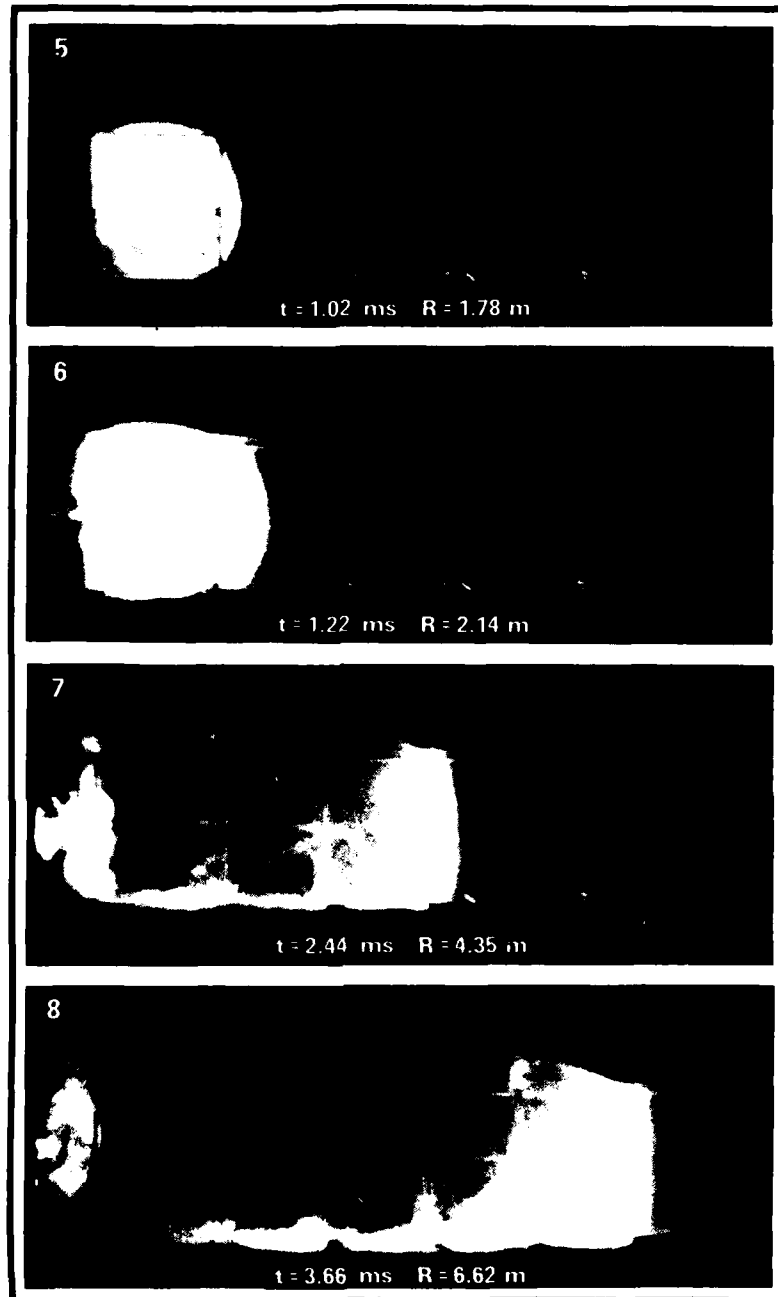


Figure 57 (Cont'd)

Selected frames from a cinematographic record showing successful initiation of detonation. The gas mixture is 6.40%  $C_2H_4$  in  $C_2H_4$ -air. The initiator charge is 18 grams of Detasheet.

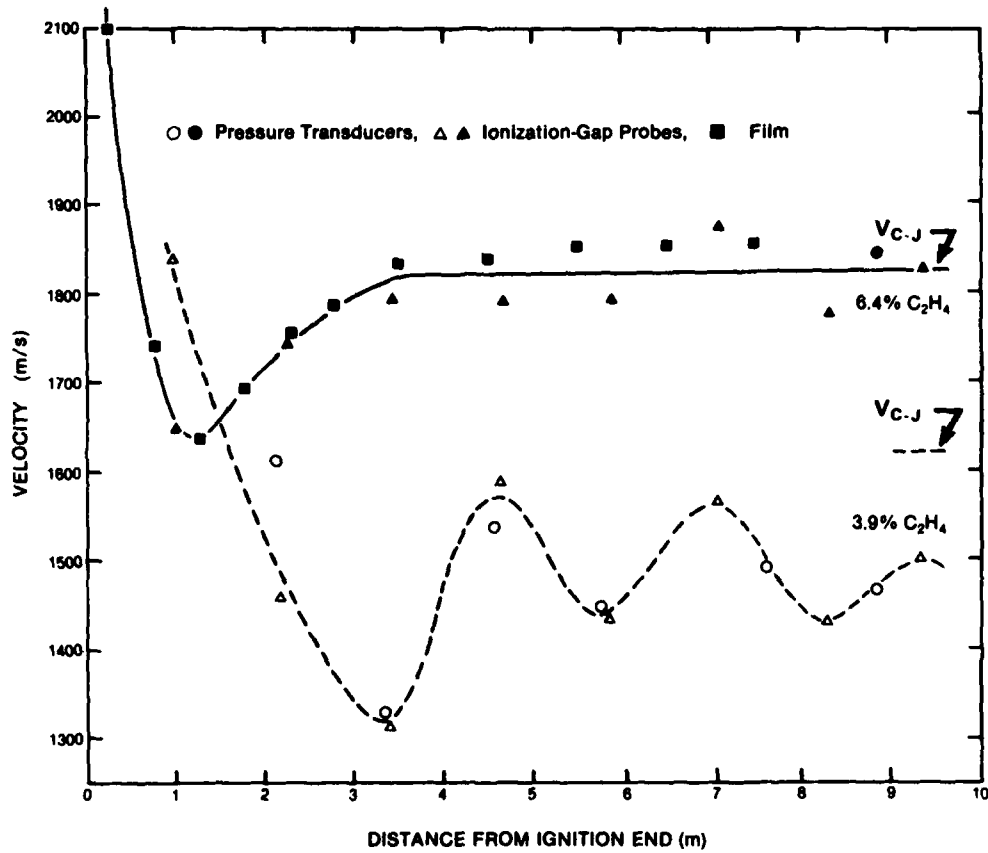


Figure 58

Detonation velocity observed at various positions along the test section showing steady propagation for 6.40% C<sub>2</sub>H<sub>4</sub> in C<sub>2</sub>H<sub>4</sub>-air and unsteady propagation for 3.90% C<sub>2</sub>H<sub>4</sub> in C<sub>2</sub>H<sub>4</sub>-air.

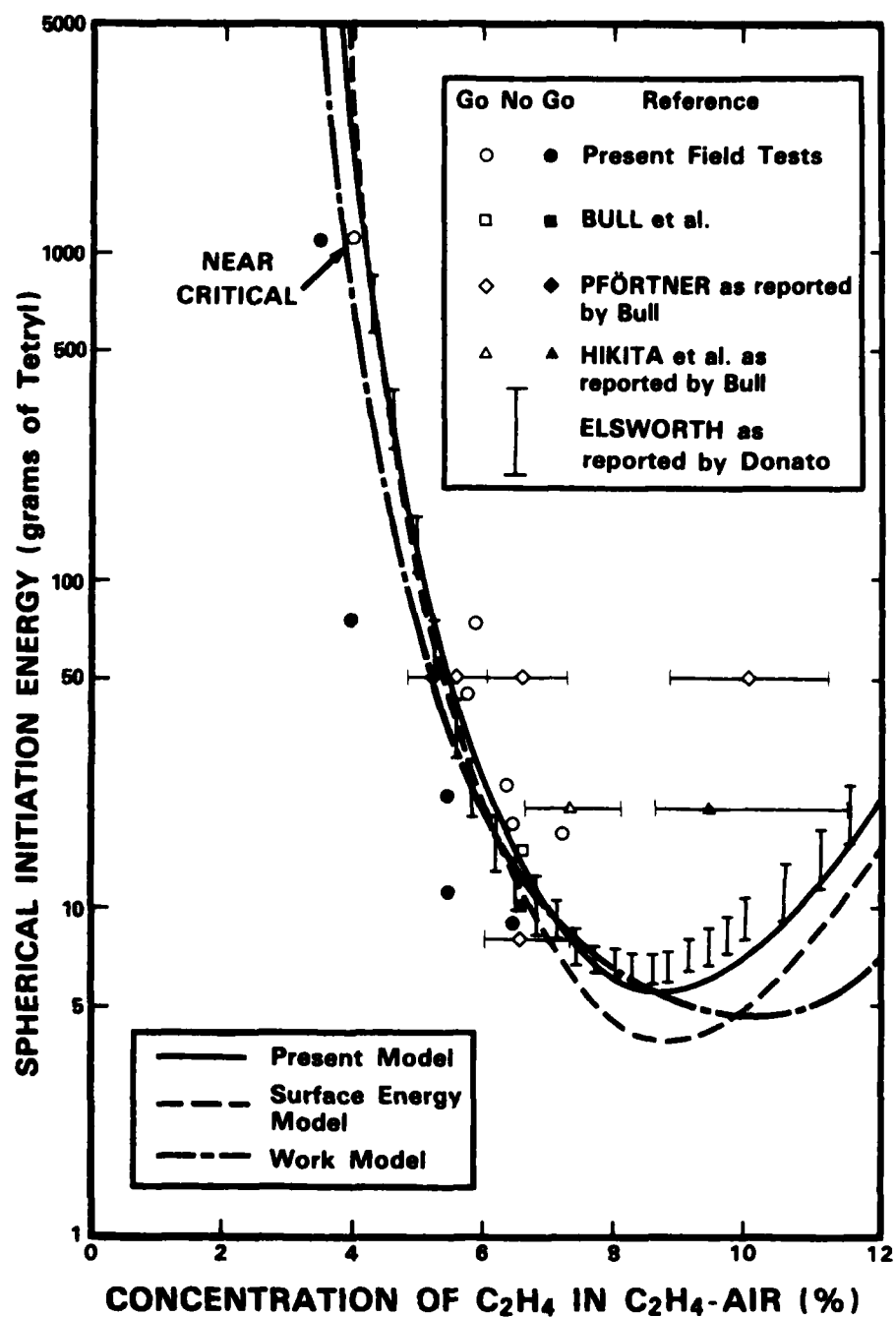


Figure 59

Spherical initiation energy (grams of tetryl) versus concentration of C<sub>2</sub>H<sub>4</sub> in C<sub>2</sub>H<sub>4</sub>-air mixtures at atmospheric pressure. Bull *et al.* (1978), Bull (1979), Donato (1982).

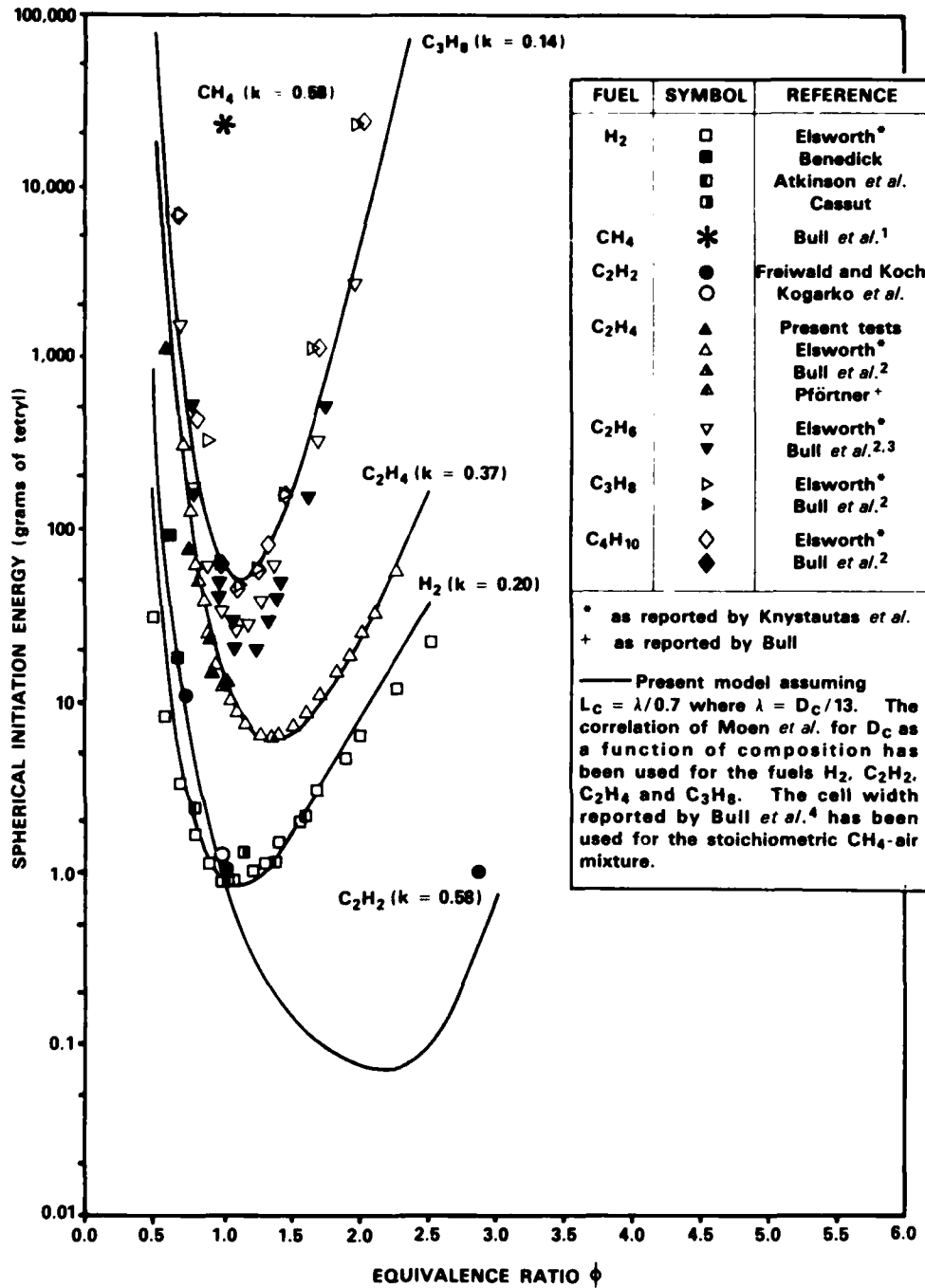


Figure 60

Spherical initiation energy (grams of tetryl) versus stoichiometry for various fuel-air mixtures. Cassut (1961), Freiwald and Koch (1963), Kogarko *et al.* (1965), Bull *et al.*<sup>1</sup> (1976), Bull *et al.*<sup>2</sup> (1978), Bull (1979), Bull *et al.*<sup>3</sup> (1979), Atkinson *et al.* (1980), Bull *et al.*<sup>4</sup> (1982), Benedick (1983), Knystautas *et al.* (1983), Moen *et al.* (1983).

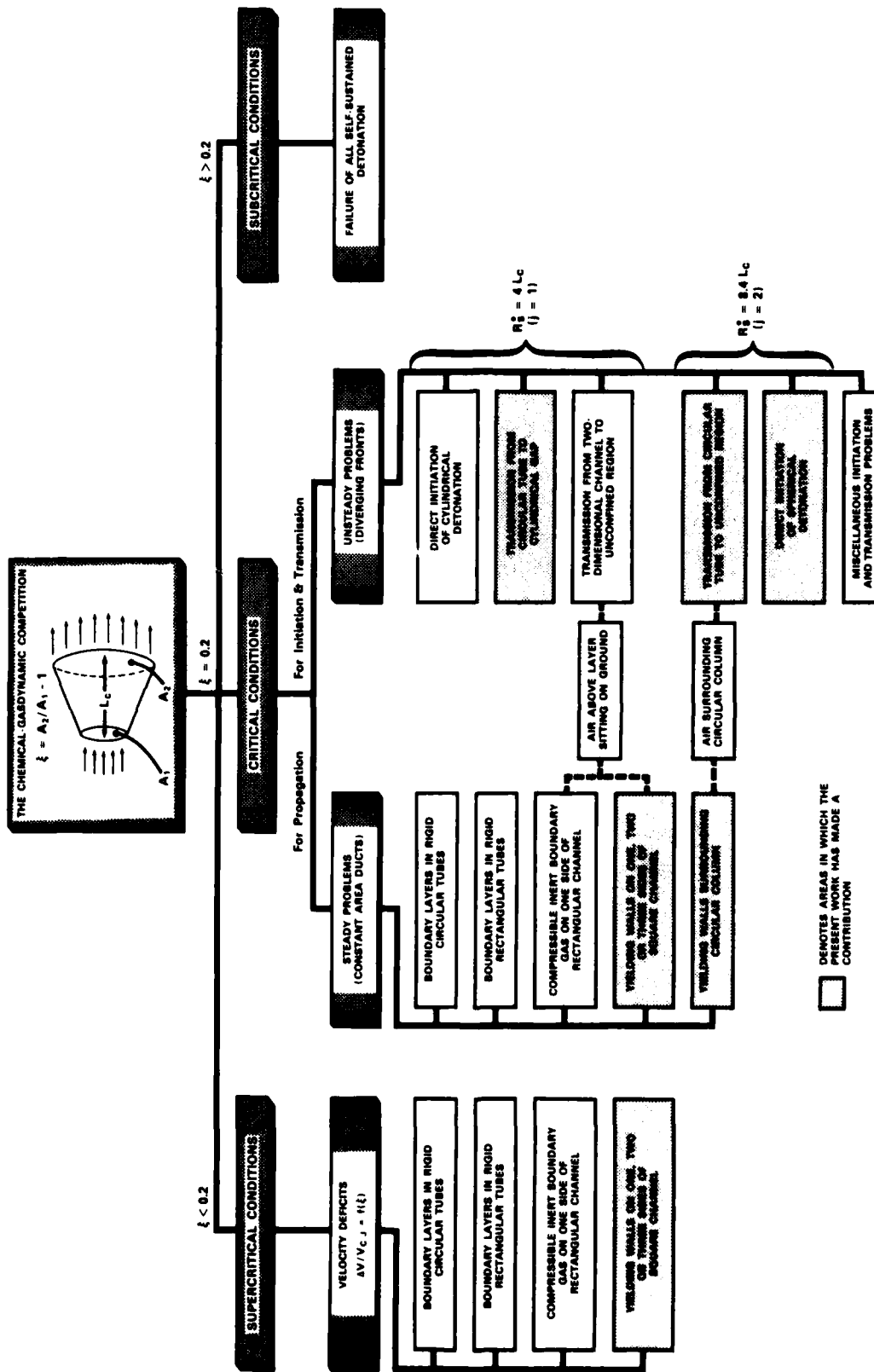


Figure 61  
 A summary of experimental studies on the influence of initial and boundary conditions on the behavior of detonations away from the spin limit.



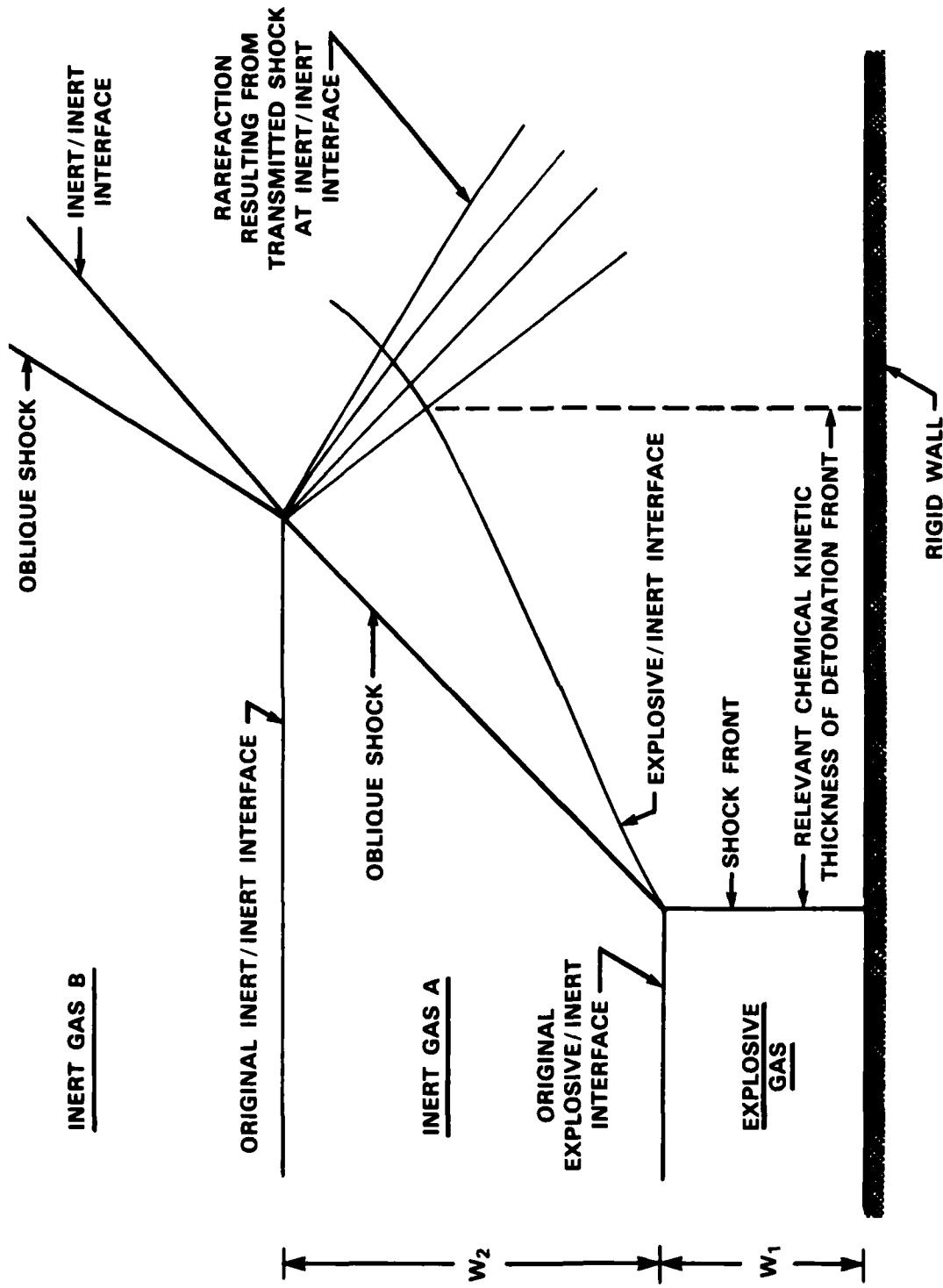


Figure 62

Proposed experimental configuration to investigate the nature of the chemical-gasdynamic competition and the magnitude of the relevant chemical kinetic thickness of the detonation front.

UNCLASSIFIED

APPENDIX A

**THE DRES LARGE-SCALE FUEL-AIR EXPLOSIVES  
TESTING FACILITY\***

---

\*Published at the Defence Research Establishment Suffield as Report SM-1051.

UNCLASSIFIED

DEFENCE RESEARCH ESTABLISHMENT SUFFIELD  
RALSTON, ALBERTA

SUFFIELD MEMORANDUM NO. 1051

THE DRES LARGE-SCALE FUEL-AIR EXPLOSIVES  
TESTING FACILITY

by

J. Funk and S. B. Murray

ABSTRACT

The large-scale fuel-air explosives (FAE) testing facility, designed and built on the experimental range of the Defence Research Establishment Suffield (DRES) in 1981, is described in some detail.

Design considerations to maximize versatility, survivability of permanent operational systems, safety and diagnostic capabilities, and to minimize turnaround time for each experiment, are discussed.

Details about the concrete test bed and important operational systems of the facility, including the gas delivery, mixing and analysing systems and the initiation system, are presented. Diagnostic capabilities to monitor the outcome of each test are described, as are operational procedures for carrying out an experiment.

To date, experiments involving up to 110 cubic meters of detonable mixture have been conducted. Improvements to the facility, evolving from these tests, are summarized.

ACKNOWLEDGEMENTS

The authors would sincerely like to acknowledge the efforts of several DRES groups as well as the assistance of several individuals involved in the design and construction of the DRES FAE testing facility.

The Field Operations Section was responsible for the primary construction of the facility. The Experimental Model Shop manufactured the steel manifolds and associated fittings. The Electronic Design and Instrumentation Group provided the instrumentation expertise and design. Steve Ward, Morrie Kirschenblatt and Richard Tarnasky were all instrumental in the detailed construction of the FAE testing facility.

TABLE OF CONTENTS

	<u>Page No.</u>
ABSTRACT .....	A-ii
ACKNOWLEDGEMENTS .....	A-iii
TABLE OF CONTENTS .....	A-iv
LIST OF FIGURES .....	A-v
1. INTRODUCTION .....	A-1
2. CONCRETE TEST PAD .....	A-3
3. GAS DELIVERY SYSTEM .....	-3
4. GAS CIRCULATION .....	A-4
5. GAS ANALYSING SYSTEM .....	A-6
6. INITIATION SYSTEM .....	A-8
7. DIAGNOSTIC SYSTEMS .....	A-9
8. SAFETY CONSIDERATIONS .....	A-11
9. CONCLUDING REMARKS .....	A-11

LIST OF FIGURES

- FIGURE A-1      PLAN VIEW OF THE DRES FAE FACILITY
- FIGURE A-2      MOUNTING CHANNELS
- FIGURE A-3      CONCRETE TEST PAD
- FIGURE A-4      GAS DELIVERY SYSTEM
- FIGURE A-5      CENTRIFUGAL BLOWER USED FOR MIXING COMBUSTIBLE GASES
- FIGURE A-6      THE GAS MIXING SYSTEM
- FIGURE A-7      ANALYSING SYSTEM SCHEMATIC
- FIGURE A-8      FUEL CONCENTRATION (%  $C_2H_4$  IN  $C_2H_4$ -AIR) VERSUS TIME (MINUTES)  
FOR A TYPICAL EXPERIMENT
- FIGURE A-9      DIAGNOSTIC SYSTEMS
- FIGURE A-10     INSTRUMENTATION AND GAS FLOW CONTROL BUNKERS

UNCLASSIFIED

DEFENCE RESEARCH ESTABLISHMENT SUFFIELD  
RALSTON, ALBERTA

SUFFIELD MEMORANDUM NO. 1051

THE DRES LARGE-SCALE FUEL-AIR EXPLOSIVES  
TESTING FACILITY

by

J. Funk and S. B. Murray

1. INTRODUCTION

When the fuel-air explosives (FAE) research program began at DRES in 1980, the need for an adequate large-scale testing facility was realized. The planning and design for this facility was completed in the spring of 1981 and the construction was completed during that summer. The facility has been actively used for experimentation since August of 1981. The work was carried out under PCN 27C10.

The testing facility was designed in an attempt to satisfy future DRES FAE experimental field requirements. The following criteria were considered to be general guidelines for the design of the experimental layout:

- i) **Versatility** - The facility must be capable of being modified quickly and easily for future, as yet undefined, FAE experiments.
  
- ii) **Accuracy** - FAE experiments depend heavily on accurate determination of fuel and other constituent concentrations. Therefore, the facility must incorporate very accurate sampling and gas analysis systems. Likewise, appropriate diagnostic systems must be employed in order to adequately determine the outcome of each experiment.

UNCLASSIFIED

- iii) **Survivability** - Owing to the destructive nature of FAE testing, all structures, equipment and instrumentation subjected to blast loading must be structurally hardened to ensure their survival.
  
- iv) **Rapid Turnover** - The nature of most FAE studies requires that several trials be conducted to obtain each valid data point or to examine phenomena. Minimizing the duration of the experiment, as well as preparation time, is therefore essential for the judicious use of the relatively short experimental period our Canadian weather permits.
  
- v) **Safety** - Because of hazards associated with the handling and detonation of FAE mixtures, the safety of personnel must be an overriding consideration.

In more physical terms, the facility must have a hard level surface upon which apparatus can be mounted. It must also be capable of supplying fuel and other gases to the experimental volume, mixing these gases homogeneously throughout, and determining species concentrations accurately. In addition, the facility must have a firing system to initiate detonation of the gaseous mixture once the intended composition is reached. This firing system must be capable of coordinating the operation of high-speed diagnostic systems for data collection.

The body of this report describes in detail the features of the DRES FAE facility. General layout and configuration of the test pad is outlined in Section 2. The gas delivery, mixing and analysis systems are described in Sections 3, 4 and 5, respectively. Initiation system details are given in Section 6. Diagnostic capabilities are discussed in Section 7. Finally, safety considerations and concluding remarks appear in Sections 8 and 9, respectively.



## 2. CONCRETE TEST PAD

The FAE testing facility is centred around a concrete test pad. The pad is 18.3 m long x 7.6 m wide x 0.3 m thick and is heavily reinforced to withstand severe shock loading. The surface of the pad incorporates a 1% grade to facilitate water drainage. Imbedded in the surface of the test pad are seven mounting channels which are oriented longitudinally along the entire length of the pad and welded firmly to the steel reinforcing grid. These mounting channels, illustrated in Figures A-1 and A-2, together with 18 mm diameter T-bolts, allow various types of experimental apparatus to be mounted securely to the test pad with ease. They also serve as trays for instrumentation cables, allowing ready access to the cables while keeping them protected.

The longitudinal axis of the test pad runs parallel to the direction of the prevailing wind. This is an important consideration since many of the planned FAE tests involve large surfaces of polyethylene which are very susceptible to damage from cross winds.

Photographs of the test pad appear in Figure A-3.

## 3. GAS DELIVERY SYSTEM

The gas delivery system is designed around three "Matheson" mass flow controllers; two having a maximum flow rate of 100 standard liters per minute (SLPM) and the third having a capacity of 400 SLPM. See the schematic in Figure A-4. Each controller can be used to regulate a variety of gases by applying a constant correction factor to the calibration curve for a specific gas.

The setpoint controls and digital readout for each mass flow controller are located inside the fuel-control bunker. High-pressure, commercially bottled gases are reduced in pressure via dual-stage regulators

before passing through solenoid shut-off valves and the mass flow controllers. For tests involving large volumes of gas, it is possible to manifold several bottles together.

These gases are then piped 50 m to the test pad through three lines, one of 18 mm diameter and two of 13 mm diameter. In addition to the flow of fuel through one line, the other two can be used to flow diluent, oxidizer, sensitizer, or to flow components of a detonation sensitive mixture for the purpose of easy ignition. Knowing the volume of the test apparatus, it is a simple matter to calculate the amount of each gas needed to bring the experimental mixture to a specified state.

#### 4. GAS CIRCULATION SYSTEM

Once gases have been introduced into the experimental volume, it is essential that they be mixed homogeneously with the initial air. Although diffusion can be used to achieve homogeneity, this process takes considerable time in large-scale experiments. The DRES facility makes use of a multipath recirculation system to mix the experimental gases. A high-capacity blower, shown in Figure A-5, is connected between two 300 mm diameter steel manifolds buried underground along the length of the test pad. This assembly has eight 100 mm diameter outlets; four located upstream of the blower (low-pressure side) and four located downstream (high-pressure side) as illustrated in Figure A-6. Any one of four 100 mm diameter steel headers can be attached to any of these eight outlets to evenly distribute the flow to various points in the test section. These headers are equipped with 100 mm diameter remotely-actuated butterfly valves which can be used to either regulate or shut off the flow. Each header extends to the centre of the test pad and is connected to the test apparatus with a short length of flexible plastic hose. The manifold assembly is also fitted with two 40 mm solenoid shut-off valves located at the upstream and downstream ends. These valves open the manifolds to atmosphere and are used for purging purposes.

A 12 mm solenoid shut-off valve is located just upstream of the blower. It is open to atmosphere during an experiment in order to maintain the pressure of the system above atmospheric pressure. Since polyethylene bags are often part of the experimental apparatus, this overpressure is useful in keeping the bag inflated. In this state, it is less susceptible to damage by wind. Small leaks in the polyethylene or at sealed joints would cause the bag to deflate if this pressure control valve did not allow additional air to enter the test volume in order to compensate for the losses.

The centrifugal blower employed has a capacity of over 20 cubic meters per minute at 100 mm H<sub>2</sub>O static head. It is equipped with an explosion-proof electric motor, a stuffing box to seal in explosive gases, and an aluminum rotor wheel to eliminate any sparks that could ignite the detonable gases being circulated.

During a typical experiment, all butterfly valves are left open to maximize circulation. When very thin polyethylene bags are used, however, the two downstream valves are partially closed to avoid overinflating the bag. The pressure control valve is also left open to ensure adequate inflation. Once the proper mixture composition has been reached, the pressure control valve is closed. After this point in time, the mixture maintains a fixed composition until firing. With this valve closed, however, small leaks begin to decrease the pressure in the bag. As the pressure approaches atmospheric pressure, the bag becomes more susceptible to destruction by winds. In this light, it is best to leave the pressure control valve open until shortly (less than 10 minutes) before firing. The small leak rate in question is, in fact, beneficial in attaining the desired mixture composition. During a typical experiment, a rich mixture is created in the test section and subsequently allowed to "leak" down to the desired composition at a slow rate.

Two minutes before firing, the two butterfly valves upstream of the blower are closed and the upstream purge valve is opened. This allows a

slug of correct mixture in the manifold to repressurize the bag in preparation for firing. This is accomplished in a few seconds. Subsequently, the downstream butterfly valves are closed and the downstream purge valve is opened, thereby isolating the experimental volume while purging the manifolds and blower with air. This eliminates the possibility of flashback through the blower which could be catastrophic.

#### 5. GAS ANALYSING SYSTEM

The most critical and difficult experimental parameter to measure in gaseous explosive testing is the concentration of a particular specie in the mixture. In the foreseeable future, the species of interest will always be some form of hydrocarbon in a gaseous state. For this reason, it was decided to employ infrared real-time gas analysis.

The core of the analysing system is a "Wilks Miran 80" infrared gas analyser which is capable of multigas analysis. Since the analyser is a sensitive instrument, it is housed in the fuel-control bunker 50 m from the test pad. It receives gas samples on a continuous basis from four locations along the test section, as shown in the schematic of Figure A-7.

In order to avoid contamination of the gas samples while flowing between the test pad and bunker, the sampling network was designed to operate at above atmospheric pressure throughout, thereby eliminating errors caused by small leaks in the sampling lines. For this reason, gas sampling pumps (to drive the gas around the sampling circuit) were mounted at the edge of the test pad. Since the mixture in the experimental volume is normally somewhat above atmospheric pressure, the short feed lines from the test section to the pumps are maintained above atmospheric pressure as well.

The pumps used are "Webster" diaphragm compressor pumps having a capacity of 30 liters per minute. This capacity was chosen to accommodate the gas analyser which has a 5.6 liter test chamber. Assuming five gas

changes are needed to purge the analyser of the previous sample, a cycle time of about one minute is possible. Since the flow rate of sample gas is high, it is returned to the experimental volume to avoid the undesirable reduction in concentration by removal of such large quantities for analysis purposes.

The system of solenoid valves shown in Figure A-7 was developed to facilitate automatic sampling from up to four individual sample locations. An electronic programmer automatically controls sample sequencing. Although the programmer is completely automatic, trial personnel have complete manual override on all valves.

During a normal sampling sequence, the programmer first opens one of the four selection valves as well as both isolation valves (located on either side of the analyser) for a time corresponding to the purge time of the analyser. Positive flow is ensured by check valves. Once the analyser has been purged, the programmer closes the selection valve as well as both isolation valves. Since infrared gas analysis is sensitive to pressure, a bleed valve is opened at this time to vent the sample to atmosphere. The programmer then initiates the gas analysing routine. Once the routine has been completed, the entire sequence begins again with another selection valve (corresponding to another sampling location). The system presently uses a two minute cycle time per sampling line. After homogeneity of the gas mixture throughout the test section has been established, all four sampling lines may be accessed simultaneously so that the analyser purge time is reduced.

As mentioned above, the analysis is sensitive to the pressure of the gas sample. The correction factor is calculated by obtaining the ratio of absolute calibration gas pressure to absolute sample gas pressure. Since the bleed valve ensures that the sample is at atmospheric pressure, the correction factor becomes the ratio of calibration gas pressure to atmospheric pressure, the latter of which is monitored throughout the course of each experiment.

The gas analysis is also sensitive to sample gas temperature. A thermocouple is used to measure sample gas temperature. The correction factor is then calculated as the ratio of sample gas temperature to calibration gas temperature. These correction factors are immediately applied to the analyser infrared absorption readings. Prior to daily use, the analyser is calibrated using both commercially available and internally prepared gas samples. A plot of ethylene concentration versus time for a complete experiment is shown in Figure A-8. The downward trend in concentration after the peak is due to small leaks at sealed joints and in the polyethylene material used in this experiment. As noted previously, these small leaks actually provide a method of reducing the fuel concentration by small amounts until the desired concentration is reached. The pressure control solenoid valve (see Gas Circulation System) is then closed, thereby holding the composition constant until firing.

Before firing, the analyser is purged with air and then isolated from the sampling system with manual valves in order to eliminate any possibility of flashbacks damaging the analyser.

To independently verify the gas analysis, a sample is trapped in a 250 cc gas sampling tube about one minute before firing. It is then taken back to the laboratory where it can be further analysed by gas chromatography or mass spectroscopy.

## 6. INITIATION SYSTEM

Once the proper gas composition has been achieved, some method of initiation must be employed to detonate the mixture. The DRES initiation system centres around a timing and firing sequencer. This sequencer incorporates a 15 second countdown before firing and a 15 second count after firing. The countdown clock is used to start high-speed cameras, high-speed tape recorders, and to charge a 1 microfarad capacitor at various preset times before the instant of firing.

At time zero, this capacitor (charged to 3,000 volts) is discharged through the firing lines. The energy pulse fires an exploding bridgewire Reynolds detonator which initiates a variable amount of solid explosive (PETN). The blast wave from this explosion in turn initiates the gaseous mixture directly. The capacitor discharge is also sufficient to initiate a slug of detonation sensitive gas with an exploding wire. Once detonation is established in the sensitive slug, it transmits to the mixture being studied. At time zero, the sequencer also produces a trigger signal which can either be used to activate instrumentation or be stored on a tape track for simplification of data reduction. After the firing pulse the sequencer continues counting for an additional 15 seconds, turning off equipment and returning the firing circuit to a safe condition.

#### 7. DIAGNOSTIC SYSTEMS

The DRES FAE testing facility was designed to be as flexible as possible regarding diagnostic methods. See Figure A-9. The test pad and instrumentation van are presently connected by 55 low-noise, underground cables (20 coaxial and 35 shielded twisted pairs). Sufficient cable has been installed to accommodate an expansion to 85 channels. Junction boxes are located both at the test pad and at the instrumentation van. This allows virtually any type of electronic instrumentation to be used with a minimum of modification or additional cable.

At present, electronic instrumentation consists of twelve piezo-electric pressure transducers and 20 ionization probes. The pressure transducers are mounted at various locations for different FAE tests. Eight transducers (PCB 113A24) are mounted directly in the experimental test section to measure the pressure-time history of the detonation wave. The remaining four pressure transducers (PCB and Kistler) are mounted in specially designed, portable, far-field gauge stands which can be moved easily around the layout up to a distance of 75 meters from the test pad. A typical gauge stand is shown to the extreme right of the lower photograph of

Figure A-3. These transducers measure far-field blast wave overpressure signatures which are recorded on a multichannel high-speed tape recording system. Honeywell, Ampex and Racal recording systems are available with frequency responses up to ~ 200 kHz. Hard copy reproduction of the pressure records can be made immediately by an oscillograph, on site, for qualitative analysis. The tape can also be digitized for quantitative computer analysis at a later date.

The ionization probes are connected to a 20-channel power supply and electronic counter which were designed and built at DRES. All channels begin counting at arrival of the firing or "det zero" pulse. As the detonation wave passes over each ionization probe, it ionizes the gas between the probe electrodes, lowering the path resistance. This is sensed by the probe unit which then stops the count of individual channels. Thus, each channel has an elapsed time from det zero which can be used to determine the velocity knowing the location of each probe. Probes can be situated strategically along the experimental test section to give an appropriate velocity profile.

Apart from electronic diagnostic methods, the DRES facility is capable of operating three high-speed cameras simultaneously with the option of locating the cameras at any of six different locations. Additional positions can be added quickly, if necessary. At present, the photographic data collection is done by a "Hycam" 16 mm high-speed camera operating at up to 20,000 half frames per second and a "Fastax" 16 mm high-speed camera operating at up to 5,000 full frames per second. These cameras are started by the timing and firing sequencer at prescribed times before det zero in order to allow them to accelerate up to speed.

In addition to electronic and photographic diagnostic systems, "smoked" foils are used to yield information about detonation wave structure. A thin metal sheet is smoked with a light layer of carbon black and fastened to the walls of the test section. The passing detonation wave "writes" on the smoked foil, leaving behind a record of the wave structure.



8. SAFETY CONSIDERATIONS

F AE testing involves extensive handling of flammable or detonable gas mixtures which can pose a serious hazard to personnel in the vicinity of the experimental layout. To minimize the possibility of accident during an experiment, only air is used to inflate the collapsible polyethylene bag or tube. As well, the ignition end of each experimental configuration is fitted with high explosives (for initiation purposes) while only air is contained within the test section. Before gas is flowed, all personnel must be inside either one of two protective bunkers located 50 m from the test pad. All experimental operations can be controlled remotely from inside these bunkers. See Figure A-10.

The gas analyser contains the only test gas permitted inside the bunker. Its analysis chamber, which is capable of withstanding 10 atmospheres overpressure, is purged with air before firing in order to eliminate the possibility of a flashback inside the bunker. All sampling lines are equipped with flame arrestors.

9. CONCLUDING REMARKS

Since the completion of the testing facility, over 80 tests have been carried out. These tests involved polyethylene tubes with diameters ranging from 0.89 to 3.66 meters, in conjunction with steel tubes having diameters from 0.30 to 1.83 meters. Throughout the tests, the facility has demonstrated its flexibility, reliability and safety, with only a few minor modifications being required.

The sampling pumps used initially were susceptible to shock waves which propagated up the sampling lines and caused occasional damage during firings. Heavier duty pumps have been received and will be installed prior to trials next season.

The mass flow controllers were limited in their application to achieving only approximate fuel concentrations due to a significant temperature effect on their performance.

All other systems operated without damage or failure throughout the trials. The test pad shows no blast effects and the analysing, mixing and gas delivery systems operated very consistently throughout the trials.

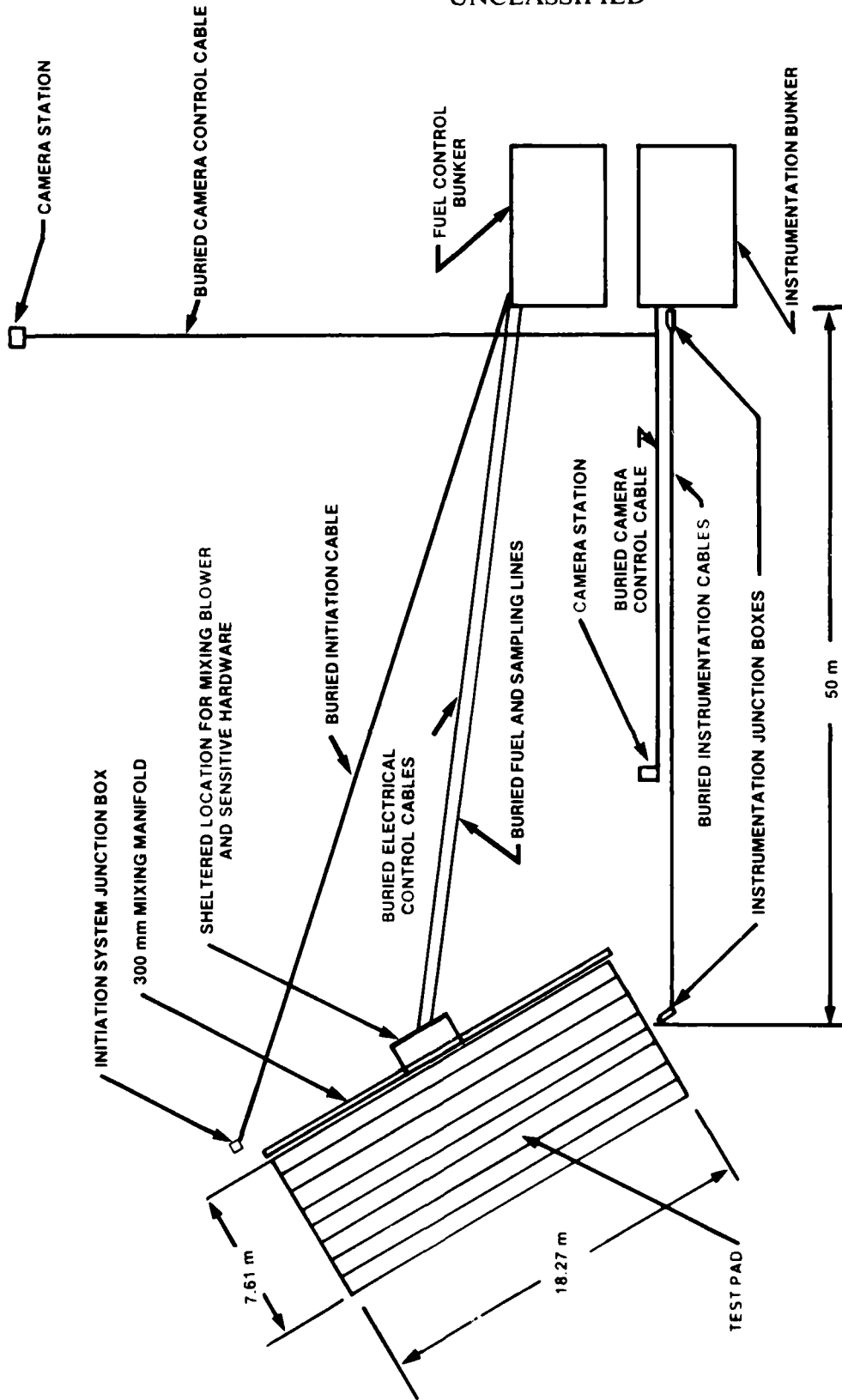


Figure A-1  
Plan View of the DRES FAE Facility

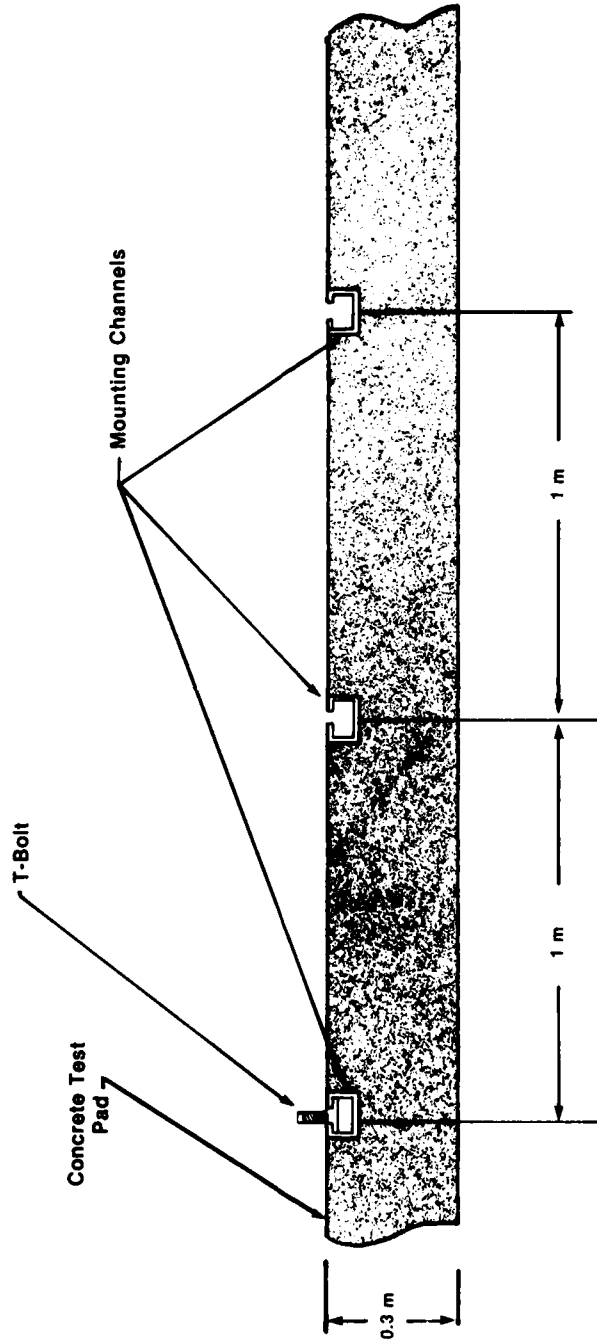


Figure A-2  
Mounting Channels

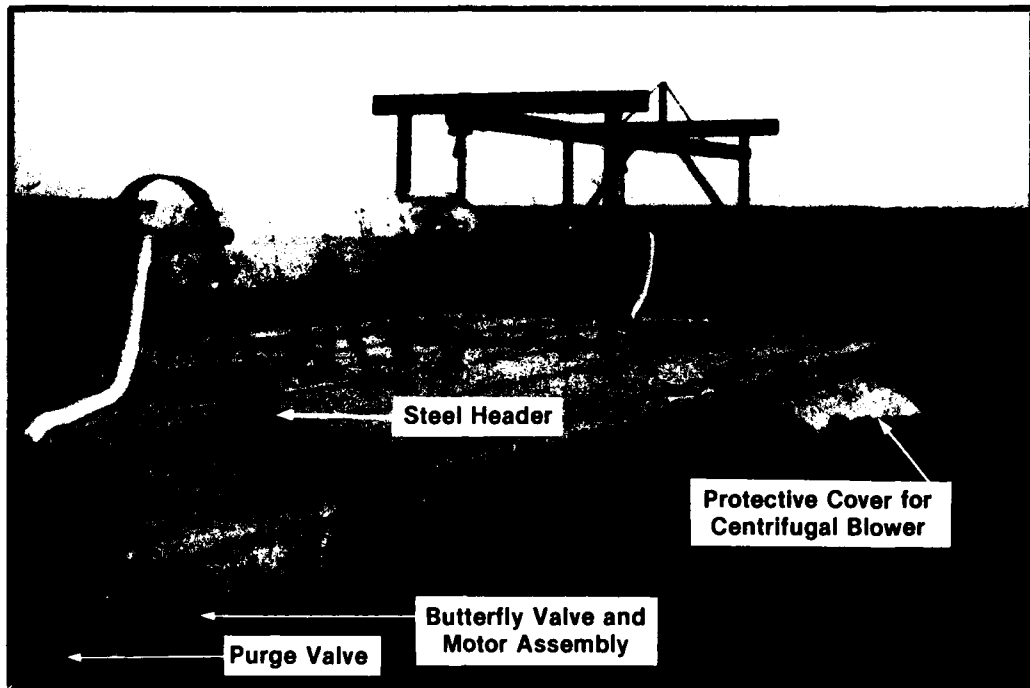


Figure A-3  
Concrete Test Pad

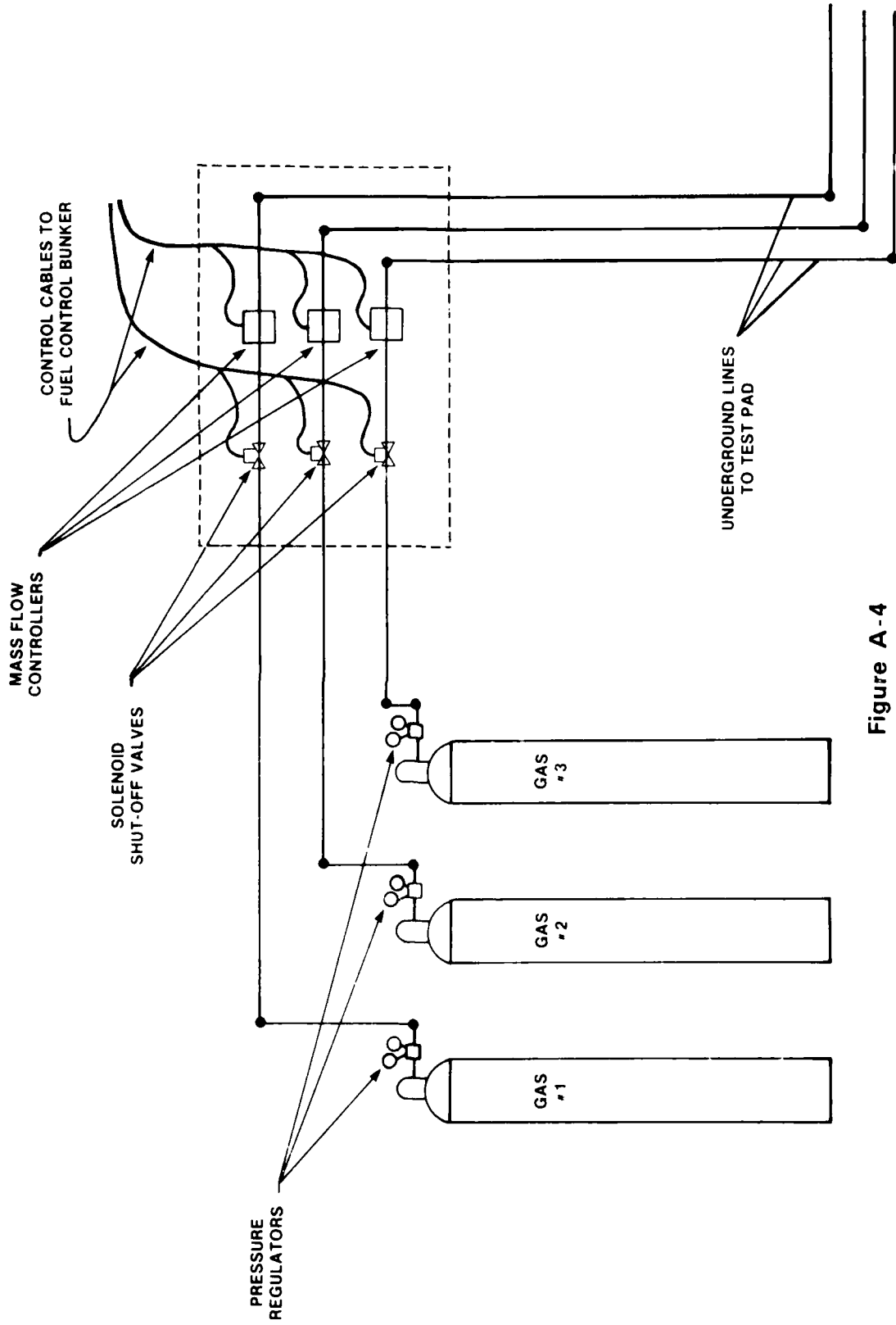


Figure A-4  
Gas Delivery System

AD-A162 631

THE INFLUENCE OF INITIAL AND BOUNDARY CONDITIONS ON  
GASEOUS DETONATION WAVES(U) DEFENCE RESEARCH  
ESTABLISHMENT SUFFIELD RALSTON (ALBERTA) S B MURRAY  
SEP 85 DRES-SR-411

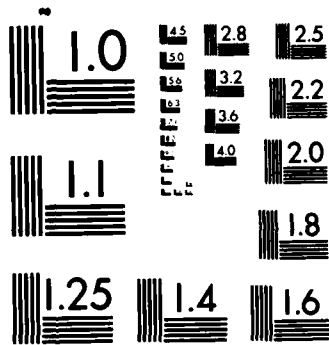
4/4

UNCLASSIFIED

F/G 19/4

NL





MICROCOPY RESOLUTION TEST CHART  
NATIONAL BUREAU OF STANDARDS-1963-A



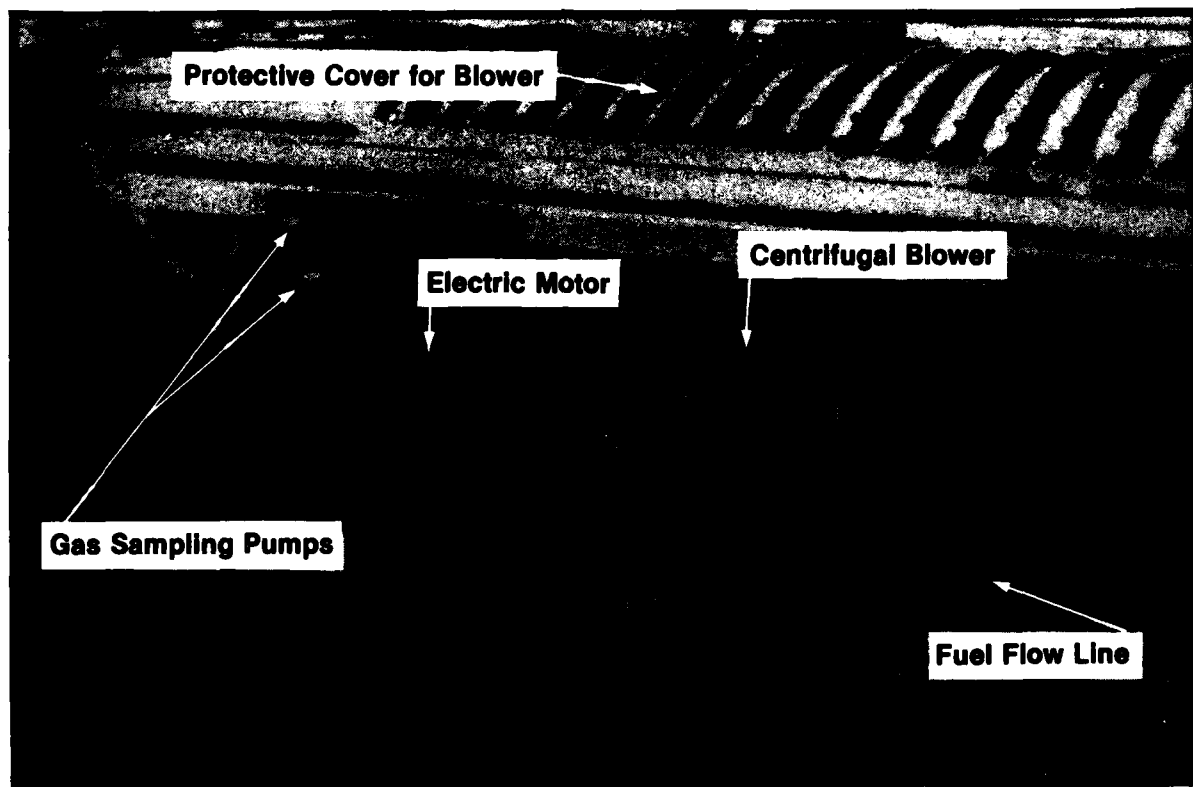


**Figure A-5**  
**Centrifugal Blower Used for Mixing Combustible Gases**

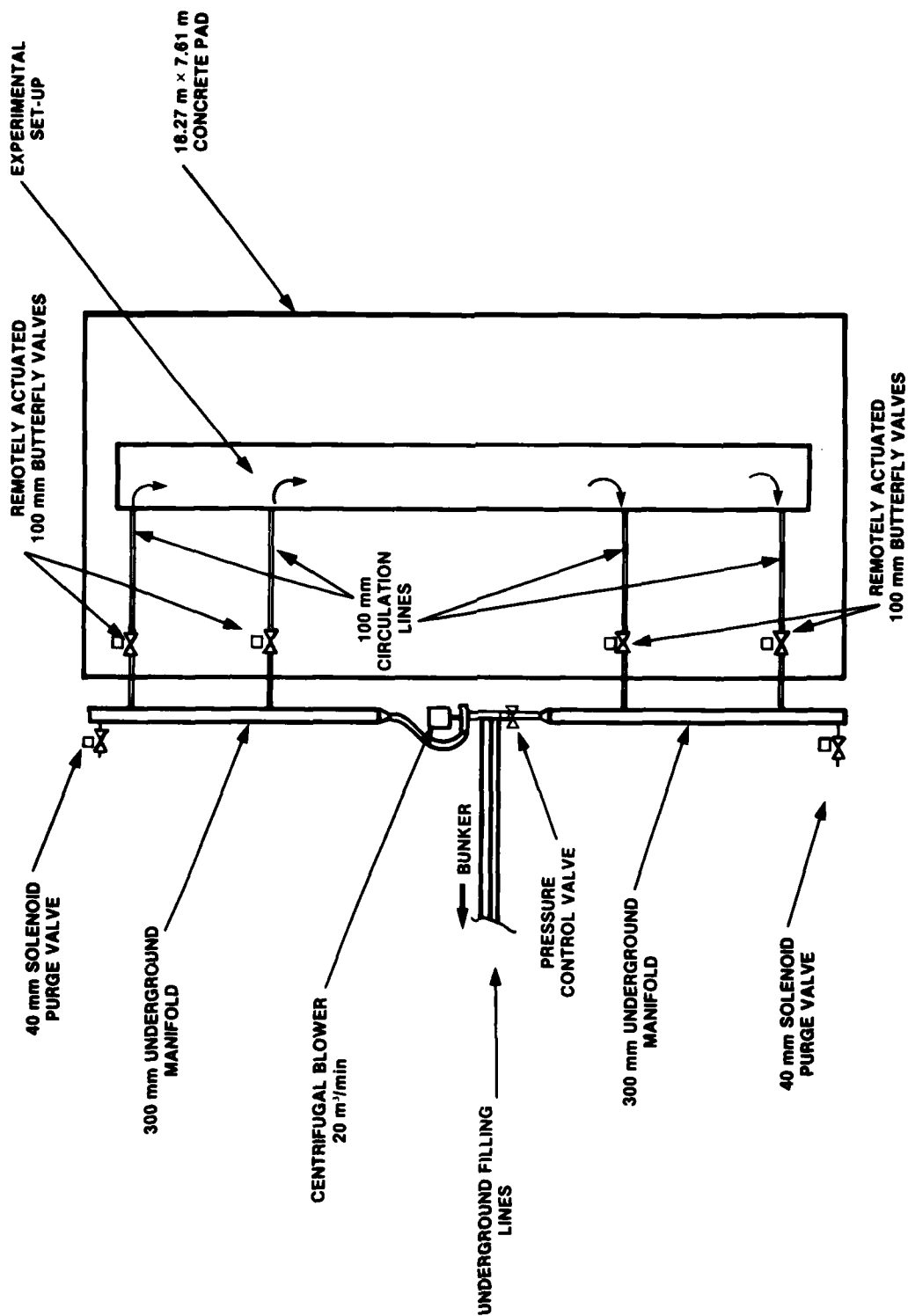


Figure A-6  
The Gas Mixing System

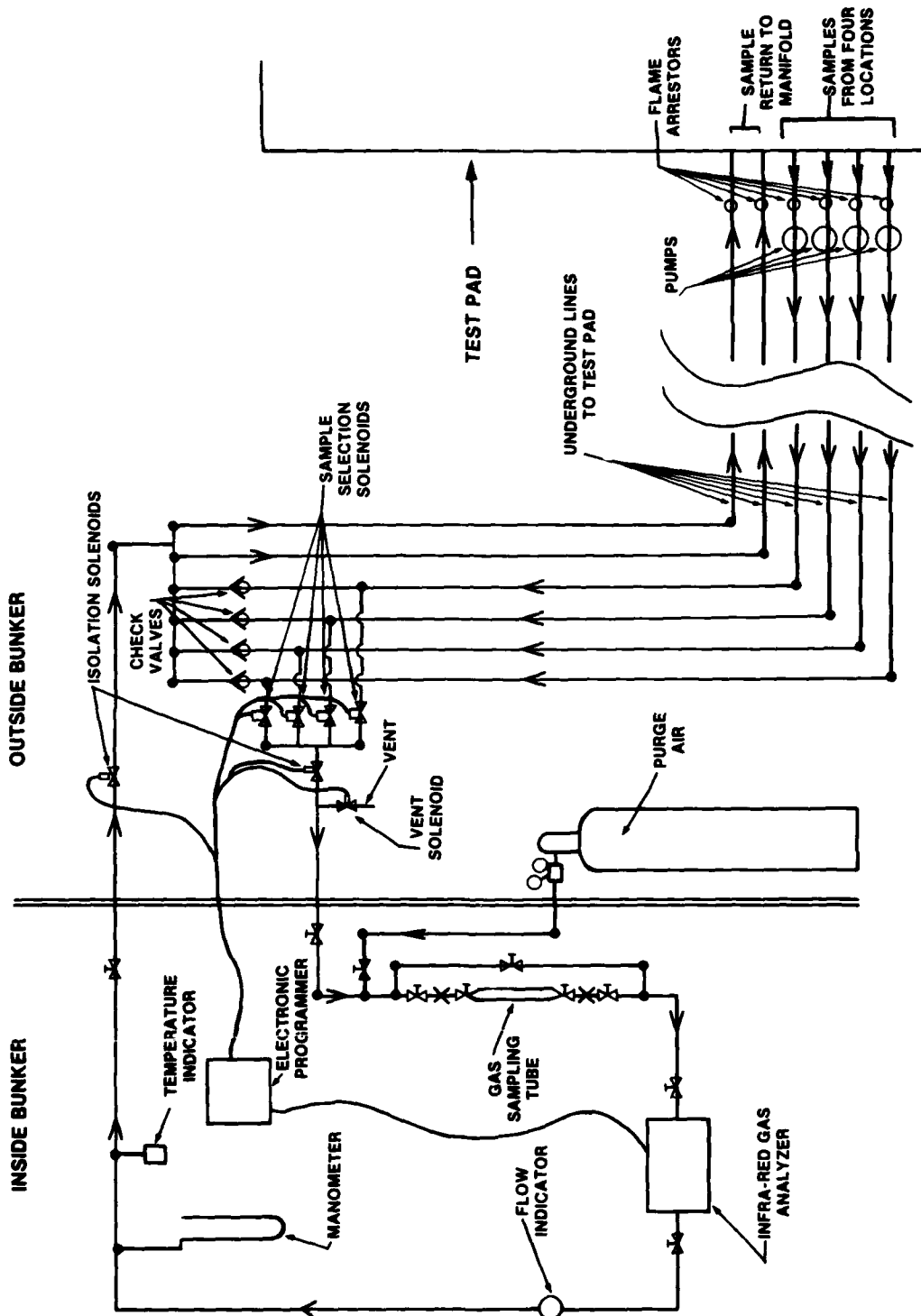


Figure A-7  
Analysing System Schematic

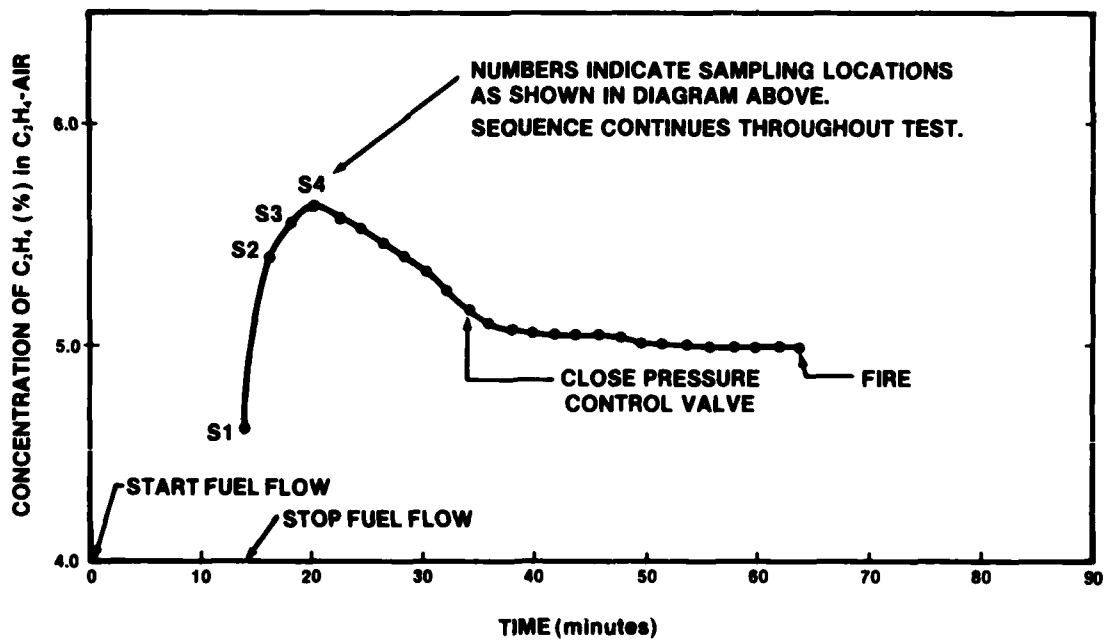
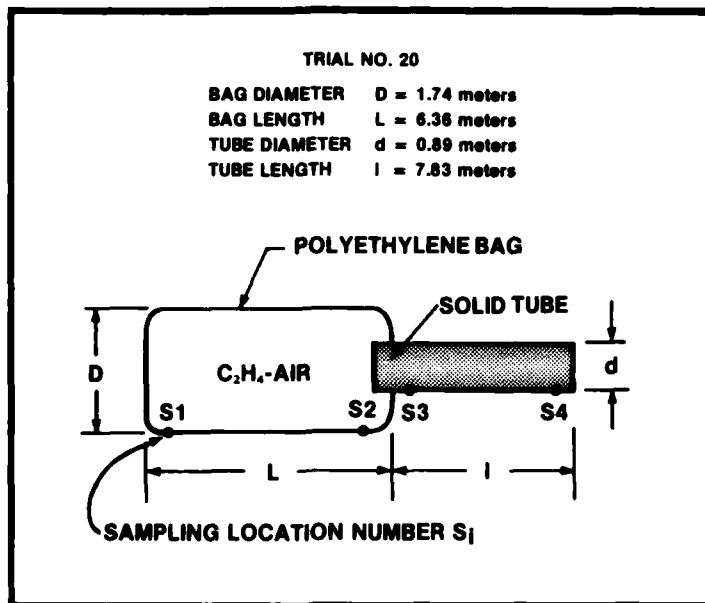


Figure A-8  
 Fuel Concentration (%  $C_2H_4$  in  $C_2H_4$ -Air) Versus Time (minutes)  
 for a Typical Experiment

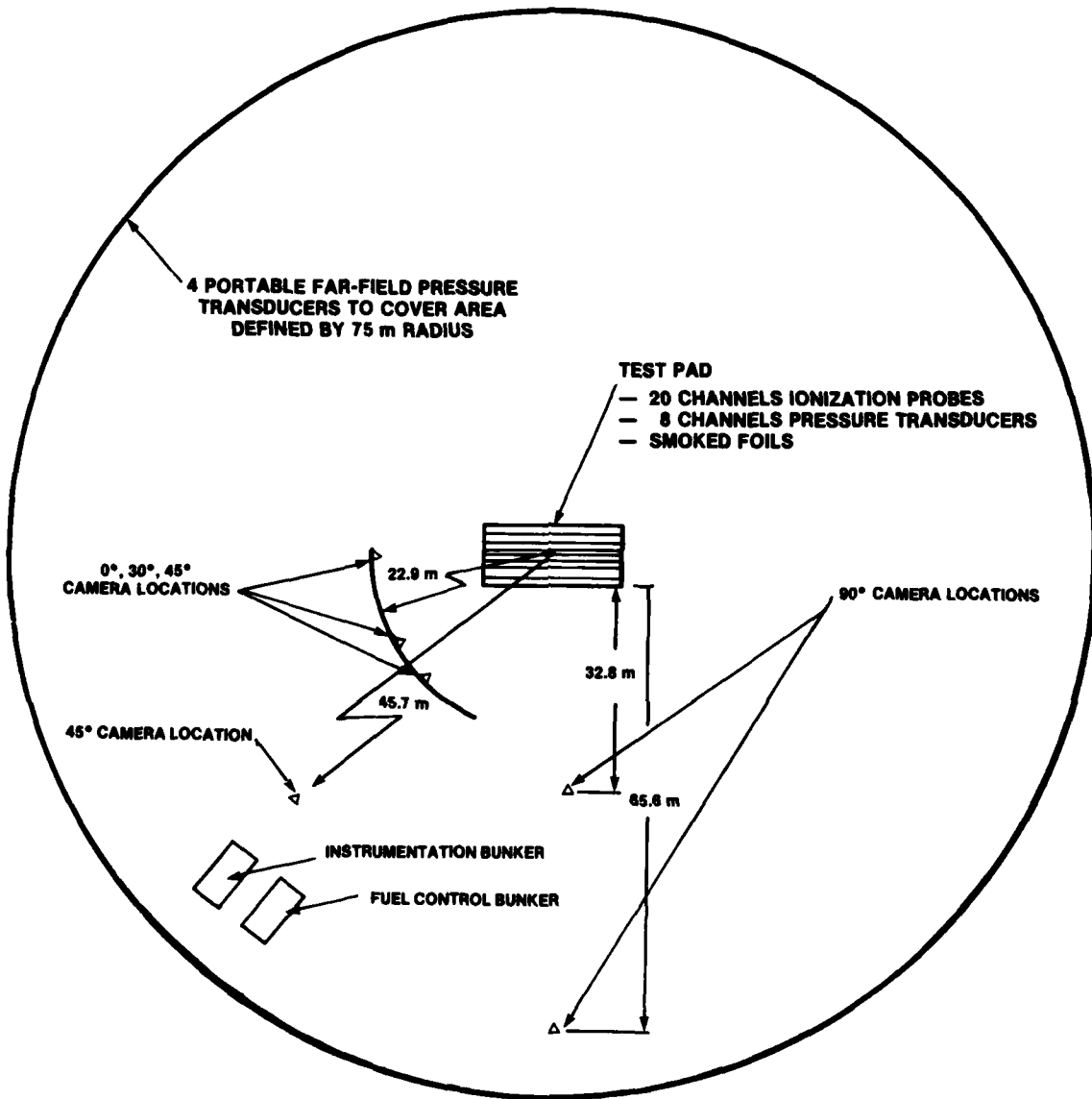


Figure A-9  
Diagnostic Systems

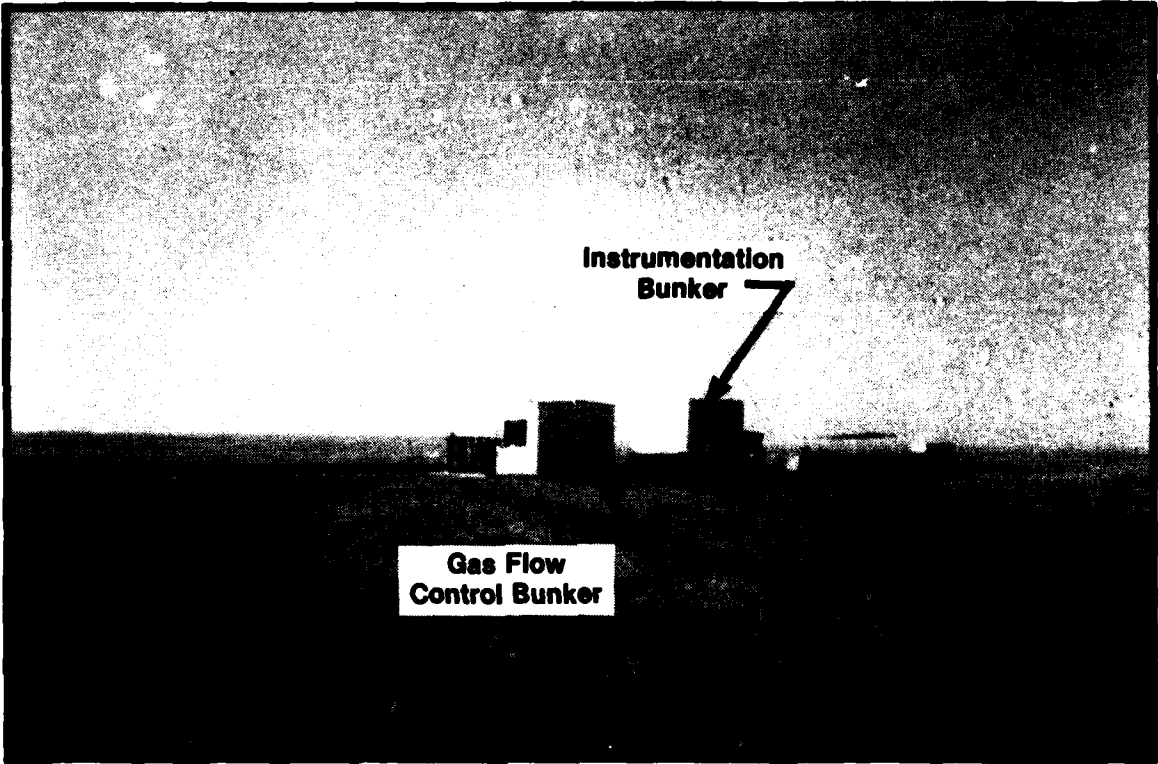


Figure A-10

Instrumentation and Gas Flow Control Bunkers

UNCLASSIFIED

APPENDIX B

APPROXIMATE ONE-DIMENSIONAL ANALYSIS FOR THE MOTION OF AN  
ACCELERATING CYLINDRICAL PISTON

---

\*Most of the derivation in this appendix is taken from Meyer, R. F. (1958)  
"The Impact of a Shock on a Movable Wall". Journal of Fluid Mechanics 3, 309.

UNCLASSIFIED

APPROXIMATE ONE-DIMENSIONAL ANALYSIS FOR THE  
MOTION OF AN ACCELERATING CYLINDRICAL PISTON

The problem of an accelerating cylindrical piston is not unlike that of a simple launcher. Figure B-1 shows the x-t diagram for a piston of specified mass being accelerated down a barrel by the gases in a high-pressure chamber. The full solution for the nonsteady flow fields both ahead of and behind the piston is indeed involved and requires a numerical approach. However, if only the piston motion is of interest, several approximate methods are available. One such method is that due to Meyer (1958), who studied the problem of a shock wave impacting a movable wall in a head-on fashion. An x-t diagram corresponding to this problem is shown in Figure B-2. It is essentially the same as the diagram shown in Figure B-1 with the exception that the high-pressure region in the shock impact problem is created by the reflection of the wave from the back surface of the piston.

The analysis which follows is due to Meyer (1958). It has been modified slightly for the present purpose in the following ways: i) the reflected shock wave has been eliminated and a quiescent high-pressure reservoir used instead; ii) different ratios of specific heats have been allowed on either side of the piston; and iii) an integral term has been added to account for the effect of cylindrical divergence on the flow field. The full characteristic equations for the regions ahead of and behind the piston are:

$$\frac{\partial}{\partial t} \left( \frac{2}{\gamma - 1} c \pm u \right) + (u \pm c) \frac{\partial}{\partial x} \left( \frac{2}{\gamma - 1} c \pm u \right) = \frac{c^2}{(\gamma - 1)C_p} \frac{\partial s}{\partial x} \quad (B-1)$$

and  $Ds/Dt = 0$ , where  $c$ ,  $u$  and  $s$  are the velocity of sound, the particle velocity and the specific entropy, respectively. If the changes in specific entropy through the shock are neglected, the flow is isentropic and



the characteristic equations reduce to:

$$\frac{\partial}{\partial t} \left( \frac{2}{\gamma - 1} c \pm u \right) + (u \pm c) \frac{\partial}{\partial x} \left( \frac{2}{\gamma - 1} c \pm u \right) = 0. \quad (\text{B-2})$$

We then have that

$$P = \frac{2}{\gamma - 1} c + u = \text{constant along } \frac{\partial x}{\partial t} = u + c \quad (\text{B-3})$$

$$\text{and } Q = \frac{2}{\gamma - 1} c - u = \text{constant along } \frac{\partial x}{\partial t} = u - c \quad (\text{B-4})$$

where P and Q are the Riemann invariants. Since changes in specific entropy are being neglected, it follows that Q must be constant everywhere ahead of the piston. Likewise, P is constant everywhere behind the piston. Since Q is constant in the flow region between the piston and the shock, the positive characteristics (lines along which P is constant) are straight lines along which the flow properties are constant.

Consider some general point  $a$  on the piston where  $a$  refers to conditions ahead of the piston and  $b$  refers to conditions behind the piston. Ahead of the piston

$$Q_a = \frac{2}{\gamma_1 - 1} c_a - u_a = \text{constant} = Q_1 \quad (\text{B-5})$$

$$\text{where } Q_1 = \frac{2}{\gamma_1 - 1} c_1. \quad (\text{B-6})$$

Here, subscript 1 refers to the uniform initial conditions of the quiescent low-pressure reservoir ahead of the piston. The above two expressions can

be rearranged to give the ratio  $c_a/c_1$  which, together with the isentropic relation, leads to

$$\frac{p_a}{p_1} = \left[ \frac{c_a}{c_1} \right]^{2\gamma_1/(\gamma_1 - 1)} = \left[ \frac{Q_1 + u_a}{Q_1} \right]^{2\gamma_1/(\gamma_1 - 1)} \quad (\text{B-7})$$

where  $p$  is the pressure. Similarly, we have for the pressure on the trailing side of the piston

$$\frac{p_b}{p_2} = \left[ \frac{c_b}{c_2} \right]^{2\gamma_2/(\gamma_2 - 1)} = \left[ \frac{p_2 - u_b}{p_2} \right]^{2\gamma_2/(\gamma_2 - 1)} \quad (\text{B-8})$$

where subscript 2 denotes the initial conditions of the quiescent high-pressure reservoir behind the piston. Note that  $u_a = u_b = u$ , the velocity of the piston. The acceleration of the piston can now be expressed in terms of the pressure difference across the piston; that is

$$\frac{du}{dt} = \frac{\Delta p}{m/A} = \frac{1}{m/A} \left\{ p_2 \left[ \frac{p_2 - u_b}{p_2} \right]^{2\gamma_2/(\gamma_2 - 1)} - p_1 \left[ \frac{Q_1 + u_a}{Q_1} \right]^{2\gamma_1/(\gamma_1 - 1)} \right\} \quad (\text{B-9})$$

Equation (B-9) can be integrated numerically for  $u(t)$ .

Now, if the geometry is not planar ( $j = 0$ ) but cylindrical ( $j = 1$ ) instead, we would replace Equations (B-3) and (B-4) by the following:

$$P = \frac{2}{\gamma - 1} c + u + \int_0^t \frac{cu}{r} dt = \text{constant along } \frac{\partial x}{\partial t} = u + c \quad (\text{B-10})$$

$$\text{and } Q = \frac{2}{\gamma - 1} c - u + \int_0^t \frac{cu}{r} dt = \text{constant along } \frac{\partial x}{\partial t} = u - c \quad (\text{B-11})$$

where the last term in each of the expressions for the invariants accounts for cylindrical divergence. Repeating the same derivation as described in Equations (B-5) through (B-9) gives the piston motion in cylindrical geometry:

$$\frac{du}{dt} = \frac{1}{m/A} \left\{ p_2 \left[ \frac{p_2 - u_b - \int_0^t \frac{cu}{r} dt}{p_2} \right]^{2\gamma_2/(\gamma_2 - 1)} - p_1 \left[ \frac{Q_1 + u_a - \int_0^t \frac{cu}{r} dt}{Q_1} \right]^{2\gamma_1/(\gamma_1 - 1)} \right\} \quad (B-12)$$

which can again be integrated numerically for  $u(t)$ . However, an iterative approach must be used because the integral term in Equation (B-12) involves  $u(t)$ , the quantity being sought.

#### REFERENCE

Meyer, R. F. (1958) "The Impact of a Shock on a Movable Wall". *Journal of Fluid Mechanics* 3, 309.

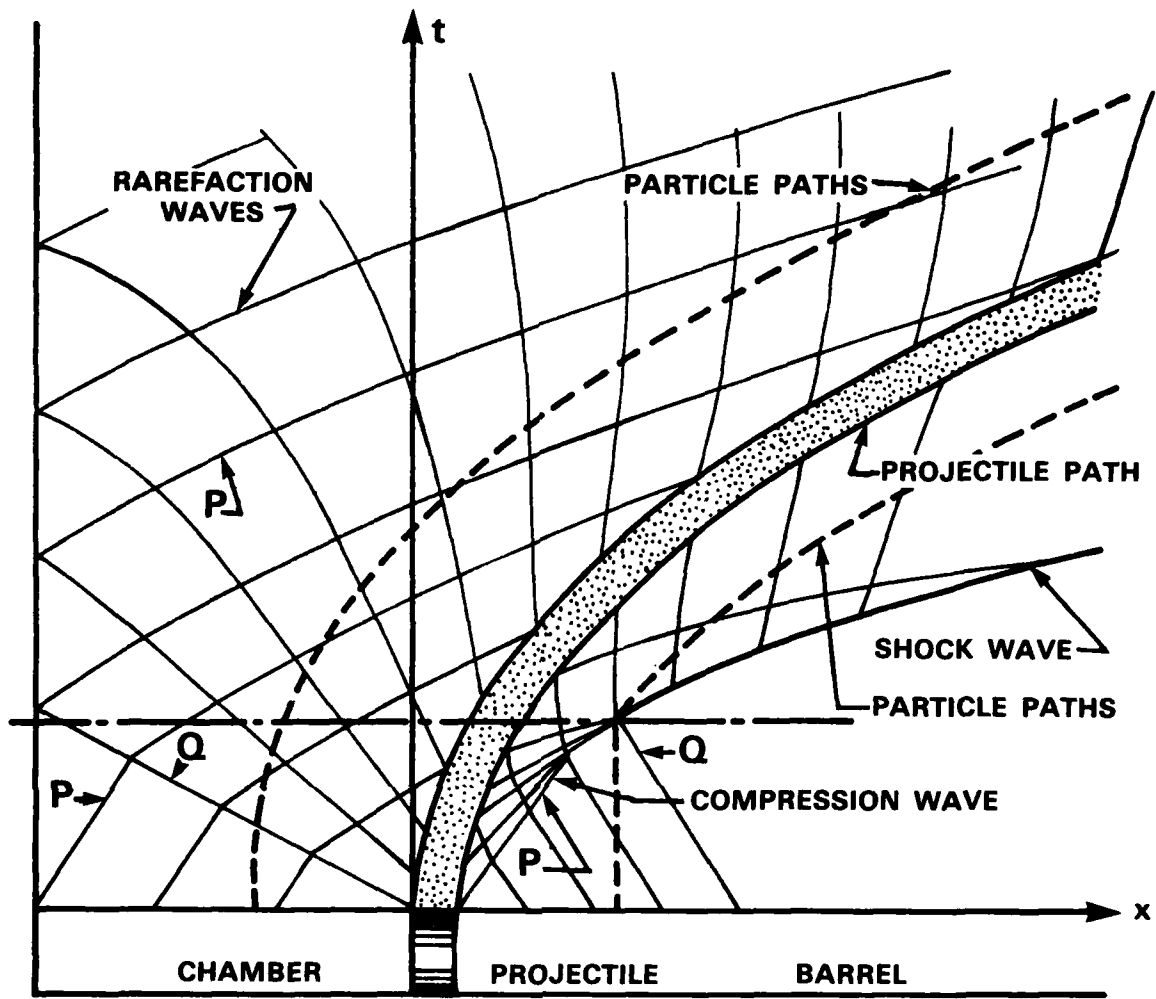


Figure B - 1

The x - t diagram for a simple launcher.

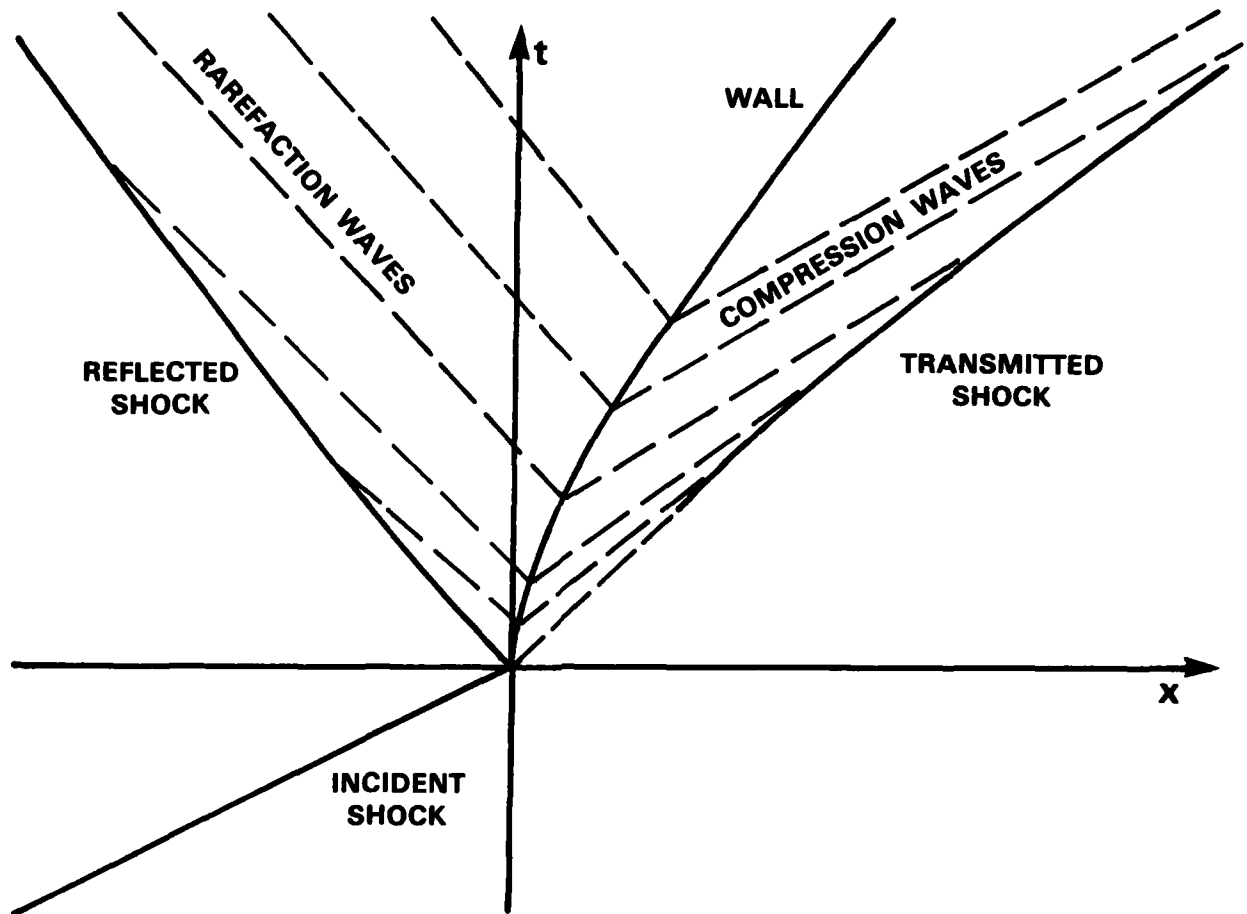


Figure B - 2

Wave diagram for the motion following the one-dimensional impact of a shock wave on a movable wall.

UNCLASSIFIED

APPENDIX C

QUASI ONE-DIMENSIONAL ANALYSIS FOR THE  
VELOCITY DEFICIT OF A DETONATION WAVE\*

---

\*Most of the derivation in this appendix is taken from Dabora, E.K. (1963) "The Influence of a Compressible Boundary on the Propagation of Gaseous Detonations". University of Michigan Technical Report 05170-1-T (Ph.D. Thesis).

UNCLASSIFIED

QUASI ONE-DIMENSIONAL ANALYSIS FOR THE  
VELOCITY DEFICIT OF A DETONATION WAVE

The classical hydrodynamic formulation for the characteristics of a general, steady, one-dimensional wave will first be presented briefly. It is assumed that the wave can be considered as a planar discontinuity, with conditions along the wave being uniform, as represented in Figure C-1. Thus, the conservation equations can be written as follows:

a. Conservation of mass:

$$\rho_1 u_1 = \rho_2 u_2 \quad (C-1)$$

b. Conservation of momentum:

$$\rho_1 u_1^2 + p_1 = \rho_2 u_2^2 + p_2 \quad (C-2)$$

c. Conservation of energy:

$$\frac{u_1^2}{2} + h_1 + q = \frac{u_2^2}{2} + h_2 \quad (C-3)$$

where  $q$  is the heat release per unit mass due to chemical reaction, and  $p$ ,  $h$ ,  $\rho$  and  $u$  are the particle pressure, enthalpy, density and velocity relative to the front, respectively. To keep the analysis general, one can assume that the gases ahead and behind the wave have different molecular weights  $m$  and ratios of specific heats  $\gamma$ . However, for simplicity, both gases are assumed to be thermally and calorically perfect. Thus, the equation of state is

$$p = \rho \frac{R_0 T}{m} \quad (C-4)$$

and the enthalpy can be written as

$$\begin{aligned}
 h &= c_p T = \frac{\gamma}{\gamma - 1} \frac{R_0}{m} T \\
 &= \frac{\gamma}{\gamma - 1} \frac{p}{\rho} = \frac{\gamma}{\gamma - 1} p v .
 \end{aligned}
 \tag{C-5}$$

Now if Equations (C-1) and (C-2) are combined, one can readily obtain

$$\frac{\frac{p_2}{p_1} - 1}{\frac{v_2}{v_1} - 1} = - \frac{u_1^2}{p_1 v_1} = -\gamma_1 M_1^2 = - \frac{u_2^2}{p_1 v_1} .
 \tag{C-6}$$

On a p-v diagram, this equation represents a straight line with a negative slope for any finite Mach number, and is commonly known as the Rayleigh line.

On the other hand, if Equations (C-1), (C-2), (C-3) and (C-5) are combined, the following can be obtained, after elimination of the velocity terms:

$$\left\{ \frac{2q}{p_1 v_1} + \frac{\gamma_1 + 1}{\gamma_1 - 1} - \frac{\gamma_2 - 1}{\gamma_2 + 1} \right\} \left\{ \frac{\gamma_2 - 1}{\gamma_2 + 1} \right\} = \left\{ \frac{p_2}{p_1} + \frac{\gamma_2 - 1}{\gamma_2 + 1} \right\} \left\{ \frac{v_2}{v_1} - \frac{\gamma_2 - 1}{\gamma_2 + 1} \right\} .
 \tag{C-7}$$

This is called the Hugoniot relation, and it can be seen that on a p-v diagram it would plot as a family of hyperbolas with a function of q and  $\gamma$ 's as a parameter.

Figure C-2 shows a schematic plot of Equation (C-6) (two straight lines) and Equation (C-7) for the adiabatic case and for two cases with heat release. The lower branch of the Hugoniot curves, in conjunction with Rayleigh lines of absolute slope less than  $\gamma_1$ , represent the deflagration mode of combustion and is not relevant to the present work. The upper branch and Rayleigh lines of absolute slope greater than  $\gamma_1$  represent shock or detonation waves. In general, a Rayleigh line intersects the Hugoniot curve at two points which represent the simultaneous solution of Equations (C-6)



and (C-7). As examples, point A represents an adiabatic shock wave with  $p_2/p_1$  and  $\rho_2/\rho_1$  greater than unity. Point B is the solution for a strong detonation wave and point B' is that for a weak wave, both of which occur for a value of  $q$  less than the limiting value. Points similar to B' are usually ruled out from entropy considerations if the detonation process is considered a shock followed by heat release. Finally, point C-J is the solution for the Chapman-Jouguet wave and is realized at the limiting value of heat release. It is the type of wave observed in detonation tubes.

As can be seen from Figure C-2, at point C-J the Rayleigh line is tangent to the Hugoniot curve. If Equations (C-6) and (C-7) are differentiated, we obtain respectively:

$$\frac{\partial \frac{p_2}{p_1}}{\partial \frac{v_2}{v_1}} = - \frac{u_2^2 \rho_2}{p_1 \rho_1} \quad (C-8)$$

and

$$\frac{\partial \left[ \frac{p_2}{p_1} \right]}{\partial \left[ \frac{v_2}{v_1} \right]} = - \frac{\frac{p_2}{p_1} + \frac{\gamma_2 - 1}{\gamma_2 + 1}}{\frac{\rho_1}{\rho_2} - \frac{\gamma_2 - 1}{\gamma_2 + 1}} \quad (C-9)$$

Equating (C-8) and (C-9), substituting  $p_1$  from (C-2) and  $u_1$  from (C-1), the solution of  $u_2$  for the C-J point is obtained:

$$u_2 = \sqrt{\frac{\gamma_2 p_2}{\rho_2}} = a_2 \quad (C-10)$$

This means that for a Chapman-Jouguet wave the burned gas immediately behind the wave travels at the local sonic speed with respect to the wave.

The conservation equations, together with the perfect gas relation and the definition of the velocity of sound, can be combined to give the changes in the thermodynamic properties across the wave in terms of the original Mach

number  $M_1$ ,  $q$  and  $\gamma$ 's. This was done by Adamson and Morrison (1958) for the simple case where no changes in molecular weight and specific heat ratio were considered. Later, Adamson (1958) generalized the solutions to cases admitting these changes. These solutions are given here without derivation:

a. Pressure ratio:

$$\frac{p_2}{p_1} - 1 = \frac{\gamma_1 F}{\gamma_2 + 1} \left[ M_1^2 - \frac{\gamma_2}{\gamma_1} \right] \quad (C-11)$$

b. Density ratio:

$$\frac{\rho_2}{\rho_1} = \frac{1}{1 - \frac{F}{\gamma_2 + 1} \left[ M_1^2 - \frac{\gamma_2}{\gamma_1} \right] \frac{1}{M_1^2}} \quad (C-12)$$

c. Temperature ratio:

$$\frac{T_2}{T_1} = \frac{m_2}{m_1} \left\{ 1 - \frac{F}{M_1^2 (\gamma_2 + 1)} \left[ M_1^2 - \frac{\gamma_2}{\gamma_1} \right] \right\} \times \left\{ 1 + \frac{\gamma_1 F}{\gamma_2 + 1} \left[ M_1^2 - \frac{\gamma_2}{\gamma_1} \right] \right\} \quad (C-13)$$

The definition of  $F$  in the above equations is:

$$F = 1 + \sqrt{1 - \frac{2(\gamma_2^2 - 1)}{\gamma_1 - 1} \frac{M_1^2}{\left[ M_1^2 - \frac{\gamma_2}{\gamma_1} \right]^2} \left\{ \frac{q}{c_{p1} T_1} - \frac{\gamma_1 - \gamma_2}{\gamma_1 (\gamma_2 - 1)} \right\}} \quad (C-14)$$

and its implication is as follows:

- $F = 1$  represents cases with limiting  $q$ ; i.e., C-J waves.
- $F = 2$  represents cases with  $q = 0$ ; i.e., adiabatic shock waves (when  $\gamma_1 = \gamma_2$ ).
- $2 > F > 1$  represents cases of strong detonation waves.

The solution for the Mach number behind the wave was also given by Adamson (1958) as

$$M_2^2 = \frac{\gamma_1}{\gamma_2} \left\{ \frac{(\gamma_2 + 1 - F) \left[ M_1^2 - \frac{\gamma_2}{\gamma_1} \right] + \frac{\gamma_2}{\gamma_1} (\gamma_2 + 1)}{\gamma_1 F \left[ M_1^2 - \frac{\gamma_2}{\gamma_1} \right] + (\gamma_2 + 1)} \right\}. \quad (C-15)$$

It is to be noted that for the C-J case  $M_2 = 1$ , and therefore Equation (C-15) yields  $F = 1$  so that the propagation Mach number of a Chapman-Jouguet wave can be found from Equation (C-14) by the relation

$$2 \left\{ \frac{q}{c_{p1} T_1} - \frac{\gamma_1 - \gamma_2}{\gamma_1 (\gamma_2 - 1)} \right\} \frac{\gamma_2 - 1}{\gamma_1 - 1} = \frac{\left( M_1^2 - \frac{\gamma_2}{\gamma_1} \right)^2}{M_1^2}. \quad (C-16)$$

Thus, if the initial thermodynamic conditions, as well as the value of heat release and  $\gamma_2$  are known, the detonation velocity can be found. In general, however, finding  $q$  and  $\gamma_2$  requires a trial and error solution that involves chemical equilibrium behind the wave [the Gordon and McBride (1976) computer program is used to obtain the solution in the present work].

Now, if some mechanism is present to promote an increase in the area of each stream tube between the shock and the C-J plane (e.g., yielding walls, boundary layer growth, etc.) then a deficit in the propagation velocity will result. The analysis that follows will make use of reasoning similar to that of Fay (1959) who investigated the effect of boundary layer growth on the detonation velocity in solid tubes. If the shock front area is  $A_1$  and the C-J plane area is  $A_2$ , which is different from  $A_1$  (see Figure C-3), then

$$A_2/A_1 = 1 + \xi \quad (C-17)$$

where  $\xi$  is the average fractional change in the area of each stream tube. The conservation equations thus become:

a. Conservation of mass:

$$\rho_1 u_1 = \rho_2 u_2 (1 + \xi) \quad (C-18)$$

b. Conservation of momentum:

$$\rho_1 u_1^2 + p_1 = (\rho_2 u_2^2 + p_2)(1 + \xi) - \int_0^\xi p \, d\xi \quad (C-19)$$

c. Conservation of energy:

$$\frac{u_1^2}{2} + h_1 + q = \frac{u_2^2}{2} + h_2 \quad (C-20)$$

To evaluate the integral term in Equation (C-19) requires a detailed knowledge of the pressure behind the shock front along the boundary within the reaction zone. However, one can define the integral as

$$\int_0^\xi p \, d\xi = p_2 \epsilon \xi \quad (C-21)$$

and note from Equation (C-11) that  $p_2/p_1$  for a shock ( $F = 2$ ) is about twice that for a detonation wave ( $F = 1$ ) when  $M_1$  is large. Thus, the value of  $\epsilon$  is between 2 and 1.

Using the same general assumptions as for the case involving no area increase, Equations (C-18), (C-19), (C-20) and (C-21), together with the definition of the speed of sound, can be combined to give:

$$2 \left[ 1 + \frac{q}{c_{p1} T_1} \right] = \left[ \frac{\gamma_2}{\gamma_1} \right]^2 \left[ \frac{\gamma_1 - 1}{\gamma_2 - 1} \right] \left\{ \frac{1}{1 - \frac{\xi \epsilon}{(1 + \gamma_2)(1 + \xi)}} \right\}^2 \frac{(\gamma_1 M_1^2 + 1)^2}{M_1^2} - (\gamma_1 - 1) M_1^2 \quad (C-22)$$

Introducing a new function  $\psi$  defined by

$$1 + \psi \equiv \left\{ \frac{1}{1 - \frac{\epsilon \xi}{(1 + \gamma_2)(1 + \xi)}} \right\}^2 \quad (C-23)$$

Equation (C-22) can be reduced to the following:

$$2 \left\{ \frac{q}{c_{p1} T_1} - \frac{\gamma_1 - \gamma_2}{\gamma_1(\gamma_2 - 1)} \right\} \frac{\gamma_2^2 - 1}{\gamma_1 - 1} = \frac{\left(M_1^2 - \frac{\gamma_2}{\gamma_1}\right)^2}{M_1^2} + \frac{\psi \gamma_2^2 \left(M_1^2 + \frac{1}{\gamma_1}\right)^2}{M_1^2} . \quad (C-24)$$

This equation is different from Equation (C-16) by only the last term which represents the effect of area change. For large  $M_1$  (i.e.,  $M_1 > 5$ ), Equation (C-24) can be reduced further to:

$$2 \left\{ \frac{q}{c_{p1} T_1} - \frac{\gamma_1 - \gamma_2}{\gamma_1(\gamma_2 - 1)} \right\} \frac{\gamma_2^2 - 1}{\gamma_1 - 1} = M_1^2 (1 + \psi \gamma_2^2) . \quad (C-25)$$

If the heat release is assumed to remain the same whether there is an area change or not, the right hand side of Equation (C-25) remains essentially constant. It should be noted that physically this is a reasonable assumption in that chemical equilibrium is expected to remain the same at the C-J plane whether there is an area change or not. This is so because the influence of an area increase would be a decrease in both pressure and temperature at that plane. If the heat release is controlled by dissociation at this point, the pressure and temperature effects would tend to cancel each other.

Noting that  $\psi = 0$  when  $\xi = 0$ , one can find, after making use of Equation (C-25), that the decrease in Mach number from the case where there is no area change to the case where  $\xi$  is finite can be written as:

$$\frac{M_1(\xi = 0) - M_1}{M_1(\xi = 0)} = \frac{\Delta M_1}{M_1(\xi = 0)} = 1 - \sqrt{\frac{1}{1 + \gamma_2^2 \psi}} , \quad (C-26)$$

or in terms of  $\xi$ :

$$\frac{\Delta M_1}{M_1(\xi = 0)} = 1 - \sqrt{\frac{\left\{ 1 - \left[ \frac{\epsilon}{1+\gamma_2} \right] \left[ \frac{\xi}{1+\xi} \right] \right\}^2}{\left\{ 1 - \left[ \frac{\epsilon}{1+\gamma_2} \right] \left[ \frac{\xi}{1+\xi} \right] \right\}^2 + \gamma_2^2 \left\{ 2 \left[ \frac{\epsilon}{1+\gamma_2} \right] \left[ \frac{\xi}{1+\xi} \right] - \left[ \frac{\epsilon}{1+\gamma_2} \right]^2 \left[ \frac{\xi}{1+\xi} \right]^2 \right\}}$$

(C-27)

Having determined the velocity or Mach number deficit, it is now possible to back substitute into Equations (C-5), (C-18), (C-19) and (C-20) in order to obtain the "modified" sonic conditions resulting from an area increase in the reaction zone. These modified conditions are summarized in graphical form in Figure C-4 for the case of  $\gamma_1 = 1.4$ ,  $\gamma_2 = 1.2$  and  $\epsilon = 1$ .

#### REFERENCES

- Adamson, T. C., Jr. (1958) Class notes from University of Michigan course on "Flame Propagation".
- Adamson, T. C., Jr. and Morrison, R. B. (1958) "On the Classification of Normal Detonation Waves". *Jet Propulsion* 25, 400.
- Fay, J. A. (1959) "Two-Dimensional Gaseous Detonations: Velocity Deficits". *Physics of Fluids* 2, 283.
- Gordon, S. and McBride, B. I. (1976) "Computer Program for Calculation of Complex Chemical Equilibrium Compositions, Rocket Performance, Incident and Reflected Shocks and Chapman-Jouguet Detonations". NASA Report SP-273.

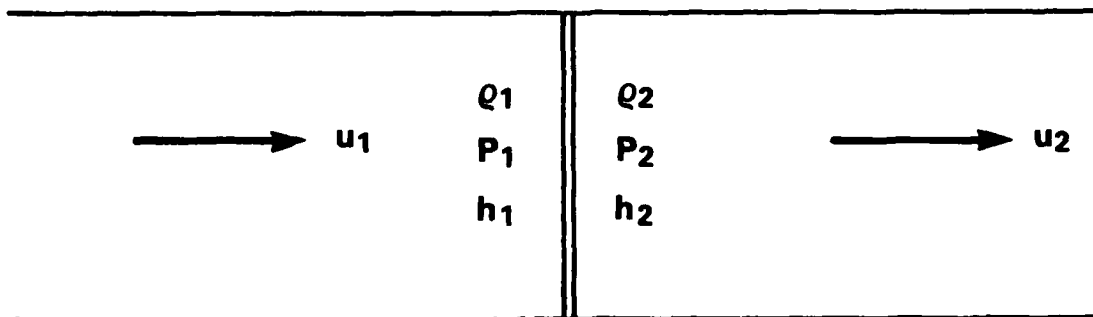


Figure C-1

One-dimensional detonation wave.

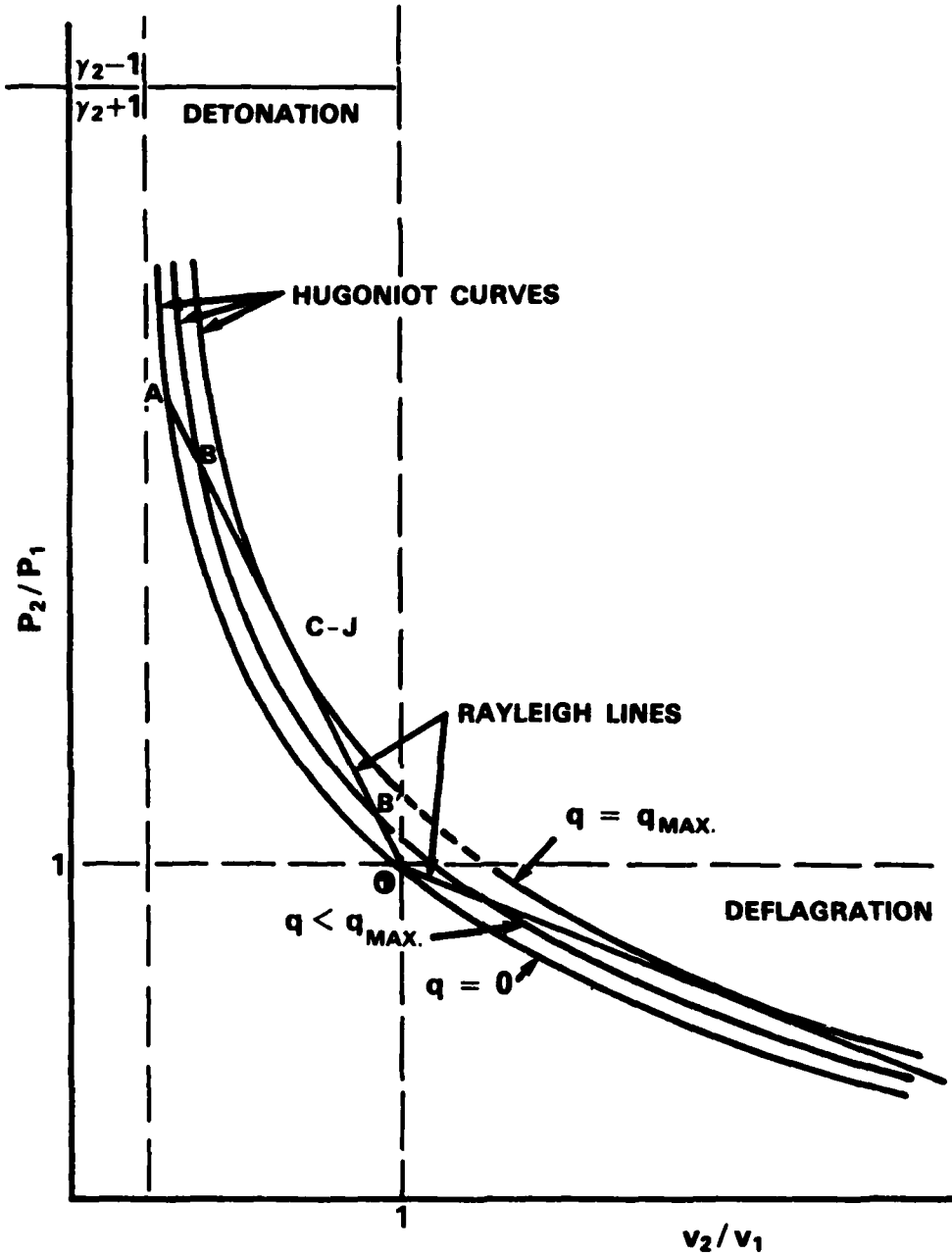


Figure C-2

Hugoniot-Rayleigh representation of shock and detonation waves.



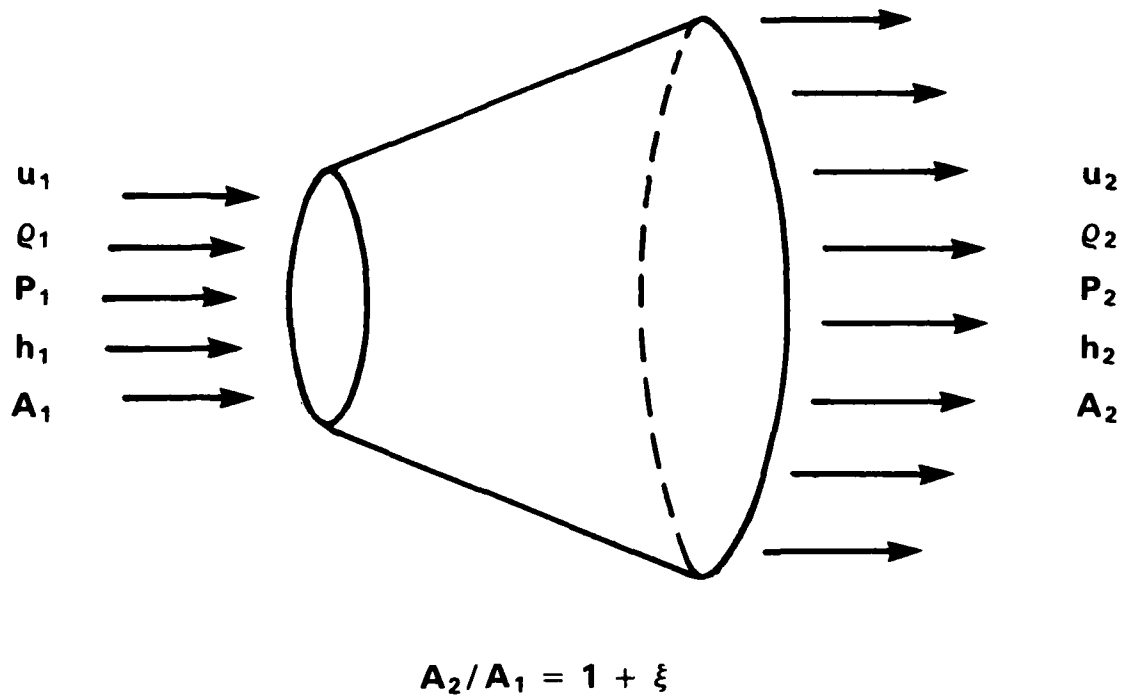


Figure C-3

Quasi one-dimensional representation of a detonation wave with area increase.

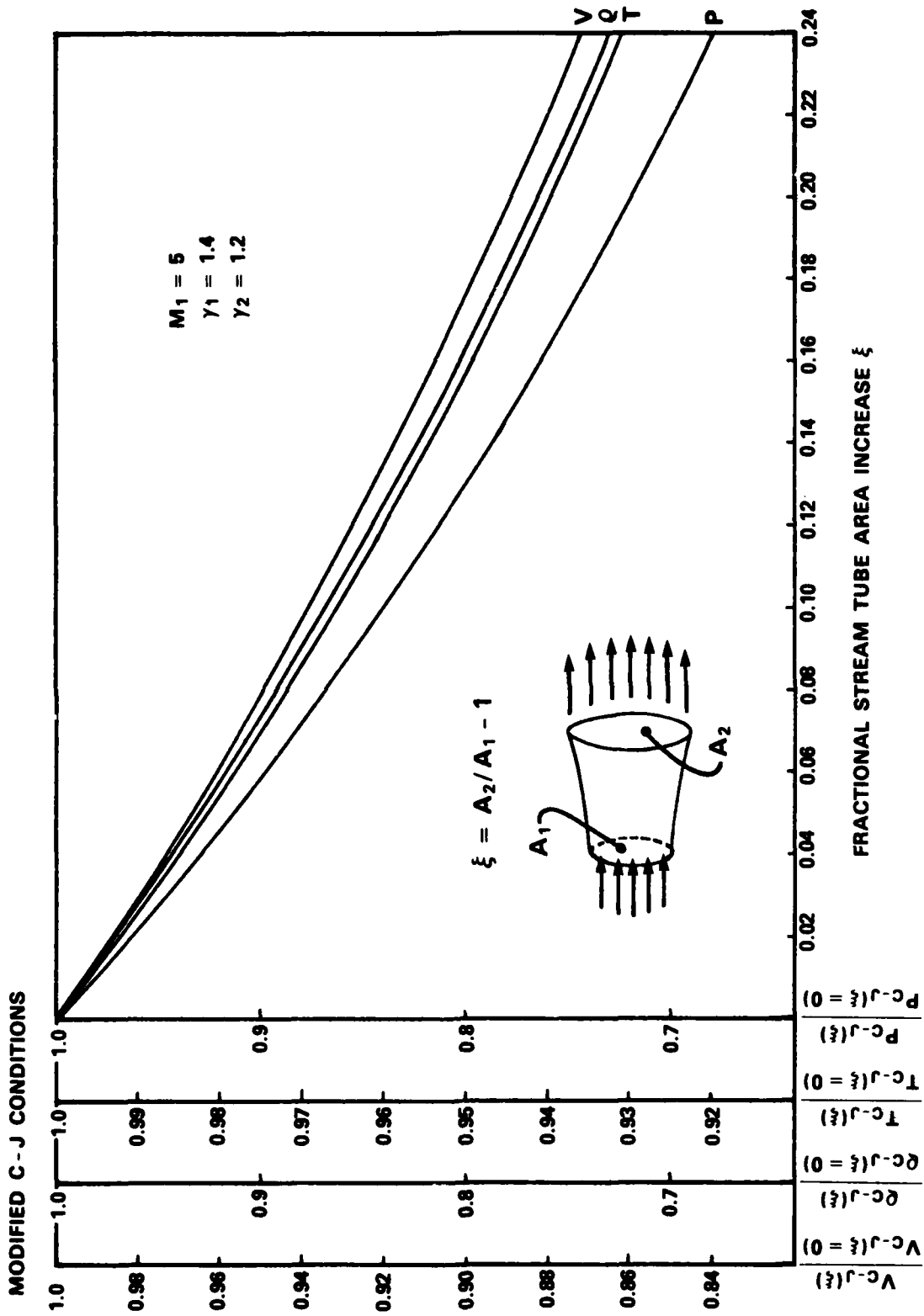


FIGURE C-4  
 CHANGES IN C-J CONDITIONS DUE TO AREA INCREASE.

**DOCUMENT CONTROL DATA - R & D**

(Security classification of title, body of abstract and indexing annotation must be entered when the overall document is classified)

1. ORIGINATING ACTIVITY Defence Research Establishment Suffield Ralston, Alberta, Canada		2a. DOCUMENT SECURITY CLASSIFICATION Unclassified	
		2b. GROUP	
3. DOCUMENT TITLE The Influence of Initial and Boundary Conditions on Gaseous Detonation Waves			
4. DESCRIPTIVE NOTES (Type of report and inclusive dates) Suffield Report 411			
5. AUTHOR(S) (Last name, first name, middle initial) Murray, Stephen B.			
6. DOCUMENT DATE Sep 1985		7a. TOTAL NO. OF PAGES 314	7b. NO. OF REFS 238
8a. PROJECT OR GRANT NO. ACN 27C10		9a. ORIGINATOR'S DOCUMENT NUMBER(S) SR 411	
8b. CONTRACT NO.		9b. OTHER DOCUMENT NO.(S) (Any other numbers that may be assigned this document)	
10. DISTRIBUTION STATEMENT Unlimited			
11. SUPPLEMENTARY NOTES Ph.D. Thesis, McGill University		12. SPONSORING ACTIVITY	
13. ABSTRACT <p>The results of five experimental investigations on the initiation, propagation and transmission of detonation have shown that the wave behavior depends on the relative rates of gasdynamic expansion and chemical energy release occurring within the cellular detonation front. The former rate is controlled by the "boundary conditions" defined by the physical system, while the latter rate depends on the chemical and physical properties of the combustible mixture. The fractional increase <math>\xi</math> in the area of the post-shock "stream tube", evaluated over a chemical kinetic distance equal to the cell length, has been identified as a parameter which satisfactorily characterizes the competition between these two rate processes. For <math>\xi</math> less than about 20%, the chemical processes survive the gasdynamic expansion and self-sustained propagation is possible. However, under these "supercritical" conditions, the wave propagates with a velocity deficit which appears to be a universal and theoretically predictable function of <math>\xi</math>.</p> <p>For <math>\xi</math> greater than 20%, the shock/reaction zone coupling breaks down, resulting in failure of the wave. The "critical" conditions for the propagation of detonation waves subjected to a wide range of expansion inducing mechanisms, including viscous boundary layers, compressible boundary gases and yielding walls, are all found to be consistent with the 20% criterion. However, the criterion becomes inapplicable as the cell size approaches the characteristic transverse dimension of the geometry.</p> <p>In the case of direct initiation or transmission of detonation from one geometry to another, the critical conditions are shown to be linked to the requirement for the diverging wave to exceed some minimum radius of curvature. Such radius is geometry dependent and satisfies the stream tube criterion. The role of the "initial conditions" in this type of problem is to guarantee survival of the wave until it achieves the minimum radius for which shock/reaction zone coupling, and hence self-sustenance, are possible.</p>			

## KEY WORDS

detonation, fuel-air, initiation, propagation, detonability, detonability limits, velocity deficits, critical energy, direct initiation, detonation diffraction, critical tube diameter, yielding boundary, transmission of detonation, critical channel width, stream tube, structure of detonation, cellular structure, shock wave, detonation wave, combustion wave, critical conditions, supercritical conditions, cell size, transverse wave spacing, compressible boundary, spinning detonation.

## INSTRUCTIONS

1. **ORIGINATING ACTIVITY** Enter the name and address of the organization issuing the document.
- 2a. **DOCUMENT SECURITY CLASSIFICATION** Enter the overall security classification of the document including special warning terms whenever applicable.
- 2b. **GROUP** Enter security reclassification group number. The three groups are defined in Appendix 'M' of the DRB Security Regulations.
3. **DOCUMENT TITLE** Enter the complete document title in all capital letters. Titles in all cases should be unclassified. If a sufficiently descriptive title cannot be selected without classification, show title classification with the usual one-capital-letter abbreviation in parentheses immediately following the title.
4. **DESCRIPTIVE NOTES** Enter the category of document, e.g. technical report, technical note or technical letter. If appropriate, enter the type of document, e.g. interim, progress, summary, annual or final. Give the inclusive dates when a specific reporting period is covered.
5. **AUTHOR(S)** Enter the name(s) of author(s) as shown on or in the document. Enter last name, first name, middle initial. If military, show rank. The name of the principal author is an absolute minimum requirement.
6. **DOCUMENT DATE** Enter the date (month, year) of Establishment approval for publication of the document.
- 7a. **TOTAL NUMBER OF PAGES** The total page count should follow normal pagination procedures, i.e., enter the number of pages containing information.
- 7b. **NUMBER OF REFERENCES** Enter the total number of references cited in the document.
- 8a. **PROJECT OR GRANT NUMBER** If appropriate, enter the applicable research and development project or grant number under which the document was written.
- 8b. **CONTRACT NUMBER** If appropriate, enter the applicable number under which the document was written.
- 9a. **ORIGINATOR'S DOCUMENT NUMBER(S)** Enter the official document number by which the document will be identified and controlled by the originating activity. This number must be unique to this document.
- 9b. **OTHER DOCUMENT NUMBER(S)** If the document has been assigned any other document numbers (either by the originator or by the sponsor), also enter this number(s).
10. **DISTRIBUTION STATEMENT** Enter any limitations on further dissemination of the document, other than those imposed by security classification, using standard statements such as:
  - (1) "Qualified requesters may obtain copies of this document from their defence documentation center."
  - (2) "Announcement and dissemination of this document is not authorized without prior approval from originating activity."
11. **SUPPLEMENTARY NOTES** Use for additional explanatory notes.
12. **SPONSORING ACTIVITY** Enter the name of the departmental project office or laboratory sponsoring the research and development. Include address.
13. **ABSTRACT** Enter an abstract giving a brief and factual summary of the document, even though it may also appear elsewhere in the body of the document itself. It is highly desirable that the abstract of classified documents be unclassified. Each paragraph of the abstract shall end with an indication of the security classification of the information in the paragraph (unless the document itself is unclassified) represented as (TS), (SI), (C), (R), or (U).  
  
The length of the abstract should be limited to 20 single-spaced standard typewritten lines, 7 1/4 inches long.
14. **KEY WORDS** Key words are technically meaningful terms or short phrases that characterize a document and could be helpful in cataloging the document. Key words should be selected so that no security classification is required. Identifiers, such as equipment model designation, trade name, military project code name, geographic location, may be used as key words but will be followed by an indication of technical context.

**END**

**FILMED**

---

*2-86*

**DTIC**